Light Sensitivity of Lactococcus lactis Thioredoxin Reductase

Skjoldager, Nicklas

Publication date:
2017

Document Version
Publisher's PDF, also known as Version of record

Light Sensitivity of *Lactococcus lactis* Thioredoxin Reductase

PhD Thesis

May 2017

Nicklas Skjoldager

DTU Bioengineering

Department of Biotechnology and Biomedicine

Technical University of Denmark (DTU)

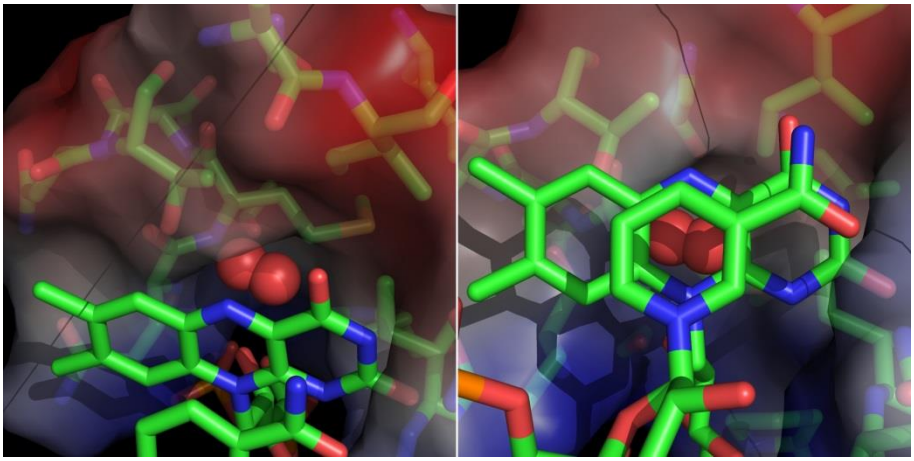

Supervisors

Associate Professor Per Hägglund, Department of Biotechnology and Biomedicine, DTU

Professor Birte Svensson, Department of Biotechnology and Biomedicine, DTU

Cover pictures: The active site in *Lactococcus lactis* thioredoxin reductase. The FAD is in complex with the $NADP^+$ on the *re*-face, while the *si*-face open space has been modeled with molecular oxygen.

Preface

The present thesis represents the results of my PhD study carried out in the Enzyme and Protein Chemistry (EPC) group and the DTU Proteomics Core (PC) group at the Department of Biotechnology and Biomedicine, Technical University of Denmark (DTU) under the supervision of Associate Prof. Per Hägglund (EPC & PC), Prof. Birte Svensson (EPC) and Associate Prof. Susanne Jacobsen (EPC). The crystallographic part of the work has been carried out at the Protein & X-ray Crystallography group, Department of Chemistry, DTU, under supervision of Associate Prof. Pernille Harris. The research was conducted in the period from January 2013 to May 2017. This project was funded by a DTU PhD scholarship.

Part of the PhD project focused on characterizing potential thioredoxin protein targets. An overview of this work is compiled in Appendix H. The main part of the PhD study has generated the data presented in chapter 2 and 3, which for now has resulted in two papers and a planned manuscript:

Björnberg, O., Viennet, T., **Skjoldager, N.**, Ćurović, A., Nielsen, K. F., Svensson, B. and Hägglund, P. *Lactococcus lactis* Thioredoxin Reductase Is Sensitive to Light Inactivation. *Biochemistry* **54**, 1628–1637 (2015). [Appendix A, referred to as **Paper 1**].

Skjoldager, N., Blanner Bang, M., Rykær, M., Björnberg, O., Davies, M. J., Svensson, B., Harris, P. and Hägglund, P. The structure of *Lactococcus lactis* thioredoxin reductase reveals molecular features of photo-oxidative damage. *Sci. Rep.* **7**, 46282 (2017). [Appendix B, referred to as **Paper 2**].

Skjoldager, N., Ryberg, L. A., Blanner Bang, M., Ignasiak, M. T., Davies M. J., Peters, G. H. J., Svensson, B., Harris, P. and Hägglund, P. *Lactococcus lactis* Thioredoxin Reductase displays increased conformational flexibility. *Planned manuscript*.

Publication not included in this PhD thesis

Navrot, N., **Skjoldager, N.**, Bunkenborg, J., Svensson, B. & Hägglund, P. A redox-dependent dimerization switch regulates activity and tolerance for reactive oxygen species of barley seed glutathione peroxidase. *Plant Physiol. Biochem.* **90**, 58–63 (2015).

Acknowledgements

First and foremost I want to thank my supervisors Associate Prof. Per Hägglund, Prof. Birte Svensson and Associate Prof. Susanne Jacobsen. Per Hägglund has been a strong resource for me, sharing his huge knowledge within thiol redox control systems through endless discussions, trying to shed light on our enigmatic enzyme. Prof. Birte Svensson is acknowledged for contributing with her great insight in protein chemistry and has been a persistent support throughout the course of the PhD study that in periods seemed rather bumpy. Associate Prof. Susanne Jacobsen has a special place in this project, as the one who got me on board at DTU. As an energetic person sharing her positive energy with me and others, she became a delighted inspiration and role model.

Associate Professor Pernille Harris Department of Chemistry, DTU, is acknowledged for supervision and support in theoretical and practical X-ray crystallography, joining me in a relentless search for collecting the best of possible diffraction data. The MAXIV synchrotron is acknowledged for beam-time and support during data-collection and the funding from BioStruct-X (EC FP7 grant agreement N°283570) and DANSCATT (The Danish Agency for Science, Technology and Innovation).

Many people are acknowledged for help during the PhD study:
Maria Blanner Bang (DTU Chemistry) is acknowledged for help in the initial stages of crystallization trials and structure solving. Mogens Kilstrup (DTU Bioengineering) is acknowledged for inspirational discussions and guidance in performing *L. lactis* growth experiments. Line Abildgaard Ryberg (DTU Chemistry) is thanked for laboratory assistance during the crystallization trials. Michael J. Davies (University of Copenhagen, Department of Biomedical Sciences) is acknowledged for discussions and guidance about the photo-inactivation mechanisms of *Ll*TrxR and for providing me access to the stopped-flow instrument. Petr Efler (former EPC) is thanked for introducing me to *L. lactis* growth experiments. Marta Teresa Ignasiak (University of Copenhagen, Department of Biomedical Sciences) is thanked for the help during the stopped-flow experiments and data analysis. Olof Björnberg (former EPC) is thanked for inspirational discussions about the

light sensitivity of *Ll*TrxR. Martin Rykær (DTU Bioengineering) is credited for performing LC-MS on digested *Ll*TrxR. Anne Blicher (DTU Bioengineering) is recognized for performing amino acid analysis on *Sa*TrxA and *Bs*TrxA. Hans Erik Mølager Christensen (DTU Chemistry) for his patience in performing ESI-MS on intact *Ll*TrxR together with me. Kristian Fog Nielsen (DTU Bioengineering) is credited for performing LC-MS on FAD from *Ll*TrxR. Neha Sharma is thanked for laboratory assistance in the kinetic characterization of *Ll*TrxA and *Ll*TrxD protein target specificity. Claes von Wachenfeldt (Lund University) in thanked for kindly donating the enzymes *Sa*TrxR, *Bs*TrxR, *Sa*TrxA and *Bs*TrxA. I also want to thank everyone at EPC, PC and Protein & X-ray Crystallography groups for help and support throughout my time at DTU.

I am grateful for the inspiration of my two lovely children, who showed me that life is more than just hard work. Finally, my deepest acknowledgement and love go to my wonderful wife who has endured many weekends and long evenings without my support. Without you I could not have made it

Nicklas Skjoldager

Lyngby, May 2017

Abstract

The thioredoxin system has evolved in all kingdoms of life acting as a key antioxidant system in the defense against oxidative stress. The thioredoxin system utilizes reducing equivalents from NADPH to reduce protein disulfide targets. The reducing equivalents are shuttled via a flavin and redox active dithiol motif in thioredoxin reductase (TrxR) to reduce the small ubiquitous thioredoxin (Trx). Trx in turn regulates the protein dithiol/disulfide balance by reduction of protein disulfide targets in *e.g.* ribonucleotide reductase, peroxiredoxins and methionine sulfoxide reductase. The glutathione system is an alternative thiol-based antioxidant system, but the glutathione biosynthesis system is not present in all organisms.

This thesis focuses on the TrxR from the lactic acid bacteria (LAB) model organism *Lactococcus lactis* ssp. *cremoris* MG1363, a strain that is glutathione- and catalase-negative, thus expected to rely mainly on the Trx system for thiol-disulfide control. *L. lactis* is an important industrial microorganism used as starter culture in the dairy production of cheese, buttermilk etc. and known to be sensitive to oxidative stress. The *L. lactis* TrxR (*Ll*TrxR) is a homodimeric flavoenzyme with each monomer consisting of a FAD- and a NADPH domain. In this type of low molecular weight (LMW) TrxR the NADPH domain rotates 66° relative to the FAD domain in order to complete a catalytic cycle. The TrxR thus exists in two conformations, referred to as FO- and FR-conformation. In the FR-conformation NADPH reduces the FAD co-enzyme, followed by rotation to the FO-conformation in which $FADH_2$ reduces the disulfide in the redox active motif of TrxR. The human TrxR belongs to the high molecular weight (HMW) TrxR involving a selenosulfide pair and functions in a different way than the LMW TrxR, which potentially makes LMW TrxR a therapeutic target.

*Ll*TrxR has been shown to be photo-inactivated by visible light exposure (λ_{max} = 460 nm), which has not been reported in other TrxR and the feature was not observed using the *E. coli* homolog (*Ec*TrxR) as control. The inactivation coincides with a shift in the absorbance spectrum of the tightly bound FAD co-enzyme and oxidation of the methyl group of the

isoalloxazine ring, as determined by MS. The extracted FAD from photo-inactivated *Ll*TrxR also displayed a positive result in a dinitrophenylhydrazine (DNPH) test, indicating the presence of a carbonyl group, *i. e.* an aldehyde. *Ll*TrxR reduces O_2 in the presence of NADPH faster than the *Ec*TrxR and the photo-inactivation is lowered at semi-anaerobic conditions and in the presence of iodine a well-known quencher of photoexcited triplet state flavin.

The present PhD study was initiated in order to identify the underlying functional and structural mechanisms behind this light sensitivity. Crystal structures of photo-inactivated *Ll*TrxR revealed oxidative damages over the course of light exposure. An increased electron density was observed around the carbon-7α of the isoalloxazine ring and to a minor degree around the carbon-8α. The Tyr237 in the vicinity of the flavin was shown to develop increased electron density at C3 position (ortho to the hydroxyl group) as a function of light exposure and was verified by MS to be associated with a +16 Da mass shift, consistent with formation of 3,4-dihydroxyphenylalanine (DOPA). A novel FAD *si*-face open space was identified in all structures of *Ll*TrxR and predicted to accommodate O_2, thus acting as an oxygen pocket. This model explains how the protein-bound FAD can function as a *de facto* photosensitizer, generating reactive oxygen species (ROS) upon light exposure. Reaction mechanisms accounting for the observed oxidations on FAD and Tyr237 were proposed with the photo-excited isoalloxazine ring generating a superoxide radical ($O_2^{\bullet-}$) at the *si*-face oxygen pocket. The one-electron deficient isoalloxazine cation can then oxidize Tyr237, which upon deprotonation forms a Tyr phenoxyl radical, a target of superoxide at the C3 position, accounting for the DOPA formation. The superoxide radicals can in addition react with the deprotonated form of carbon-7α of the isoalloxazine, which via a Russel mechanism accounts for the observed aldehyde formation. Another distinct feature of *Ll*TrxR is that it crystallizes mainly in FR-conformation, both with and without $NADP^+$ co-crystallization. *Ll*TrxR was only obtained in FO-conformation in reduced environment during the crystallization in the presence of DTT and absence of $NADP^+$. Interestingly, a mixed FO-FR conformation of the homodimer was also obtained in the presence of phosphate, indicating that the two monomers might function asynchronically.

The oxygen pocket is arising from the Met43 bending way from the *si*-face towards Pro15. Three methionines, Met18, Met43 and Met67 are bending towards the residue of Pro15 constituting (what in this work is referred to as) a methionine-proline motif.

Identification of key residue surrounding the oxygen pocket makes it possible to predict TrxR from other organisms harboring the FAD *si*-face oxygen pocket, including organisms such as *Bacillus subtilis* (*Bs*TrxR) and pathogens such as *Staphylococcus aureus* (*Sa*TrxR), *Streptococcus pyogenes* and *Bacillus anthracis*. A comparative photo-inactivation of TrxR from *L. lactis*, *S. aureus* and *B. subtilis* reveals that *Sa*TrxR and *Bs*TrxR are much less sensitive to light-inactivation than *Ll*TrxR, though *Sa*TrxR exhibited a similar rate of O_2 reduction in the presence of NADPH as *Ll*TrxR. Light exposure of *L. lactis* cell extract showed a prominent drop in TrxR activity and after 12 h about 35% of the *Ll*TrxR remained. Preliminary experiments of light exposed living *L. lactis* cells kept at 4°C, indicate that light exposure is in fact lethal, under the applied conditions. Cell extracts from the same 17 h *in vivo* irradiated cells showed ~14% remaining TrxR activity. The present investigation shows that TrxR light sensitivity might be a widespread phenomenon among bacteria, particular within the phylum of *Firmicutes*. This feature can potentially be exploited in clinical light therapy, *e.g.* in targeted blue light therapy of selected drug-resistant pathogenic bacteria.

Dansk resumé

Thioredoxin systemet er udbredt inden for alle taksonomiske former af liv og fungerer som et vigtigt antioxidantsystem i forsvaret mod oxidativt stress. Thioredoxin systemet anvender reduktive ækvivalenter fra NADPH til at reducere disulfidbindinger i proteiner. Reduktionsækvivalenterne overføres via et flavin- og redox-aktivt dithiol-motiv i thioredoxin reduktase (TrxR) for derigennem at reducere det lille allestedsnærværende thioredoxin (Trx). Trx regulerer dernæst protein dithiol/disulfid balancen ved reduktion af disulfidbindinger i proteiner, heriblandt ribonukleotidreduktase, peroxiredoxiner og methioninsulfoxidreduktase. Glutathion systemet er et alternativt thiolbaseret antioxidantsystem, men glutathion biosyntese apparatet er ikke udbredt i alle organismer.

Denne afhandling fokuserer på TrxR fra modelorganismen inden for mælkesyrebakterier *Lactococcus lactis* ssp. *cremoris* MG1363, en stamme der er glutathione- og katalase-negativ, og som derfor forventes hovedsageligt at basere sig på Trx-systemet til thiol-disulfidkontrol. *L. lactis* er en vigtig industriel mikroorganisme, der anvendes som starterkultur i mejeriproduktionen af ost, kærnemælk etc. og udviser følsom overfor oxidativt stress. *L. lactis* TrxR (*Ll*TrxR) er et homodimert flavoenzym med hver monomer bestående af et FAD- og et NADPH-domæne. I denne lavmolekylære (LMW) type af TrxR roterer NADPH-domænet 66° i forhold til FAD-domænet for at fuldbringe en katalytisk cyklus. TrxR eksisterer således i to konformationer, der benævnes FO- og FR-konformation. I FR-konformationen reducerer NADPH FAD co-enzymet, efterfulgt af rotation til FO-konformationen, hvorefter $FADH_2$ reducerer disulfidbindingen i det redox-aktive motiv af TrxR. Den humane TrxR tilhører den højmolekylære (HMW) type af TrxR, der involverer et selenosulfidpar og har en anden bagvedliggende mekanisme end LMW TrxR, hvilket potentielt gør LMW TrxR til et terapeutisk mål.

*Ll*TrxR har ved synlig lyseksponering (λ_{max} = 460 nm) vist sig at blive foto-inaktiveret, en egenskab, som ikke er rapporteret for nogen anden TrxR, og som heller ikke blev observeret i *E. coli* homologen (*Ec*TrxR) i kontrolforsøgene. Den inaktiverede *Ll*TrxR har et ændret absorptionsspektrum for det tætbundne FAD co-enzym og er oxideret på

methylgruppen i isoalloxazin ringen, bestemt med MS. Den ekstraherede FAD fra foto-inaktiveret *Ll*TrxR viste også et positivt resultat i en dinitrophenylhydrazin-test (DNPH), hvilket indikerer tilstedeværelsen af en carbonylgruppe, dvs. et aldehyd. *Ll*TrxR reducerer O_2 i nærvær af NADPH hurtigere end *Ec*TrxR, og inaktiveringen sænkes under semi-anaerobe betingelser og i tilstedeværelse af iodid ioner, en velkendt quencher af foto-exciteret triplet tilstand af flavin.

Det nærværende ph.d.-studium er fokuseret på at identificere de bagvedliggende funktionelle og strukturelle mekanismer for denne lysfølsomhed. Krystalstrukturer af foto-inaktiveret *Ll*TrxR afslørede oxidative skader i løbet af lyseksponering. En øget elektrondensitet blev observeret omkring carbon-7α på isoalloxazin ringen og i mindre grad omkring carbon-8α. Tyr237 i nærheden af flavinen viste sig at udvikle forøget elektrondensitet ved C3-position (ortho til hydroxylgruppen) som funktion af lyseksponering og blev verificeret vha. MS til en +16 Da masseforøgelse i overensstemmelse med dannelsen af 3,4-dihydroxyphenylalanin (DOPA). Et ikke tidligere beskrevet FAD *si*-side kavitet blev bestemt i alle strukturer af *Ll*TrxR og identificeret til at kunne akkommodere O_2, som en oxygenlomme. Denne model kan forklare hvordan det proteinbundne FAD kan fungere som en *de facto* fotosensibilisator, der genererer reaktive oxygen specier (ROS) ved lyseksponering. Reaktionsmekanismer der kunne forklare de observerede oxidationer på FAD og Tyr237, blev fremsat med udgangspunkt i dannelsen af superoxid radikalen ($O2^{\bullet-}$) på *si*-siden af den foto-exciterede isoalloxazin ring. Den monovalente isoalloxazin kation kan derefter oxidere Tyr237, som ved deprotonering danner en Tyr-phenoxyl radikal, som superoxid angriber i C3-positionen, hvorved dannelsen af DOPA finder sted. Superoxid radikalerne kan desforuden reagere med den deprotonerede form af carbon-7α på isoalloxazinen, som via en Russel reaktionsmekanisme fører til den observerede aldehyddannelse. Et andet særpræg ved *Ll*TrxR er, at den krystalliserer hovedsagelig i FR-konformation, både med og uden $NADP^+$ ko-krystallisering. *Ll*TrxR krystalliserede kun i FO-konformation i reducerende miljøer i tilstedeværelse af DTT og fravær af $NADP^+$. Tillige blev en blandet FO-FR konformation af homodimeren krystalliseret i tilstedeværelse af phosphat, hvilket

indikerer, at de to monomerer måske fungerer asynkront. Oxygenlommen opstår som følge af at Met43 bøjer væk fra *si*-siden mod Pro15. Tre methioniner, Met18, Met43 og Met67 bøjer mod Pro15, der samlet udgør (hvad der i dette arbejde betegnes som) et methionin-prolin motiv.

Aminosyrer involveret i dannelsen af iltlommen er blevet kortlagt, hvilket er udgangspunktet i forudsigelsen af TrxR fra andre organismer, der besidder samme FAD *si*-side oxygenlommen. Herunder TrxR fra organismer som *Bacillus subtilis* (*Bs*TrxR) og patogener såsom *Staphylococcus aureus* (*Sa*TrxR), *Streptococcus pyogenes* og *Bacillus anthracis*. En komparativ foto-inaktivering af TrxR fra *L. lactis*, *S. aureus* og *B. subtilis* afslørede, at *Sa*TrxR og *Bs*TrxR er meget mindre følsomme over for lysinaktivering end *Ll*TrxR, selvom *Sa*TrxR udviser en tilsvarende O_2-reduktion i tilstedeværelse af NADPH som *Ll*TrxR. Lyseksponering af *L. lactis* celleekstrakt udviste et betydeligt fald i TrxR aktivitet og efter 12 timer var ca. 65% af *Ll*TrxR inaktiveret. Foreløbige forsøg med levende *L. lactis* celler belyst ved 4°C, tyder på at lyseksponering faktisk er letal under de givne betingelser. Celleekstrakter fra de samme 17 timer *in vivo* bestrålede celler viste ~86% TrxR inaktivering. Den beskrevne undersøgelse viser, at lysfølsomheden hos TrxR kan være en udbredt egenskab blandt bakterier, særligt inden for phylum af *Firmicutes*. Denne egenskab kan potentielt udnyttes ved klinisk lysbehandling, f.eks. i målrettet blå-lysbehandling af udvalgte antibiotikaresistente patogene bakterier.

Table of Contents

Abbreviation

$AADP^+$	3-Aminopyridine adenine dinucleotide phosphate
AhpC	Alkyl hydroperoxide reductase
AMP	Adenosine monophosphate
BLUF	Blue-light-utilizing FAD
Cry	Cryptochrome
dNDP	Deoxyribonucleoside diphosphate
DNPH	2,4-Dinitrophenylhydrazine
DOPA	3,4-dihydroxyphenylalanine
Dps	DNA-binding protein from starved cells
DTNB	5,5'-Dithio-bis-(2-nitrobenzoic acid), *i.e.* Ellman's reagent
FAD	Flavin adenine dinucleotide (oxidized)
$FADH_2$	Flavin adenine dinucleotide (two-electrons reduced)
FMN	Flavin mononucleotide
GdmCl	Guanidinium chloride
Gpx	Glutathione peroxidase
GR	Glutathione reductase
Grx	Glutaredoxin
GSH	Glutathione (reduced)
GSSG	Glutathione (oxidized)
HMW	High molecular weight
LAB	Lactic acid bacteria
LMW	Low molecular weight
LOV	Light-oxygen-voltage
Msr	Methionine sulfoxide reductase
NAD^+	Nicotinamide adenine dinucleotide (oxidized)
NADH	Nicotinamide adenine dinucleotide (reduced)
$NADP^+$	Nicotinamide adenine dinucleotide phosphate (oxidized)
NADPH	Nicotinamide adenine dinucleotide phosphate (reduced)

PAPS	3'-phosphoadenosine-5'-phosphosulfate reductase
PDT	Photodynamic therapy
PEG	Polyethylene glycol
PMA	Phenylmercuric acetate
Prx	Peroxiredoxins
RF	Riboflavin
RMSD	Root Mean Square Deviation
rNDP	Ribonucleoside diphosphate
RNR	Ribonucleotide reductase
RNS	Reactive nitrogen species
SEC	Size exclusion chromatography
Spx	Bacterial redox sensor
TNB	2-nitro-5-thiobenzoic acid
Tpx	Thiol peroxidase

Table 1. Enzymes investigated in this thesis.

Abbreviation of enzyme	**Enzyme**	**Organism**
*Ll*TrxR	Thioredoxin Reductase	*Lactococcus lactis*
*Ll*TrxA	Thioredoxin	*Lactococcus lactis*
*Ll*TrxD	Thioredoxin	*Lactococcus lactis*
*Ll*NrdH	Glutaredoxin-like protein	*Lactococcus lactis*
*Ec*TrxR	Thioredoxin Reductase	*Escherichia coli*
*Ec*Trx1	Thioredoxin	*Escherichia coli*
*Sa*TrxR	Thioredoxin Reductase	*Staphylococcus aureus*
*Sa*TrxA	Thioredoxin	*Staphylococcus aureus*
*Bs*TrxR	Thioredoxin Reductase	*Bacillus subtilis*
*Bs*TrxA	Thioredoxin	*Bacillus subtilis*

Chapter 1. Introduction

1.1 Oxidative stress

Although oxygen is essential to many organisms as electron acceptor in aerobic respiration pathways, these processes unavoidably generates so-called reactive oxygen species (ROS), which are partially reduced forms of oxygen that are toxic to cells. ROS are also generated from external sources such as smoke, radiation etc. (Imlay, 2008). In the mid-1950s the 'free-radical theory' was proposed by D. Harman, which states that aging is related to endogenous oxygen radicals generated in cells resulting in a pattern of accumulative damage of cell components (Harman, 1956). Because of the high concentration of oxygen in the atmosphere and its ability to penetrate cell membranes due to its hydrophobic character, cells are equipped with a variety of antioxidant defense systems to remove the generated ROS, but it was not until 1969 with the characterization of the superoxide scavenging enzyme superoxide dismutase (SOD) that mechanistic support was provided for the 'free-radical theory' (McCord and Fridovich, 1969). Oxidative stress is characterized by an imbalance within the cell between the generation of ROS and the antioxidant defenses (Finkel and Holbrook, 2000), and may be the most inevitable of biological problems because it involves the least-specific reaction: univalent electron transfer (Imlay, 2008).

1.1.1 Chemical properties of reactive oxygen species (ROS)

In 1950s Rebeca Gerschman and co-workers suggested that oxygen toxicity originated from the formation of partially reduced oxygen species (Gerschman et al., 1954). Ground state molecular oxygen (O_2) is a stable biradical, with two spin-aligned electrons occupying separate π-anti bonding orbitals (π*), see figure 1. Because of spin restrictions of ground state molecular oxygen it can only accept one electron at a time from organic molecules with spin-paired electrons. Since most organic molecules are poor univalent electron-donors molecular oxygen cannot easily oxidize amino acids and DNA, *e.g.* via a 2-electron

addition reactions. However, molecular oxygen reacts fast in a one-electron transfer, as the unpaired electrons of dioxygen readily interact with unpaired electrons from transition metals such as iron in [Fe-S] clusters and organic radicals (Imlay, 2003; Nonell and Flors, 2016).

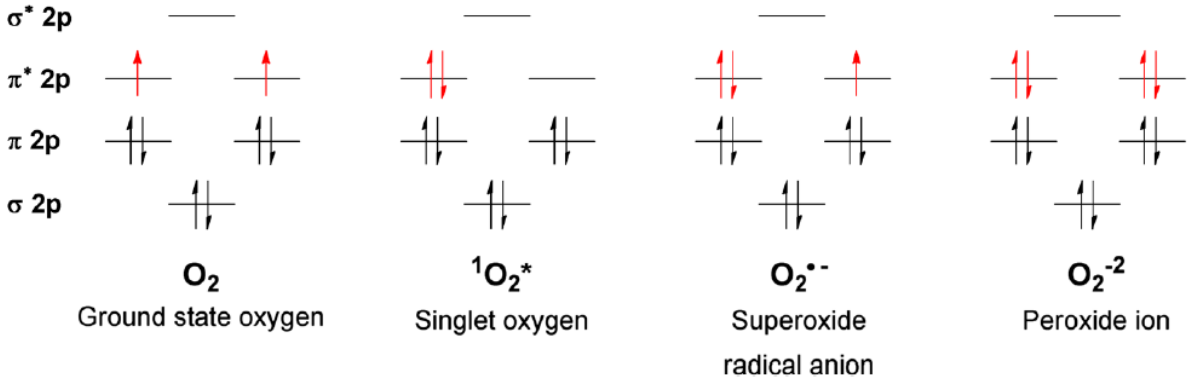

Figure 1. Molecular–orbital diagrams for selected oxygen species with the electrons in focus highlighted in red. Molecular oxygen (O_2) with two unpaired electrons with parallel spin in each π-anti bonding orbitals (π*). Superoxide anion (O_2^-) is a radical with an unpaired single electron in its π* orbital. Peroxide ion (deprotonated hydrogen peroxide, H_2O_2) is a closed-shell molecule with full electron occupancy of its π* orbitals. Singlet oxygen is an excited form of molecular oxygen derived through energy transfer, resulting in paired electrons with opposite spins. See text for more details. Figure from (Nonell and Flors, 2016).

Addition of one electron to molecular oxygen gives rise to the superoxide radical anion ($O_2^{\bullet-}$). Further one electron reduction of $O_2^{\bullet-}$ results in the formation the peroxide ion (hydrogen peroxide (H_2O_2) in the protonated form) see figure 1. Hydrogen peroxide can react further to give a hydroxyl radical (HO•) and a hydroxide anion (OH^-), with HO• being the most reactive of all ROS, as discussed below.

The one-electron reduction potential of O_2 is relatively low, $E°$ = –0.16 V (for oxygen concentration of 1 M, pH 7 as the standard state), compared to the much higher reduction potentials of $O_2^{\bullet-}$ (+0.94 V), see figure 2. However, the superoxide anion has a limited reactivity with electron rich centers due to its negative charge and thus a limited spectrum of biomolecules can react with it. Protonation of O_2^- gives the peroxyl radical which is a

better oxidant with an increased reduction potential of +1.06 V (Buettner, 1993), but with a pK_a = 4.8 the concentration of the protonated species is low and might not have a significant role at physiological pH (Sawyer and Valentine, 1981). One electron reduction of superoxide gives hydrogen peroxide with a reduction potential of +0.94 V. Hydrogen peroxide can decompose to generate hydroxyl radical (HO•) and a hydroxide anion (OH^-), but because of the stability, due to the oxygen-oxygen bond, the reactivity is however limited. The hydroxyl radical on the other hand does not have any of these features and with an unpaired electron and a reduction potential of +2.33 V it is the most powerful oxidant and reacts at diffusion-limited rates with most biomolecules, see figure 2 (Imlay, 2003; Nonell and Flors, 2016).

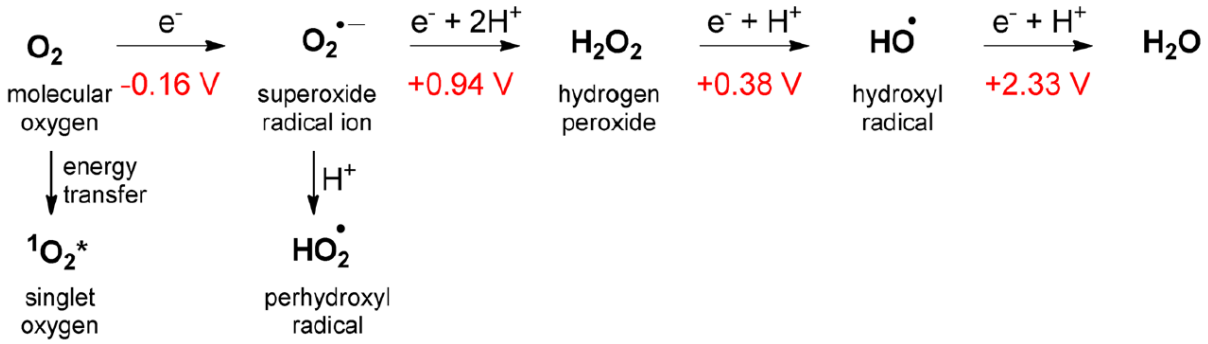

Figure 2. Formation of ROS through energy- and electron-transfer reactions with reduction potentials in red. 1 M dioxygen is used as the standard state for the first step. See text for details. Modified from (Nonell and Flors, 2016).

Singlet oxygen is an excited form of molecular oxygen derived through energy transfer, resulting in paired electrons with opposite spins (figure 1 and 2). Singlet oxygen is often referred to as $^1O_2$ or $^1\Delta_g^-$, and has energy of 95 kJ/mol above the ground state molecular oxygen (triplet state molecular oxygen, more precisely referred to as $^3\Sigma_g^-$ or $^3O_2$).

1.1.2 Sources of ROS and scavenging systems

Exogenous sources of ROS can be generated by environmental factors such as UV light, ionizing radiation and pollutants. Typical redox-cycling quinone-like compounds such as paraquat, menadione and the anticancer drug doxorubicin, also can give rise to ROS. These electron-shuttle quinones are typically reduced by flavo-enzymes forming a radical, which in turn reduces O_2 to superoxide (O'Brien, 1991; Winterbourn, 2008).

O_2^- and H_2O_2 are generated *in vivo* as side-reactions of metabolic redox-enzymes, through inadvertent univalent electron transfer to O_2. It is hypothesized that this process occurs due to autoxidation of the enzyme-bound reduced flavin cofactors in respiratory dehydrogenases before the enzyme has passed on the reducing equivalent to the redox-moities (Messner and Imlay, 2002). For example enzymes like fumarate reductase in the respiratory chain has been shown to be involved in ROS formation (Imlay, 1995). Membrane vesicles from glucose-grown cells showed that about 0.2% and 0.4% of the consumed oxygen was released as O_2^- and H_2O_2, respectively (Gonzalez-Flecha and Demple, 1995; Imlay, 2008). *E. coli* mutants unable to scavenge hydrogen peroxide were shown to accumulate about 14 µM H_2O_2 *in vivo* (Seaver and Imlay, 2001).

In plants production of singlet oxygen ($^1O_2$) is occurring in the photosystems as a consequence of over-reduction of the intersystem electron carriers, among others triplet chlorophylls in the reaction center of photo-system II and in the antenna system. In photosynthetic membranes, $^1O_2$ is quenched by chromophores like β-carotene, offering protection from singlet oxygen under normal conditions (Krieger-Liszkay, 2005). Singlet oxygen can be generated in small amounts *in vivo* without the involvement of light. Some biological hydroperoxides can generate singlet oxygen, fx can two lipid hydroperoxides react with one another and decompose to generate an alcohol and an aldehyde upon release of a singlet oxygen (Miyamoto et al., 2014). Another source of $^1O_2$ is photosensitizers, which are described in section 1.1.3.

NADPH oxidases are transmembrane proteins using electrons from NADPH in the cytoplasm to transfer electrons across the membrane, producing superoxide in the extracellular environment (Cross and Segal, 2004). NADPH is part of the innate immune

system (in-born immunity system) and is activated during infections, *e.g.* microorganisms entering the organisms, which causes a so-called respiratory burst (first discovered by high O_2 consumption). NADPH oxidases are located on fx phagocytes (neutrophils and macrophages) in association with pattern recognition receptors, making it possible to recognizing conserved structures on the surface of microorganisms, before ingesting the invading cell (Cross and Segal, 2004; Panday et al., 2015). The engulfed microbe is then killed by superoxide generation.

During the electron transport chain in mitochondria transfer of a single electron to O_2 yields superoxide. Superoxide can potentially be generated from complex I, II and III when the mitochondria are not making ATP or when there is a too high NADH/NAD^+ ratio in the mitochondrial matrix, though the complex I is regarded as the major source of superoxide (Murphy, 2009; Sabharwal and Schumacker, 2014). SOD can disproportionate O_2^- to form hydrogen peroxide and molecular oxygen (reaction 1.1) (McCord and Fridovich, 1969). In the mammalian mitochondria there are two SOD; SOD1 located in the inter membrane space and SOD2 operating in the matrix (Miller, 2012).

$$2\ O_2^- + 2\ e^- + 2\ H^+ \rightarrow \quad H_2O_2 + O_2 \qquad (1.1)$$

E. coli sodA sodB double mutant strain devoid of cytoplasmic SODs was shown to grow well anaerobically. Under aerobic growth the strain was highly sensitive to hydrogen peroxide and paraquat, a redox-cycling compound generating superoxide. This was the first experiment demonstrating the importance of enzymatic catalysis for superoxide depletion *in vivo* (Carlioz and Touati, 1986).

Further reduction of hydrogen peroxide occurs non-enzymatically through the metal-catalyzed Fenton reaction (1.2):

$$H_2O_2 + Fe^{2+} \rightarrow \quad OH^- + FeO^{2+} + H^+ \quad \rightarrow OH^- + HO\bullet + Fe^{3+} \qquad (1.2)$$

Fe^{2+} (ferrous ion) is the primary reactant catalyzing the Fenton reaction. It is important to emphasize that these ions need to be accessible in a free form; ions incorporated into enzymes or iron-storage proteins are not involved in the Fenton reaction. Copper(I) ions

also catalyze the Fenton reaction, but the biological significance is limited due to the low intracellular concentrations of this ion (Imlay, 2003).

The primary origin of reducing donors of Fe^{3+} (ferric ions) is not fully understood (reaction 1.3). The original idea that superoxide was the main reductant of Fe^{3+} (Haber–Weiss reaction) was ruled out due to the low concentration of superoxide. More abundant reductants like NAD(P)H and glutathione are however less reactive with Fe^{3+} (Halliwell, 1982; Winterbourn, 1979). More likely candidates are reduced $FADH_2$ and cysteines, but other reductants may also be involved (1.3) (Woodmansee and Imlay, 2002; Park and Imlay, 2003).

$$Donor^{red} + Fe^{3+} \rightarrow Donor^{ox} + Fe^{2+} \quad (1.3)$$

The hydroxyl radical is the most damaging ROS and there is no known enzymatic activity acting directly on this ROS. Therefore most organisms are equipped with very effective H_2O_2 scavenging enzymes, for example catalase, which decomposes H_2O_2 to H_2O and O_2 (reaction 1.4) utilizing a heme iron center and operates at diffusion-limiting rates (Imlay, 2003):

$$2\ H_2O_2 \rightarrow 2\ H_2O + O_2 \quad (1.4)$$

Other hydrogen peroxide scavengers are the peroxiredoxins (Prx) that are cysteine-dependent enzymes that reduce peroxides. Among this group of enzymes are the thiol peroxidase (Tpx) and the alkyl hydroperoxidase (AhpC), which are hydrogen peroxide scavengers (1.5) and thus particularly important in catalase-negative organisms (Jaeger, 2007):

$$2\ –SH + H_2O_2 \rightarrow -S-S- + 2\ H_2O \quad (1.5)$$

$$2\ –SH + R\text{-}OOH \rightarrow -S-S- + 2\ H_2O + R\text{-}H \quad (1.6)$$

Tpx and AhpC are in general reduced by Trx and alkyl hydroperoxide reductase (AhpF), respectively. AhpC has a large hydrophobic site, which can accommodate substrates ranging from H_2O_2 to more complex organic hydroperoxides (reaction 1.6) such as cumene

hydroperoxide and operates in complex with AhpF to decrease the H_2O_2 leakage (Dubbs and Mongkolsuk, 2007). H_2O-forming NADH oxidases are mentioned in section 1.4.3.

Glutathione peroxidase (Gpx) is a GSH-dependent peroxidase found in eukaryotes that can also decompose hydrogen peroxide. Gpx-like homologs are known in bacteria, fx under oxidative stress in *E. coli* a Trx-dependent Gpx-like homolog is expressed (Arenas et al., 2010). In mammals eight Gpx have been identified so far, displaying different roles in the cell. The variety in Gpx homologs points to the fact that hydrogen peroxide is not only toxic, but also functions as signaling molecule, *e.g.* in the insulin signaling pathway, hence the need for the tightly regulated H_2O_2 homeostasis (Brigelius-Flohé and Maiorino, 2013).

Hordeum vulgare (barley) glutathione peroxidase 2 (*Hv*Gpx2) has in addition to its H_2O_2 scavenging function the special feature that it reversibly dimerizes at low levels of H_2O_2. The dimerized *Hv*Gpx2 has a 5-fold lower activity than the monomer. At higher levels of H_2O_2 the monomer dimerizes to a lesser extent (~20% at 20 mM H_2O_2), thus scavenging H_2O_2 more efficiently. Though these results were obtained *in vitro*, it seems as a way for *H. vulgare* to regulate the H_2O_2 homeostasis *in vivo* (Navrot et al., 2015). An opposite response to H_2O_2 is described for 2-Cys Prx in the so-called floodgate model, where 2-Cys Prx prevents the gradual buildup of toxic H_2O_2, but hyper-oxidizes in the presence of rapid rising H_2O_2, leading to inactivation, thus allowing signaling cascades of H_2O_2 (Wood et al., 2003; Poole et al., 2004).

In prokaryotes hydrogen peroxide also acts as a signaling molecule that operates at low concentration *in vivo*, which insures to stimulate biological responses and to activate specific biochemical pathways upon oxidative stress (Stone and Yang, 2006). The transcription factor OxyR regulates the H_2O_2 response in *E. coli*. Cys199 of OxyR is oxidized to sulfenic acid (R-SOH) by H_2O_2, which in turn reacts with Cys208 to generate an intramolecular disulfide bond. The oxidized OxyR organizes as a tetramer that binds to its specific DNA promoter region of antioxidant defense genes. OxyR is regenerated to its reduced form by glutaredoxin (Grx), releasing OxyR from the promoter site (Toledano et al., 1994; Hillion and Antelmann, 2015). Gram-positive bacteria use a different sensor of

H_2O_2, namely PerR. In *B. subtilis* PerR works as a repressor of ROS scavenger genes like catalase. Only PerR bound to Fe^{2+} can bind to DNA. When the H_2O_2 level rises it oxidizes the Fe^{2+} to Fe^{3+}, which leads to a conformational change that releases the binding to DNA, thus activating the ROS operon. With these features PerR appears to be dedicated to prevent Fenton chemistry in the cell (Imlay, 2014). Spx is a RNA-promoter-binding protein conserved among Gram-positive bacteria and regulates transcription of thiol stress response genes like thioredoxin, thioredoxin reductases, thiol peroxidase and methionine sulfoxide reductase. Opposite to OxyR and PerR, Spx is an hydrogen peroxide independent regulator (Zuber, 2009; Hillion and Antelmann, 2015). SoxR is another transcription factor involved in regulation of ROS. SoxR binds one $[2Fe\text{-}2S]^{+}$ cluster per monomer, while a second domain includes a DNA-binding motif. Upon exposure to superoxide-generating redox-cycling compounds the clusters are quickly oxidized to the $[2Fe\text{-}2S]^{2+}$ state. The cluster oxidation twists the SoxR dimer, which alters the conformation of the bound DNA, directing the promoter motifs so that RNA polymerase can initiate transcription (Watanabe et al., 2008; Imlay, 2014).

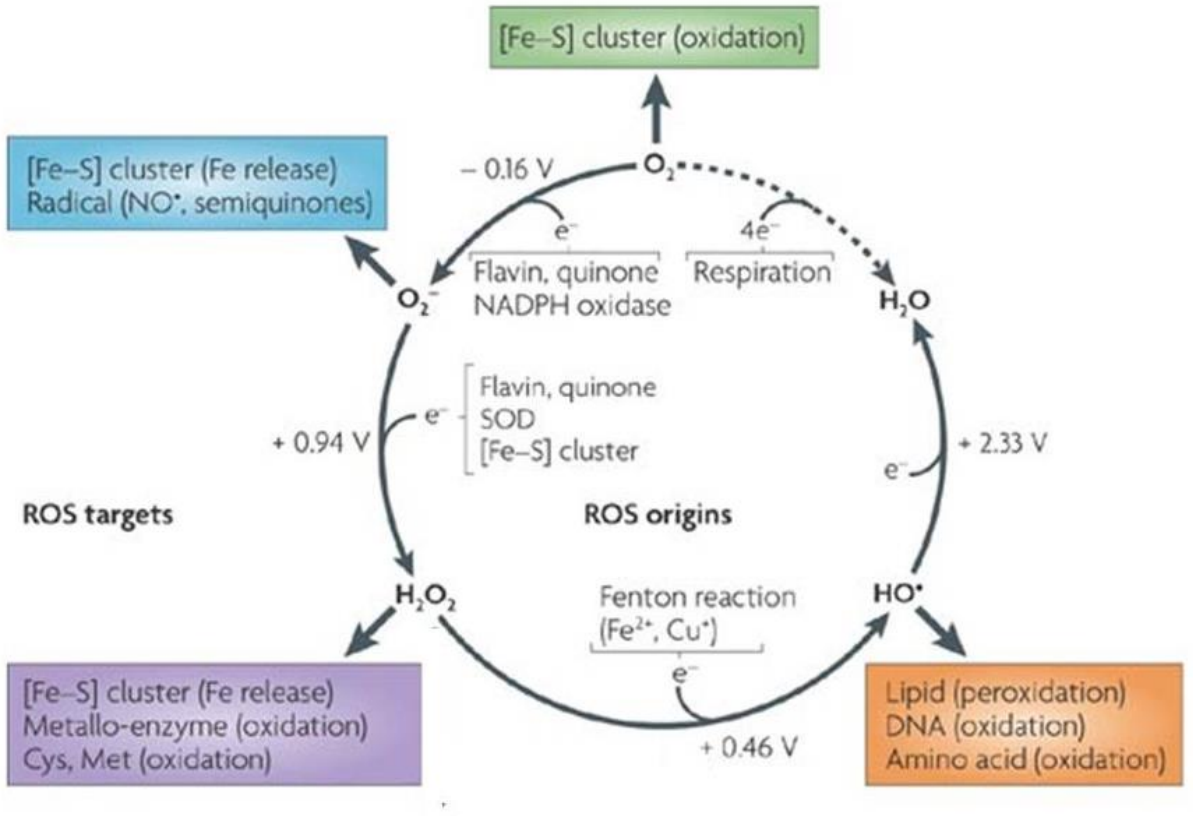

Figure 3. Overview of ROS and their respective targets. Molecular oxygen can receive a single electron from flavins, quinones (like paraquat, menadione and doxorubicin) and NADPH oxidase. Superoxide reacts with [Fe-S] clusters with Fe^{2+} release and nitric oxide (NO) and semiquinones. Superoxide can be further reduced to give H_2O_2 by electron donors like flavin and quinones or be disproportionated by SOD. H_2O_2 reacts with [Fe-S] clusters, metallo-enzymes and cysteine and methionine residues (see later). Hydroxyl radicals can be generated from hydrogen peroxide by Fe^{2+} or Cu^+, and as the most potent of oxidants it can react with lipids, DNA and proteins/amino acids (see later). Modified from (D'Autréaux and Toledano, 2007).

1.1.3 Photosensitizers and photochemical reactions involving ROS

Photosensitizers can briefly be described as molecules that upon excitation at an appropriate wavelength are capable to absorb and transfer energy to another molecule in a photochemical process. During irradiation the photosensitizer is photo-excited via a one-photon transition ($h\nu$) from its ground state, S_0, to the singlet excited state S_n (figure 4). The S_n excited state will relax to give the lowest excited singlet state S_1, which followed by intersystem crossing generates the photosensitizer triplet state T_1. The lifetime of T_1 is

longer (µs) than that of S_1 (ns), allowing the triplet state photosensitizer to react in one of two ways defined as Type I and Type II mechanisms. In the Type I mechanism the excited photosensitizer reacts with a substrate to generate a free radical by hydrogen abstraction or electron transfer (figure 4). This free radical can then in turn react with O_2 to generate ROS such as the superoxide radical. In the type II mechanism singlet oxygen is generated by the excited triplet state photosensitizer (Derosa and Crutchley, 2002). Here, triplet oxygen, $^3\Sigma_g^-$ (molecular oxygen in its ground state) is excited into singlet oxygen $^1O_2$ ($^1\Delta_g^-$) by the excited triplet state photosensitizer through a collision based energy transfer process (Derosa and Crutchley, 2002).

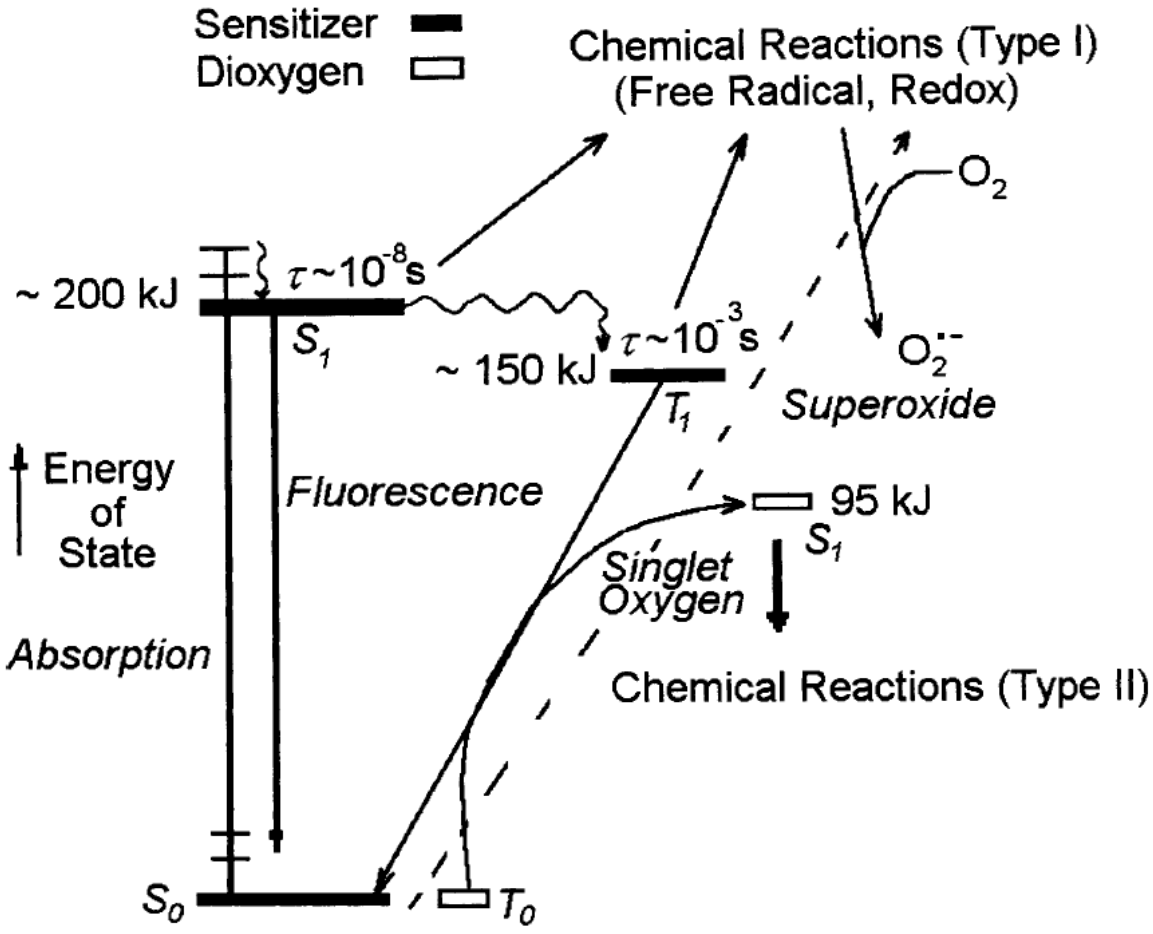

Figure 4. Extended Jablonski diagram displaying the photo-generation of excited photosensitizers. State energies are represented by thick lines; photosensitizers in different states (black) and dioxygen as $^3O_2$ and $^1O_2$ (white). For details see text. Figure from (Derosa and Crutchley, 2002).

Exogenous photosensitizers are used in photodynamic therapy (PDT), for example in cancer treatment. The photosensitizer is applied to the target (*e.g.* cancer cells) and exposed to irradiation resulting in ROS formation and destruction of the targeted cells. It is possible to target the photosensitizers to specific sites by conjugating them to antibodies, peptides, proteins and other ligands of specific cellular receptors (Abrahamse and Hamblin, 2016). Effective photosensitizers should follow the listed criteria: (1) High absorbance coefficient matching the emission spectrum of the light source. (2) A triplet state energy of approximately 95 kJ/mol, to insure effective energy transfer to $^3O_2$. (3) High quantum yield in the triplet state and long triplet lifetime. (4) High photostability. There are several examples of UV-Vis absorbing molecules generating high yields of singlet oxygen upon irradiation. For example Rose Bengal, eosin, and methylene blue are all very effective chemically synthesized photosensitizers, which possess triplet states of appropriate energies for sensitization of $^3O_2$ (Derosa and Crutchley, 2002).

Besides exogenously added photosensitizer, naturally *in vivo* occurring molecules such as protoporphyrin IX, riboflavin and curcumin can act as photosensitizers. Natural photosensitizer have been used as starting compounds to design exogenous photosensitizer with desired properties by introducing chemical modifications to change the λ_{max} of absorbance. Derivates of for example riboflavin where the N-10 group is substituted with different chemical groups are also used to modulate the λ_{max}, for example to an ethylamine giving a cationic riboflavin with a λ_{max} = 440 nm, which was used in inactivation of bacteria (Eichner et al., 2015; Maisch et al., 2014). Isoalloxazine has also been modified at C6, C7, C8 and C9 to map the photochemical properties, in order to optimize the singlet oxygen formation (Sikorska et al., 1998).

1.1.4 Damage caused by ROS

ROS oxidize DNA, lipids, iron-sulfur-clusters and proteins which can lead to inactivation, loss-of-function, growth defects and eventually cell death (Imlay, 2003). The various ROS have preferences for certain targets and the following description will give an overview of

different types of ROS-mediated reactions. As this work focuses on protein oxidations with special emphasis on reactivity of individual amino acid residues towards specific ROS, this part is more elaborated.

The highly reactive species hydroxyl radicals (HO•) can oxidize nearly all biological molecules with rate constants close to the diffusion limit. Therefore most reactions involving HO• are site-specific, *e.g.* observed in the proximity of the site of generation, such as metal binding sites of Fe^{2+} and Cu^{+} (Davies, 2016).

Protein oxidation

Approximately 68% of the dry weight of cells consists of protein, which potentially is the major target for oxidative damage (Davies, 2003). The two sulfur-containing amino acids cysteine and to a lesser extent methionine have the most reactive residues in direct oxidation reactions. They both have the special characteristic that they participate in enzymatic as well as non-enzymatic reversible redox reactions (Kim et al., 2014).

Cysteines are readily oxidized by mild oxidants such as H_2O_2 and nitric oxide (NO). The reactivity of cysteine is dependent on its pK_a, as the thiolate anion is more prone to react. In the initial oxidation of cysteine sulfenic acid (Cys-SOH) is formed. This modification is reversible and can in the absence of neighboring Cys residues be directly reduced to R-SH by thioredoxin or glutathione, the latter resulting in a mixed disulfide (Lo Conte and Carroll, 2013). Cys-SOH can be further oxidized to generate sulfinic acid (Cys-SO_2H) and sulfonic acid (Cys-SO_3H), see figure 5, upper panel (Lo Conte and Carroll, 2013). Figure 5, lower panel, indicates the various cysteine modifications (Spadaro et al., 2010).These modifications can induce specific conformational changes in the protein, a feature that can modify the activity/binding capacities of fx transcription factors to DNA, which often involves ROS induced sulfenic acids that establish a disulfide bond with a cysteine thiol group. A well-established mechanism is the intramolecular disulfide bond formation in ROS induced transcription factors, *e.g* OxyR a positive promoter of peroxide detoxification genes as described above (Zheng et al., 1998; Åslund et al., 1999).

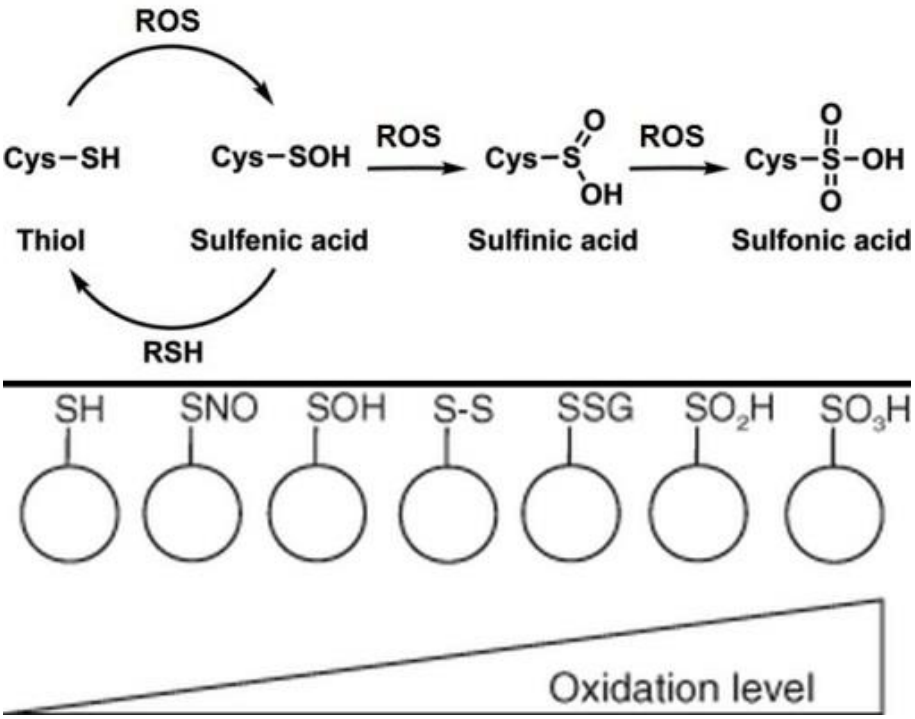

Figure 5. Upper panel: Thiol groups can reversibly be oxidized to sulfenic acid by ROS and be reduced back to thiols (R-SH) by fx sulfiredoxins. Figures modified from (Lo Conte and Carroll, 2013). Lower panel: Schematic overview of redox-based Cys modifications. Cys thiol (SH), S-nitrosothiol (SNO), sulfenic acid (SOH), disulphide (S–S), S-glutathionylation (SSG), sulfinic acid (SO_2H) and the irreversible sulphonic acid formation (SO_3H) (Spadaro et al., 2010).

Cysteines react with reactive nitrogen species (RNS) such as nitric oxide (NO), nitrous acid (HNO_2) and peroxynitrous acid to form S-nitrosothiols (Hougland et al., 2013). NO is a free radical that is involved in cellular signaling and is generated from arginine, NADPH and oxygen by nitric oxide synthase (Alderton et al., 2001).

Methionines can reversibly be oxidized to methionine sulfoxide (Met-SO) by oxidants such as HOCl, H_2O_2, $^1O_2$ and HO•. The generated Met-SO can be further oxidized to methionine sulfone (figure 6, upper panel), which is an irreversible reaction (Drazic and Winter, 2014). The Met-SO can be reduced back to methionine by methionine sulfoxide reductases (Msr). Protein bound Met-SO can occur in two enantiomer forms, S and R, which is reduced by

MsrA and MsrB, respectively. MsrA can reduce both free and protein bound Met-(S)-SO sulfoxide (figure 6, lower panel).

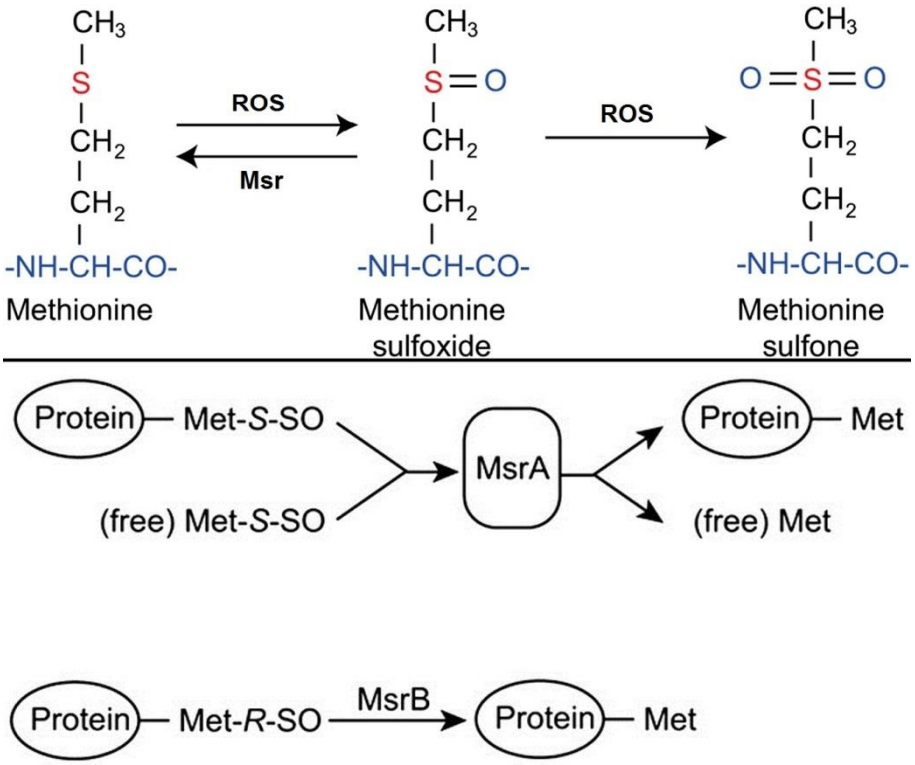

Figure 6. Upper section: Oxidation of methionine to methionine sulfoxide (Met-SO) by ROS. Met-SO can further be oxidized to give methionine sulfone in an irreversible reaction. Lower section: There are two types of methionine sulfoxide reductases, MsrA and MsrB, the first coverts S-enantiomer form of Met-SO, Met-(S)-SO, both free and protein bound, to methionine, while the latter converts Met-(R)-SO, mainly protein bound. Figure modified from (Drazic and Winter, 2014).

Aromatic residues are also a target of ROS. Single electron subtraction from tyrosine generates a radical-cation, which upon deprotonation due to its very low *p*Ka value turns into a tyrosine phenoxyl radical (Tyr-O•). Superoxide reacts readily with phenoxyl radicals at C1 (*para*, relative to -OH in Tyr) and C3/C5 (*ortho*, relative to -OH in Tyr), due to resonance stabilization (Möller et al., 2012), see figure 7. This gives rise to a hydroperoxide intermediates via an addition reaction, predominantly at C1 or C3/C5 position of the ring (Winterbourn et al., 2004). The hydroperoxy intermediates are quickly decomposed to give either the parent tyrosine by release of O_2 or are converted into the respective hydroxy

groups, as either 3,4-dihydroxyphenylalanine (DOPA) or 4-alanyl-4-hydroxy-cyclohexadienone (Nagy et al., 2009). •NO_2 can also react with Tyr-O• generating 3-nitrotyrosine, which is an important post-translational modification (Kikugawa et al., 1994; Ischiropoulos, 2009).

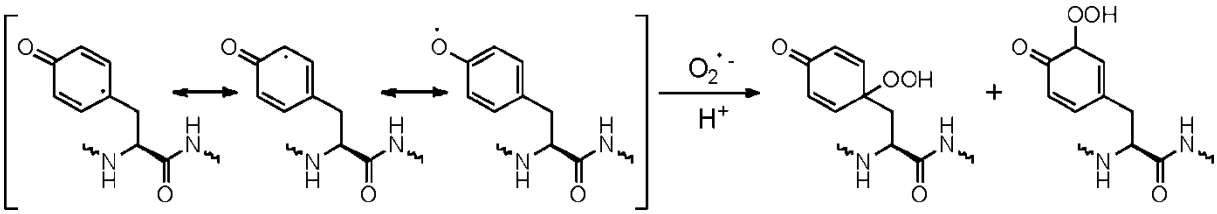

Figure 7. Resonance stabilization of tyrosine phenoxyl radical, which upon reaction with superoxide gives hydroperoxide intermediates, mainly at C1 and C3/C5 of the ring. Figure from (Möller et al., 2012).

Hydroperoxide formation is also observed from tryptophan radicals reacting with superoxide, see figure 8 (Fang et al., 1998; Davies, 2016). Tryptophan can as well be nitrated by reaction with RNS, generating nitrotryptophan with the nitro group potentially at multiple positions (Nuriel et al., 2011).

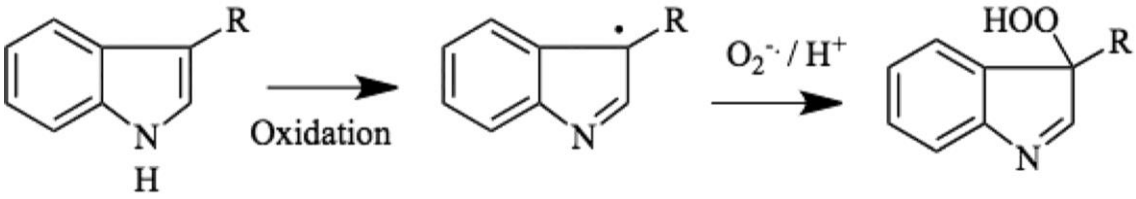

Figure 8. Oxidation of tryptophan gives rise to tryptophan indolyl radical, which readily reacts with superoxide giving Trp-hydroperoxide species. Figure from (Davies, 2016).

Five amino acid residues react rapidly with singlet oxygen ($^1O_2$) under physiological pH; methionine, cysteine, tyrosine, histidine and tryptophan (Wilkinson et al., 1995). Both cysteine and methionine react with singlet oxygen to give zwitterions with peroxide-like character (figure 9). Methionines, in the free amino acid form, exposed to singlet oxygen the zwitterions react with a second methionine giving two moles of methionine sulfoxide

(Sysak et al., 1977). The corresponding cysteine zwitterions can generate disulfides (cysteine, R-S-S-R), but also thiosulfinate (R-S(O)-S-R) and oxy acids, *e.g.* sulfinic acid and sulfonic acid (Davies, 2003). But a clear understanding of the fate of these zwitterionic peroxides is yet to be established, and they are not yet characterized in proteins (Davies, 2016).

Tyrosine, histidine and tryptophan react with $^1O_2$ generating short-lived endoperoxides (heterocyclic compound containing peroxide), that upon ring-opening generate hydroperoxides (Wright et al., 2002; Davies, 2003, 2016), see figure 9.

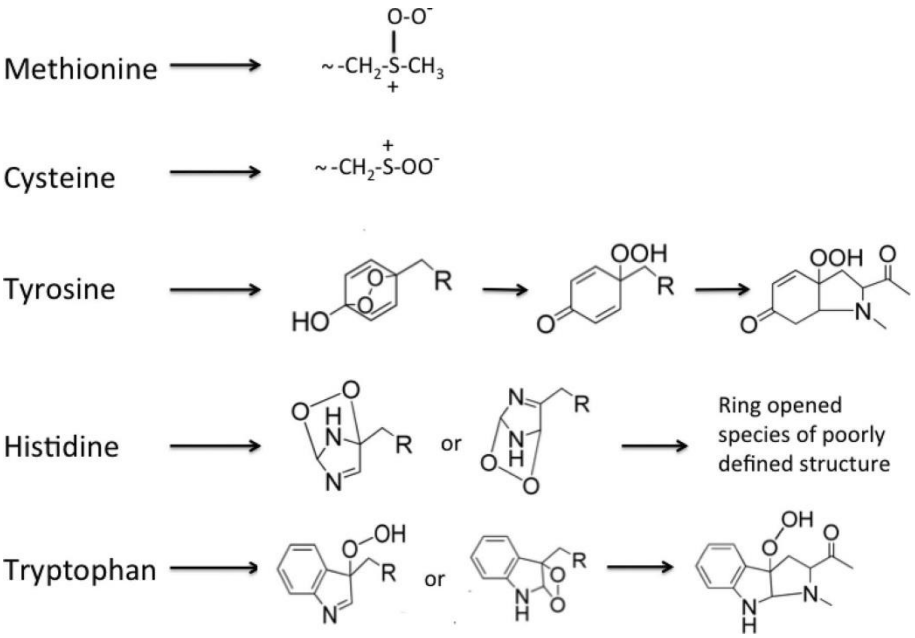

Figure 9. Reaction of singlet oxygen ($^1O_2$) with selected amino acids. Methionine and cysteine react with $^1O_2$ generating peroxide zwitterions. Upon addition of singlet oxygen to tyrosine, histidine and tryptophan, short-lived endoperoxides is formed, that can ring-open to give hydroperoxides. Figure from (Davies, 2016).

Most of the current knowledge of ROS-based oxidation of amino acids is from experiments with single amino acids. Less information is available about oxidations of peptides or intact proteins. It is evident that local electrostatic environment plays a key role in the reactivity

of various oxidants towards specific amino acid residues, which further increases the complexity of predicting protein oxidations.

Oxidation of iron-sulfur-clusters by superoxide can inactivate enzymes belonging to the family of [4Fe-4S] dehydratases, like *E. coli* dihydroxy-acid dehydratase, fumarase A and B, and mammalian aconitase. For O_2^-, inactivation takes place as the cluster is oxidized upon generation of H_2O_2. The oxidized cluster is destabilized and releases the catalytic ferrous ion, see reactions 1.7 and 1.8, resulting in enzyme inactivation (Flint et al., 1993).

$$\text{Enz-[4Fe-4S]}^{2+} + O_2^- + 2\ H^+ \rightarrow \text{Enz-[4Fe-4S]}^{3+} + H_2O_2 \qquad (1.7)$$

$$\text{Enz-[4Fe-4S]}^{3+} \rightarrow \text{Enz-[3Fe-4S]}^{+} + Fe^{2+} \qquad (1.8)$$

Hydrogen peroxide inactivates [4Fe-4S] dehydratase enzymes as well. In contrast to the Fenton reaction (1.2) where hydrogen peroxide reacts with "free" Fe^{2+}, it appears that reaction with enzyme bound $[4Fe\text{-}4S]^{2+}$ does not involve an hydroxyl radical as reaction product, since no protein damage was observed when exposing [4Fe-4S] dehydratases to H_2O_2. The alternative reaction involves a two-step oxidation of H_2O_2 upon cluster oxidation with concomitantly release of Fe^{3+}, see reactions 1.9 and 1.10 (Jang and Imlay, 2007).

$$\text{Enz-[4Fe-4S]}^{2+} + H_2O_2 \rightarrow \text{Enz-[4Fe-4S/O]}^{2+} + H_2O \qquad (1.9)$$

$$\text{Enz-[4Fe-4S/O]}^{2+} + H^+ \rightarrow \text{Enz-[3Fe-4S]}^{+} + Fe^{3+} + OH^- \qquad (1.10)$$

The release of free iron in the above reactions further contributes to the Fenton reaction, leading to generation of highly reactive hydroxyl radicals.

DNA oxidation

Iron(II) ions has a strong affinity toward DNA and Fe^{2+} has even been shown to have DNA sequence preferences (Rai et al., 2001). As Fe^{2+} bound to DNA reacts with hydrogen peroxide the Fenton reaction takes place, generating the hydroxyl radical (HO•) (1.2). This makes the DNA a more prone target for Fenton-mediated oxidation, as hydroxyl radicals

can abstract electrons from deoxyribose and nucleobases or add directly to unsaturated nucleobases. The DNA radicals in turn generate a variety of different DNA damages, reaction 1.11 (Dizdaroglu et al., 1991; Imlay, 2003). The DNA-binding protein from starved cells (Dps) is designed to protect the DNA oxidation by Fe^{2+} and hydrogen peroxide detoxification. Dps exhibits iron(II) sequestration, where the bound Fe^{2+} reacts with hydrogen peroxide in the active site (reaction 1.12). This ferroxidase activity requires two iron(II) to reduce hydrogen peroxide to two water molecules (Calhoun and Kwon, 2011), thus preventing the hydroxyl redical formation of the Fenton reaction.

$$HO\bullet + DNA \rightarrow H_2O + damage \quad (1.11)$$

$$2\ Fe^{2+} + H_2O_2 + 2\ H_2O \rightarrow 2FeOOH\ (\text{Dps ferroxidase center}) + 4H^+ \quad (1.12)$$

Lipid oxidation

Hydrogen peroxide (H_2O_2) and superoxide ($O_2\bullet^-$) also react with unsaturated fatty acids incorporated into lipid membranes, leading to lipid peroxidation, which destabilizes the membranes (Bielski et al., 1983; Farmer and Mueller, 2013). This phenomenon is more widespread in mammalian cells with higher content of polyunsaturated fatty acids, thus *E. coli* with lowered amount of monounsaturated fatty acids showed increased resistance to oxidative damage (Pradenas et al., 2012). Singlet oxygen, generated as described previously, was observed to account for more than 80% of the non-enzymatic lipid peroxidation in *Arabidopsis thaliana* under normal growth conditions (Triantaphylidès et al., 2008).

1.2 Thiol redox control systems

Thiol groups in the cytosol are in general maintained in the reduced state in an NADPH-dependent manner through specific redox-based protein pathways. These protein systems are based on redox-active cysteines, ensuring reduction of selected target proteins (Gilbert and Mclean, 1963). In the following two widespread systems are presented, the glutathione system and the thioredoxin system.

1.2.1 The glutathione system

The glutathione system is based on NADPH, the flavoprotein glutathione reductase (GR), glutathione (GSH) and glutaredoxin (Grx). The reducing equivalent of NADPH is first transferred to FAD co-enzyme of GR, which in turn reduces oxidized glutathione (GSSG) to two reduced glutathiones (GSH). GSH is a tripeptide consisting of γGlu-Cys-Gly, where glutamate is linked with an isopeptide bond from its side chain to the N-terminal of the cysteine (GSSH is the oxidized form with two glutathiones linked by a disulfide bond). Grx is a small redox-active protein with the conserved active-center CPYC, in *E. coli* consisting of 85 residues, which is non-enzymatically reduced by two GSH (Holmgren, 1989; Meyer et al., 2009; Fernandes and Holmgren, 2004), see figure 10. GSH is present in most eukaryotes and Gram-negative bacteria, but the genes encoding enzymes involved in the biosynthesis of glutathione are lacking in most Gram-positive *e.g. L. lactis*. Interestingly, upon addition of GSH to minimal medium *L. lactis* displayed significantly increased resistance to H_2O_2 in strains able to accumulate GSH (Li et al., 2003). Besides GSH other low molecular weight thiol compounds involved in cytosolic redox homeostasis have been identified, *e.g.* mycothiol (MSH) in *Actinomycetes* and bacillithiol (BSH) in *Firmicutes* (Loi et al., 2015).

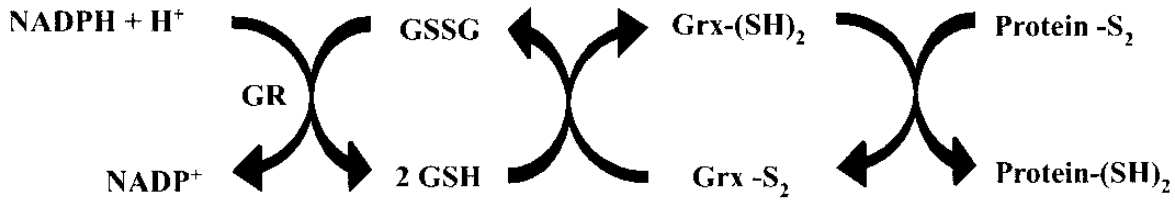

Figure 10. The flow of electrons from NADPH to GR, which in turn reduces a GSSG to two GSH. The two generated GSH non-enzymatically reduce the active redox-center of Grx. Grx can then reduce selected target proteins (Holmgren, 1989).

1.2.2 The thioredoxin system

Thioredoxins (Trx) are small ubiquitous redox active proteins with a molecular weight of approximately 12–14 kDa found in organisms ranging from archaea to mammals. The thioredoxin system consists of NADPH, thioredoxin reductase (TrxR) and thioredoxin (Trx). Similar to GR, TrxR also contains a tightly bound FAD co-enzyme that is reduced by NADPH. In low molecular weight TrxR transfer of electrons from the FAD to the active site cysteines takes place via an inter-domain rotation in the enzyme, while no such rotation occurs in high molecular weight TrxRs that also have a different enzymatic mechanism, involving two different redox-centers, a disulfide and a selenylsulfide (section 1.3.1). The reduced TrxR reduces the Trx that in turn reduces disulfide bonds in specific target proteins, see figure 11 (Lu and Holmgren, 2014).

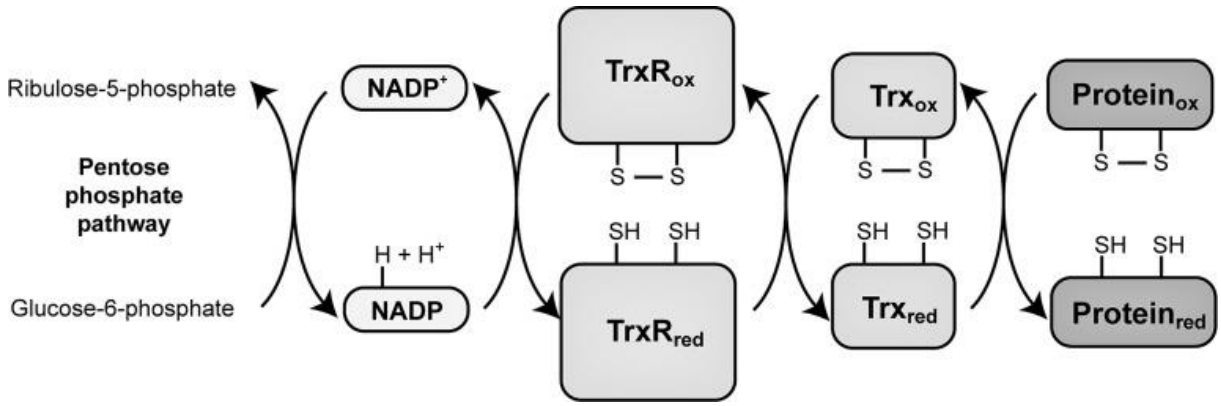

Figure 11. Flow of reducing equivalents in the thioredoxin system. Electrons from NADPH, generated through the pentose phosphate pathway is transferred through the thioredoxin system via redox-active cysteines. The reduced thioredoxin reductase ($TrxR_{red}$) transfers its reducing equivalent to thioredoxin (Trx), which in turn can reduce disulfide bonds in selected target proteins. Figure modified from (Lee et al., 2013).

Thioredoxin was first discovered as an electron donor to ribonucleotide reductase (RNR), the enzyme responsible for reducing ribonucleoside diphosphate (rNDP) to deoxyribonucleoside diphosphate (dNDP), the precursor for DNA synthesis, thus essential for cell proliferation (Laurent et al., 1964; Moore et al., 1964; Holmgren and Sengupta, 2010). In 1976 Grx was discovered as an alternative electron donor for RNR (Holmgren, 1976). *In vivo* studies of Trx and Grx systems in yeast and *E. coli* show cross-talk between the two systems. In *E. coli* viable double mutants missing parts of both systems appeared to be able to substitute for each other (Muller, 1996; Prinz et al., 1997). In addition to RNR many other protein targets have been discovered (Arnér and Holmgren, 2000) including methionine sulfoxide reductase (Ma et al., 2011), arsenate reductase (ArsC) (Li et al., 2007), peroxiredoxin (Rouhier et al., 2001), 3'-phosphoadenosine-5'-phosphosulfate (PAPS) reductase (Chartron et al., 2007) and the transcription factor OxyR (Åslund et al., 1999). In plants Trx regulates enzymes involved in the dark reaction of photosynthesis for example malate dehydrogenase and fructose-bisphosphatase (Balmer et al., 2004, 2003). In addition Trx reduces target proteins involved in the germination process of cereal seeds, for example the barley limit dextrinase inhibitor (Jensen et al., 2012) and barley α-amylase inhibitor (BASI) (Maeda et al., 2006; Björnberg et al., 2012). In order to screen for and identify novel target proteins several different types of proteomics based methodologies have been developed and applied (Hägglund et al., 2008, 2010; Montrichard et al., 2009; Lee et al., 2013).

Trxs in general have the highly conserved active site motif WC[G/P]PC, which is distributed across all kingdoms (Lu and Holmgren, 2014). The structure of thioredoxin consists of the so-called thioredoxin fold composed of four-stranded β-sheet surrounded by three flanking α-helices. In addition Trx contains one more α-helix and one more β-strand located in the N-terminal region (Holmgren et al., 1975; Katti et al., 1990; Martin, 1995). In mammalian cells there are at least two Trx, the cytosolic Trx1 and the mitochondrial Trx2. Trx2 has cysteines only in the active site, whereas Trx1 has three additional cysteines, involved in activity regulation and NO signaling (Lu and Holmgren, 2014). *E. coli* possesses two thioredoxins, Trx1 and Trx2, encoded by *trxA* and *trxC*,

respectively. Trx2 contains two additional CXXC motifs located in an N-terminal domain of 32 amino acids that coordinate to a Zn^{2+} ion (Collet et al., 2003). Trx1 and Trx2 appear to have similar *in vivo* functions, but are regulated differently. Double knockout mutants of *trxA* and *trxC* in *E. coli* are found to be viable (Ritz et al., 2000). In other bacteria, *e.g.*, *Rhodobacter sphaeroides*, *Bacillus subtilis* and *Anacystis nidulans*, Trx 1 is required for viability (Zeller and Klug, 2006).

Examples of other bacteria with multiple putative thioredoxins are *Helicobacter pylori*, *Mycobacterium tuberculosis* and *Bacillus subtilis*. *H. pylori* has a Trx1 with a classical active site motif and an atypical Trx2 with a CPDC active site. *H. pylori* Trx1 shows similar catalytic efficiency, k_{cat}/K_M, as that of *E. coli* Trx1 in a reaction with DTNB as the final electron acceptor. Trx1 can reduce alkyl hydroperoxide reductase (AhpC), while Trx2 showed no activity (Baker et al., 2001). *M. tuberculosis* has three thioredoxins, TrxA, TrxB and TrxC, of which only TrxB and TrxC are reduced by TrxR. Both TrxB and TrxC can reduce *M. tuberculosis* thiolperoxidase (Tpx), but only TrxC can reduce AhpC (Lu and Holmgren, 2014). In addition to the essential classical thioredoxin (TrxA), *B. subtilis* possesses several putative Trx including two non-essential thioredoxin-like genes *ytpP* and *ydpP*, which were shown to be induced by bacterial redox sensor (Spx) to a 3-fold increased level in the presence of diamine (Nakano et al., 2003). In addition, the two Trx-like thiol-disulfide oxidoreductases StoA and ResA attached on the outside of the inner cell membrane are reduced by the membrane bound CcdA, which in turn is reduced by TrxA. StoA and ResA transfer electrons to periplasmic proteins involved in spore cortex synthesis and cytochrome c synthesis, respectively (Erlendsson et al., 2004, 2003).

The interaction between Trx and its target protein is responsible for the regulation of many different cellular signaling pathways. Thus understanding basic Trx recognition patterns are the common feature of the redox regulation (Lee et al., 2013). The mechanism of reduction of thioredoxin targets is initiated by the thiolate anion of the more N-terminal active site Cys of Trx makes a nucleophilic attack at the targeting disulfide (figure 12, A), which results in an intermediate mixed disulfide complex between Trx and the target protein. This is followed by attack by the more C-terminal Cys in Trx on the intermolecular

disulfide (figure 12, B), ending the catalytic reduction cycle by the formation of a disulfide bond in the Trx and a reduced target protein (Collet & Messens 2010).

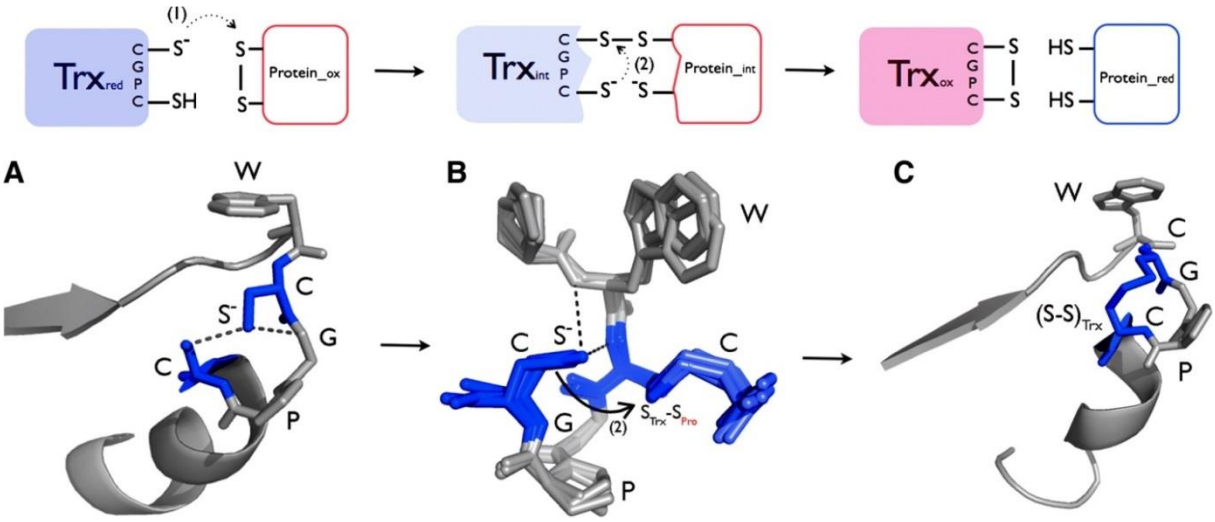

Figure 12. Mechanism of reduction of thioredoxin targets. The reaction mechanism of the conserved CGPC motif of Trx with target proteins involves a nucleophilic substitution reaction (S_N2). (A) The thiolate anion of the more N-terminal active site Cys makes a nucleophilic attack at the targeted disulfide. This thiolate anion is stabilized by two hydrogen bonds of the NH of the glycine and the thiol of the C-terminal Cys (1). (B) This results in an intermediate mixed disulfide complex between Trx and the target protein. The more C-terminal Cys attacks in a nucleophilic attack the more N-terminal Cys (2). (C) The catalytic reduction cycle ends in the establishment of a disulfide bond in the Trx and releases the reduced target protein with two free thiols on the cysteines (pdb 1TRV) (Collet and Messens, 2010).

Trx-target crystal structures have been obtained using covalently trapped stable complexes by Cys→Ser mutagenesis of the cysteine (those not involved in first nucleophilic attack) in the active sites of the two proteins. Examples of structures complexes obtained are Trx-barley α-amylase inhibitor (BASI) from *H. vulgare* (Maeda et al., 2006) and Trx-3′-phosphoadenosine-5′-phosphosulfate Reductase (PAPS) from *E. coli* (Chartron et al., 2007). In *H. vulgare* the thioredoxin is a type h (Trx h) with a target recognition loop that is involved in stabilizing backbone-backbone hydrogen binding with the BASI (Maeda et al., 2006). The surface of PAPS reductase contains a depression in which Trx helix 2 and the active site fit into (Chartron et al., 2007) and calorimetric measurements reveal that this

interaction is driven mainly by entropy and to a lesser extent by enthalpy (Palde and Carroll, 2015).

1.3 Thioredoxin reductase (TrxR)

Thioredoxin reductase (TrxR) is a member of the family of pyridine nucleotide-disulfide oxidoreductases that uses the isoalloxazine ring of a tightly bound FAD to shuttle reducing equivalents from NAD(P)H to redox-active cysteine residues. Most noteworthy members of this enzyme family includes TrxR, glutathione reductase (GR), trypanothione reductase (TryR), alkyl hydroperoxide reductase (AhpF), lipoamide dehydrogenase, and mercuric reductase (Russel and Model, 1988; Cohen et al., 1994; Tartaglia et al., 1990; Argyrou and Blanchard, 2004). In this work the thioredoxin reductase is referred to as TrxR, other terms like NADPH-dependent thioredoxin reductase (NTR) are mainly used for plants. TrxR is a homodimer flavoprotein with an FAD in each monomer. Two major classes of TrxR have evolved, high molecular weight (HMW) TrxR of 55 kDa for each subunit and low molecular weight (LMW) TrxR of 35 kDa for each subunit (Williams et al., 2000). HMW TrxRs are found in higher eukaryotes as well as unicellular parasites and insects and contain a mobile C-terminal flexible extension with an additional selenocysteine-containing redox-active motif (Gromer et al. 2003; Nordberg & Arnér 2001; Lu & Holmgren 2014). In HMW TrxRs the NADPH is positioned at the *re*-face of FAD and reducing equivalents are directly transferred to a redox-active CVNVGC motif positioned on the *si*-face (Fritz-Wolf et al., 2007, 2011). The reduced dithiol then transfers its electrons to the selenocysteine-containing active site which in turn reduces the CXXC motif in Trx (Biterova et al., 2005). This is in contrast to LMW TrxRs, involving a conformational shift, as elaborated below.

1.3.1 Structure and mechanism

LMW TrxR are present in archaea, bacteria, fungi and plants and are distinct from HMW TrxRs with regard to structure and mechanism. The monomer is composed of an FAD

domain and an NADPH domain, which are structurally similar to those of glutathione reductase (Waksman et al., 1994), see figure 13.

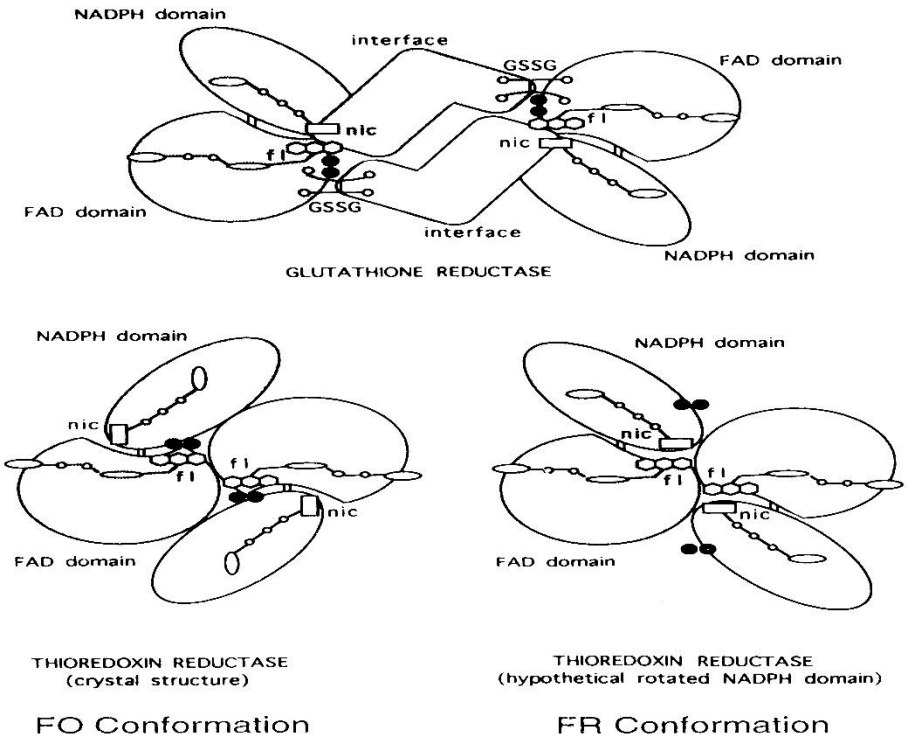

Figure 13. Comparison of glutathione reductase and TrxR. Top: Glutathione reductase transfers electrons from the NADPH (nic) to FAD (fl) so that oxidized GSSG can be reduced on the opposite site of the isoalloxazine ring. Bottom: TrxR in the two proposed conformations that were later confirmed by X-ray crystallographic structures. In the left structure the NADPH is distant from the FAD, but upon conformational change (lower right structure) the nicotinamide is positioned in vicinity of the FAD allowing transfer of two electrons (Waksman et al., 1994).

The active site containing a CXXC motif is located in the NADPH domain. One major difference from glutathione reductase is that TrxR can adopt two conformations, FO (Flavin Oxidized) and FR (Flavin Reduced). The two conformations were first proposed from EcTrxR crystal structures (Waksman et al., 1994) and later evidence supported by experiment with intrinsic and extrinsic quenchers (Mulrooney and Williams, 1997). The term FO refers to "FAD Oxidizing" and FR to "FAD Reducing" (Lennon and Williams, 1997). The two domains are linked by a two-stranded β-sheet. The NADPH domain can

rotate 67° relative to the FAD domain, transferring electron from NADPH through FAD to the active site cysteines. Figure 14 A shows *Ec*TrxR in the FO conformation (PDB code 1TDF) with $NADP^+$ (obtained by soaking the crystal in buffer with $NADP^+$) on the surface of the protein and the active site cysteines located on the *re*-side of the isoalloxazine of the FAD. Upon rotation to the FR conformation (PDB code 1F6M), shown in figure 14 B, the $NADP^+$ analogue $AADP^+$ (3-aminopyridine adenine dinucleotide phosphate) is translocated to the vicinity of the FAD allowing a two-electron reduction, while the cysteines are exposed on the surface of the protein. This exposure allows the protein target thioredoxin (in grey) to be reduced by the cysteines (Lennon et al., 2000).

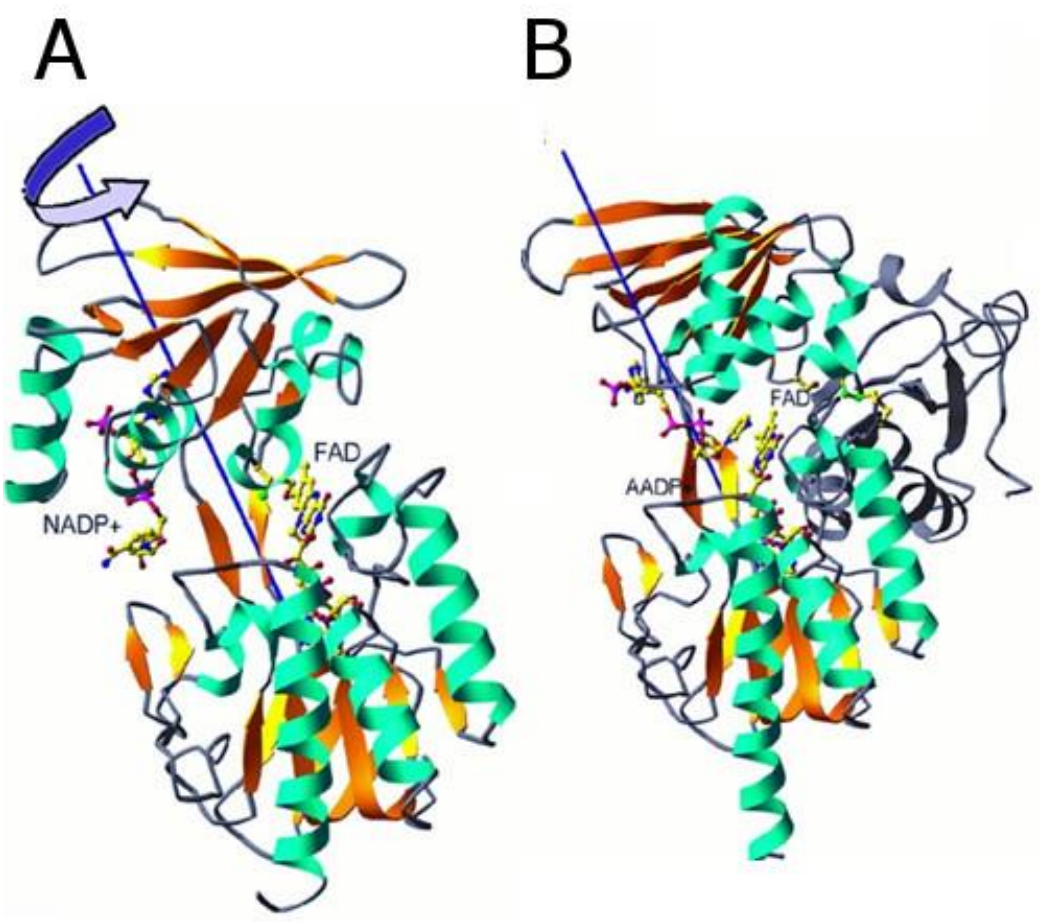

Figure 14. *Ec*TrxR in FO (A) and FR (B) conformation. In the FR conformation the *Ec*TrxR is trapped in the crystal with *Ec*Trx1, which is shown in grey (Lennon et al., 2000).

Apparent equilibrium constant (K_{eq}) of the FO⇆FR equilibrium for wildtype *Ec*TrxR was determined to be approximately K_{eq} = 2.6 based on measurements of the changes in extinction coefficient of FAD upon establishment of FAD-NADPH charge transfer complexes in the electron transfer from NADPH to FAD (Lennon and Williams, 1997). A plausible model is that NADPH in the initial step binds to the NADPH cleft exposed on surface of TrxR in the FO conformation, followed by the conformational switch to bring NADPH and the FAD in proximity. This assumption is further supported by analysis of high-resolution structures of *Helicobacter pylori* TrxR, where rigid-body rotation of the NADPH-domain modeled with bound $NADP^+$ can rotate from FO to FR conformation without any re-adjustments of the conformation of $NADP^+$ (Gustafsson et al., 2007). Mulrooney and Williams (1997) showed that FAD fluorescence intensity was increased when trapping $EcTrxR_{C138S}$ in FR conformation, upon reaction of the active Cys135 with phenylmercuric acetate (PMA). This result is most likely a consequence of the quenching effect of the cysteine in the vicinity of the isoalloxazine ring is lowered as the TrxR is shifted towards the FR conformation, as cysteine is known to quench riboflavin triplet state (Cardoso et al., 2004). Comparing the fluorescence emission of *Ll*TrxR gave a 3-fold higher quantum yield than *Ec*TrxR (Paper 1, Appendix A, figure S5). This result could be interpreted as the equilibrium of *Ll*TrxR is shifted more towards the FR conformation as compared to EcTrxR equilibrium, but there could be many other factors influence fluorescence yield.

Trx1-TrxR interactions in *E. coli* consist of a 6 residues loop (70-76) in Trx that binds into a groove at the NADPH domain. Trx Arg73 interacts with the Arg130 at one side of the groove in TrxR. On the other side of the groove Phe141 and Phe142 of TrxR fit into the hydrophobic pocket of Trx consisting of Trp31, Ile60, Gly74 and Ile75 (Lennon et al., 2000). A loop in the FAD domain of the TrxR was later identified as critical in the Trx recognition, as confirmed by site-directed mutagenesis in *E. coli*, *Hordeum vulgare* and *Arabidopsis thaliana*. Mutants having key residues changed to alanine exhibited significant loss in activity as detected in DTNB assays (Kirkensgaard et al., 2014).

1.3.2 Flavins, flavoproteins and flavoenzymes

Flavins are yellow-colored compounds with the general structure 7,8-dimethyl-10-alkylisoalloxazine. If the N-10 position is linked to a ribityl group the compound is called riboflavin (RF), which is the precursor of the cofactors flavin mononucleotide (FMN) and flavin adenine dinucleotide (FAD), see figure 15. Commonly riboflavin is referred to as vitamin B_2.

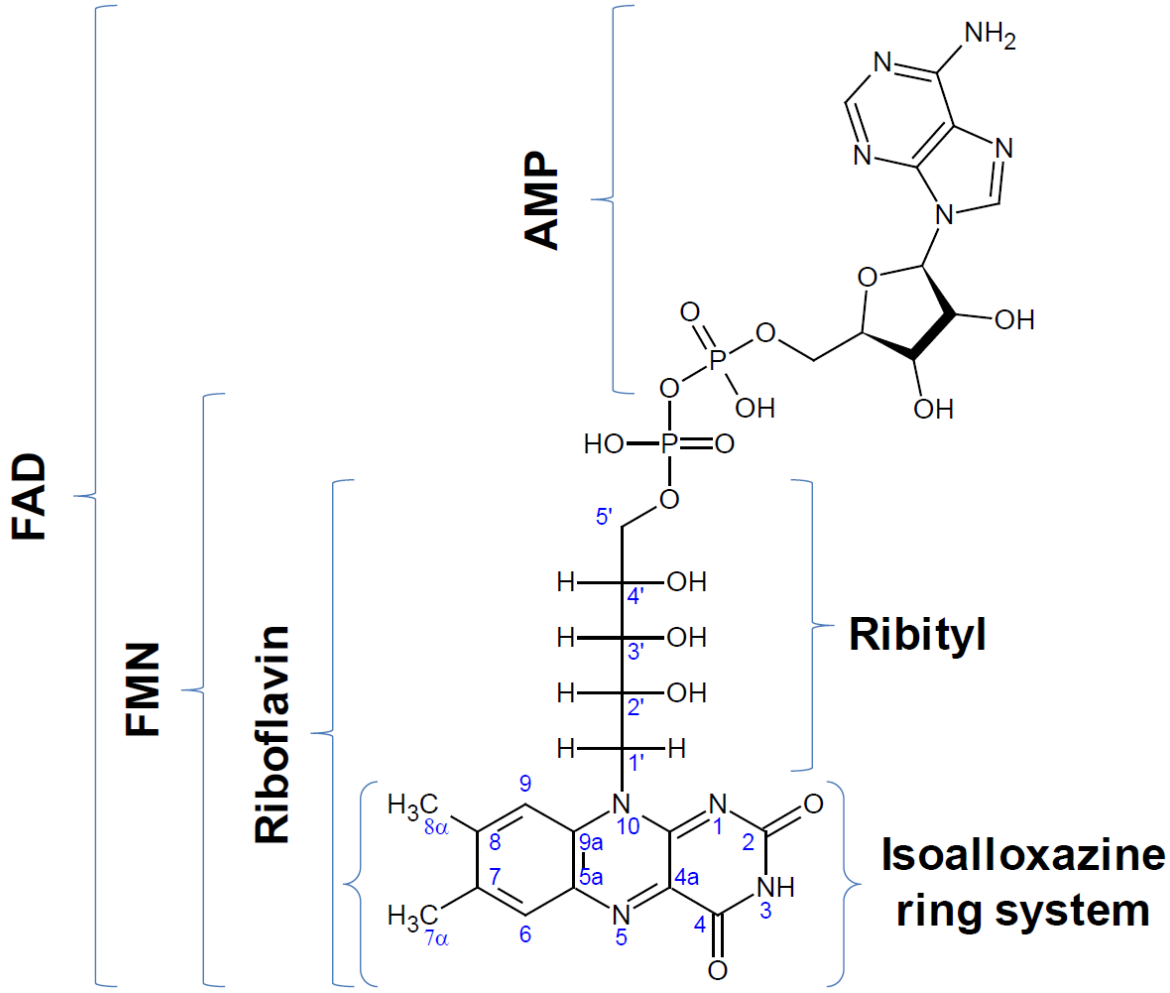

Figure 15. Structure of oxidized FAD with IUPAC numbering (Heelis, 1982). Flavins are referred to as 7,8-dimethylisoalloxazine alkylated at the N10 position. If the N-10 is attached to a ribityl group the molecule is riboflavin. 5'-phosphorylation gives flavin mononucleotide (FMN) and a further adenosine monophosphate bound to this phosphate gives flavin adenine dinucleotide (FAD).

Most flavins *in vivo* act as co-enzymes, mainly in the form of FMN or FAD (Edwards, 2006). Protein bound FMN and FAD can be involved in both one- and two-electron transfer. Upon receiving one electron the oxidized flavin is transformed into a free radical state, referred to as a flavosemiquinone. The fully reduced flavin is formed by addition of a second electron to the flavosemiquinone (figure 16). The flavins can also occupy different protonation states, which are determined by the local environment in the specific protein. The pK_a can change dramatically upon these changes, and as a consequence some flavoenzymes can stabilize semiquinones, while others cannot (Heelis, 1982; Edwards, 2006).

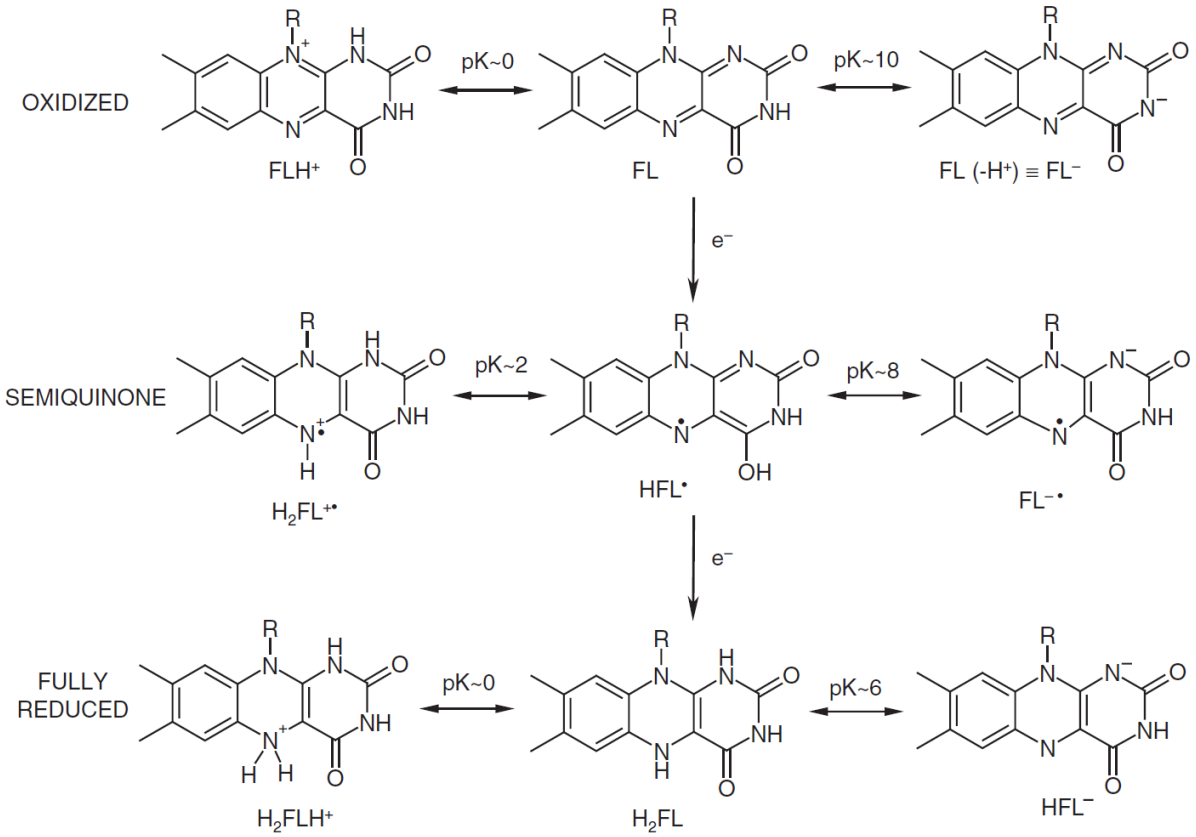

Figure 16. Redox and acid-base equilibria for flavins. A one-electron transfer to oxidized flavin leads to semiquinone (HFL·) and yet another electron leads to the fully reduced form (H_2FL) (Heelis, 1982). Figure from (Edwards, 2006).

The UV-Vis spectrum of *Ec*TrxR has characteristic absorbance peaks at ~380 and 456 nm. The extinction coefficient of FAD bound to TrxR was determined to be 11300 M^{-1} cm^{-1} at 456 nm, the same as of free FAD at 450 nm (Williams et al., 1967). Upon a full two-electron reduction of the FAD to $FADH_2$ with dithionite the peaks diminish, but the FAD is rapidly re-oxidized in the presence of molecular oxygen (figure 17).

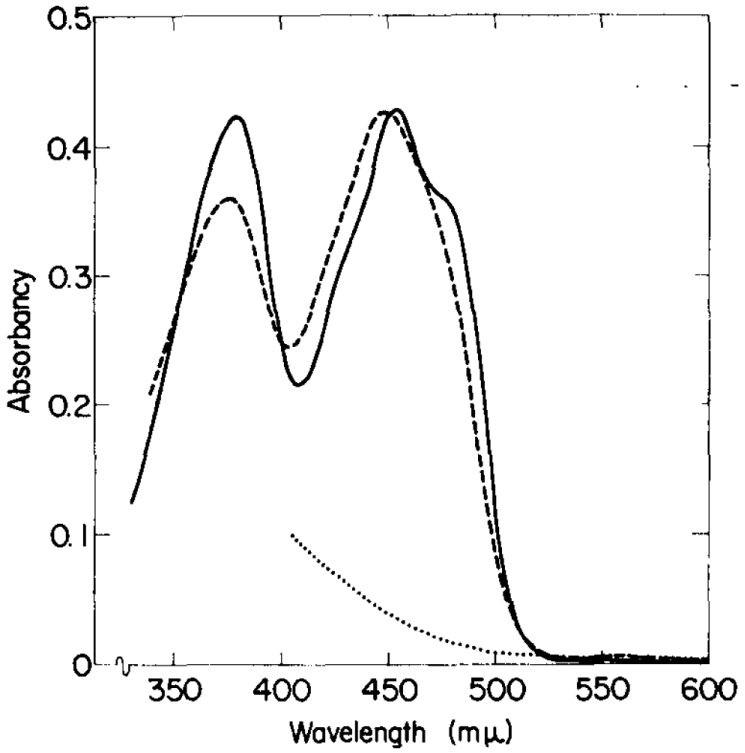

Figure 17. Changes in FAD absorbance spectrum from *Ec*TrxR. Enzyme in 50 mM potassium phosphate, pH 7.6, with 7 M urea. (-). After adding excess sodium dithionite, the absorbance decreases (·····). After mixing with air the spectrum was restored (- - -). (Williams et al., 1967).

Covalently bound FAD

In some flavoenzymes the flavin is covalently attached to the protein through C8α (Edmondson and Newton-Vinson, 2001; Heuts et al., 2009). The covalent bond to C8α is formed through a nucleophilic reaction of the anionic residues attacking the C8α methide group (figure 18). The residues involved are a deprotonated tyrosine (Trickey et al., 1999;

Efimov and McIntire, 2004), cysteine (Kenney et al., 1974) or histidine (Koetter and Schulz, 2005; Jin et al., 2008).

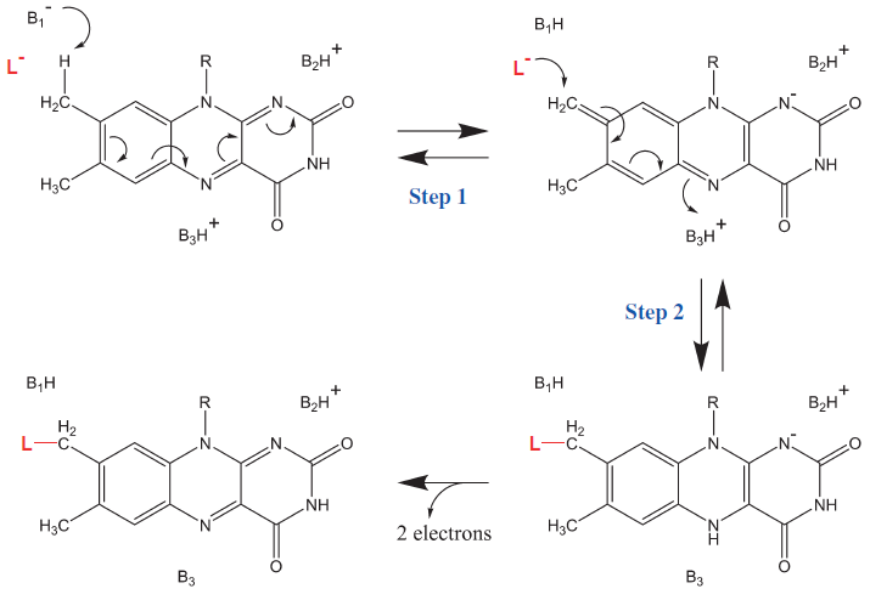

Figure 18. General mechanism for covalent C8α flavinylation. Upon loss of one proton at C8α the generated methide group becomes a center of a nucleophilic attack for anions. L^- represents tyrosine, cysteine or histidine. B1-B3 represents acid/bases in the active site. Figure from (Heuts et al., 2009).

Oxidation of FAD and change in redox potential

Experimental data and theoretical calculations on 7,8-substituted flavin analogues predict major changes in the oxidation-reduction potentials as a result of these modifications. The C8α is the best studied with regard to modification (Edmondson and Ghisla, 1999). An 8-formylflavin will have a change in redox potential from –208 mV to –90 mV, whereas an acid or a hydroxyl group in the same location change the redox potential to –165 and –170 mV, respectively (Edmondson and Singer, 1973). In *Ec*TrxR the difference in redox potential of the flavin and the active site disulfide at pH 7.6 is only 7 mV (O'Donnell and Williams, 1983; Lennon and Williams, 1996), thus small changes in the redox potential upon flavin modification will disable electron transfer to the disulfide, thereby inactivating the TrxR.

1.4 *Lactococcus lactis* and LAB

Lactic acid bacteria (LAB) are a group of Gram-positive, non-sporulating, anaerobic or facultative aerobic cocci or rods, included mainly in the phylum of *Firmicutes*, class *Bacilli* and order *Lactobacillales* (Quinto et al., 2014). LAB do not comprise a monophyletic group of bacteria, rather they are characterized by their ability to ferment sugars to lactic acid as the major end product (König and Fröhlich, 2009). Though most LAB species belongs to the order of *Lactobacillales*, a few LAB belong to *Actinobacteria* (Makarova and Koonin, 2007).

L. lactis has because of its importance in the dairy industry and its relative small genome of 2.5 Mbp (Bolotin et al., 2001; Wegmann et al., 2007) served as a model organism in the characterization of LAB. *L. lactis* is classified to as "GRAS" (Generally Recognized As Safe) and is widely used in the dairy industry as a starter culture in cheese production, with the acidification causing precipitation of the milk proteins, as well as in yogurt and buttermilk production. *L. lactis* is mesophilic (optimal growth temperature around 30°C) and regarded as microaerophilic fermenting LAB. Though *L. lactis* is in general described as a microaerophilic bacterium, this term might be inadequate (Condon, 1983), as it does grow well even under aerated conditions and its common habitats in nature are on plant and animal surfaces.

1.4.1 Metabolism under anaerobic conditions

Heterofermentative LAB convert hexoses to xylulose 5-phosphate, which is converted to acetyl phosphate and glyceraldehyde 3-phosphate by phosphoketolase. Acetyl phosphate will depending on the cellular stress conditions be converted into either ethanol or acetate (Papadimitriou et al., 2016), see figure 19. Homofermentative LAB on the other hand solely converts hexoses through glycolysis generating two ATP, two NADH and two molecules of pyruvate. *L. lactis* is a homofermentative bacterium and converts carbohydrates mainly into lactic acid via fermentative metabolism when grown under anaerobic conditions (Condon, 1987; Felipe et al., 1998), see figure 19. Through the

reduction of pyruvate to lactic acid by lactate dehydrogenase (LDH) the NADH is reoxidized/regenerated to NAD^+, providing the required oxidant to make the glycolysis running.

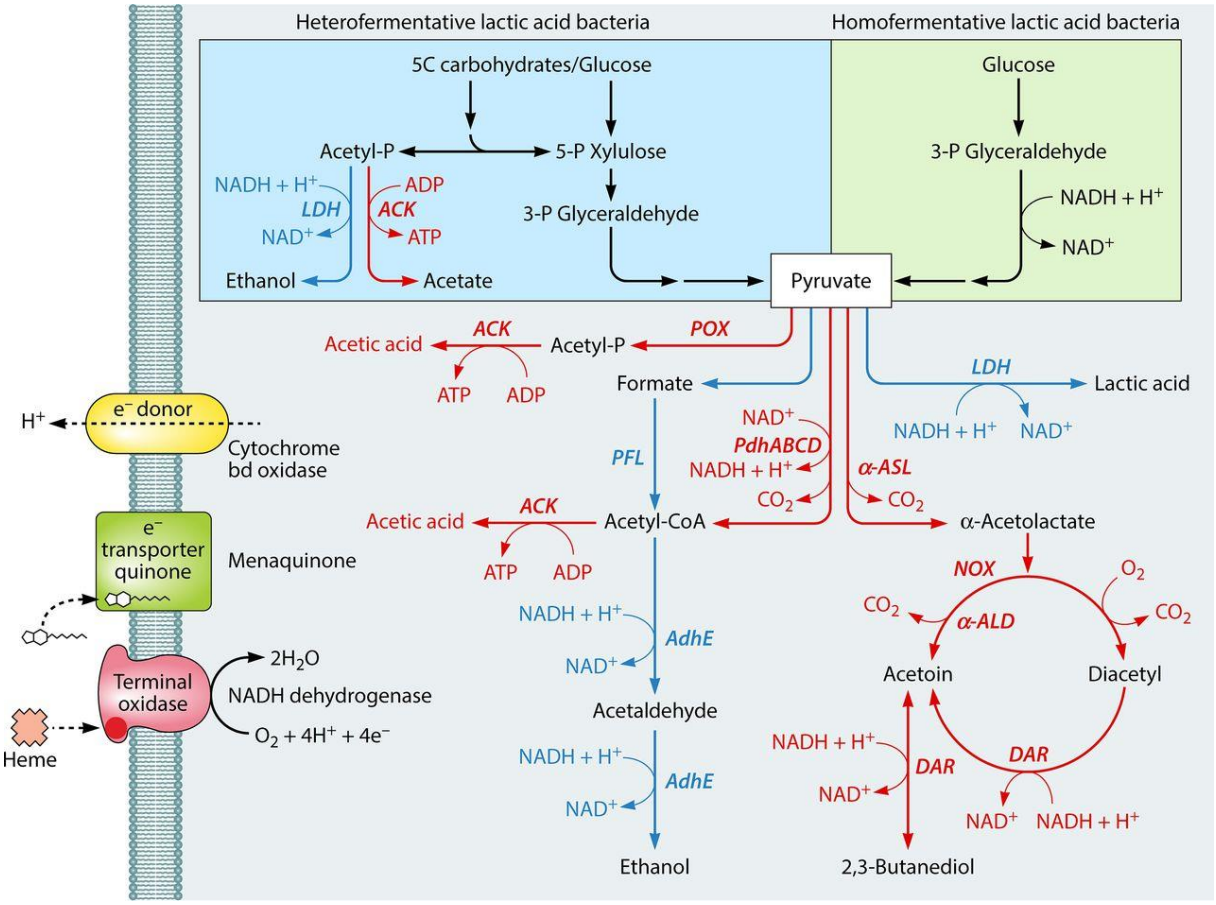

Figure 19. Overview of carbohydrate metabolism in LAB. Arrows and enzymes mainly induced during unstressed fermentative conditions (blue), during respiration and/or stress conditions (red), or common reactions and enzymes (black) are indicated. LDH, lactate dehydrogenase; ACK, acetate kinase; POX, pyruvate oxidase; PFL, pyruvate formate lyase; PdhABCD, pyruvate dehydrogenase complex; α-ASL, α-acetolactate synthase; AdhE, alcohol dehydrogenase; NOX, NADH oxidase; α-ALD, α-acetolactate decarboxylase; DAR, diacetyl reductase. Figure from (Papadimitriou et al., 2016).

1.4.2 Metabolism under aerobic conditions and respiration in LAB

The NADH/NAD^+ ratio is the main determinant regulating shifts from homolactic fermentation to mixed-acid fermentation in *L. lactis* (Garrigues et al., 1997). In the presence of intracellular oxygen the NADH/NAD^+ ratio is lowered due to enhanced expression of NADH oxidase and NADH peroxidase (Miyoshi et al., 2003). The competition for NADH molecules lowers the activity of LDH and shifts the fermentation towards the mixed-acid fermentation. Under this metabolic phenotype pyruvate can be converted into formate and acetyl-CoA by pyruvate formate lyase (PFL). Acetyl-CoA is further transformed into acetaldehyde and ethanol by alcohol dehydrogenase (AdhE). At intracellular conditions with surplus of carbohydrates and low pH less pyruvate is converted to lactic acid by LDH, and the excess pyruvate is metabolized through α-acetolactate synthase (α-ASL) generating α-acetolactate. α-acetolactate is mainly decarboxylated to diacetyl at high oxygen levels in a non-enzymatic fashion. At lower levels of oxygen α-acetolactate is mainly converted to acetoin by α-acetolactate decarboxylase (α-ALD). Diacetyl is converted to acetoin via diacetyl reductase (DAR), which depending on cellular redox state can further reduce acetoin to 2,3-butandiole while regenerating NAD^+. Under cellular conditions where the NAD^+ concentration is high due to AdhE activity the pyruvate is converted by pyruvate dehydrogenase complex (PdhABCD) to acetyl-CoA and NADH (Papadimitriou et al., 2016), see figure 19. Under these aerobic conditions a shift from homolactic fermentation towards mixed-acid fermentation with acetate, acetoin, diacetyl and ethanol as the main metabolites (Miyoshi et al., 2003).

In LAB the respiration can be induced by addition of exogenous heme and in some cases heme and menaquinone (Duwat et al., 2001; Lechardeur et al., 2011). The heme-dependent cytochrome activates the respiration, which causes a metabolic shift towards activation of pyruvate oxidase (POX) generating acetyl phosphate, which is dephosphorylated to acetic acid by acetate kinase (ACK) to form ATP (figure 19). Action of the respiration metabolism in LAB has shown to improve fitness and markedly increased growth yield. In *L. lactis* activation of the respiration induces expression of genes encoding cytochrome bd

oxidase, menaquinone biosynthesis and heme uptake as-well as increasing the biomass and in general improving the robustness of *L. lactis* (Pedersen et al., 2012). In *L. lactis* inhibition of the lactate dehydrogenase activity during the respirational growth has shown to stimulate respiration leading to increased growth and robustness (Arioli et al., 2013).

1.4.3 Removal of oxygen

As described above aerobic condition leads to mixed-acid fermentation resulting in an altered redox state. Most *Lactobacilli* and *Lactococci* have as described above no functional electron-transfer chain and further more does not contain any heme-containing enzymes such as catalase (Poole, Higuchi, et al., 2000). Their aerotolerance is dependent on O_2 scavenging enzymes, serving to remove intracellular oxygen, but also to utilize O_2 as a final electron acceptor (Miyoshi et al., 2003; Baker et al., 2014). The flavo-protein AhpF (Nox-1) transfers reducing equivalents from NADH to FAD and reduced O_2 to H_2O_2. When AhpF is linked to the peroxidase AhpC, the latter reduces H_2O_2 further to 2 H_2O without H_2O_2 leakage as detected with an oxygen electrode upon addition of catalase (Niimura et al., 1995). Another NADH oxidase is H_2O-forming NADH-oxidase Nox-2, in *L. lactis* referred to as NoxE. This 4-electron reduction from oxygen to water performed by NoxE from *L. lactis* is found to be 6-fold higher than the coupled NADH oxidase/NADH peroxidase system (AhpF/AhpC). But the expression levels of NoxE vs. AhpF/AhpC upon oxidative stress might explain the difference in the kinetic parameters (Jiang et al., 2005). Expression of NoxE in *S. cerevisiae*, which does not possess this gene, led to a 5-fold decrease in NADH accumulation and a 6-fold decrease in the $NADH/NAD^+$ ratio (Heux et al., 2006).

1.4.4 Thioredoxin system in *L. lactis*

In general bacteria can be classified in three groups according to their antioxidant systems. 1. Bacteria with Trx system, GSH system, and catalase. 2. GSH-negative bacteria and 3. Catalase-negative bacteria (Lu and Holmgren, 2014). Being catalase-negative *L. lactis* is in the third group with strains with and without GSH. For that reason *L. lactis* was expected to depend exclusively on its thioredoxin system in order to maintain the cytoplasm in a

reduced state. Interestingly though, a Δ*trxB1* mutant of the GSH-negative *Lactococcus lactis* subsp. *cremoris* (strain MG1363), which lacks TrxR, was shown to be viable under aerated static conditions even without DTT supplemented to the growth medium (Vido et al., 2005). This result is surprising as related Gram-positive bacteria like *B. subtilis* (Scharf et al., 1998) and *S. aureus* (Uziel et al., 2004) appear to be depend on the thioredoxin system for survival. It should however be noted that the *L. lactis* mutant Δ*trxB1* was severely diminished in its growth and hardly grew within the first 7 hours (and next data point was at 24 hours where it showed same OD as the wild-type). Even though some *L. lactis* strains lack Grx and GSH synthesis genes (like most LAB), these strains were shown to import and utilize GSH if it was added to the medium (Li et al., 2003).

L. lactis contains two paralogues of thioredoxin; the classical TrxA and in addition a protein denoted *Ll*TrxD with the atypical redox-active site motif WCG**D**C. *Ll*TrxD is prevalently found in Gram-positive bacteria and has a higher redox potential of –243 mV as compared to *Ll*TrxA's of –259 mV. Interestingly, *Ll*TrxD showed no activity with insulin as substrate and was not reduced by *Ec*TrxR (Björnberg et al., 2014). *Ll*TrxA and *Ll*TrxD showed same turnover values (k_{cat} = 26–27 s^{-1}) with *Ll*TrxR in DTNB assays. To investigate the atypical nature of *Ll*TrxD, the aspartic acid (Asp31) in the active site was mutated to proline or asparagine in order to change the electrostatic environment. But of the D31P and D31N *Ll*TrxD mutants, only D31P gained a minor activity in insulin disulfide reduction assays, and none of them were able to be reduced by *Ec*TrxR (Björnberg et al., 2014). The physiological properties of *Ll*TrxA and *Ll*TrxD were further investigated in Δ*trxA*, Δ*trxD*, Δ*trxA*Δ*trxD* deletion mutants of *L. lactis* (Efler et al., 2015). The growth of a Δ*trxA* deletion mutant diminished under non-stress conditions and was considerably impaired under various oxidative stress conditions. On the other hand, the Δ*trxD* mutant showed almost the same growth as the wildtype, also under oxidative stress conditions. Only in the presence of arsenate and tellurite the Δ*trxD* mutant became differentiated from the wildtype. Under non-stress conditions the Δ*trxA*Δ*trxD* double-knockout mutant was significantly impacted, indicating partially overlapping functions of *Ll*TrxA and *Ll*TrxD (Efler et al., 2015).

1.4.5 *L. lactis* TrxR light sensitivity

This section describes the basis for the *Ll*TrxR light sensitivity, which was established before the start of my PhD project, thus being the starting point for the subsequent work described in this thesis. More detailed descriptions are found in Paper 1 (Appendix A). The *Ll*TrxR light sensitivity was discovered by postdoc Olof Björnberg *et al.* at Enzyme and Protein Chemistry group (DTU) in the summer of 2011. The first hints began with difficulties to reproduce enzyme kinetic measurements of recombinantly produced *Ll*TrxR, as the enzyme lost a significant part of its activity after just a few hours on ice. This was as opposed to *Ec*TrxR that appeared much more stable. Several conditions for *Ll*TrxR were examined, like buffer conditions, the solubility and stability of the enzyme, as well as the integrity of the DNA clone. After several "interrogations" it became clear that *Ll*TrxR is sensitive to light and just the mere ambient daylight in the laboratory was enough to inactivate the enzyme. After taking the proper precautions to keep the *Ll*TrxR away from light, the k_{cat} values obtained with the *Ll*TrxA as substrate was in the same range as for *Ec*TrxR. After this realization a more detailed investigation of the light based inactivation of *Ll*TrxR was initiated. The results were later published in Biochemistry 2015 (Paper 1).

Standardized conditions for light inactivation was established using a compact 1225 Lumen (21 watt) fluorescent lamp with a color temperature of 6500 K corresponding to a maximum intensity λ_{max} = 460 nm (Manufacture Leuci (Relco group)). The inactivation of *Ll*TrxR was performed in the cold room (4°C) with the enzyme solution in an original Eppendorf tube 20 cm below the lamp. This standardized setup is the basis for the photo-inactivation experiments, as described in section 2.4.2. These types of lamps typically have spectral lines at 405, 435, 545, 610 and 710 nm, with the color temperature of the specific lamp defined by the identities of the individual lines.

Important findings in Paper 1

Activity

- *Ll*TrxR is sensitive to visible light using a light source as described above
    - A half-life of ~35 min light exposure using a DTNB assay with Trx
- *Ec*TrxR and *Hv*NTR2 appear to be much more robust towards light

Spectral changes in UV-Vis and fluorescence

- A blue shift of the 456 nm peak is observed (λ_{max} = 440–445 nm) over the course of light exposure
- The 380 nm peak is lowered and an increase at 300–330 nm is observed during light exposure
- Fluorescence emission of *Ll*TrxR excited at 450 nm shows a 3-fold higher quantum yield than *Ec*TrxR. Upon light irradiation the emission intensity was lowered and a small shift in the maximum emission from 515 to 510 nm was observed. The fluorescence emission spectrum of irradiated *Ec*TrxR did not change

Oxygen exposure

- Irradiation of *Ll*TrxR in a semi anaerobic system, using glucose, glucose oxidase and catalase as molecular oxygen scavengers, clearly protected the enzyme from inactivation. A control, made without glucose, showed the same sensitivity towards light as previously observed
- *Ll*TrxR reduces molecular oxygen (O_2) in the presence of NADPH faster than *Ec*TrxR. Interestingly, light inactivated *Ll*TrxR showed a slightly higher O_2 reduction ability, as compared to non-irradiated.
- Addition of iodide, a well-known quencher of photoexcited triplet state flavin, clearly protected *Ll*TrxR from light inactivation, indicating the isoalloxazine ring acting as a photosensitizer.

FAD oxidation

- Mass spectrometry of heat-extracted FAD from irradiated *Ll*TrxR revealed a mass gain of 13.979 Da, which unambiguously corresponds to the addition of one oxygen atom and loss of two hydrogen atoms, consistent with conversion of a methyl group to an aldehyde.
- A minor ion with a mass gain of 29.9743 Da was observed, corresponding to a further addition of an oxygen atom.
- The presence of an aldehyde at the place of one of the methyl groups of the isoalloxazine ring was verified by treatment with 2,4-dinitrophenylhydrazine (DNPH), a molecule known to react with carbonyl groups forming insoluble red/orange precipitates.
- Aldehyde formation at C8α has in the literature not been reported to cause the observed blue shift.
- Reduction of the 8-formylflavins are known to absorb at a wavelength at above 500 nm, due to resonance stabilization of the conjugated isoalloxazine system, but liberated FAD from irradiated *Ll*TrxR, did not show the absorbance band between 500–600 nm upon reduction.
- On this account it was concluded that the most likely location of the aldehyde formation is on C7α.

Other conditions during light exposure were tested like addition of *Ll*TrxA and *Ll*NrdH, superoxide dismutase, FAD and riboflavin (20 μM), DTT (2 mM), and tryptophan (1 mM). Only the addition of FAD and riboflavin (20 μM) provided some protection. pH lowered to 4.0 seemed to provide some protection towards photo-inactivation.

1.5 Objectives and hypotheses of the present investigation

At the onset of this project, studies of the *L. lactis* thioredoxin system had revealed that the recombinantly expressed *Ll*TrxR is sensitive to light (previous section and Paper 1). In order to explore this novel feature of TrxR in greater detail, the following set of questions were raised and used as a basis for the experimental work:

- What are the underlying structural features responsible for the light sensitivity of TrxR?
    - The local micro environment around the FAD in *Ll*TrxR
    - The FO-FR conformational equilibrium of *Ll*TrxR
- What molecular mechanisms can explain the observed light sensitivity of TrxR?
    - Change in redox potential of FAD
    - Restrictions in conformational dynamics
- Which types of oxidations are generated over the course of irradiation?
    - What plausible mechanisms can explain the observed oxidations?
- What is the biological relevance of the light sensitivity of TrxR?
    - Light sensitivity of *Ll*TrxR in *L. lactis* cell extracts
    - Light sensitivity of *Ll*TrxR *in vivo*
    - General viability of *L. lactis* upon visible light exposure
- Is light sensitivity a common feature of TrxR from organisms related to *L. lactis*?

The methodology used to address the above questions is based protein expression and purification followed by characterization of involved proteins using techniques such as; X-ray crystallography, enzymatic activity assay of irradiated *Ll*TrxR, SDS-PAGE, size exclusion chromatography (SEC), MS, stopped-flow spectrometry, fluorescence measurement and growth of *L. lactis* for cell extract and *in vivo* irradiation for monitoring viability and *Ll*TrxR activity.

A general biochemical characterization of photo-inactivated *Ll*TrxR (non-crystallographic data) is presented in chapter 2, while chapter 3 focuses entirely on the three-dimensional structures of *Ll*TrxR. Chapter 4 is combining the results with concluding remarks and perspectives to address the above questions.

Chapter 2. Characterization of photo-inactivated thioredoxin reductase

2.1 Introduction

This chapter describes some of the non-crystallographic results obtained by the characterization of the photo-inactivated *Ll*TrxR. Some data are included in the two published articles (Paper 1 and Paper 2), while some are not compiled in a manuscript yet.

2.2 Results and discussion

2.2.1 Reconstitution of photo-inactivated *Ll*TrxR

The following data is included in the published article (Paper 1), but is elaborated here in more details. In order to examine to what extent the light-sensitivity of the *Ll*TrxR activity indeed is a consequence of FAD oxidation, an experiment was performed to reconstitute light-inactivated *Ll*TrxR by replacing the oxidized FAD with exogenous FAD. *Ll*TrxR (20 µM), exposed to light for 3 h (~7% remaining activity), and a control wrapped in tin foil were added 600 times excess of exogenous FAD and subsequently mixed with the denaturing agent guanidinium chloride (GdmCl) to gradually reach a final concentration of 2 or 3 M followed by incubation for 21 h with gentle shaking at 4 °C. After the incubation the samples were diluted in several steps to reach a final concentration of 100 mM GdmCl. After concentrating the samples to ~1 mL and buffer exchange to buffer without GdmCl by size exclusion chromatography (SEC), the activity was measured with *Ll*TrxA in a DTNB assay. As seen from figure 20 the activity of *Ll*TrxR increased from 7% to ~40% following reconstitution with exogenous FAD in 2 and 3 M GdmCl suggesting that successful (at least partial) reconstitution was achieved. This experiment was repeated on another occasion with 1 and 2 M GdmCl giving similar increase in activity upon reconstitution (data not shown). However, addition of exogenous FAD to non-denatured *Ll*TrxR only increased activity from 7% to 11%, suggesting that partial unfolding is necessary in order to exchange the tightly bound FAD.

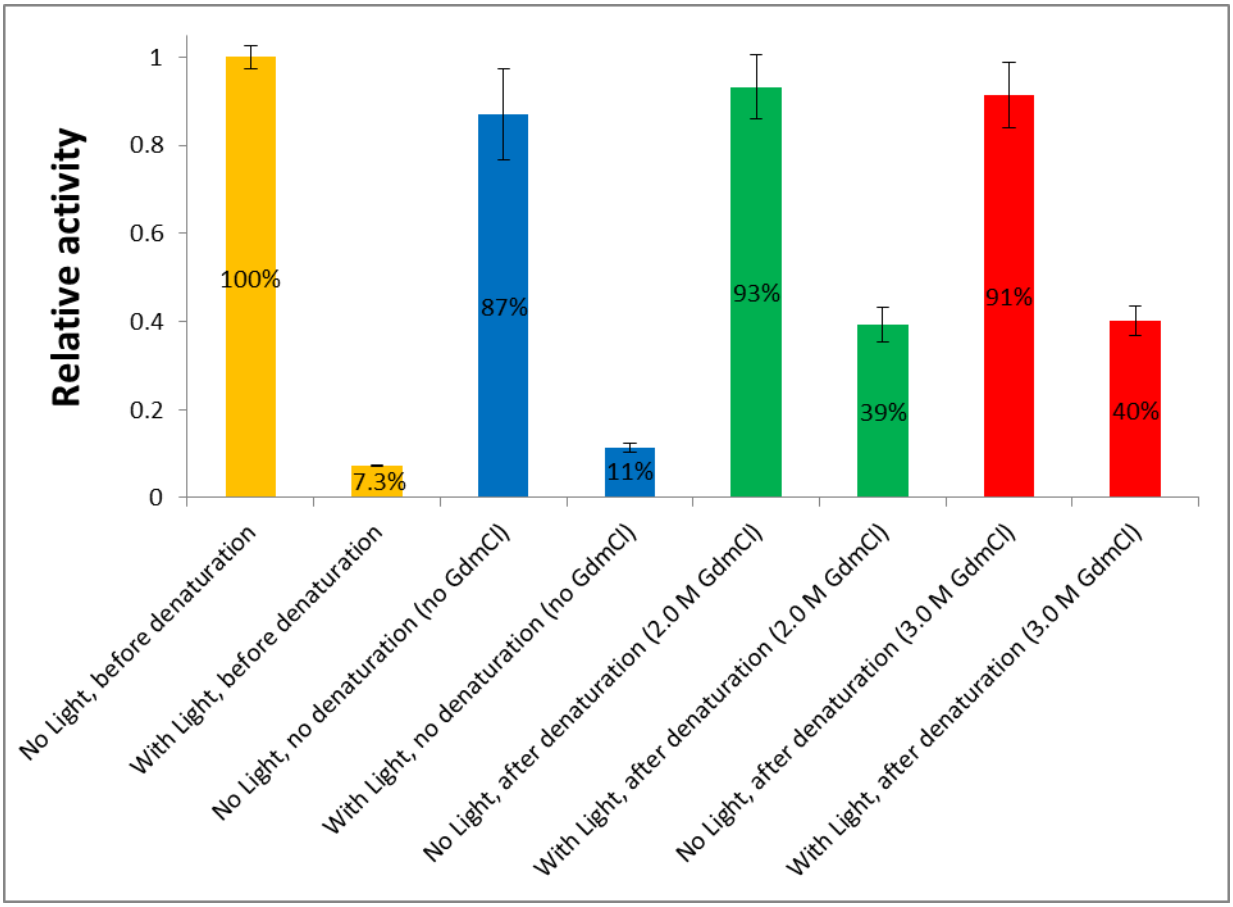

Figure 20. Relative activity of *Ll*TrxR, quantified by DTNB reduction with NADPH and *Ll*TrxA. After 3 h photo-inactivation ~7% activity remains. After reconstitution of FAD in the presence of 2 or 3 M GdmCl, approximately 40% of the original activity was recovered. With no denaturing agent present during the FAD reconstitution only a minor increase in activity was observed. *Ll*TrxR from samples which were light protected and treated with GdmCl showed no increase in activity, as compared to the one with no denaturing agent. The error bars indicate the standard deviations.

As judged from the UV-Vis spectra of the photo-inactivated *Ll*TrxR with reconstituted FAD in the presence of 2 or 3 M GdmCl, the FAD absorbance peak is red-shifted towards the native form with a maximum at 456 nm, indicating that FAD was indeed exchanged with exogenous FAD. In the control without GdmCl the blue-shifted peak was only slightly changed upon incubation with exogenous FAD from λmax = 441 nm to λmax = 444 nm (figure 21). Even though the successful reconstitution demonstrates that the oxidation of the FAD has strong influence on the activity of *Ll*TrxR, the activity was not fully recovered after replacing the photo-oxidized FAD. It can therefore be suggested that photo-

inactivation involves other modifications, which impairs the activity of the enzyme, for example tyrosine oxidation in the vicinity of the FAD as was observed in the crystal structure of light exposed *Ll*TrxR (chapter 3). Another possibility is that FAD is covalently cross-linked to the polypeptide, preventing exchange of oxidized FAD. Such a covalent bond to FAD could be envisaged by a hemiacetal formation with Tyr237/Tyr133 and the 7-formyl group at the isoalloxazine ring in FR and FO conformation, respectively.

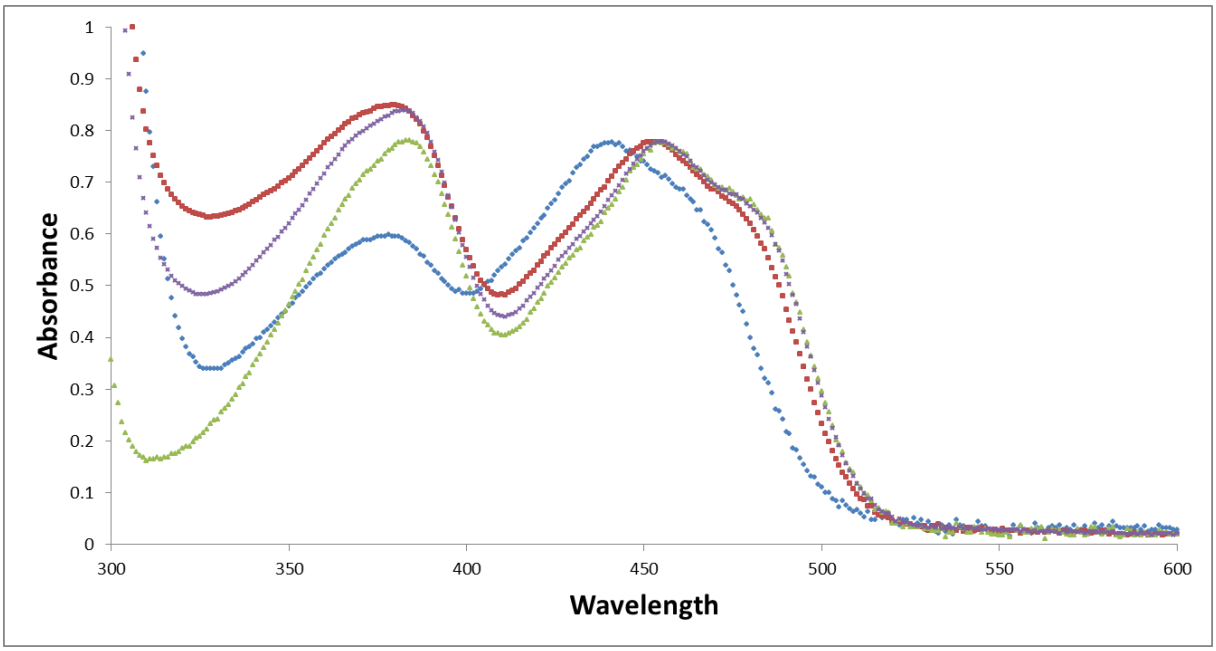

Figure 21. UV-Vis spectra of *Ll*TrxR, with and without light exposure, before and after reconstitution of FAD using 2.0 M GdmCl. A clear blue shift (λ_{max} = 441 nm) is observed for the light-exposed sample before denaturation (blue), as compared to light protected *Ll*TrxR having λ_{max} = 456 nm (green). After reconstitution of FAD in the presence of 2.0 M GdmCl the light-exposed sample obtains a λ_{max} = 452 nm (red), while light-protected maintains a λ_{max} = 456 nm (purple). Similar shifts are observed when FAD is reconstituted in presence of 3.0 M GdmCl. The spectra were normalized to the 450 nm peak for comparison.

2.2.2 Direct DTNB reduction by NADPH via *Ll*TrxR

In order to evaluate the disulfide reductase activity of photo-inactivated *Ll*TrxR independent of Trx, a direct DTNB reduction experiment was performed (NADPH → *Ll*TrxR → DTNB). *Ll*TrxR was first photo-inactivated for 2 h along a control wrapped in foil. The activity was then determined in an assay with higher concentration of DTNB (8 mM) and *Ll*TrxR (250 nM) than in the standard assay using Trx, as described in section

2.2.1. As seen from figure 22, the activity after irradiation was decreased to ~22% of the original activity, which is in the same range as when assayed with *Ll*TrxA (26%) in the standard assay (section 2.4.2). This result indicates that the light inactivation is not a consequence of specific impaired capacity of *Ll*TrxR to reduce Trx, but rather related to a general incapability act as a disulfide reductant.

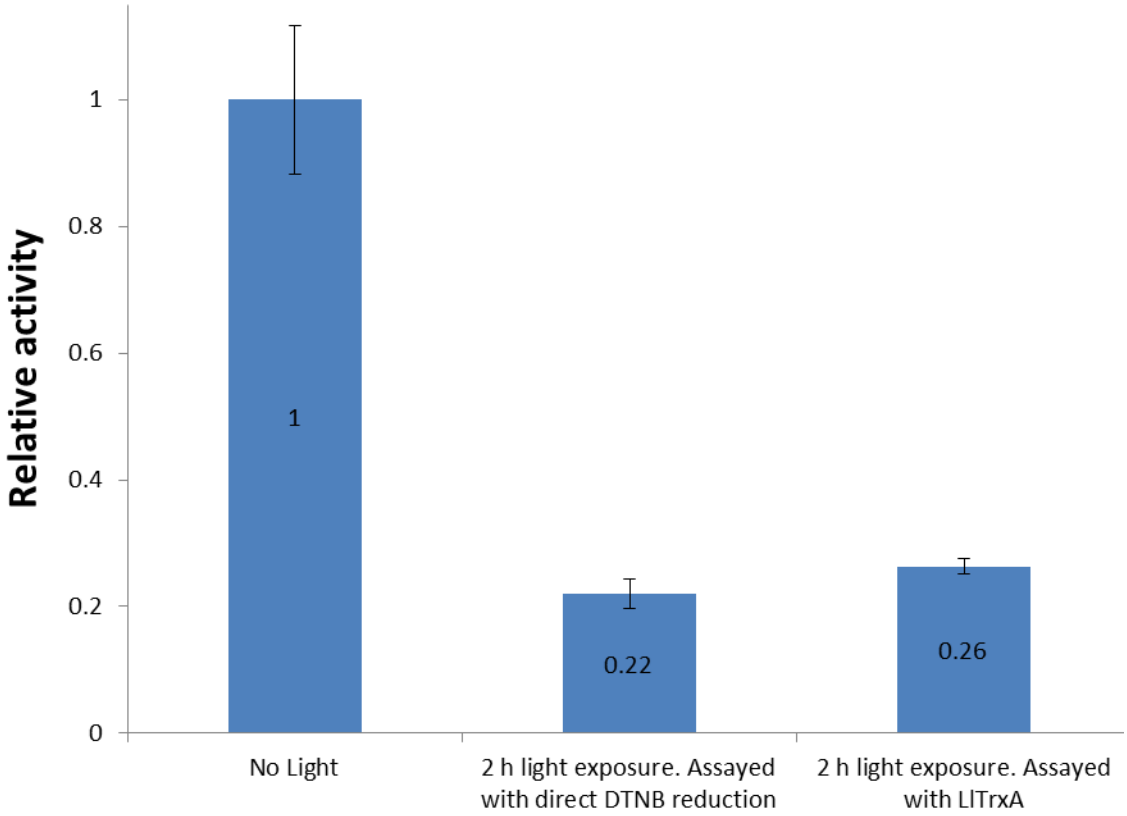

Figure 22. Relative initial rates of DTNB reduction by *Ll*TrxR (incubated 2h with or without light), with no thioredoxin. The assay is performed with higher concentration of DTNB (8 mM) and *Ll*TrxR (250 nM) and fueled by a standard concentration of NADPH (0.2 mM). As seen the activity is diminished to 22% after irradiation, which is in the same range (26%) of decrease as observed as when assayed in the standard DTNB assay using *Ll*TrxA as electron shuttle, as described in section 2.2.1. The error bars indicate the standard deviations.

2.2.3 Optimizing the separation of photo-inactivated *Ll*TrxR

Size exclusion chromatography (SEC) of 16 h (2.5% remaining activity) irradiated *Ll*TrxR using 100 mM potassium phosphate pH 7.4, 1 mM EDTA as separation buffer, reveals the presence of three distinct species (figure 23). The presence of the two minor peaks suggests that light-inactivation induce formation of low-abundant species with altered hydrodynamic volumes. The species with the smallest hydrodynamic volume elutes at 147 mL, the main component elutes at 126 mL, while the species with the largest hydrodynamic volume elutes at 110 mL on a HiLoad Superdex 75, prep grade, 26/60 column (GE Healthcare). No significant FAD absorption at 445 nm (the λ_{max} of this light exposed sample) and 380 nm is detected in the 145 mL peak whereas the 110 mL peak has detectable FAD absorption. The 280/445 nm ratios are 7.7 and 6.1 for the 110 mL and 126 mL peaks, respectively. SEC of non-irradiated *Ll*TrxR also displays a very small fraction of the same 110 mL peak (data not shown). However, the photo-induced species seem to maintain a hydrodynamic radius close to the native form of the protein suggesting maintained structural integrity.

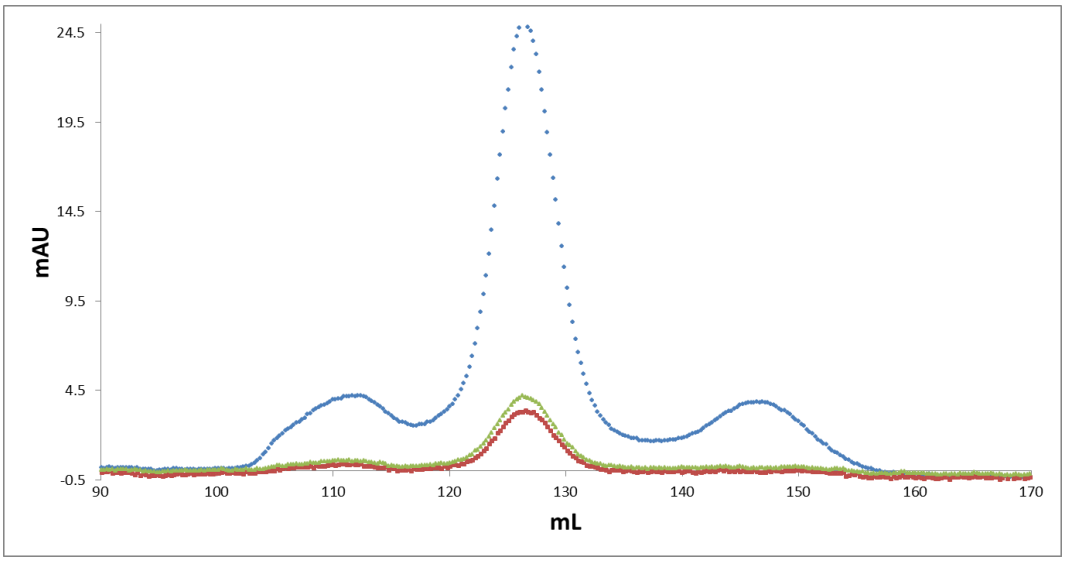

Figure 23. Size exclusion chromatogram of irradiated *Ll*TrxR using HiLoad Superdex 75, prep grade, 26/60 column (GE Healthcare). Absorbance was monitored at 280 nm (blue), 380 nm (red) and 445 nm (green). The separation buffer was 100 mM potassium phosphate pH 7.4, 1 mM EDTA. Three distinct species eluted from the column with peaks at 110, 126 and 147 mL with the middle peak being the major. The 110 and 127 mL peaks display FAD absorbance at 380 and 445 nm, while the 147 mL peak does not display any detectable absorbance at these wavelengths.

SDS-PAGE of DTT-reduced light-exposed *Ll*TrxR revealed a minor band corresponding to dimeric *Ll*TrxR (described in more detail in section 2.2.5) as seen in figure 24. In addition the band corresponding to monomeric *Ll*TrxR in the photo-inactivated sample becomes less defined (more blurry) as compared to non-irradiated protein. The bands of the 110 and 147 mL peaks were too weak to detect dimer formation.

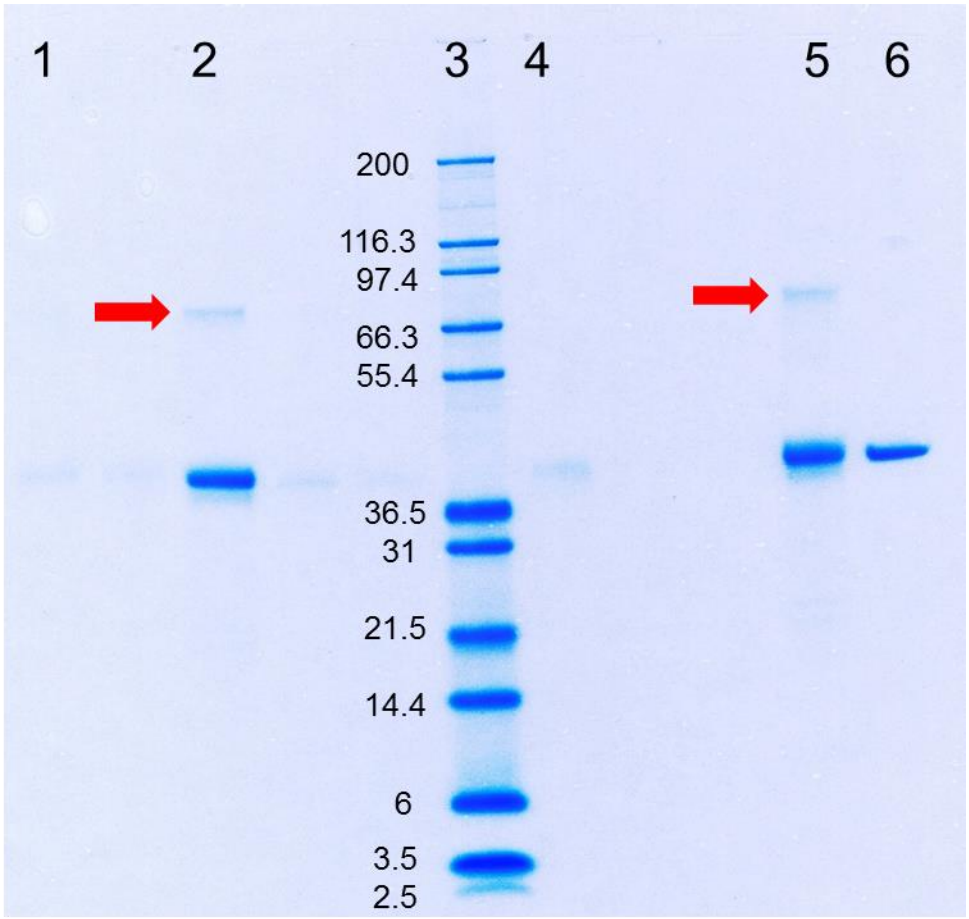

Figure 24. SDS-PAGE of DTT-reduced light-exposed *Ll*TrxR, before and after SEC separation into three different species. Lanes 1, 2 and 3 is *Ll*TrxR from SEC peak 110, 126 and 147 mL, respectively. Lanes 5 and 6 are before SEC, with and without light exposure, respectively. Dimer formation correlating with the mass of ~72 kDa (red arrows) is observed at lanes 2 and 5. The bands of the monomer around 36 kDa in lanes 2 and 5 are less defined (more blurry) and compared to the band of the light protected sample (lane 6). The concentration of *Ll*TrxR from the two minor peaks (lanes 1 and 4) are too low to detect a potential dimer band. Mark 12 is used as molecular weight standard (lane 3).

Several attempts were made to improve the separation of the different forms of photo-inactivated *Ll*TrxR, in order to obtain a homogenous preparation for crystallization trials. The most successful approach was to apply 1 mL irradiated *Ll*TrxR (typically 50 µM) on a HiLoad Superdex 75, prep grade, 16/60 column (GE Healthcare) using 10 mM HEPES, 200 mM NaCl, 2 mM EDTA, pH 7.0 with a flowrate of 1 mL min^{-1} and subsequently dialyzing the fractions of the main peak against the crystallization buffer. As seen from figure 25, this procedure resulted in improved separation of the main peak from the two minor peaks, as exemplified by chromatograms of 120 and 360 min photo-inactivated *Ll*TrxR. As in the SEC experiments outlined above (figure 23) the presence of two low-abundant peaks are observed after photo-inactivation at 47 and 59.5 mL with the main peak eluting at 52.5 mL as monitored with 280 nm absorbance (figure 25). The species with the largest hydrodynamic volume (eluting at ~47 mL) is the first to be observed during irradiation and is also observed in the non-irradiation population, though to a very small extent. The species with a smallest hydrodynamic volume (eluting at ~59.5 mL) is observed after prolonged light-inactivation and does not display FAD absorbance suggesting that the co-factor is absent. This protocol was judged to provide sufficient resolution in order to isolate the major peak of the photo-inactivated *Ll*TrxR prior to crystallization trials.

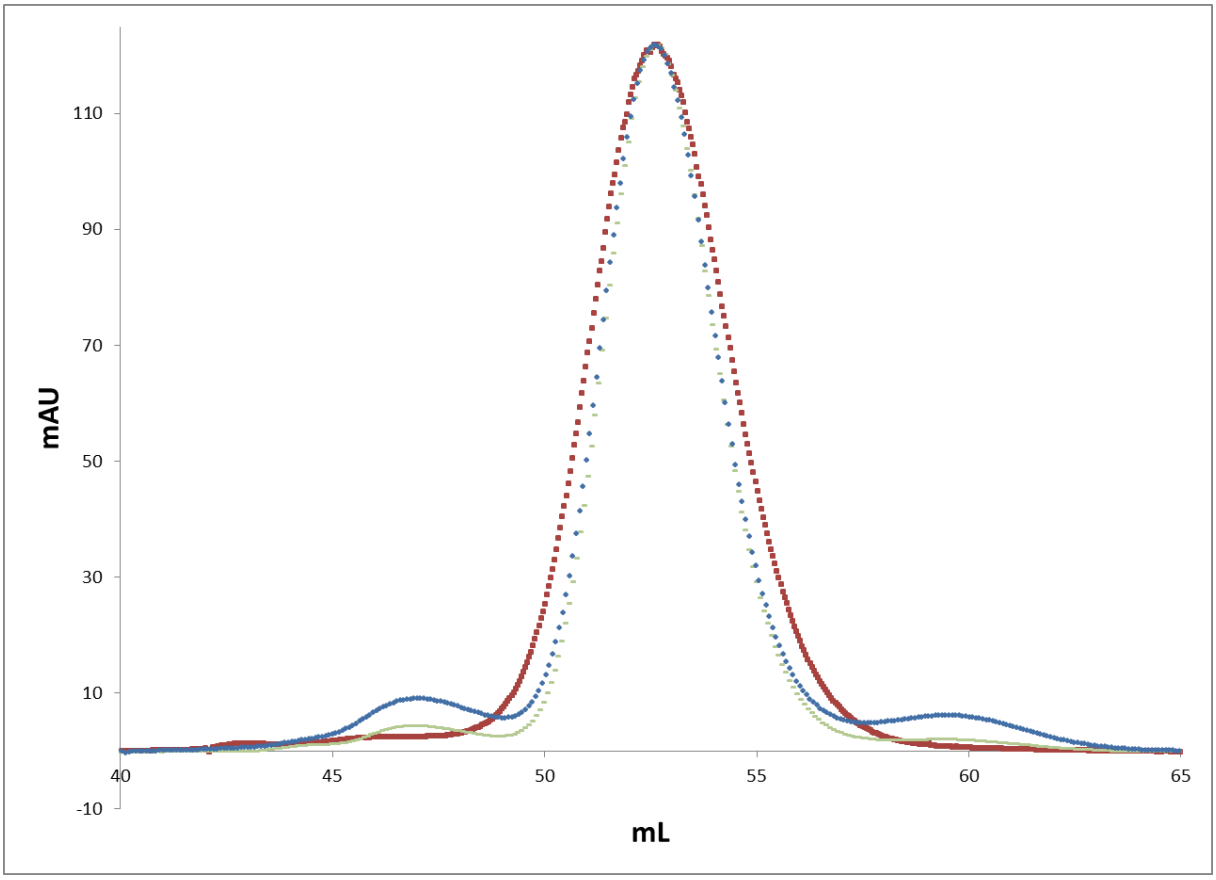

Figure 25. Preparative SEC of irradiated *Ll*TrxR for crystallization purpose. Chromatograms showing 280 nm absorbance of *Ll*TrxR applied on HiLoad Superdex 75, prep grade, 16/60 column using 10 mM HEPES, 200 mM NaCl, 2 mM EDTA, pH 7.0 with a flowrate of 1 mL min^{-1}. No light (red), 120 min light (green) and 360 min light (blue). The chromatograms were normalized for comparison.

2.2.4 Mass spectrometry on intact *Ll*TrxR

Light-protected and photo-inactivated (16 h) *Ll*TrxR was analyzed by mass spectrometry. When analyzed in the non-denatured and light-protected form *Ll*TrxR appears as a dimer with the expected M_w of 73532.00 Da including the tightly bound FAD (figure 26).

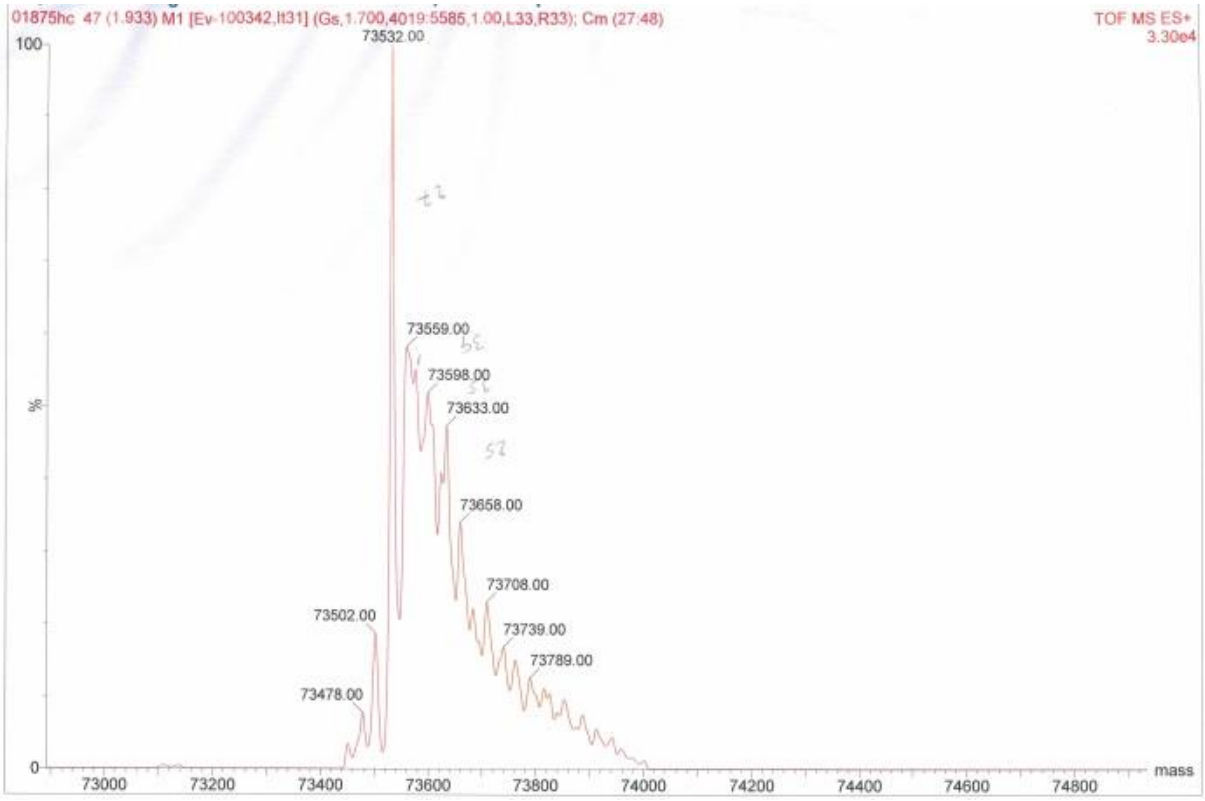

Figure 26. Deconvoluted mass spectrum of light-protected and native *Ll*TrxR. The main peak of 73532.0 Da matches the theoretical M_w of the oxidized dimeric *Ll*TrxR with two FAD bound (73532.6 Da).

In the denatured form light-protected *Ll*TrxR instead appears as a monomer without bound FAD (M_w 35981 Da), as seen in figure 27.

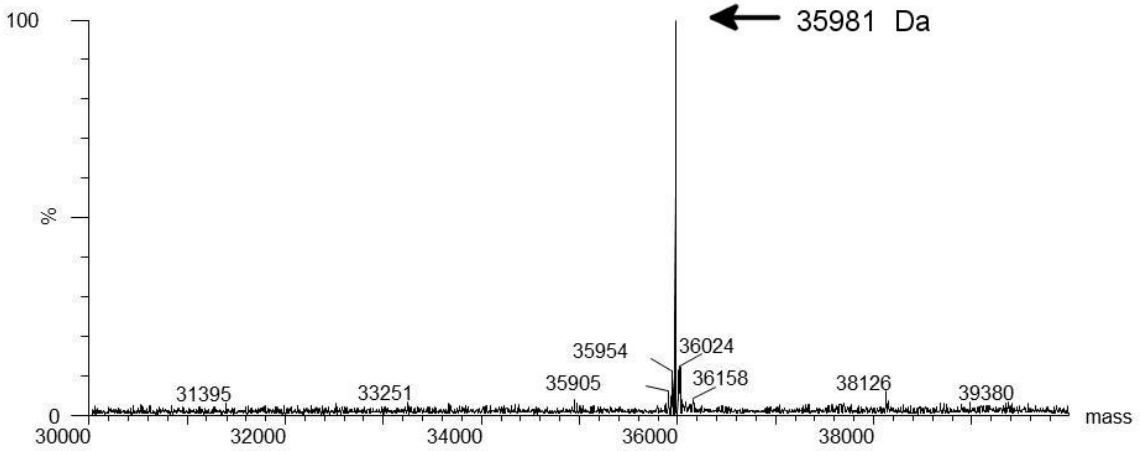

Figure 27. Deconvoluted mass spectrum of light-protected denatured *Ll*TrxR. The main peak of 35981 Da matches the predicted theoretical M_w of the oxidized *Ll*TrxR polypeptide of 35980.74 Da.

Upon photo-inactivation the mass of the denatured *Ll*TrxR is increased with a not well-defined main peak of ~36074 Da, which indicates a more heterogenous population of modified polypeptides (figure 28).

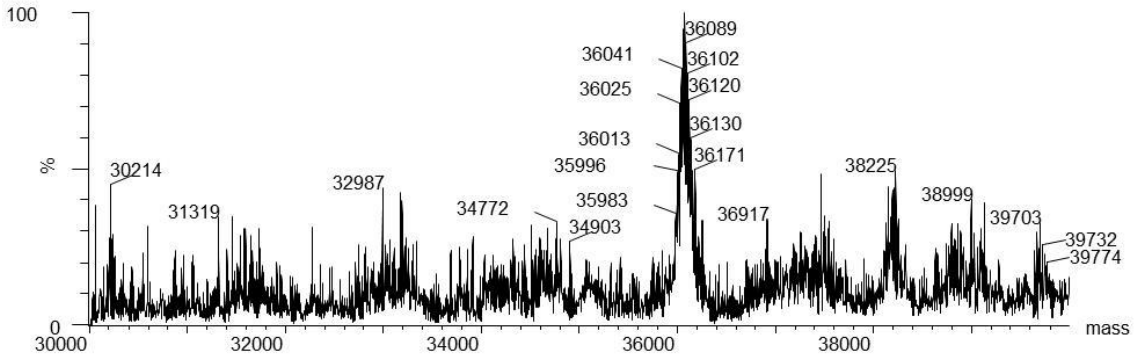

Figure 28. Deconvoluted mass spectrum of photo-inactivated denatured *Ll*TrxR. The main peak with a maximum at 36074 Da is not well-defined, which indicates a heterogeneous population of modified polypeptides.

One oxidative modification that was later discovered in the crystal structure (and verified by LC-MS peptide mapping of the GluC digested protein) was Tyr237 converted to 3,4-dihydroxyphenylalanine (DOPA) (chapter 3), but other oxidations on the protein cannot be excluded.

FAD extracted from *Ll*TrxR with formic acid was also examined. The light-protected FAD gave the expected mass with +1.01 Da increase arising from the protonated form of the monoisotopic mass (785.15 Da), see figure 29.

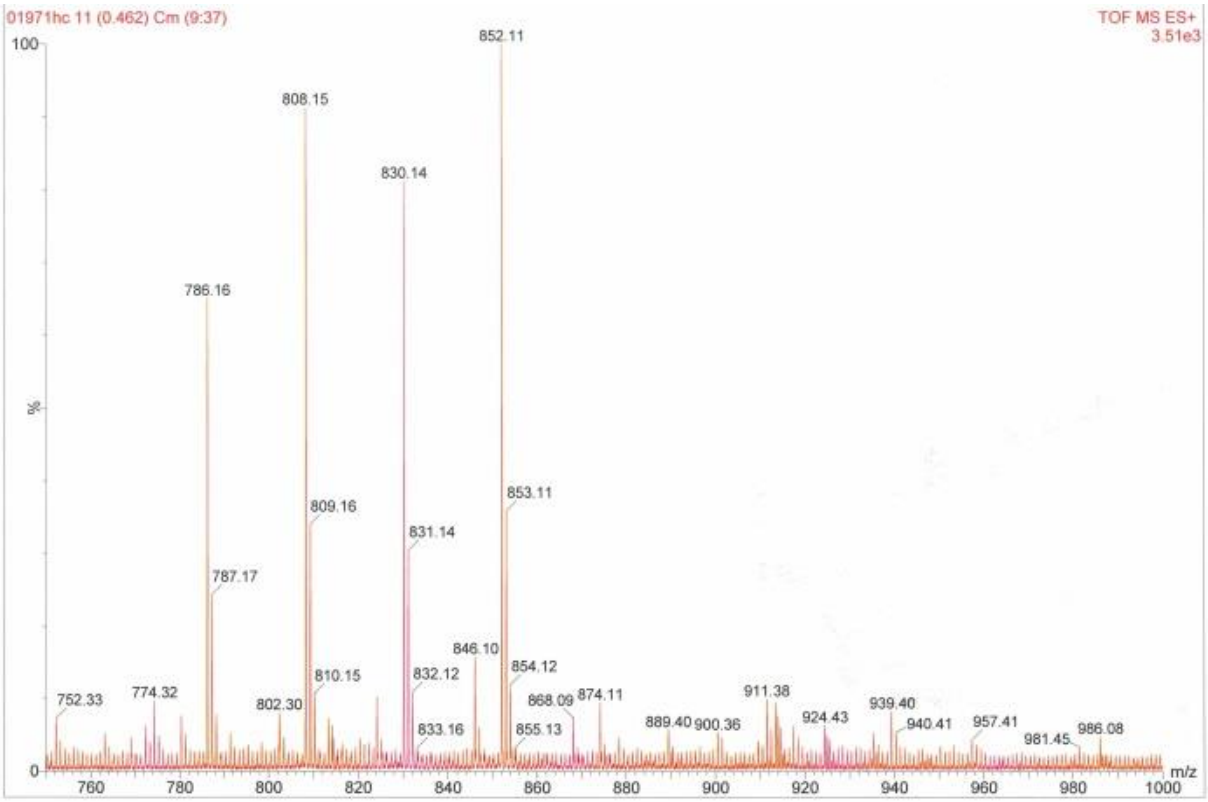

Figure 29. Mass spectrum of FAD released from non-irradiated *Ll*TrxR. The theoretical monoisotopic mass of FAD is 785.15 Da and in the spectrum the protonated form is observed at 786.16 m/z. Sodium adducts account for peaks at 808.15, 830.14 and 852.11 Da.

FAD released from the light exposed *Ll*TrxR (16 h) verified the previous results (Paper 1, supplementary figure S6) giving +13.98 Da (800.14 m/z) and +29.98 Da (816.14 m/z) mass increases (figure 30).

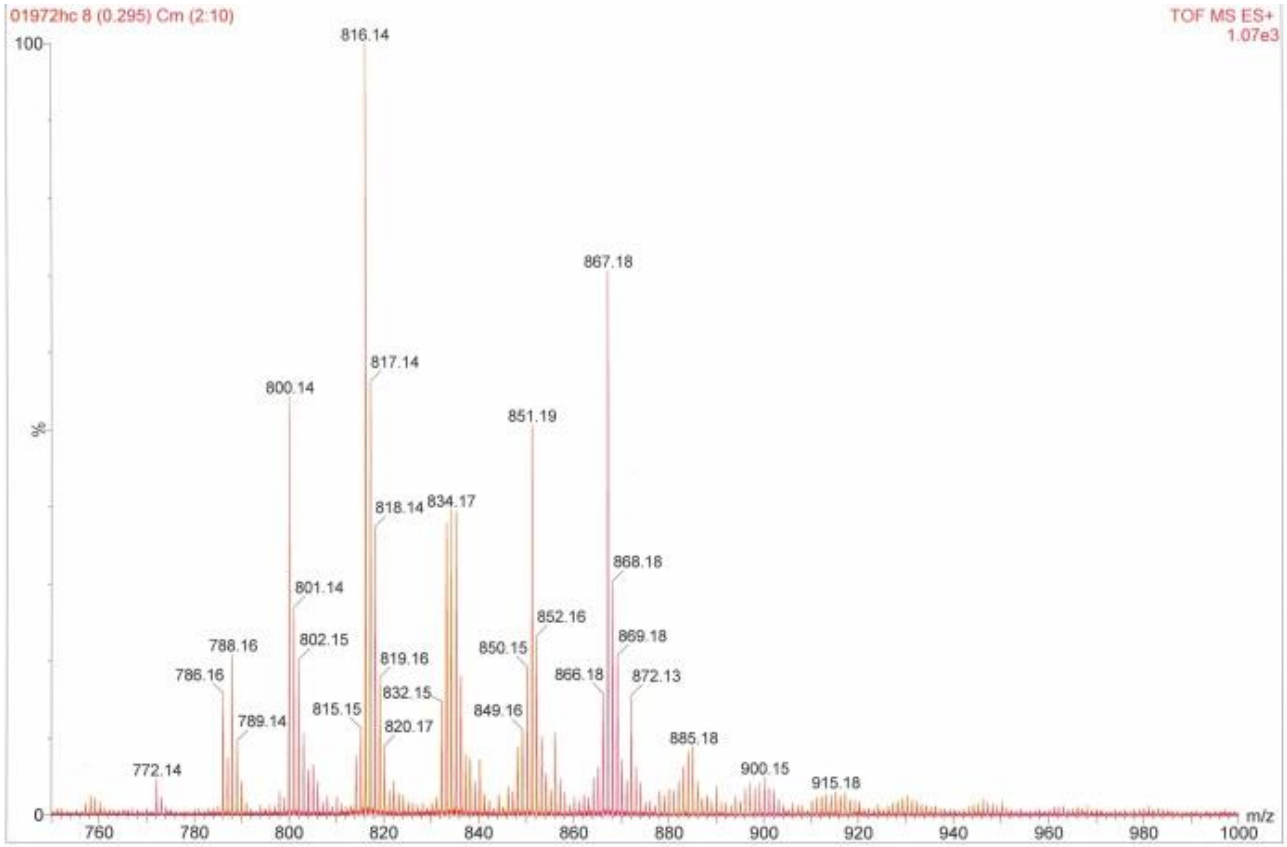

Figure 30. Mass spectrum of FAD released from 18 h irradiated *Ll*TrxR. The intensity of the unmodified FAD is very weak (786.16 m/z). Peaks at 800.14 (aldehyde formation) and 816.14 m/z (carboxylic acid/aldehyde+alcohol) are observed in alignment with previous data (Paper 1, supplementary figure S6).

The 800.14 m/z peak corresponds to a mass increase of 13.98 Da (from the unmodified FAD at 786.16 m/z) that can be explained by an aldehyde formation at one of the two methyl groups on the isoalloxazine ring, as already reported (Paper 1). The 816.14 m/z peak identified indicates a further addition of an oxygen atom to the FAD. This total mass increase of 29.98 Da could originate from an oxidation of the aldehyde to carboxylic acid or from the formation of a hydroxyl group at the other methyl group.

2.2.5 Partial GluC protease digestion of photo-inactivated *Ll*TrxR

To test if photo-inactivation affects the FO/FR equilibrium of *Ll*TrxR the protein was digested with GluC, an endoproteinase that selectively cleaves peptide bonds on the C-terminal side of glutamic acid residues. The strategy was inspired inspired by Mulrooney & Williams 1997, who demonstrated that native *Ec*TrxR trapped in FR conformation, showed specific cleavage sites upon partial GluC digestion, as a consequence of altered surface-accessible residues.SDS-PAGE was performed on samples of light-protected and photo-inactivated (16 h) *Ll*TrxR digested with GluC for 1½ h (lanes 2 and 3, respectively), 3 h (lanes 4 and 5, respectively) and 6 h (lanes 6 and 7, respectively), see figure 31. In the photo-inactivated samples proteolytically generated bands were observed at ~5 and ~14 kDa (red circles), whereas the light-protected *Ll*TrxR seems to be more resistant to protease digestion. Bands with similar masses were previously observed in *Ec*TrxR trapped in FR conformation exposed to GluC proteolysis (Mulrooney and Williams, 1997).

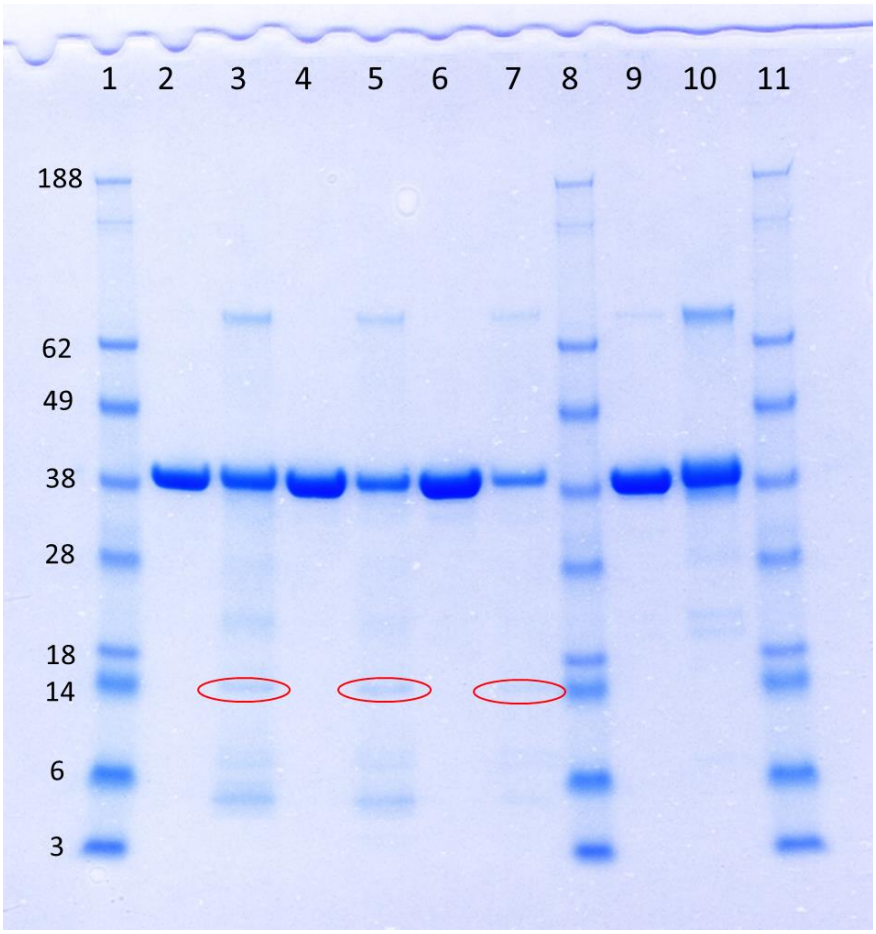

Figure 31. Limited GluC proteolysis of photo-inactivated and light-protected *Ll*TrxR. Lanes 2, 4, 6 and 9: Light-protected *Ll*TrxR GluC digested for 1½, 3, 6 and 0 h, respectively. Lanes 3, 5, 7 and 10: Photo-inactivated *Ll*TrxR (16 h irradiated) GluC digested for 1½, 3, 6 and 0 h, respectively. The 14 kDa bands in lanes 3, 5 and 7 are indicated with red circles, arising as a consequence of GluC cleavage of irradiated *Ll*TrxR. Lanes 1, 8 and 11: Molecular weight standards: SeeBlue® protein ladder with masses given in kDa.

As already described a non-reducible dimer is observed (~72 kDa) and the monomer band (36 kDa) becomes more blurry in photo-inactivated *Ll*TrxR (figure 31). Interestingly, for the photo-inactivated *Ll*TrxR both the monomer and dimer appear to be susceptible to GluC digestion, while the monomer from the light protected *Ll*TrxR appears to be GluC resistant. In the non-digested samples weak bands are observed at ~28, ~22 and ~24 kDa, which are most likely caused by light-induced oxidative damage that may induce fragmentation of the polypeptide backbone, though these are only minor products, as judged from the intensities of the bands.

The 14 kDa band was only observed in *Ec*TrxR when trapped in FR conformation with phenylmercuric acetate (PMA) (Mulrooney and Williams, 1997). Similarly a 14 kDa band is observed for irradiated *Ll*TrxR (figure 31), but not observed for the non-digested irradiated LlTrxR, suggesting that it appears as a consequence of GluC cleavage of irradiated *Ll*TrxR. Though it has to be mentioned that a major difference compared to Mulrooney & Williams, 1997 is that the efficiency of the proteolytic digestion is much lower for *Ll*TrxR. N-terminal sequence analysis of the 14 kDa band from *Ec*TrxR concluded that it originates from the amino terminus and a cleavage site at Glu123 or Glu124 (Appendix C for sequences) was suggested, yielding peptides with molecular weights of 13,569 and 13,440 kDa, respectively (Mulrooney and Williams, 1997). Similar masses are predicted from cleavage sites Glu123, Glu124 or Glu125 in *Ll*TrxR (Appendix C), which could be a plausible explanation for the observed band of approximately 14 kDa. These glutamates are all located in the NADPH domain. A comparison of the results of GluC proteolysis of *Ll*TrxR with the experiments with *Ec*TrxR (Mulrooney and Williams, 1997), suggests that the appearance of the band of approximately 14 kDa is correlated with the enzyme being the FR conformation. But the fluorescence data (section 2.2.7 and Paper 1, supplementary figure S5) indicates that FO/FR equilibrium of irradiated *Ll*TrxR might be shifted towards the FO conformation. If this is the case, then the GluC digested photo-inactivated *Ll*TrxR band at ~14 kDa is due to slower dynamics of the NADPH domain, rather than a shift in the FO/FR equilibrium towards the FO conformation.

2.2.6 Stopped-flow spectrophotometry of *Ll*TrxR reduced by NADPH

The spectral differences of the various flavin (e.g. FAD and FMN) redox-ionic-electronic states make it possible to monitor the kinetics of the different steps in TrxR catalysis by measuring the absorbance changes using stopped-flow spectrophotometry. To elucidate the characteristics of the reductive half-reaction (electron transfer from NADPH to FAD) of *Ll*TrxR, a stopped-flow approach was employed as described in Lennon & Williams (1997). By measuring the changes in absorbance of FAD upon establishment of FAD-NADPH charge transfer complexes it is possible to get insight into the different parts of the reductive cycle (Lennon and Williams, 1997).

The first phase observed within the first millisecond after mixing TrxR and NADPH, is seen as (1) a decline in the 456 nm absorbance, (2) with a simultaneous formation of a broad band centered around 580 nm, which is assigned to be a pre-reductive formation of NADPH-FAD_{ox} charge transfer complex (Blankenhorn, 1975), see figure 32. The second phase of FAD reduction is the decay of NADPH-FAD_{ox} charge transfer complex, characterized with (1) an increased rate in the ε_{456nm} diminishment, (2) a decline in the ε_{580nm}, (3) while the 700 nm band formation starts. The latter assigned to represent the $NADP^+$-FAD_{red} charge transfer complex (Blankenhorn, 1975). The third phase is observed as (1) the complete formation of $NADP^+$-FAD_{red} charge transfer complex and (2) is characterized by a slower decrease in ε_{456nm} and ε_{580nm}, (3) while the ε_{700nm} increases (figure 32). FAD reduction can only occur in the FR conformation. As proposed by Lennon & Williams, 1997, the second phase represents FAD reduction of the part of the enzyme population that already was in the FR conformation at the onset of phase 1, while the third phase represents reduction of FAD in the part of the enzyme population that has shifted from the FO to the FR conformation within phase 1 and 2. By determining the absorbance change between the starting points of phase 2 and phase 3 the apparent K_{eq} of the FR/FO equilibrium can thus be estimated (Lennon and Williams, 1997). The absorbance values at the starting points are then used to calculate the ratio of how much the 456 nm extinction coefficient has decreased. As an example if the diminishment in A_{456nm} in phase 2 and 3 is 60% and 23%, respectively, then the apparent FR/FO equilibrium is $K_{eq} = 60/23 = 2.6$.

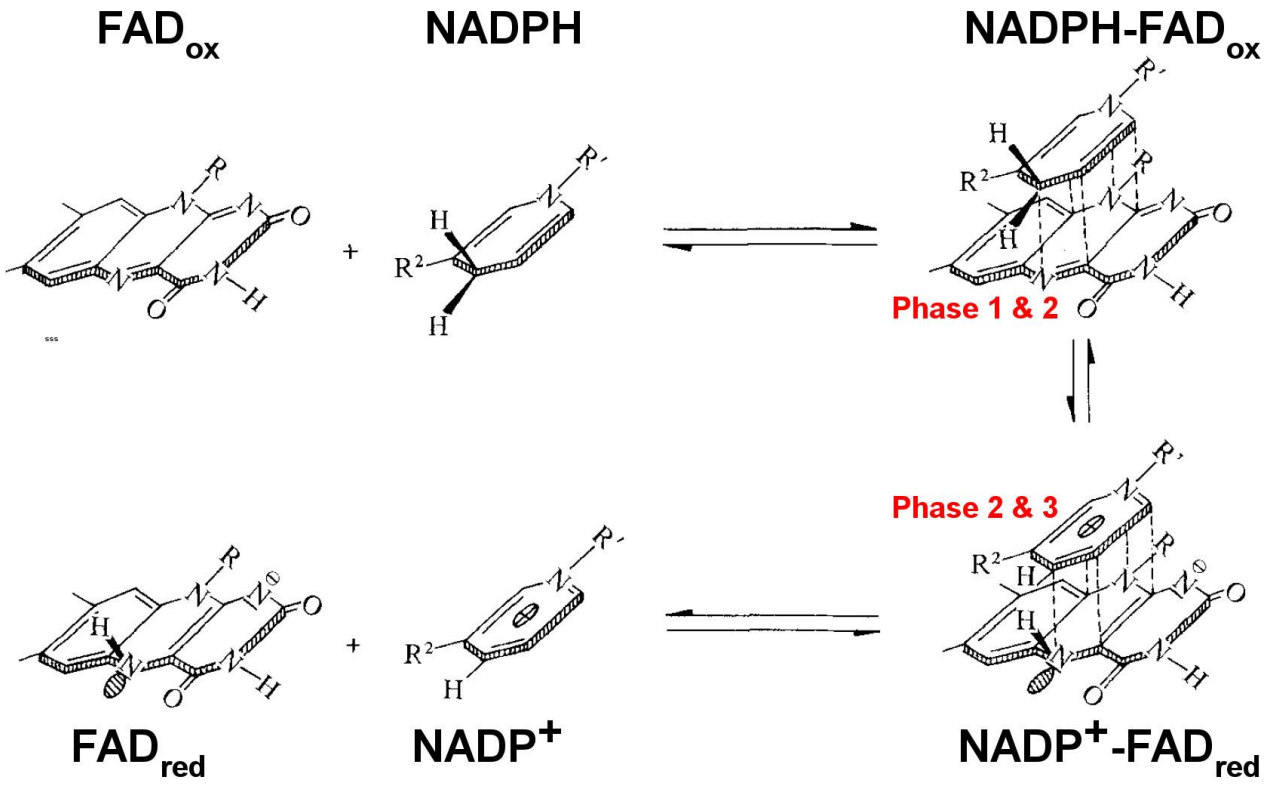

Figure 32. Establishment of charge-transfer complexes between FAD (isoalloxazine) and NADPH (nicotinamide). First, the formation of NADPH-FAD$_{ox}$ charge-transfer complex gives rise to the absorbance band center around 550 nm. Second, the NADP$^+$-FAD$_{red}$ charge-transfer complex is observed as a broad absorbance band around 700 nm. Eventually, the dissociation of the complex gives FAD$_{red}$ and NADP$^+$, which do not absorb in the above regions, indicating that the reductive half-reaction is completed. Note that what is referred to as FAD$_{red}$, is more correctly a FADH$^-$ that has not received the last proton yet. R^2 is methanamide. Note the orientation of the R^2 group, which in NAD(P)H is a primary amide group (discussed in section 3.2.4.2). Modified from (Blankenhorn, 1976).

Here the reductive half-reaction of both *Ec*TrxR and *Ll*TrxR were examined by stopped-flow spectrometry using an instrument connected to both a photomultiplier tube (PMT) set to the wavelength of interest and a photodiode array detector (PDA). However the very low absorbance intensities at 580 and 700 nm were difficult to differentiate from noise in the PMT setup, so eventually the final experiments were performed with PDA, giving full scans during the reaction. TrxR (40 µM) and NADPH (500 µM) were deoxygenated and mixed in a 1:1 ratio in the sample cell. As seen from figures 33 and 34, both *Ll*TrxR and *Ec*TrxR display fast decline in the 456 nm extinction coefficient, upon mixing with

NADPH. The half-life of 456 nm is determined to be 0.015 s and 0.016 s for *Ll*TrxR and *Ec*TrxR, respectively.

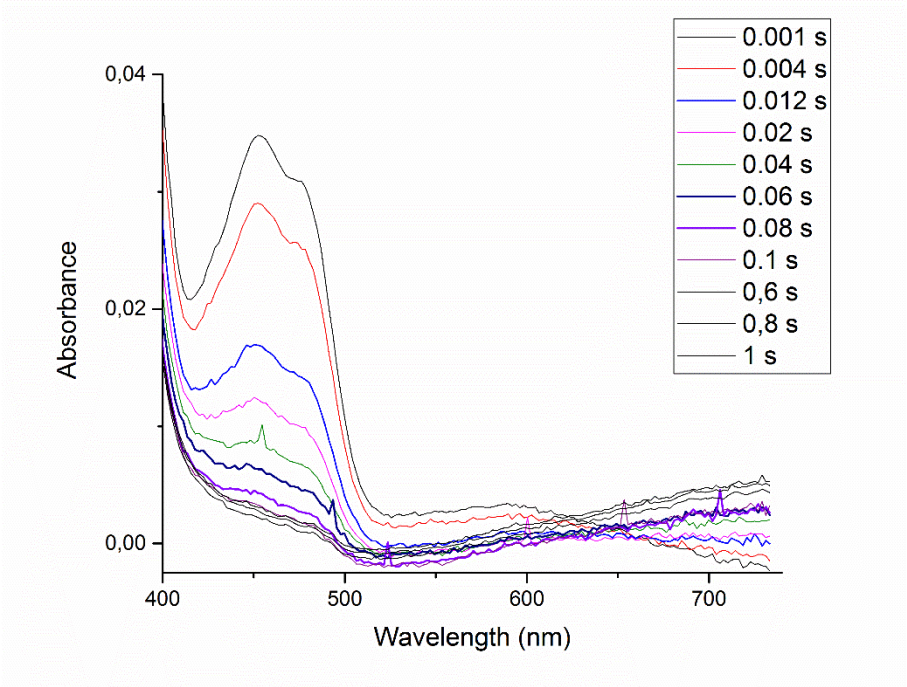

Figure 33. Stopped-flow spectroscopic data of the reductive half-reaction of 20 µM *Ll*TrxR mixed with 250 µM NADPH. In the very first ms of the reductive half-reaction the extinction coefficient of the main peak at 456 nm decreases rapidly. Already within the first 2 ms, a peak at 580 nm appears, which is gone after 12 ms. Interestingly, *Ll*TrxR forms a very intense and long-lived band in the region ~600–720 nm.

Both enzymes have already reached their maximum extinction coefficient at the 580 nm band within the dead time of the instrument. This makes it impossible to calculate the apparent K_{eq}, as the time point of the beginning of the second phase cannot be determined. Therefore it was not possible to accurately determine the FO/FR equilibrium constant in contrast to the previous results reported for *Ec*TrxR (Lennon and Williams, 1997). However, the data shows some other interesting differences in the spectroscopic features of the two enzymes. Remarkably an intense and long-lived band at 700 nm is formed in *Ll*TrxR (figure 33). Even after 1 s the band is still very strong and appears stable. Using

the assignments from the Blankenhorn articles (Blankenhorn, 1975, 1976) this band corresponds to the $NADP^+$-FAD_{red} charge-transfer complex, stabilized in the FR conformation of *Ll*TrxR. In *Ec*TrxR the band at 700 nm is short-lived and appears at the same time as the 580 nm band is observed in the very first milliseconds (figure 34). The half-life of the 700 nm band is 0.055 s and 0.021 s for *Ll*TrxR and *Ec*TrxR, respectively, though the intensity of the band from *Ec*TrxR is too low to give an accurate estimation of this value.

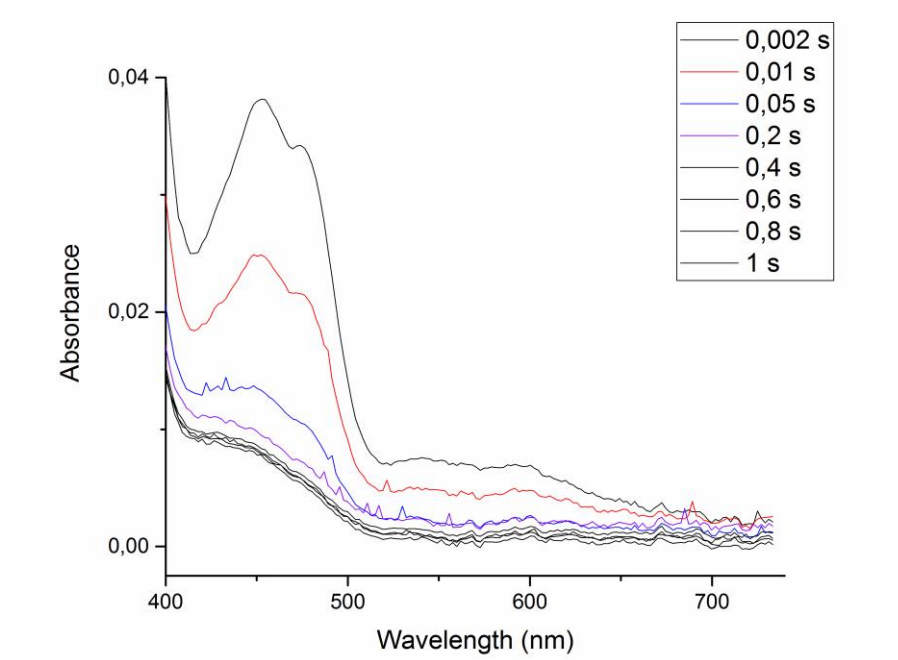

Figure 34. Stopped-flow spectroscopic data of the reductive half-reaction of 20 µM *Ec*TrxR mixed with 250 µM NADPH. In the first 10 ms of the reductive half-reaction the extinction coefficient of the main peak at 456 nm decreases rapidly. The peak centered around 580 nm is only observed within the first 2–10 ms. Contrary to *Ll*TrxR, *Ec*TrxR does not form a strong band at 700 nm, and the changes in absorbance in this region is minute over the course of the reductive half-reaction.

Based on stopped-flow data for *Ec*TrxR (Lennon and Williams, 1997) it was proposed that the rate-limit of the third phase of the reductive half-reaction is neither a consequence of $NADP^+$ release from the enzyme nor reduction with a second equivalent of NADPH, but

instead limited by the conformational change between FO and FR. Based on the observed longer life-time and more intense 700 nm band in *Ll*TrxR it can be speculated that the conformational switch between FO and FR is slower in *Ll*TrxR compared to *Ec*TrxR. Alternatively, the long life-time of the third phase of the reductive reaction may reflect a stabilization of the reduced flavin in *Ll*TrxR in complex with $NADP^+$. Figure 35 shows the references of TrxR mixed with buffer versus mixed with NADPH.

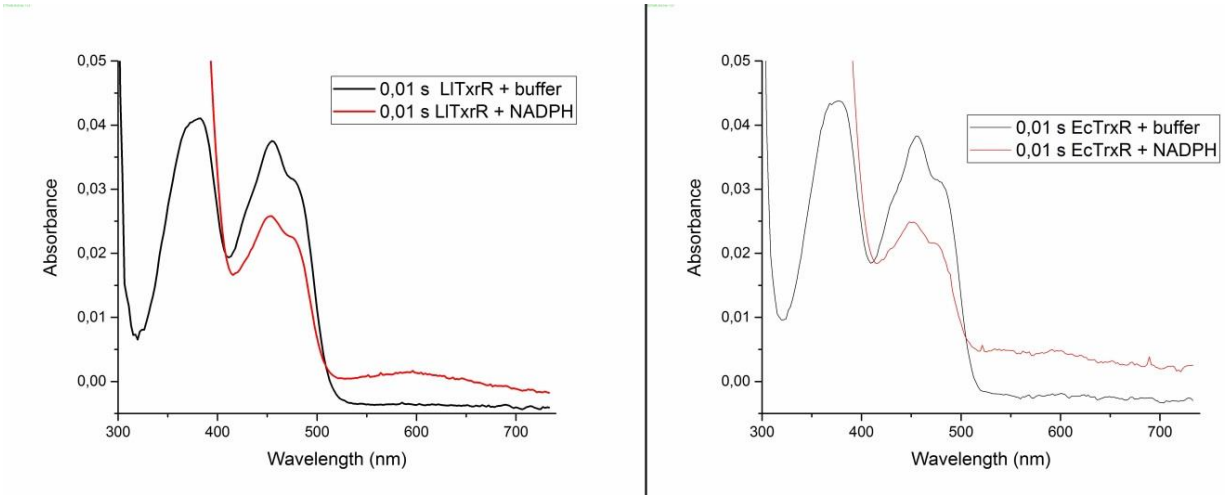

Figure 35. Comparing 20 µM *Ll*TrxR (left) and 20 µM *Ec*TrxR (right) mixed with buffer (black line) or 250 µM NADPH (red line). A broad low intensity band is seen centered around 580 nm for *Ll*TrxR and as a more permanent increase from ~520-720 nm for *Ec*TrxR after mixing with NADPH. These broad bands are seen even within the dead time of the instrument, which makes it impossible to determine the start of phase 2 and phase 3 (red line). TrxR mixed with buffer gives the characteristic oxidized FAD absorbance spectrum (black line).

*Ll*TrxR light inactivated under standard condition for 3 h was also subjected to stopped-flow analysis (figure 36). The inactivated *Ll*TrxR shows very different absorbance changes during reduction. Firstly the decline in ε_{456nm} is not complete as seen for native *Ll*TrxR. The inactivated *Ll*TrxR is not fully reduced as judged from the 456 nm peak after 1 s. A plausible explanation for this inefficient reduction could be that the oxidized FAD has altered chemistry properties and redox potential. Secondly, the absorbance in the 500–720

nm region remains essentially unchanged throughout the measurements. This feature is in strong contrast to the non-irradiated *Ll*TrxR (figure 33).

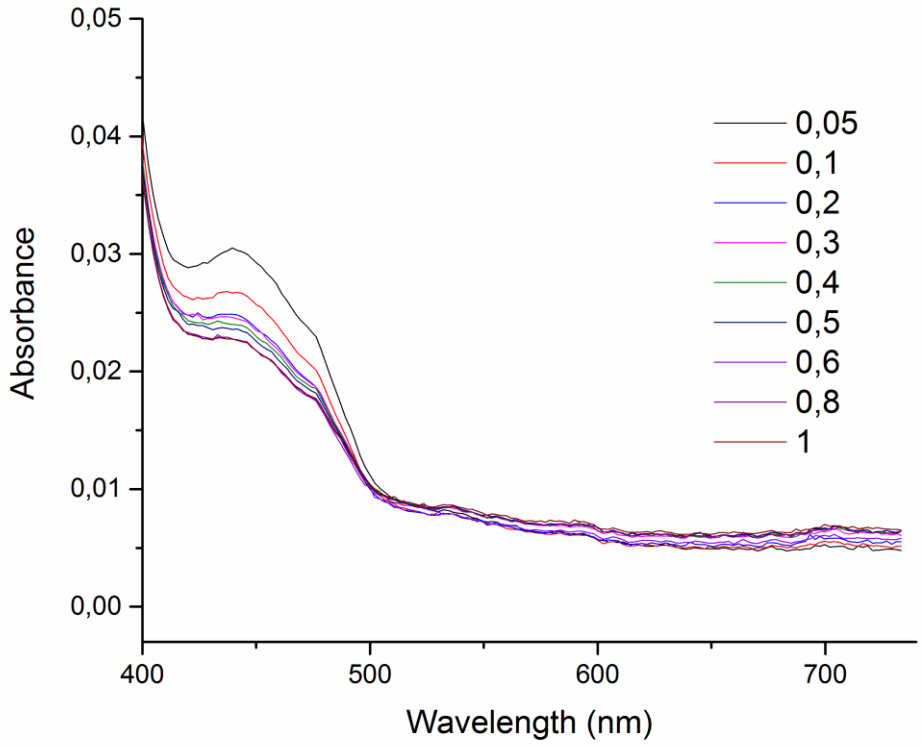

Figure 36. The spectrum of the reductive half-reaction of light inactivated (3 h) *Ll*TrxR (30 µM) show distinct features compared to the light protected samples. Firstly, the irradiated *Ll*TrxR does not seem to be fully reduced within the recorded time (1 s), as judges from the 456 nm absorbance. Generally only minor changes in the 450 nm peak appear and the 500–700 nm region has a higher absorbance that appears more or less constant over the course of the recorded time.

2.2.7 Fluorescence of FAD bound and released from *Ll*TrxR

The maximum fluorescence emission signal of *Ll*TrxR excited at 450 nm is shifted from 515 nm to 505 nm in the photo-inactivated enzyme. Interestingly, the fluorescence intensity yield also decreases in the inactivated form (figure 37). The lowered quantum yield of FAD could either be a direct consequence of a change in the oxidized FAD's ability to form hydrogen bonds with the protein or it could be because of the FO/FR equilibrium constant

of *Ll*TrxR is shifted towards the FO conformation. The latter is surported by the observation that an increase in quantum yield was observed when *Ec*TrxR was trapped in FR conformation with PMA (Mulrooney and Williams, 1997). When the FAD is heat-extracted from *Ll*TrxR the fluorescence intensities of the native and photo-inactivated forms are identical, underlining that the change in fluorescence intensities of bound FAD is in fact a consequence of the protein environment around the flavin. After the FAD is released from the protein, the minor blue-shift of the irradiated sample still remains.

The quantum yield of 450 nm excited *Ec*TrxR is about 3-fold lower than that of *Ll*TrxR (Paper 1, supplementary figure S5). With the above argumentation this indicates that the *Ec*TrxR is shifted towards the FO conformation, relative to *Ll*TrxR. Another explanation could be that the hydrogen-bonding pattern surrounding the FAD of *Ec*TrxR and *Ll*TrxR are different. However, the local environment surrounding the FAD appears to be similar in the crystal structures of *Ll*TrxR and *Ec*TrxR (section 3.2.4.2). As mentioned in the Paper 1 the decrease in quantum yield may also be a consequence of more rigidly fixed isoalloxazine ring system in the FO conformation (Heelis, 1982).

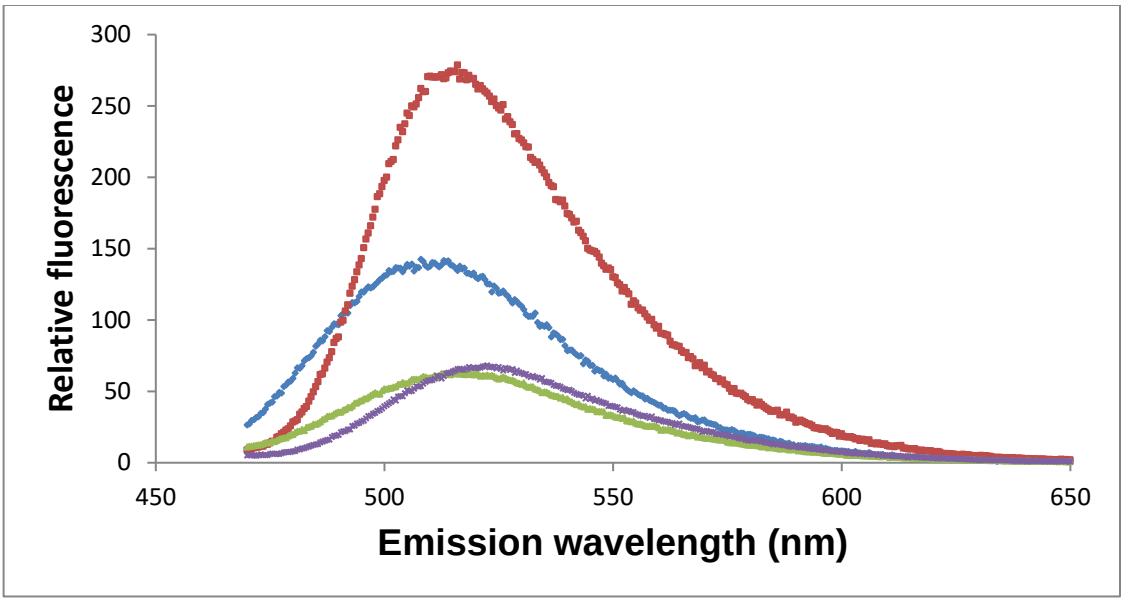

Figure 37. FAD fluorescence spectra from *Ll*TrxR, protein bound or released (red and purple, respectively) and from irradiated *Ll*TrxR, protein bound and released (blue and green, respectively). After irradiation the quantum yield of FAD diminishes and the maximum is shifted from 515 nm to 505 nm. Upon release from *Ll*TrxR the quantum yield is similar for the two FAD molecules. Excitation wavelength is 450 nm.

2.2.8 Light inactivation and activity of *Ll*TrxR, *Sa*TrxR, *Bs*TrxR and *Ec*TrxR

In order to examine the light sensitivity of other thioredoxin reductases, TrxR from *S. aureus* (*Sa*TrxR) and *B. subtilis* (*Bs*TrxR) were compared to *Ll*TrxR and *Ec*TrxR. The background for selecting TrxR from these organisms was that both belong to the *Firmicutes* phylum as *L. lactis*, with *B. subtilis* sharing the same class (Bacilli). The inactivation was performed in the same way as done previously with *Ll*TrxR with controls wrapped in foil. The activity was determined in an NADPH/TrxA assay measuring increase in absorbance at 412 nm. Controls wrapped in foil did not exhibit significant changes in activity and are not included in the figure.

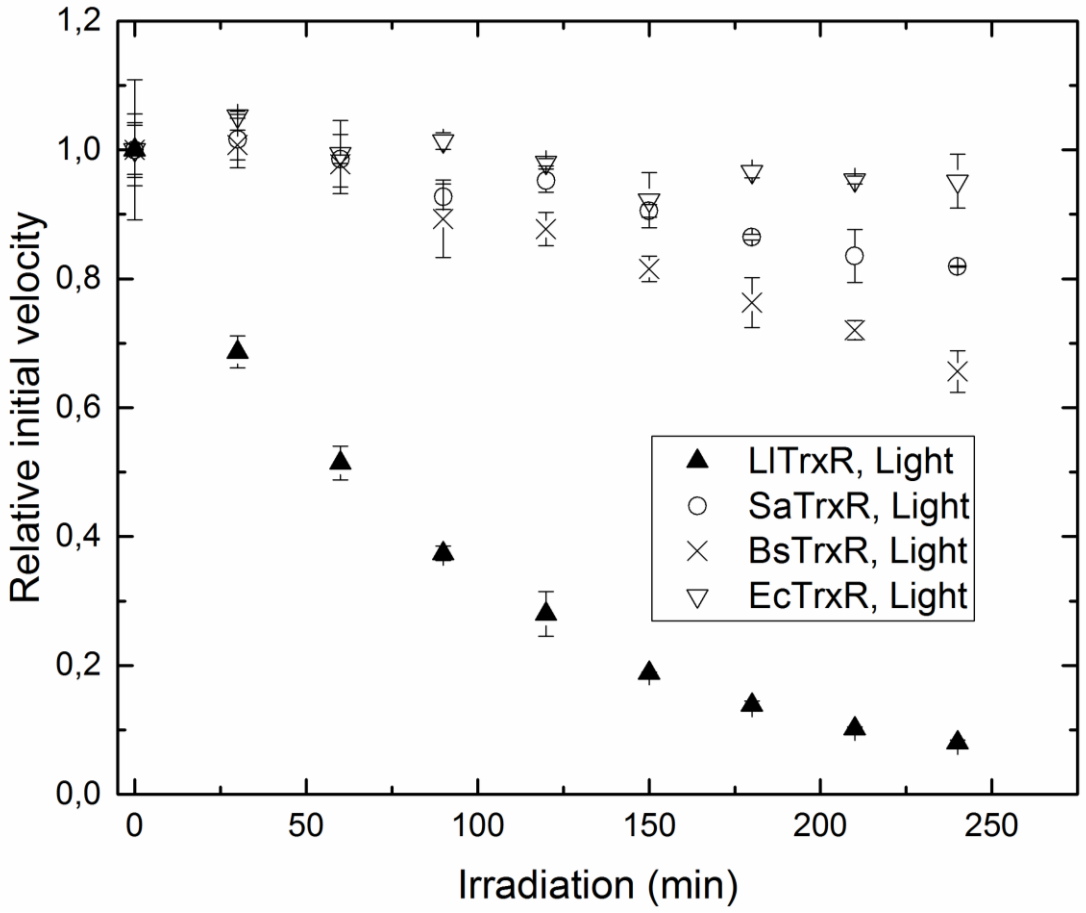

Figure 38. Relative activity of TrxRs from *L. lactis* (▲), *S. aureus* (○), *B. subtilis* (×) and *E. coli* (▽), as a function of irradiation time. With a remaining activity of 8% after 240 min irradiation *Ll*TrxR display higher light sensitivity than the other TrxR. *Bs*TrxR, *Sa*TrxR and *Ec*TrxR have a remaining activity of 65, 82 and 95% after 240 min of light exposure. The error bars indicate the standard deviations.

As seen from figure 38 *Ll*TrxR displays a much higher sensitivity towards visible light that *Bs*TrxR, *Sa*TrxR and *Ec*TrxR. After 240 min of light exposure *Ll*TrxR remained 8.0% activity, while *Ba*TrxR, *Sa*TrxR and *Ec*TrxR had 66, 82 and 95% activity remaining. It has to be noted that the half-life of the *Ll*TrxR activity in this experiment is ~60 min, while the previously determined half-lives have been determined to ~35 min (Paper 1).

The 240 min photo inactivated/protected *Ll*TrxR from this experiment was used to confirm the presence of Tyr237 oxidation to 3,4-dihydroxyphenylalanine (DOPA) observed in the photo-inactivated *Ll*TrxR structures (Paper 2, supplementary figure S1a and S1b).

*Bs*TrxR and *Sa*TrxR do show higher photo-sensitivity than *Ec*TrxR, but not to the same extent as *Ll*TrxR. The structure of *Sa*TrxR (PDB 4GCM) and the predicted structure of *Bs*TrxR, both reveal the same FAD *si*-face oxygen pocket as described in *Ll*TrxR (see section 3.2.5). This observation suggests that other factors also influence the degree of light sensitivity of these enzymes. As discussed in section 3.2.7, the presence of the disulfide near the flavin in FO conformation may quench the excited state of the isoalloxazine.

2.2.9 Oxygen Reduction by TrxRs in presence of NADPH

During the characterization of *Ll*TrxR it was discovered that it exhibits a much higher rate of O_2 reduction than the *E. coli* homologue and that the capacity to reduce O_2 was retained in the photo-inactivated enzyme (Björnberg et al., 2015). The most likely product of this reaction is hydrogen peroxide, *e.g.* two-electron transfer from NADPH to O_2. It is thus conceivable that the ability to reduce O_2 may be linked to the generation of ROS during light exposure, as both processes require molecular oxygen in the vicinity of the isoalloxazine ring. In order to determine the O_2 turnover of the TrxR from *S. aureus and B. subtilis*, NADPH oxidation was monitored as decrease in 340 nm with varying TrxR concentrations. Figure 39 shows the initial NADPH oxidation as function of TrxR concentration, with the slopes giving the turnover values displayed in table 2.

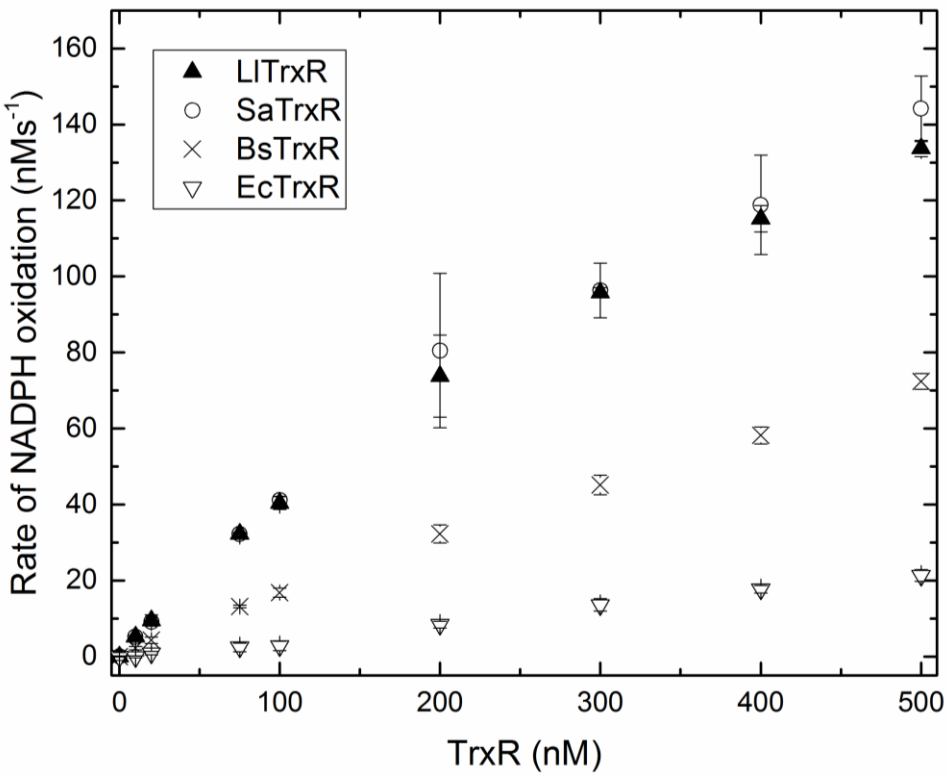

Figure 39. The initial velocity of NADPH oxidation as a function of TrxR concentration. *Ll*TrxR (▲) and *Sa*TrxR (○) display approximately the same degree of NADPH oxidation, while *Bs*TrxR (×) has approximately the half activity. *Ec*TrxR (▽) shows the lowest NADPH oxidation rate of the four investigated TrxRs. The error bars indicate the standard deviations.

Table 2. The NADPH turnover is calculated based on the slopes in figure 39 and *Ll*TrxR light-inactivation data are from figure 38.

	NADPH oxidation turnover (s^{-1})	Relative NADPH turnover (*Ec*TrxR as reference)	Photo-inactivation, 240 min (percentage)
***Ll*TrxR**	0.270 ± 0.0150	6.1	92
***Sa*TrxR**	0.286 ± 0.0153	6.4	18
***Bs*TrxR**	0.143 ± 0.0023	3.2	34
***Ec*TrxR**	0.045 ± 0.0012	1	5

Combining the ability to reduce O_2 with the degree of light sensitivity of the four TrxR no clear correlation is observed. *Ec*TrxR exhibits the lowest O_2 reduction and highest light robustness. *Sa*TrxR on the other hand has the same NADPH turnover as *Ll*TrxR, but is

much less light-sensitive than *Ll*TrxR. The same is the case when comparing *Sa*TrxR with *Bs*TrxR, with the latter being more light-sensitive and having lower NADPH turnover. This indicates that different factors are in play for the two processes. First and foremost, both processes depend on the ability to accommodate molecular oxygen close to the isoalloxazine ring, which will be elaborated in detail from the structures in section 3.2.5. Other factors determining the kinetics of NADPH oxidation are the rate of electron transfer from FAD to molecular oxygen, exchange of $NADP^+$ with NADPH and accommodation of a new O_2 in the active site. The rate of light inactivation is dependent on several factors; the generation of triplet state flavin, the life-time of the triplet state and its ability to generate ROS (most likely O_2^- and/or $^1O_2$) and finally the rate with which the ROS generates oxidative protein modifications. Taking all these factors into account, it might not come as a surprise that there is not a clear correlation between O_2 reduction and light sensitivity, as this would require that the two processes depend on the same rate-limiting factors. In chapter 3 the structures of *Ll*TrxR and *Sa*TrxR are compared and differences in the environment of ROS formation are discussed.

L. lactis utilizes the NADH oxidases Nox-1 and Nox-2 during aerobic growth to reduce molecular oxygen to restore the NAD^+ pool, producing H_2O_2 and H_2O, respectively (Higuchi et al., 1999). These flavo-enzymes display a different mechanism involving O_2 reduction through a covalent C4a-peroxyflavin intermediate, often stabilized by a positive charge (McDonald et al., 2011), that can further dissociate to form hydrogen peroxide (Kemal et al., 1977; Mattevi, 2006). NADH oxidases depending on these types of reduction mechanisms typically operate with k_{cat} values above 100 s^{-1} (Niimura et al., 1995). The rate of TrxR catalyzed O_2 reduction is of a different order of magnitude, and it seems unlikely to depend on the same C4a-peroxyflavin intermediate mechanism.

2.2.10 Cell extract inactivation and activity of native *Ll*TrxR

The *Ll*TrxR examined so far has been recombinantly expressed in *E. coli*. In order to evaluate the sensitivity of native TrxR in an environment resembling the conditions *in vivo*,

cell extracts of mid-late exponential phase cultures of *L. lactis* MG1363 and *E. coli* K-12 were subjected to irradiation over a period of 12 h. At different time points TrxR activity was determined in a coupled assay with NADPH and the respective Trx using DTNB as final electron acceptor. A clear decrease in DTNB reduction was observed in the *L. lactis* cell extract over the course of irradiation, indicating loss of *Ll*TrxR activity, while the activity in the *E. coli* cell extract was unchanged (figure 40 and 41). After 12 h the TrxR activity (relative initial velocity) was diminished to ~35% in the *L. lactis* cell extract, in an assay with addition of recombinant *Ll*TrxA. The slower rate of inactivation of native *Ll*TrxR compared to the recombinant enzyme is likely due to light-quenching by endogenous chromophores.

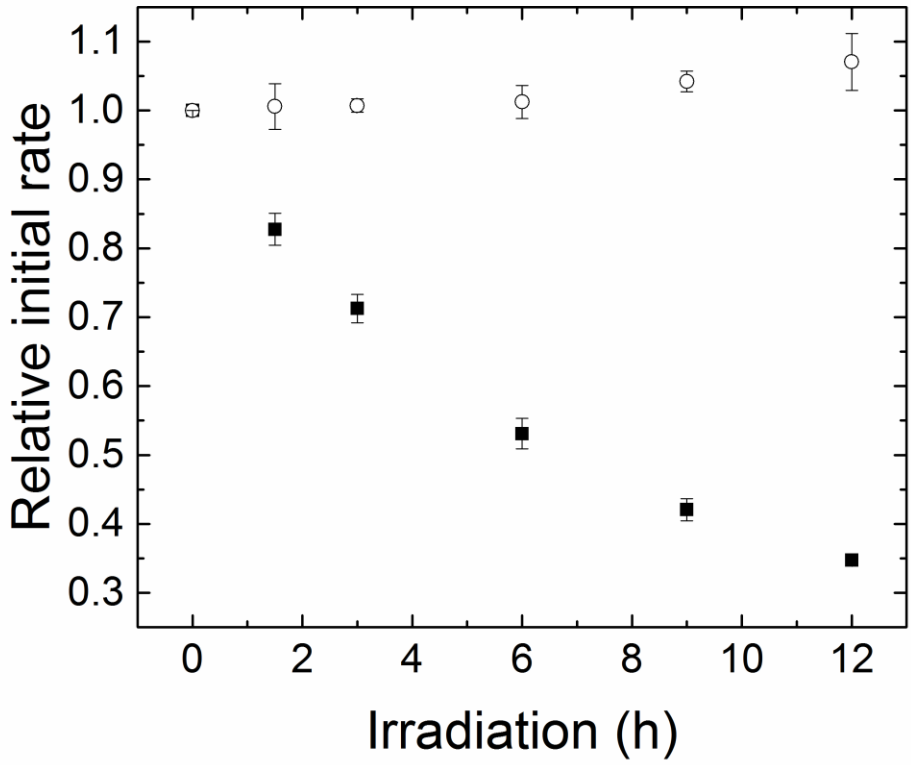

Figure 40. Activity of *Ll*TrxR in cell extract was quantified by DTNB reduction with NADPH and *Ll*TrxA. Light exposed cell extracts (■) and light protected controls (○) wrapped in foil and relative initial rates were calculated at various time points. After 12 h light exposure ~65% of the activity was lost, while the light protected showed no impact. The error bars indicate the standard deviations.

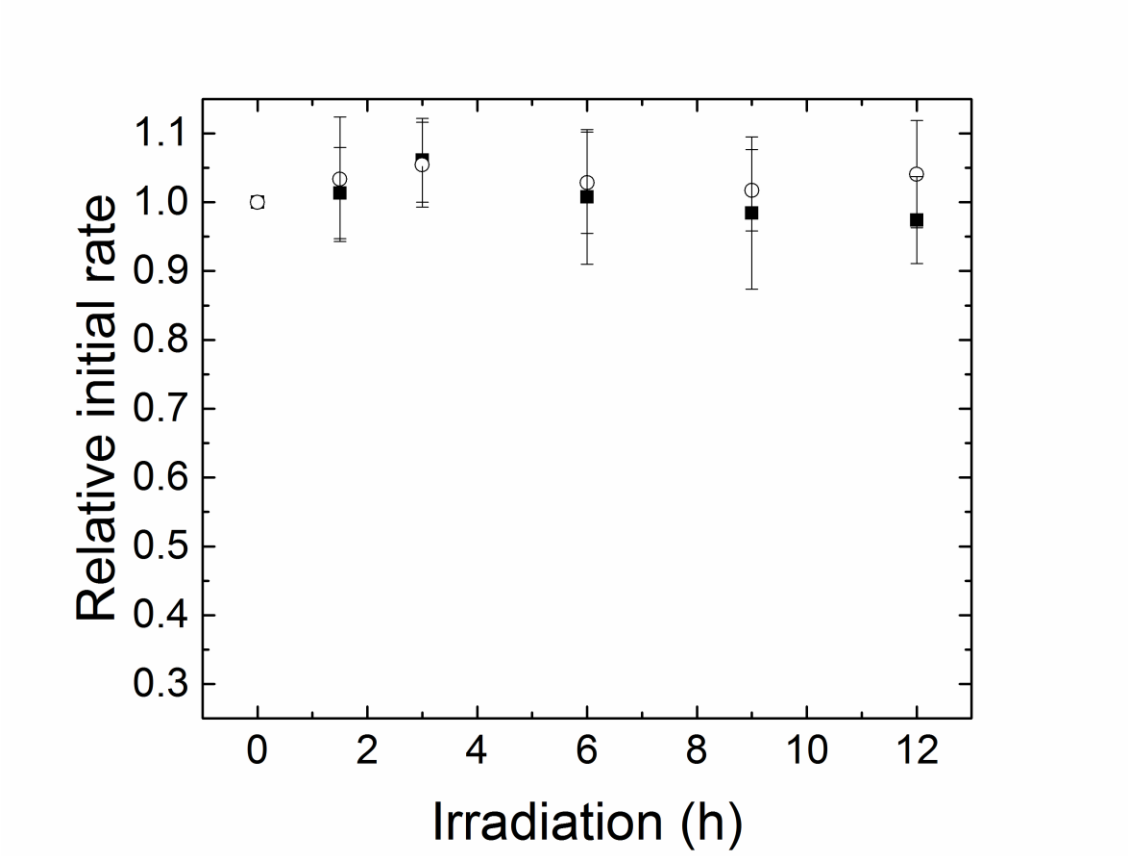

Figure 41. Activity of *Ec*TrxR in cell extract was quantified by DTNB reduction with NADPH and *Ec*Trx1. Light exposed cell extracts (■) and light protected controls (○) wrapped in foil. After 12 h light exposure no significant loss of activity was observed, as compared to the light protected sample. The error bars indicate the standard deviations.

These results underlines that native *Ll*TrxR is indeed sensitive to light, even in the natural environment. Assuming an exponential decay of the photo-inactivation of *Ll*TrxR, the graph has the equation $y = e^{-0.094x}$ ($R^2 = 0.98$), giving a half-life of 7.4 h of inactivation, significantly higher than the ~35 min half-life of the recombinant *Ll*TrxR (Björnberg et al., 2015). The activity was also measured without addition of thioredoxin (*Ll*TrxA and *Ec*Trx1) in the assay, which gave the same overall picture, though the final remaining activity of light inactivated *Ll*TrxR after 12 h was ~45% rather than 35%. The assay performed with thioredoxin significantly boosted the DTNB reduction, suggesting the TrxR in the cell extract is not the rate limiting factor of the thioredoxin system *in vivo*.

2.2.11 Photo-inactivation of TrxR in intact *L. lactis* cells

After confirming the inactivation of native *Ll*TrxR in *L. lactis* cell extract the next step was to evaluate the light sensitivity of *Ll*TrxR in intact cells. Given that TrxR is the electron donor for NrdH in *L. lactis*, which in turn transfers electrons to ribonucleotide reductase, responsible for maintaining the deoxynucleoside triphosphate (dNTP) pool needed for DNA replication, an active TrxR is of crucial importance to the proliferating cell. Although *L. lactis* MG1363 with a *trxB1* knockout has been reported to be viable (Vido et al., 2005), the growth of this knockout strain was critically low, especially in the first 7 h. In other organisms like *B. subtilis* TrxR has been reported essential for survival (Scharf et al., 1998).

In order to measure the correlation of TrxR activity and viability of *in vivo* irradiated cells, large amounts of cell mass is required and the irradiation is performed on harvested exponentially growing cells maintained in physiological sodium chloride at 4–5°C with a very high cell density (OD_{450} = 2-3). This simplified system has the advantage that it prevents cell growth (lowers the metabolism) and translation of new TrxR during irradiation, while enabling Colony Forming Unit (CFU) measurements. A potential drawback is that intracellular O_2 levels may be increased because the activity of the NADPH oxidases (NOX proteins) is lower than normal at the low temperature of 4–5°C. The experimental model may thus not accurately resemble the actual *in vivo* state in metabolically active bacterial cells, but it provides a conceptual idea as to whether visible light can impact viability and activity of *Ll*TrxR in the cell. After light exposure cells were harvested, CFU determined and pellets were examined for TrxR activity. As this experiment only has been performed once with one time point after 17 h of visible light exposure, the results should be viewed as preliminary. Although the dilution of light exposed cells are out of range the results still indicate that visible light indeed impacts the ability for *L. lactis* to form colonies, as the light protected controls are consistent in colony formation (table 3).

Table 3. Colony Forming Unit (CFU) of *L. lactis* from standard agar plates (D=8.5cm) after 17 h of visible light exposure. Each of the three biological replicates (#1, #2 and #3) has been made in technical duplicate (10^{-6} and 10^{-7} dilution in 0.9% NaCl).

Sample	Colony count	Sample	Colony count
Light#1 (dilution 10^{-6})	0	**No Light#1 (dilution 10^{-6})**	16
Light#1 (dilution 10^{-7})	0	**No Light#1 (dilution 10^{-7})**	2
Light#2 (dilution 10^{-6})	0	**No Light#2 (dilution 10^{-6})**	28
Light#2 (dilution 10^{-7})	0	**No Light#2 (dilution 10^{-7})**	2
Light#3 (dilution 10^{-6})	0	**No Light#3 (dilution 10^{-6})**	13
Light#3 (dilution 10^{-7})	0	**No Light#3 (dilution 10^{-7})**	2

The relative *Ll*TrxR inactivation (using initial rates) in cell extract from the light exposed cells, also clearly confirmed the light sensitivity *in vivo*. As seen from table 4, about 10% of the *Ll*TrxR activity remained in the cell extract (comparing the light exposed with controls wrapped in foil as 100%) and slightly more activity remained when NrdH was added to the assay to boost the DTNB reduction.

Table 4. Remaining activity of *Ll*TrxR in cell extract from living *L. lactis* cells exposed to visible light for 17 h, using the initial activity rates, made in technical duplicate for all three biological triplicates (#1, #2 and #3). The relative inactivation is a measure of comparison with the control samples wrapped in foil (100%). The activity of *Ll*TrxR in the cell extract was quantified by DTNB reduction with NADPH and ±*Ll*NrdH. An overall slightly lower relative inactivation is measured when using *Ll*NrdH.

Sample	Percentile remaining *Ll*TrxR activity	Percentile remaining *Ll*TrxR activity (NrdH)
Light#1	10.6	16.0
Light#1	13.4	17.6
Light#2	9.6	13.2
Light#2	8.8	12.7
Light#3	12.6	11.4
Light#3	6.3	14.0
Average	10.3 ±2.6	14.2±2.3

Figure 42 shows the same results as table 4, just giving as absolute initial velocity of DTNB reduction. Here the effect of NrdH added to the assay is clearly visualized.

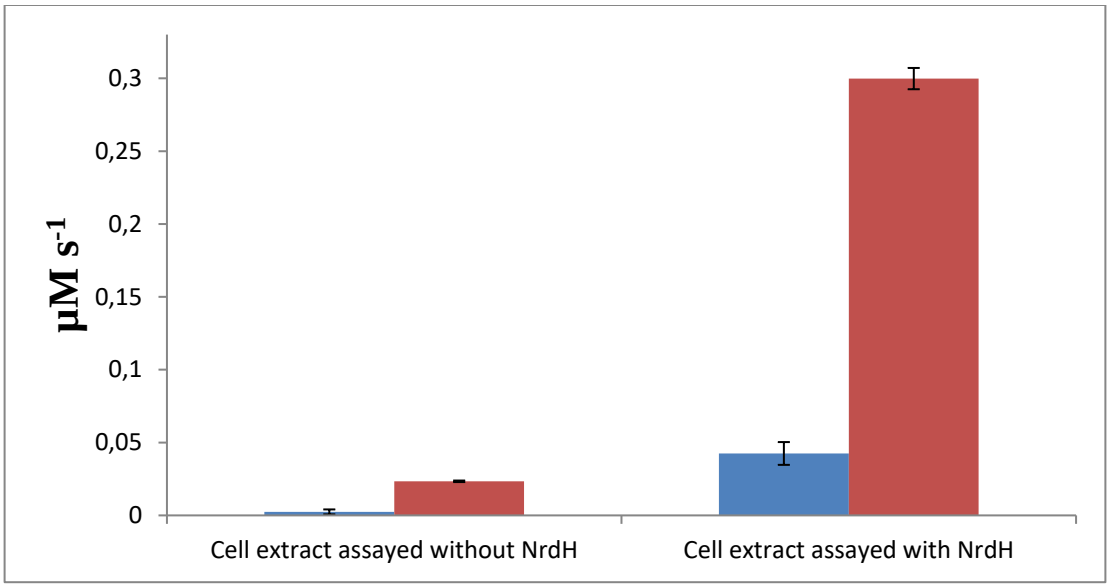

Figure 42. Inactivation of TrxR in cell extract from living *L. lactis* cells exposed to visible light for 17 h (blue), using the initial activity rates of biological triplicates. The activity of *Ll*TrxR in the cell extract was quantified by DTNB reduction with NADPH and ±*Ll*NrdH. *Ll*NrdH is serving to boost the signal, as seen when using *Ll*TrxA in section 2.2.10. A markedly higher DTNB reduction is measured when using *Ll*NrdH in the assay facilitating the electron flow to DTNB. Controls were wrapped in foil (red). The error bars indicate the standard deviations.

Obviously, the experiment needs to be repeated with more technical replicates of the CFU in a measurable dilution range and preferably with several time points over the course of irradiation. *E. coli* would serve as a good control organism, as *Ec*TrxR would be expected to be unimpacted. To confirm the connection between the TrxR sensitivity/robustness and the viability of the cells, the genes encoding the *L. lactis* and *E. coli* TrxR could be switched through recombination. If this leads to light robust *L. lactis* and light sensitive *E. coli* cells this would further strengthen the biological importance of TrxR light sensitivity. A more subtle approach would be to introduce selected mutations in TrxR predicted to cause light sensitivity/robustness, see chapter 3.

2.4 Materials and methods

2.4.1 Protein production, purification and concentration determination

The genetic constructs were made using the pET15b expression vector as previously described (Björnberg et al., 2014). Purification of recombinant N-terminal His-tagged *Ll*TrxR, *Ec*TrxR, *Ll*TrxA, *Ll*TrxD and *Ll*NrdH were prepared using single colonies of *E. coli* Rosetta DE3 strains, containing the plasmids, inoculated into 50 mL LB medium and incubated at 37°C overnight, followed by dilution into fresh 1 L LB medium to reach OD 0.1. Cultures were incubated until OD_{600} of 0.6, IPTG was added (0.1 mM final) and growth continued with individual specifications; *Ll*TrxR (6 h, 30°C), *Ec*TrxR (ON, 20°C), *Ll*TrxA (5 h, 30°C), *Ll*TrxD (5 h, 30°C) and *Ll*NrdH (3h, 37°C). The culture was placed on ice for 30 min, centrifuged (30 min, 4°C, 3000 *g*) and cell pellets were stored at -18°C. Cell pellets were thoroughly resuspended in 15 mL Bugbuster protein extraction reagent (Novagen) containing 25 U Benzonase nuclease (Merck) and incubated at RT for 30 min with slow shaking followed by 30 min centrifugation (16,000g, 4°C). TrxR was added 12 µmol FAD together with the Benzonase. Supernatants were filtered (pore size 0.45 lm) and applied onto HisTrap columns (GE Healthcare) equilibrated with loading buffer 30 mM Tris-HCl pH 8.0, 500 mM NaCl, 10 mM imidazole for *Ll*TrxA, *Ll*TrxD and *Ll*NrdH, while 20 mM potassium phosphate pH 7.4, 500 mM NaCl, 10 mM imidazole was used for the TrxR. Target proteins were eluted using a linear gradient of 10–100% elution buffer (the same buffer containing 400 mM imidazole). Fractions selected based on chromatograms and SDS–PAGE were pooled and dialyzed against 30 mM Tris/HCl, pH 8 for *Ll*TrxA, *Ll*TrxD and *Ll*NrdH, concentrated to ~5 mL (Amicon Ultra 6-8 MWCO), applied to a HiLoad Superdex 75, prep grade, 16/60 or 26/60 column (GE Healthcare) eluted by 30 mM Tris/HCl pH 8, 200 mM NaCl, dialyzed against 30 mM Tris/HCl, pH 8, concentrated (Amicon Ultra 6-8 MWCO), aliquoted and stored at -80°C. After His-trap purification the TrxR were dialyzed against 100 mM potassium phosphate, 1 mM EDTA, pH 7.4, concentrated (Amicon Ultra 6-8 MWCO) without further purification, aliquoted and stored at -80°C. Concentrations of *Ll*TrxA, *Ll*TrxD and *Ll*NrdH were determined using the

previously established extinction coefficients (Björnberg et al., 2014), while the concentrations of *Ll*TrxR, *Ec*TrxR, *Sa*TrxR and *Bs*TrxR were determined by the FAD absorbance, ε_{456} = 11,300 M^{-1} cm^{-1} (Williams et al., 1967).

Recombinant *Sa*TrxR, *Bs*TrxR, *Sa*TrxA and *Bs*TrxA were kindly donated by Claes von Wachenfeldt (Lund University) and had been purified essentially as described above for *Ll*TrxR and *Ll*TrxA. Concentration determinations of *Sa*TrxA and *Bs*TrxA were done by aid of amino acid analysis after hydrolysis for 24 h in 6 M HCl (Barkholt and Jensen, 1989). The molar extinction coefficients (ε_{280}) determined were 14,911 and 14,585 M^{-1} cm^{-1} for *Sa*TrxA and *Bs*TrxA, respectively.

2.4.2 Photo-inactivation of TrxR (standard condition)

Aliquots of *Ll*TrxR produced as described in section 2.4.1 were thawed on ice and diluted to 50 µM (unless stated otherwise) in 100 mM potassium phosphate pH 7.5, 2 mM EDTA, 0.1 mg/mL BSA. Photo-inactivated *Ll*TrxR for crystallization and stopped-flow spectrophotometry was diluted in buffer without BSA (100 mM potassium phosphate pH 7.5, 2 mM EDTA). Photo-inactivation was performed in Eppendorf tubes kept 20 cm below a 1225 Lumen (21 W) fluorescent lamp with a color temperature is 6500 K corresponding to a maximum intensity λ_{max} = 460 nm (Manufacture Leuci (Relco group)) at 4 °C, as standardized previously (Björnberg et al., 2015). Light exposure time performed on *Ll*TrxR varied from 20 to 360 min. The activity assays of *Ll*TrxR were performed immediately after the light exposure period. Controls were treated similarly and wrapped in foil during the light exposure period. The same standardized procedure was performed using *Ec*TrxR, *Sa*TrxR and *Bs*TrxR. To the extent it was possible the TrxR were protected from any ambient light sources.

2.4.3 Reconstitution of irradiated *Ll*TrxR with exogenous FAD

*Ll*TrxR was irradiated for 3 h under standard conditions as described in section 2.4.2. The activity was determined in the presence of 20 nM *Ll*TrxR, 2 µM *Ll*TrxA, 0.20 mM NADPH, and 0.20 mM DTNB (Ellman, 1959) in a 1 mL cuvette, measuring 2-nitro-5-

thiobenzoic acid (TNB) formation at 412 nm. Standard buffer used was 100 mM potassium phosphate pH 7.5, 2 mM EDTA, 0.1 mg/mL BSA. Six hundred times excess of exogenous FAD (12 mM final) was added, relative to enzyme-bound FAD (20 µM) in 1 mL. Subsequently GdmCl was gradually added to reach a concentration of 2.0 or 3.0 M, followed by 21 h incubation with gentle shaking at 4°C. The control was added buffer without GdmCl to reach the same enzyme concentration. The samples were then diluted in 100 mM potassium phosphate pH 7.5, 2 mM EDTA, and 0.1 mg/mL BSA, in several steps to reach GdmCl concentrations of 1, 0.5, and 0.1 M followed by incubations for 18, 1.5, and 3 h, respectively, at 4 °C. The samples were then concentrated to 1 mL by ultrafiltration (Ultra-15 10 kDa MWCO, Amicon), loaded on a PD-10 column (GE Healthcare), and eluted samples were further concentrated (Ultra-0.5 10 kDa MWCO, Amicon) to a final volume of ~0.5 mL. The *Ll*TrxR activity of the samples before and after reconstitution was analyzed as described above and compared to controls incubated without GdmCl. The enzyme concentration was determined by the intensity of the maximum absorbance of peak around 450 nm and adjusted to the defined concentration in the assay.

2.4.4 Direct DTNB reduction via TrxR

*Ll*TrxR was diluted in 100 mM potassium phosphate pH 7.5, 2 mM EDTA, 0.1 mg/mL BSA, to 20 µM and irradiated for 2 h under standard conditions. Controls were wrapped in foil. The ability for *Ll*TrxR to reduce DTNB directly was monitored in a 200 µL format using 8 mM DTNB, 250 nM *Ll*TrxR and 0.2 mM NADPH as final concentrations. The 412 nm increase was monitored spectrophotometrically for 90 s and the initial rates were calculated from the linear slopes (n = 4). The activity of *Ll*TrxR assayed with *Ll*TrxA was determined in the presence of 20 nM *Ll*TrxR, 2 µM *Ll*TrxA, 0.20 mM NADPH, and 0.20 mM DTNB.

2.4.5 Size exclusion chromatography and SDS-PAGE of *Ll*TrxR

Inactivated *Ll*TrxR (section 2.4.2) or light protected *Ll*TrxR (section 2.4.1) were purified by size exclusion chromatography for preparative and analytical purposes. *Ll*TrxR was applied to a HiLoad Superdex 75, prep grade, 16/60 or 26/60 column (GE Healthcare) and eluted by 100 mM potassium phosphate pH 7.4, 1 mM EDTA (analytical purpose) or 10 mM HEPES, 200 mM NaCl, 2 mM Na-EDTA, pH7.0 (for crystallization purpose) at a flow rate of 1.0 ml min^{-1}. Fractions from analytical SEC of *Ll*TrxR were further analyzed by SDS-PAGE; *Ll*TrxR was denatured under reducing condition (4.0 µL lithium dodecyl sulfate, LDS (4x), 1.0 µL DTT (1.0 M) and 11.0 µL sample) and analyzed by SDS-PAGE (Novex® NuPAGE).

2.4.6 Mass spectrometry on intact *Ll*TrxR

Light inactivated and light protected (16 h) *Ll*TrxR were analyzed on an LCT Premier mass spectrometer (Waters, Milford, MA) with a nano-electrospray (nanoES) ion source for native intact protein mass spectrometry. Data was collected in positive ion mode and the instrument was calibrated using 100 mg/mL CsI in 50% (v/v) isopropanol. *Ll*TrxR (21 µM) was exchanged into 100 mM ammonium acetate/ammonium hydroxide, pH 7.4 (Micro Bio-Spin P-6 chromatography columns; Bio-Rad) and sprayed from nano-electrospay capillaries. Analysis of FAD was performed after denaturing *Ll*TrxR with 3% (V/V) formic acid. Analysis of denatured *Ll*TrxR was performed on a Synapt G2-S*i* HSMS (Waters) in positive ion mode.

2.4.7 Partial GluC proteolysis of photo-inactivated *Ll*TrxR

*Ll*TrxR (section 2.4.1) was diluted in 100 mM potassium phosphate pH 7.5, 2 mM Na-EDTA, 0.1 mg/mL BSA to a concentration of 50 µM and irradiated overnight under standard conditions (section 2.4.2). Controls were wrapped in foil. GluC was added in 20:1 ratio relative to *Ll*TrxR (w/w) and the mixtures were incubated at 37°C. At 1½, 3 and 6 h aliquots where removed and the proteolysis was terminated by addition of 0.3 volume of

8% trichloroacetic acid (TCA). From each sample 10 µg *Ll*TrxR was denatured under reducing condition (4.0 µL LDS(4x), 1.0 µL DTT (1.0 M), 1.0 µL MilliQ H_2O and 10 µL sample) and analyzed by SDS-PAGE (Novex® NuPAGE).

2.4.8 Stopped-flow spectrophotometry

An SX20 Stopped-Flow Spectrometer (Applied Photophysics) with a 150 W Ozone producing Xenon lamp, was used to measure kinetics in the reductive half-reaction of TrxR. Both phododiode array (PDA) and photomultiplier (PMT) were used as a detectors. The total drive volume was adjusted to 120 µL. The temperature was kept constant at 10°C. Buffer was used to equilibrate the instrument and TrxR mixed with buffer was used as a reference. Enzyme concentrations after mixing were 20 µM, 20 µM and 30 µM for *Ec*TrxR, *Ll*TrxR and irradiated *Ll*TrxR, respectively. The NADPH:enzyme ratio was kept at 12.5 for all measurements. At all point during the experiment the enzymes were kept away from direct light. NADPH was dissolved in argon-purged MilliQ water to a final concentration of 50 mM, quantified by absorbance measurement (ε_{340} = 6220 M^{-1} cm^{-1}) and stored at -80°C. NADPH and the enzymes were diluted in 100 mM potassium phosphate, pH 7.5 immediately before measurements. Light exposed *Ll*TrxR was diluted in 100 mM potassium phosphate, pH 7.5 to 60 µM and irradiated for 3 h under standard conditions (section 2.4.2). Buffers used for dilution of NADPH and enzymes were contained in vials with septum, and were made anaerobic by bubbling for at least 20 min with molecular nitrogen (AGA Gas (Nitrogen 4.0), 99.9 % purity), before use. Diluted NADPH and enzyme solutions were then further made anaerobic by blowing molecular nitrogen above the solutions for another 20 min. The irradiated *Ll*TrxR sample was deoxygenated for 45 min.

2.4.9 Fluorimetry

*Ll*TrxR was diluted in buffer 100 mM potassium phosphate pH7.5, 2 mM Na-EDTA, 0.1 mg/mL BSA, to a concentration of 5 µM and irradiated O.N. as described in section 2.4.2. Control was wrapped in foil. Fluorescence emission spectra of the *Ll*TrxR samples were recorded (PerkinElmer luminescence spectrometer LS55). Excitation and emission wavelengths (10 nm slit widths) were 450 and 470−700 nm, respectively. FAD was heat-extracted from the *Ll*TrxR by incubating at 75 °C for 20 min. After centrifugation, the supernatants were subjected to fluorescence emission measurements as above.

2.4.10 Light inactivation and activity of *Ll*TrxR, *Sa*TrxR, *Bs*TrxR and *Ec*TrxR

Enzymes were diluted in 100 mM potassium phosphate pH 7.5, 2 mM EDTA, 0.1 mg/mL BSA to final concentration of 20 µM. Samples were simultaneously photo inactivated (section 2.4.2) and samples were withdrawn at intervals (0, 30, 60, 90, 120, 150, 180, 210, and 240 min) during the inactivation and assayed with their respective thioredoxins (20 nM TrxR, 2 µM TrxA, 0.2 mM NADPH and 0.2 mM DTNB) in a 0.2 mL cuvette, measuring TNB formation at 412 nm. All time points were measured in minimum triplicate and the initial rates were used and converted into relative activities.

2.4.11 Oxygen Reduction by TrxRs in the presence of NADPH

*Ll*TrxR, *Ec*TrxR, *Sa*TrxR and *Bs*TrxR were diluted in buffer 100 mM potassium phosphate pH 7.5, 2 mM EDTA, 0.1 mg/mL BSA and NADPH oxidation assayed in buffer containing a final concentrations of 0.2 mM NADPH, forcing O_2 to be the electron accepter. The NADPH oxidation was measured as a decrease in absorbance at 340 nm over 5 min using a quartz cuvette. The initial rates were subtracted the background reaction with no TrxR. All concentrations were measured in minimum triplicate. ε_{340nm} = 6220 $M^{-1}cm^{-1}$ was used to calculate the NADPH oxidation rates. The NADPH oxidation turnover (s^{-1}) was calculated from the slope in the plot of NADPH oxidation as function of TrxR concentration.

2.4.12 Cell extract inactivation and activity of native *Ll*TrxR

Lactococcus lactis subsp. *cremoris* (strain MG1363) was grown in SA medium (Jensen and Hammer, 1993) containing 1% (w/v) glucose and 2 mg/L lipoic acid (GSAL medium). *E. coli* K-12 (strain MG1655) was grown in LB-medium. One liter synchronized cell culture (in biological triplicate) at exponential phase (OD_{600} 0.6–0.7) was placed on ice for 30 min and then centrifuged (4°C). The cell pellet was resuspended in 0.9% NaCl and distributed in ten 2 mL screw-cap microcentrifuge tubes, centrifuged, and the pellets were stored at -20°C until use. Proteins were extracted by adding 600 µL 100 mM potassium phosphate pH 7.5, 1 mM EDTA and 400 µL glass beads ≤ 106 µm (Sigma) to each tube and performing bead beating on a FastPrep FP120 homogenizer (Qbiogene), setting 6 for 30 s, followed by 1 min rest on ice. Bead beating was repeated 6 times followed by centrifugation for 15 min at 13,000g. Benzonase (2 µL) was added to pooled supernatants (~4.5 mL) and incubated for 1 h at 21°C. The protein concentration was determined (Bio-Rad Protein Assay, Life Science Research) using BSA as a standard and the samples were aliquoted and stored at -20°C. Cell extracts were thawed, diluted 1:1 with 100 mM potassium phosphate pH 7.5, 1 mM EDTA and transferred to original 1.5 mL Eppendorf tubes with 6x3 mm magnets, and placed on a stirrer in a cold room at 4°C. The samples were irradiated as described in section 2.4.2. Control samples wrapped in foil are referred to as “No Light”. After 0, 1.5, 3, 6, 9 and 12 h cell extracts were withdrawn and stored at -20°C for subsequent activity measurements. TrxR activity was assayed as DTNB reduction monitored at 412 nm in 150 µL format with 100 mM potassium phosphate, pH 7.5, 2 mM EDTA, 0.20 mM DTNB and 0.20 mM NADPH. For *L. lactis* 30 µL of undiluted cell extract was used in the assay while the *E. coli* cell extracts were diluted 3 times in 100 mM potassium phosphate, pH 7.5, 1 mM EDTA before being added to the assay mixture. The activity of the cell extracts was measured directly or after addition of their respective recombinant thioredoxins (5 µM final concentration), *Ll*TrxA and *Ec*Trx1 (Björnberg et al., 2014). The presence of thioredoxin in the assay boosted the signal ~4 and ~2.3 times for *L. lactis* and *E. coli*, respectively. The initial activities were determined in at least technical triplicates for each biological triplicate.

2.4.13 *Ll*TrxR activity and CFU of light treated *L. lactis*

Lactococcus lactis subsp. *cremoris* (strain MG1363) was grown in SA medium (Jensen and Hammer, 1993) containing 1% (w/v) glucose and 2 mg/L lipoic acid (GSAL medium). Synchronized cell culture (400 mL in biological triplicate) in exponential phase (OD_{450} ~0.5) was placed on ice for 20 minutes and then centrifuged for 5 minutes (5000g, 4°C). Supernatants were discarded and the pellets were resuspended in 100 mL sterile 0.9% NaCl. The resuspended cells were divided in 2x50 mL in glass test tubes (height: 20 cm, diameter: 2.5 cm) and one was wrapped in aluminium foil to protect from light. The cultures were irradiated with a lamp (described in section 2.4.2) kept in a 5 cm distance from the test tubes in the cold-room (4°C). Magnetic stirrers ensured that the whole cell culture was exposed to light. After 17 h irradiation 100 µL cell culture was diluted and plated on GM17 (Oxoid) plates and incubated at 30°C for colony count the preceding day. The rest of the cell cultures were centrifuged (3000g, 4°C), supernatant decanted and the pellets were resuspended in 1 mL 0.9% NaCl and transferred to microcentrifuge tubes with screw cap and centrifuged (4000g, 4°C). Supernatants were removed and pellets stored at -20C. Proteins were extracted by adding 400 µL 100 mM potassium phosphate pH 7.5, 1 mM EDTA and 300 µL glass beads ≤ 106 µm (Sigma) to each tube and performing bead beating on a FastPrep FP120 homogenizer (Qbiogene), setting 6 for 30 s, followed by 1 min rest on ice. Bead beating was repeated 6 times followed by centrifugation for 20 min at 11,000g. The activity was determined from 40 µL cell extract in 1 mL total volume in the presence of 0.20 mM NADPH, and 0.20 mM DTNB and ±5 µM *Ll*NrdH, measuring TNB formation at 412 nm. The initial activities were determined in duplicate for each biological triplicate.

Chapter 3. Crystal structures of *L. lactis* Thioredoxin Reductase

3.1 Introduction

This chapter describes the crystal structures of *Lactococcus lactis* subsp. *cremoris (*strain MG1363*)* thioredoxin reductase (*Ll*TrxR) with Uniprot accession number A2RLJ5 and expressed by the gene annotated *trxB1* (Wegmann et al., 2007). Altogether 27 datasets have been processed, but only a limited number of these structures were subjected to analysis in this chapter which focuses on the structures that display features in relation to the light sensitivity and the FO/FR conformations. This results in a total number of 9 structures (table 5).

Table 5. *Ll*TrxR crystal structures included in this chapter. Characteristics are conformations (FR-FR, FO-FO and FO-FR), presence of co-enzyme ($NADP^+$) and visible light exposure. Published structures with PDB entries are indicated.

#	Conformation	$NADP^+$	Light exposure	PDB	Section
1	FR-FR	-	-	-	3.2.3; 3.2.4; 3.2.5
2	FO-FO	-	-	5MJK	3.2.3; 3.2.4; 3.2.5
3	FO-FR	-	-	-	3.2.3; 3.2.4; 3.2.5
4	FR-FR	+	-	5MH4	3.2.3.3.2.4; 3.2.5; 3.2.6
5	FR-FR	+	30 min	5MIP	3.2.6
6	FR-FR	+	60 min	5MIQ	3.2.6
7	FR-FR	+	120 min	5MIR	3.2.6
8	FR-FR	+	180 min	5MIS	3.2.6
9	FR-FR	+	240 min	5MIT	3.2.6

3.2 Results and discussion

3.2.1 Crystallization of *Ll*TrxR

Initial trials were performed with Structure Screen 1 (MD1-01) and Structure Screen 2 (MD1-02) from Molecular Dimensions (Jancarik and Kim, 1991; Wooh et al., 2003), which gave crystals from the condition 500 mM Li_2SO_4, 15% (w/v) PEG8000 by the hanging drop vapor diffusion method (2 µL 8–10 mg mL^{-1} protein mixed with 2 µL reservoir solution). The crystals obtained under these conditions were having high mosaicity and low diffraction grading and therefore manual optimization of the crystallization conditions was initiated. Many different crystallization conditions were tested before obtaining good crystals to differentiate single atom increase in the electron maps caused by the light-induced oxidation. In this process, spanning over a period of more than two years, it was discovered that *Ll*TrxR could be obtained in different conformations as determined by the presence of phosphate, DTT and $NADP^+$ during crystallization (Appendix D).

FO-FR conformation

The mixed conformation structures referred to as FO-FR, where the dimer has one monomer in FO- and the other in FR-conformation, was only obtained when the protein was crystallized with the standard protein buffer (100 mM potassium phosphate, 1 mM EDTA, pH 7.4). Yellow crystals appeared after ~10 d (figure 43). Although the crystals at first glance appeared well-defined under microscope, they did not diffract very well, and small cracks tended to appear in the surface during longer incubation in the drop. The best crystal diffracted to 2.57 Å and led to the structure solved with mixed FO-FR conformation. Crystallization conditions are summarized in table 6.

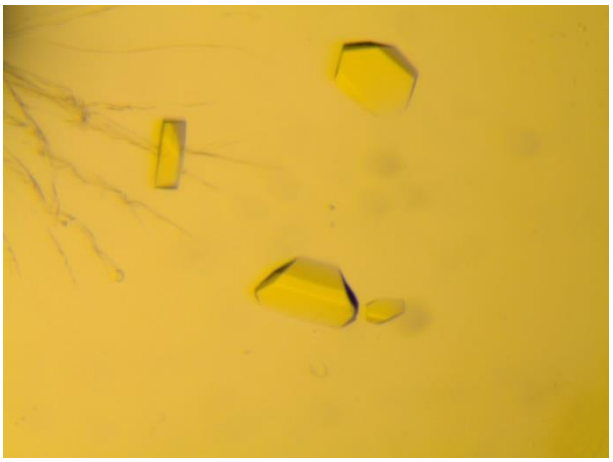

Figure 43. *Ll*TrxR was obtained in the mixed FO-FR conformation of the homodimer only when phosphate was present in the drop during crystallization.

FR-FR conformation

Structures in FR-FR conformation were obtained using protein buffer 10 mM HEPES, 2 mM EDTA, pH 7.0, with or without co-crystallization with $NADP^+$. Bright yellow octahedron crystals (100 µm) appeared after about 5 d and grew to about 200 µm in length by 14 d (figure 44).

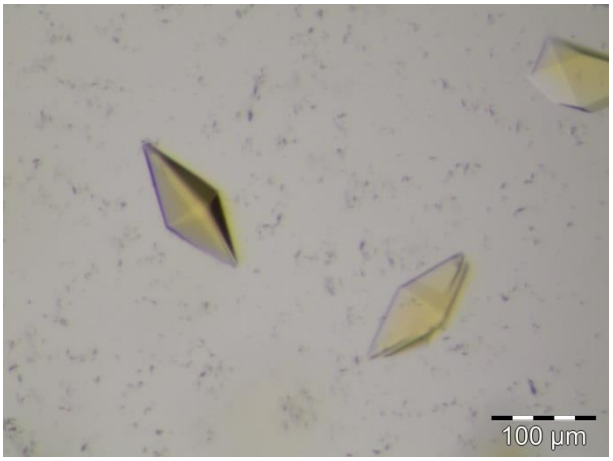

Figure 44. *Ll*TrxR crystallized in the FR-FR conformation of the homodimer, which appeared to be a consequence of removing phosphate in the protein buffer. FR-FR conformations were obtained with or without co-crystallization with $NADP^+$.

Addition of $NADP^+$ to the hanging-drop appeared to stabilize the crystals, which grew more readily and became sharper in their morphology. Crystallization conditions are summarized in table 6.

For the crystallization trials of *Ll*TrxR exposed to light, it turned out that the longer the visible light exposure time of *Ll*TrxR, the more difficult it was to obtain good crystals. The longest irradiation time still obtaining suitable crystals of *Ll*TrxR was 240 min. Crystallization attempts trial of 360 min irradiated *Ll*TrxR seemed unable to generate single crystals.

FO-FO conformation

Finally, structures in FO-FO conformation were obtained in the presence of DTT during crystallization using the protein buffer 10 mM HEPES, 2 mM EDTA, pH 7.0, without $NADP^+$. Only non-irradiated *Ll*TrxR could crystallize in the FO conformation. Crystals appeared after ~14 d. Crystallization conditions are summarized in table 6.

Table 6. Summarized crystallization conditions for the respective structures. Specific details for protein preparation, protein-reservoir ratio etc. are described in Materials and Methods section 3.3.5. Structure determination with molecular replacement and subsequent refinement performed are described in section 3.3.6.

#	Characteristics	Protein buffer	Reservoir conditions	Data collection
1	FR-FR (No light)	10 mM HEPES, 2 mM EDTA, pH 7.0	35% PEG1500, 400 mM Li_2SO_4	I911-3, MAXII, Sweden
2	FO-FO (No light)	10 mM HEPES, 2 mM EDTA, pH 7.0	20% PEG4000, 400 mM Li_2SO_4. Added 20 mM DTT to the drop	I911-3, MAXII, Sweden
3	FO-FR (No light)	100 mM potassium phosphate, 1 mM EDTA, pH7.4	15% PEG4000, 400 mM Li_2SO_4	I911-3, MAXII, Sweden
4	FR-FR(No light) $NADP^+$	10 mM HEPES, 2 mM EDTA, pH 7.0	35% PEG1500, pH 8.0, 400 mM Li_2SO_4. Added 5 mM $NADP^+$ to the drop	ID30A-1, ESRF, France
5	FR-FR (30 min) $NADP^+$	10 mM HEPES, 2 mM EDTA, pH 7.0	35% PEG1500, pH 6.0, 400 mM Li_2SO_4 Added 5 mM $NADP^+$ to the drop	I911-3, MAXII, Sweden
6	FR-FR (60 min) NADP	10 mM HEPES, 2 mM EDTA, pH 7.0	35% PEG1500, pH 6.0, 400 mM Li_2SO_4 Added 5 mM $NADP^+$ to the drop	I911-3, MAXII, Sweden
7	FR-FR (120 min) $NADP^+$	10 mM HEPES, 2 mM EDTA, pH 7.0	35% PEG1500, pH 6.5, 400 mM Li_2SO_4 Added 5 mM $NADP^+$ to the drop	I911-3, MAXII, Sweden
8	FR-FR (180 min) $NADP^+$	10 mM HEPES, 2 mM EDTA, pH 7.0	35% PEG1500, pH 7.5, 400 mM Li_2SO_4 Added 5 mM $NADP^+$ to the drop	I911-3, MAXII, Sweden
9	FR-FR (240 min) $NADP^+$	10 mM HEPES, 2 mM EDTA, pH 7.0	35% PEG1500, pH 6.5, 400 mM Li_2SO_4 Added 5 mM $NADP^+$ to the drop	I911-3, MAXII, Sweden

3.2.2 Quality of the structures

In total 9 structures are presented in this work. All seven structures in FR-FR conformation were solved in space group $P4_12_12$ containing one protein molecule in the asymmetric unit. The one structure presented here in FO-FO conformation was solved in space group $P2_1$ with four protein molecules in the asymmetric unit (two homodimers). The single structure obtained in the mixed FO-FR conformation was solved in space group P1 with four protein molecules in the asymmetric unit (two homodimers). The best structures were covering residue 5–307 (the wild-type N-formyl methionine numbered as residue 1) and the worst 6–306. Data collection and refinement statistics for the models are summarized in table 8. In the structure obtained in FO-FO conformation the B-factors are higher in the NADPH domain as compared to the structures obtained in FR-FR conformation. The mixed conformation FO-FR structure has the highest B-factors, which is ascribed to the general lower quality of the crystal and diffraction data (table 8).

All structures contain an FAD molecule with well-defined electron density and typically with B-factors ~ 21–25 $Å^2$. Structures co-crystallized in the presence of $NADP^+$ were all in FR conformation with $NADP^+$ perfectly oriented in the NADPH cavity, with B-factors ~22–29 $Å^2$. Only the two structures with lower resolutions, e.g. FO-FR and FR-FR (with $NADP^+$, no light), have higher B-factors of the co-enzymes, albeit in the same range as the B-factors of the surrounding protein (table 8).

Appendix G provides electron density maps for visual inspection (wall-eyed stereo) of selected motifs and features described in this work.

After refinement the φ and ψ angles of the peptides backbone were mainly within the favored regions and with only few outliers. Details on the Ramachandran plots, as calculated from the PDB validation reports (wwPDB) are provided in table 7.

Table 7. Ramachandran plot statistics.

#	Characteristics	Favored regions (%)	Allowed regions (%)	Outliers (%)
1	FR-FR (No light)	93.4	6.0	0.66
2	FO-FO (No light)	97.3	2.5	0.25
3	FO-FR (No light)	91.4	7.01	1.59
4	FR-FR(No light) $NADP^+$	96.0	3.7	0.33
5	FR-FR (30 min) $NADP^+$	94.4	5.0	0.66
6	FR-FR (60 min) NADP	94.4	5.0	0.66
7	FR-FR (120 min) $NADP^+$	97.0	3.0	0
8	FR-FR (180 min) $NADP^+$	95.7	3.6	0.66
9	FR-FR (240 min) $NADP^+$	96.7	3.3	0

Table 8. Data collection and refinement statistics (molecular replacement).
One crystal was used to determine each structure. Values in parentheses are for highest-resolution shell.

	#1 *Ll*TrxR FR-FR No light – – Unpublished	#2 *Ll*TrxR FO-FO No Light – – (PDB 5MJK)	#3 *Ll*TrxR FO-FR No Light – – Unpublished	#4 *Ll*TrxR FR-FR No Light $NADP^+$ – (PDB 5MH4)	#5 *Ll*TrxR FR-FR 30 min Light $NADP^+$ – (PDB 5MIP)	#6 *Ll*TrxR FR-FR 60 min Light $NADP^+$ – (PDB 5MIQ)	#7 *Ll*TrxR FR-FR 120 min Light $NADP^+$ – (PDB 5MIR)	#8 *Ll*TrxR FR-FR 180 min Light $NADP^+$ – (PDB 5MIS)	#9 *Ll*TrxR FR-FR 240 min Light $NADP^+$ – (PDB 5MIT)
Data collection									
Space group	$P4_12_12$	$P2_1$	$P1$	$P4_12_12$	$P4_12_12$	$P4_12_12$	$P4_12_12$	$P4_12_12$	$P4_12_12$
Cell dimensions									
a, *b*, *c* (Å)	120.5, 120.5, 60.65	73.61, 132.26, 73.5	65.86, 73.81, 73.72	120.54, 120.54, 60.47	121.43, 121.43, 60.7	121.46, 121.46, 60.71	121.17, 121.17, 60.62	120.92, 120.92, 60.45	120.69, 120.69, 60.33
α, β, γ (°)	90, 90, 90	90, 112.62 90	108.84, 100.26, 86.149	90, 90, 90	90, 90, 90	90, 90, 90	90, 90, 90	90, 90, 90	90, 90, 90
Monomers in ASU	1	4	4	1	1	1	1	1	1
Resolution (Å)	42.75–1.80 (1.90–1.80)	47.36–2.00 (2.05–2.00)	50.0–2.57 (2.64–257)	85.24–2.14 (2.22–2.14)	42.94–2.00 (2.05–2.00)	42.95–1.92 (1.97–1.92)	42.86–2.00 (2.05–2.00)	60.45–1.81 (1.84–1.81)	60.34–1.80 (1.84–1.80)
R_{merge}	0.091 (1.58)	0.088 (0.826)	0.164 (1.14)	0.127 (1.74)	0.116 (1.224)	0.096 (1.461)	0.073 (0.509)	0.088 (1.063)	0.134 (1.783)
I/σ (I)	18.94 (1.3)	12.2 (1.8)	6.69 (1.01)	12.3 (1.3)	13.24 (1.74)	15.69 (1.18)	20.13 (3.66)	17.5 (1.9)	14.6 (1.5)
CC(½)	99.9 (55.5)	99.7 (63.3)	98.4 (50.3)	99.7 (47.7)	99.8 (61.9)	99.9 (49.5)	99.9 (88.9)	99.9 (52.1)	99.9 (31.7)
Completeness (%)	99.8 (99.7)	99.0 (98.4)	94.5 (94.6)	99.9 (100)	96.2 (98.1)	99.6 (99.8)	99.8 (100.0)	99.9 (99.9)	99.8 (98.9)
Redundancy	6.5 (6.4)	3.8 (3.8)	1.9 (1.9)	8.4 (8.5)	6.6 (6.5)	7.4 (6.3)	7.5 (7.8)	10.2 (8.1)	13.5 (10.7)
Refinement									
Resolution (Å)	42.75–1.80	47.36–2.00	29.15–2.57	49.37–2.14	42.94–2.00	42.95–1.92	42.86–2.00	54.13–1.81	54.03–1.80
No. reflections	537,521 (78,817)	332,553 (24,494)	75400 (5,702)	210,842 (20,402)	198,639 (14,547)	260,449 (16,150)	231,711 (17,615)	423,277 (19,394)	560,996 (25,330)
R_{work} / R_{free}	0.2125/0.2513	0.2299/0.2760	0.2519/0.3031	0.1767/0.2373	0.1895/0.2404	0.1947/0.2276	0.1826/0.2166	0.1895/0.2320	0.1937/0.2335
No. atoms									
Protein	2347	9,356	9,562	2,347	2,347	2,347	2,347	2,347	2,347
Ligand/ion	87	232	222	118	125	125	125	125	125
Water	247	409	102	166	224	239	247	256	250
B-factors									
Protein	32.6	35.1	47.7	44.3	34.7	35.3	31.5	29.9	31.4
Ligand/ion	35.7	25.1	30.4	39.1	33.5	33.6	28.0	27.4	29.3
FAD	20.4	21.7	30.4	35.5	24.8	24.3	21.5	20.9	22.7
$NADP^+$	-	-	-	35.2	28.7	29.6	22.3	22.3	23.1
Water	42.3	33.2	31.1	50.2	44.7	44.8	40.1	39.5	40.9
R.m.s. deviations									
Bond lengths (Å)	0.019	0.015	0.011	0.018	0.019	0.019	0.018	0.022	0.019
Bond angles (°)	1.9	1.7	1.7	2.0	2.2	2.0	2.1	2.3	2.1

3.2.3 Overall structure of *Ll*TrxR

The overall structure of *Ll*TrxR is similar to other low molecular weight (LMW) TrxRs (Waksman et al., 1994; Kirkensgaard et al., 2009) which are composed of an NADPH and an FAD binding domain (figure 45). The secondary structure of each monomer consists of 11 α-helices and 19 β-strands. The FAD-domain consists of residues 1–111 and 244–308 and the NADPH-domain consists of residues 117–238 (Appendix E, 1). The two domains are connected by two short anti-parallel strands (residues 112–116 and 239–243), allowing the NADPH domain to rotate relative to the FAD domain, which brings the active site cysteines (Cys134 and Cys136) in vicinity of the FAD (FO conformation) or expose them on the surface (FR conformation) (figure 45).

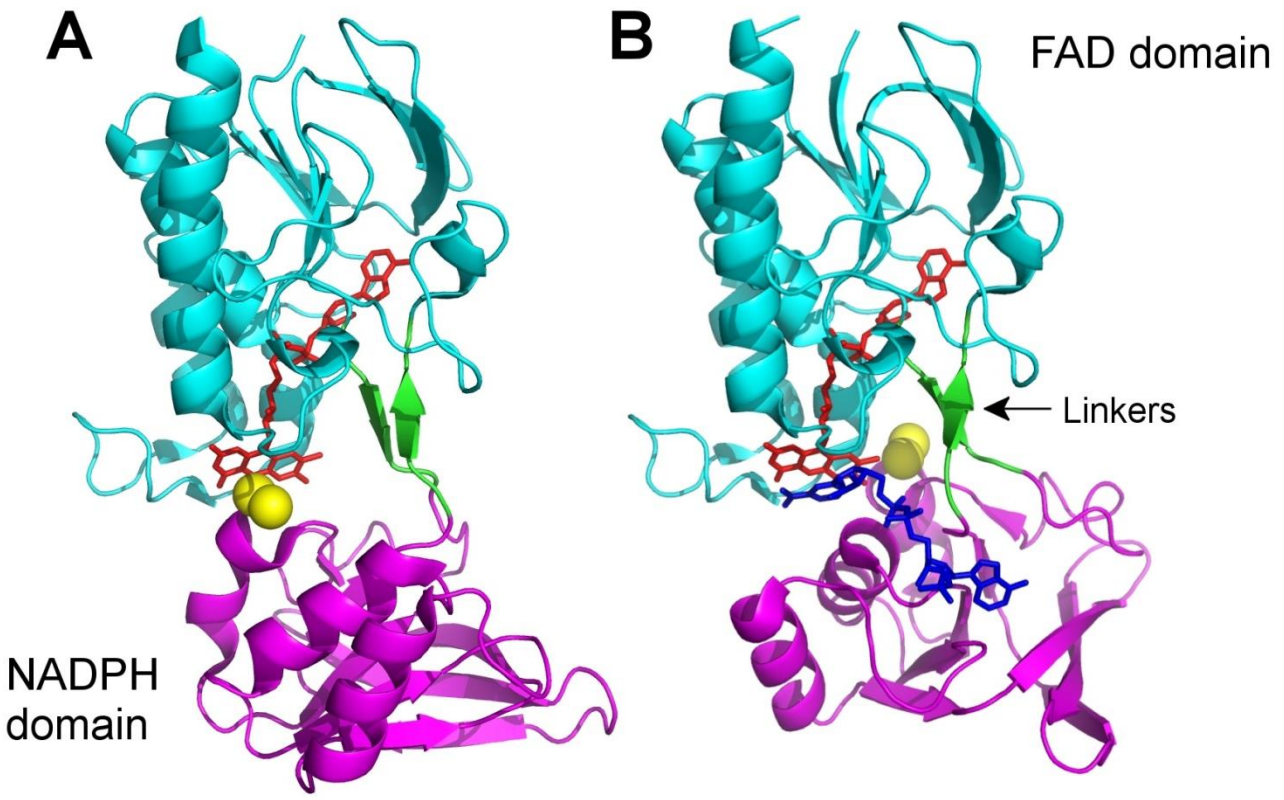

Figure 45. The overall structure of one monomer of *Ll*TrxR in FO conformation (A) and FR conformation (FR). The FAD and NADPH domain are represented in cyan and magenta, respectively, while the linkers connecting the two domains are in green. The FAD (red) is present in both structures, while $NADP^+$ (blue) only is mapped in the FR conformation (B). During the conformational shift from FO to FR the NADPH domain rotates 66° clockwise, transferring the sulfurs (yellow) of the active cysteines from the vicinity of FAD to the surface of the enzyme.

Comparing *Ll*TrxR to the well-described *Ec*TrxR, the most conspicuous difference is the insertion at residues 267–271 (SGIHG) in the *Ec*TrxR structure (figure 46). This insertion is only seen in the Gram-negative bacteria, as evaluated from multiple sequence alignment (Appendix C). The loop is located in the FAD domain and only has interaction with the FAD domain of the neighboring monomer, thus it is not directly implicated in FO/FR dynamics.

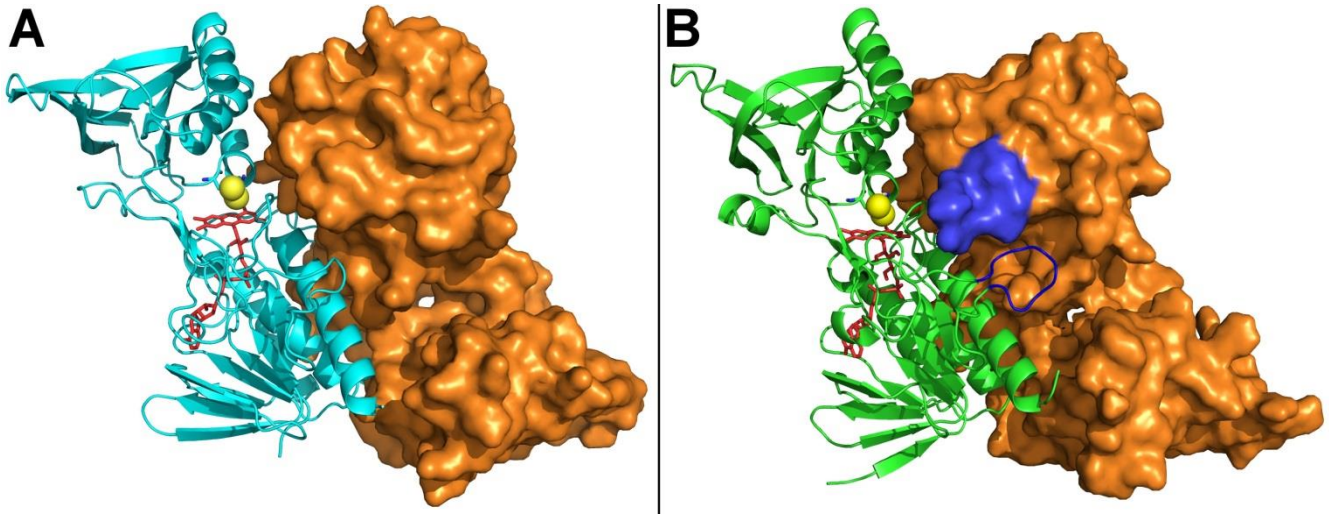

Figure 46. Homodimeric organization of *Ll*TrxR (A) and *Ec*TrxR (B) in FO conformation, presented as secondary structure and as accessible surface area (orange). The FAD and sulfur of active cysteines are colored in red and yellow, respectively. *Ec*TrxR harbors the insertion at residues 267–271 (SGIHG), presented in blue, which is not found in *Ll*TrxR and related TrxR (Appendix C).

3.2.4 FAD and NADPH domains

3.2.4.1 FO and FR conformation of *Ll*TrxR

The *Ll*TrxR structures are obtained in FR conformation (figure 47, B), which was unexpected since all available structures of LMW TrxR from other organisms are in FO conformation, except for the special case of the engineered complex between *Ec*TrxR and *Ec*Trx (Lennon et al., 2000). *Ll*TrxR crystallized in FO conformation (figure 47, A) only when non-irradiated and under reducing conditions in the presence of DTT. The propensity of *Ll*TrxR to crystallize in the FR conformation, regardless of co-crystallization with $NADP^+$, may indicate that the FO/FR equilibrium is shifted towards this conformation. Superposition of *Ll*TrxR C_α-atoms with the structure of *Ec*TrxR (Waksman et al., 1994;

Lennon et al., 2000), gave RMSD of 0.426 Å and 1.137 Å for the enzyme in FR (PDB 1F6M) and FO conformation (PDB 1TDE), respectively (figure 47).

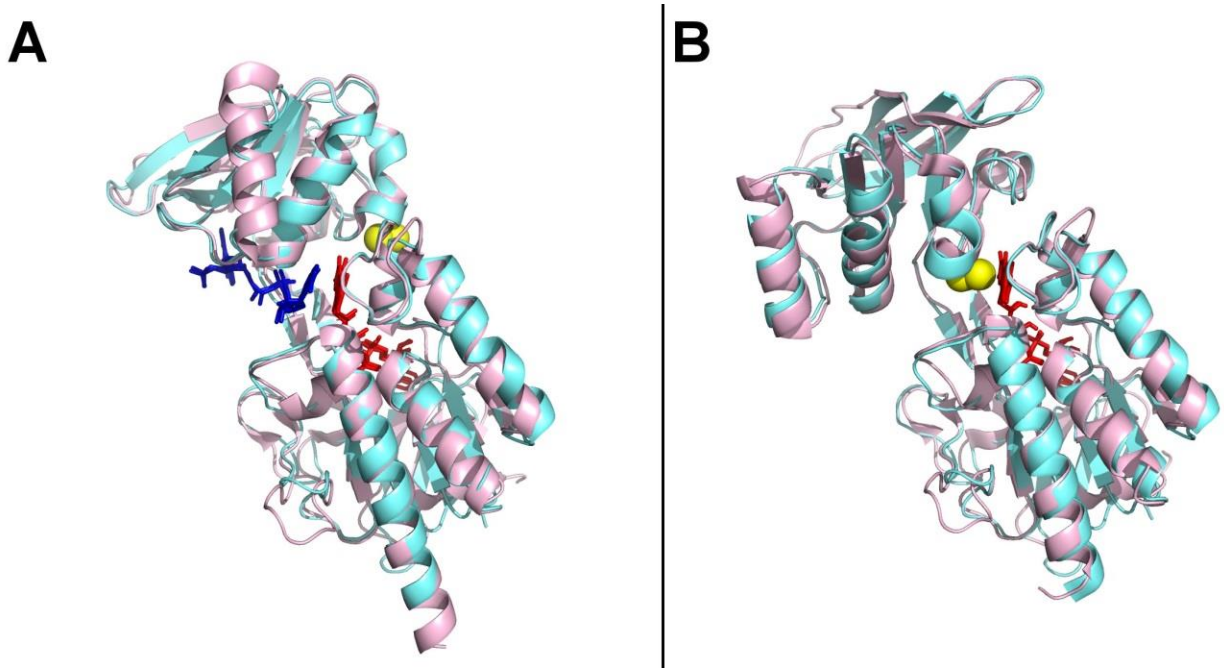

Figure 47. Overall superposition of *Ll*TrxR (cyan) and *Ec*TrxR (light pink) in FR (A) and FO (B) conformations with RMSD values of 0.426 and 1.137 Å, respectively. The FAD (red sticks), as well as $NADP^+$ and the $NADP^+$ analog $AADP^+$ (blue sticks) align well as indicated. The active site disulfide bond is marked as yellow spheres.

In both the FR and FO conformations the FAD (red sticks), as well as $NADP^+$ and the $NADP^+$ analog $AADP^+$ (blue sticks in the FR conformation) align well as indicated. The active site disulfide bond is marked as yellow spheres.

The relative orientation of the structural domain thus matches perfectly with the *E. coli* enzyme and consolidates the model first proposed by Waksman et al. (1994) where the NADPH domain rotates 66° relative to the FAD domain in order to switch between the FO and FR conformations in the catalytic cycle, placing the FAD in proximity with the active cysteines motif ($_N$CXXC$_C$) and the NADP(H), (figure 48).

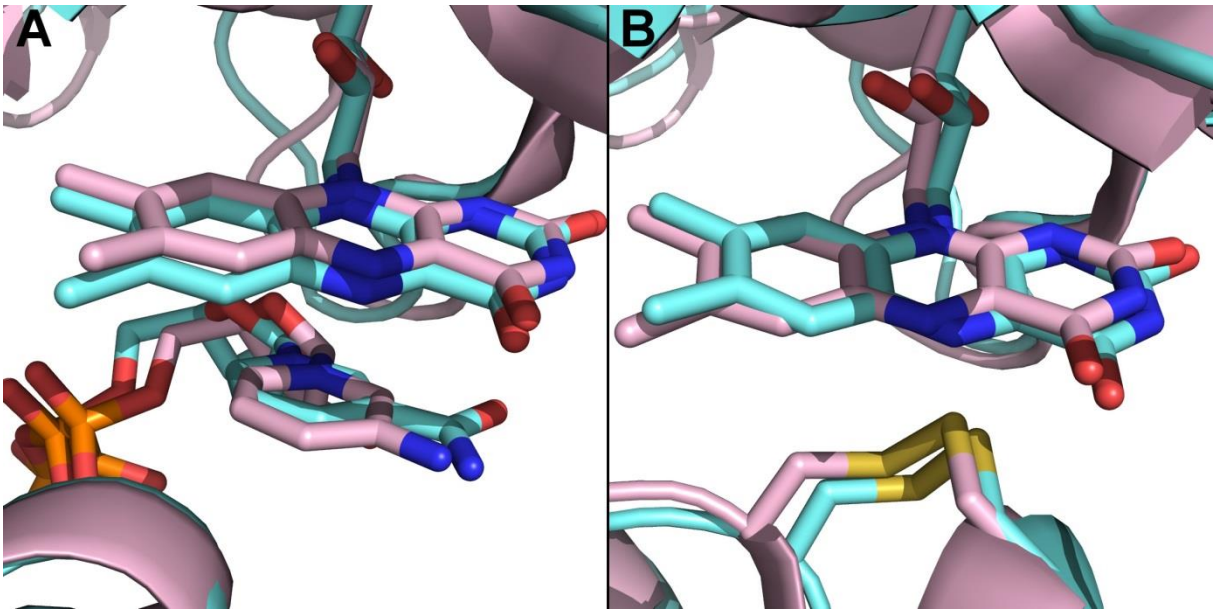

Figure 48. Superposition of the active site of *Ll*TrxR (cyan) and *Ec*TrxR (light pink) in FR (A) and FO (B) conformations. Both $NADP^+$/$AADP^+$ and the disulfide bridges are oriented identically relative to the FAD in both *Ll*TrxR and *Ec*TrxR.

The structure obtained in FR-FR conformation without $NADP^+$, has a clearly increased electron density in the NADPH cavity at two locations where $NADP^+$ has the phosphates PN and P3 (figure 49). These electron densities are assigned to sulfates present in the crystallization conditions. Phosphate P3 is stabilized by Arg175, Arg176 and Arg180 (constituting the motif responsible for binding NADPH rather NADH) while PN is stabilized only by Arg180. The presence of sulfate in the crystallization conditions could help stabilizing the protein in FR conformation.

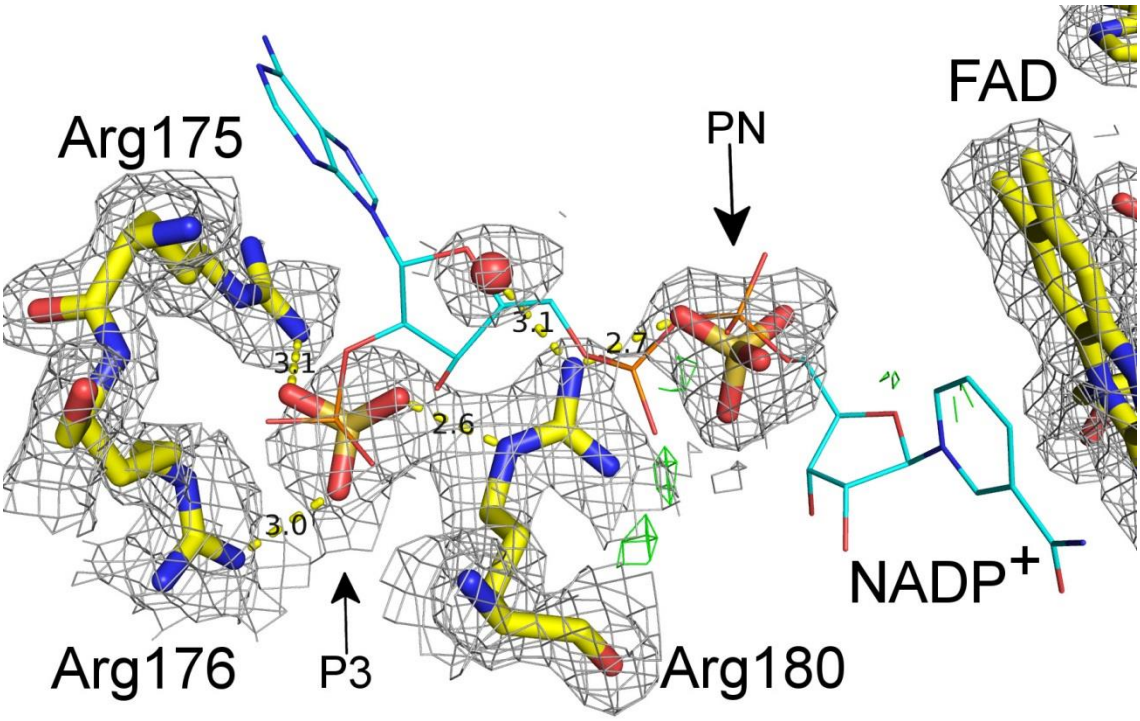

Figure 49. Structure of *Ll*TrxR obtained without $NADP^+$ in FR-FR conformation modelled with a $NADP^+$ molecule. Two sulfates are located at sites of $NADP^+$ phosphates (PN and P3). The PN phosphate is stabilized with Arg180 and P3 phosphate is stabilized by Arg175, Arg176 and Arg180. The $NADP^+$ is modeled by superimposing *Ll*TrxR obtained with $NADP^+$.

Similarly, the FO-FR structure has an increased electron density in the NADPH cavity of the monomer obtained in FR conformation. As sulfate and phosphate are present in the crystallization conditions the electron density could be assigned to either of them, but was modelled as a phosphate ion. The presence of phosphate during the crystallization process is probably the likely explanation why *Ll*TrxR crystallizes in the mixed FO-FR conformation. Whether it is the consequence of the NADPH cavity phosphates or interactions to the surface of LlTrxR is not clear. But it can be eliminated that the crystallization of FO-FR conformation is a pH phenomenon, as structures in FR-FR could be obtained in the pH range 6.0–8.0. This result potentially shows that the monomers do not necessarily undergo a synchronized conformational shift, but rather an unsynchronized mechanism, where the two monomers can rotate their NADPH domains independently of one another. Of course it could also simply be a crystallographic phenomenon with no biological relevance, but the variety in the conformations obtained, indicates that *Ll*TrxR has higher degrees of conformational freedom as compared to other TrxR structures studied.

3.2.4.2 Co-enzyme interactions

In order to map the interaction of the co-enzymes with the *Ll*TrxR, contacts found with LigPlot$^+$ (Laskowski and Swindells, 2011). Interaction with the FAD and surrounding protein were as expected unchanged in FO and FR conformation (Appendix E, 2). Noteworthy conserved hydrogen bounding residues to the isoalloxazine include Asn51, Gln285 and Ile286. In complex with NADP$^+$ Asn51 forms hydrogen bonds to both N3 (FAD) and the oxygen amide (NADP$^+$), see figure 50.

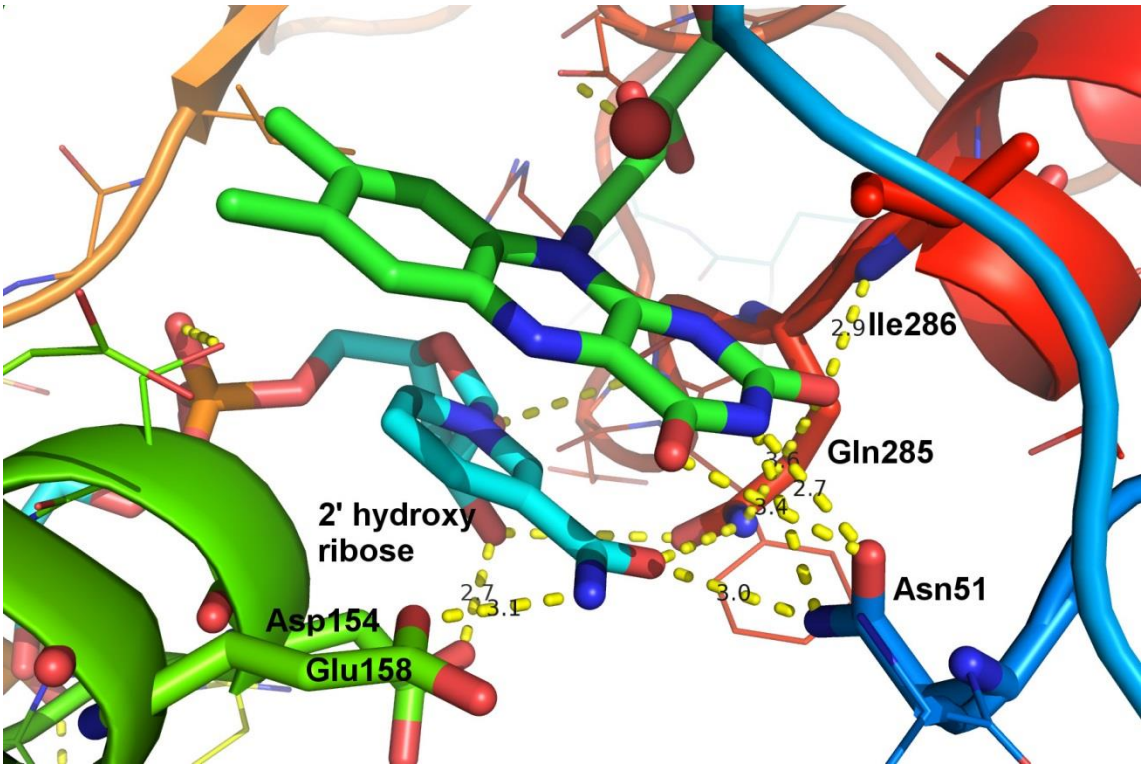

Figure 50. Interactions between the isoalloxazine/nicotinamide and the surrounding protein obtained in FR conformation with complex with NADP$^+$. Selected hydrogen bonds between the NADP$^+$ and the FAD are marked with dashed lines and distances are in angstrom (Å).

The orientation of the amide group of nicotinamide at the *re*-face of FAD is similar to the nicotinamine of AADP$^+$ in *Ec*TrxR (PDB 1F6M), but different from the orientation proposed by Blankenhorn 1976, located at the *re*-face of FAD and with the nicotinamide orienting towards the C5a and C6 atoms of FAD (figure 32). The FAD-NADP$^+$ complex is stabilized by the interaction between the C5 oxygen and the

N3 of FAD with the nitrogen (3.2 Å) and the oxygen (3.5 Å) of the nicotinamide, respectively. The redox-active carbon of the nicotinamide is in a 3.2 Å distance from the redox-active N5 of FAD allowing the reducing equivalent to be transferred (figure 51).

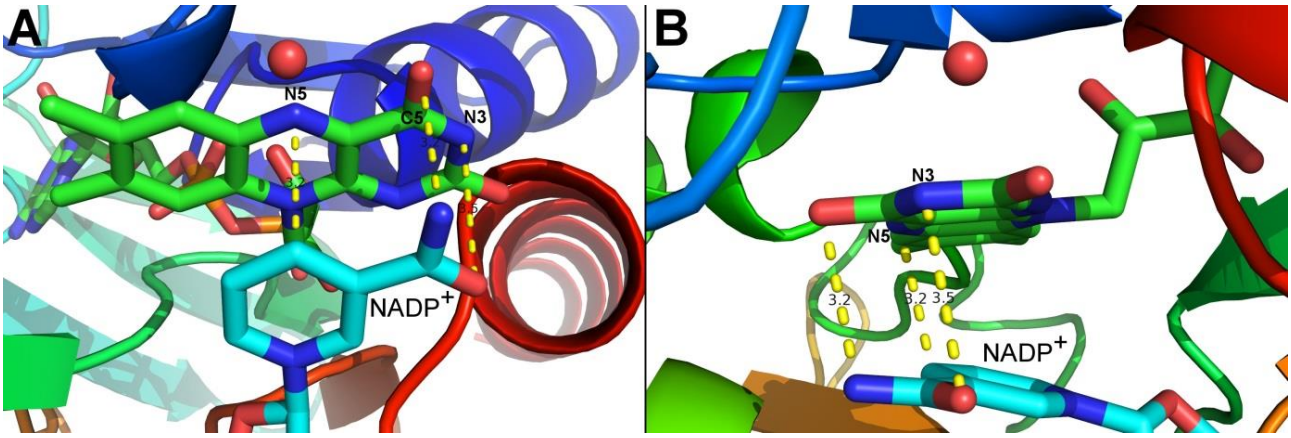

Figure 51. FAD-NADP+ complex of *Ll*TrxR. Hydrogen bonds stabilize the complex between the C5 oxygen and the N3 of FAD with the nitrogen (3.2 Å) and the oxygen (3.5 Å) of the nicotinamide, respectively (A,B). The nicotinamide is not parallel to the FAD, but rather tilted with the redox active carbon facing towards the redox active N5 (3.2 Å) of FAD (B).

Comparing co-factor interactions of *Ll*TrxR and *Ec*TrxR, could potentially explain the observed differences, *e.g.* in stopped-flow kinetics and FAD quantum yield. Comparing *Ll*TrxR and *Ec*TrxR interactions with FAD reveals that all interactions to the isoalloxazine ring are identical. The main differences identified are the two *Ec*TrxR residues Ser13 and Thr35 that are hydrogen bonded to the ribose of the nucleotide (Appendix E, 3). The interactions of $NADP^+$ (*Ll*TrxR) compared to the interactions of $AADP^+$ (*Ec*TrxR) in FR conformation show that the most noteworthy difference is at residue Asn51 (Appendix E, 4). The lack of interaction between $AADP^+$ and this residue is probably a result of the structural difference between 3-aminopyridine and nicotinamide (longer distance (4.88 Å) from 3-aminopyridine to Asn51); Asn51 is located identically in the two TrxR. $Tyr292_{EcTrxR}$ is hydrogen bonding to 3' hydroxyl ribose and not identified in *Ll*TrxR ($Phe283_{LlTrxR}$ at same position), but the 3' hydroxyl ribose in *Ll*TrxR is actually hydrogen bonded to the backbone of Arg284. Even though $LigPlot^+$ did assign $Arg176_{EcTrxR}$ as involved in hydrogen bonding/salt bridge, the three arginines Arg175/Arg176/Arg180 (*Ll*TrxR) and Arg176/Arg177/Arg181 (*Ec*TrxR) are actually identical in

hydrogen bonding to P3 phosphate of $NADP^+$/$AADP^+$, as verified by manual inspection. Overall, the co-factor interactions of *Ll*TrxR and *Ec*TrxR are highly similar and interactions mapped here are not likely to explain the differences in stopped-flow data and FAD quantum yield. Rather the distinguishing features of the two homologous enzymes are more likely found in the dynamics of the FO/FR conformations, as analyzed from inter-dimer and inter-domain contacts.

3.2.4.3 Interdimer- and interdomain-contacts of TrxR

The stopped-flow kinetics data (section 2.2.6) indicated that *Ll*TrxR seems to be more stabilized in FR conformation as compared to *Ec*TrxR. This result was further supported by the tendency of *Ll*TrxR to crystallize in FR conformation. As the FO/FR equilibrium might have impact on the light sensitivity as described in section 3.2.7, the inter-dimer and inter-domain contacts stabilizing the FO and FR conformation were analyzed. The inter-dimer and inter-domain contacts relevant for the FO/FR equilibrium concern contacts of the NADPH domain and the neighboring monomer. The program $LigPlot^+$ (Laskowski and Swindells, 2011) was applied to structures of *Ll*TrxR, *Ec*TrxR in both FO and FR conformation and to *Sa*TrxR in FR conformation to map differences, followed by manual inspections in the structures. For better overview only hydrogen bonds originating from NADPH-FAD domain contacts and NADPH domain neighboring monomer contacts are listed in the table 9. Complete tables of all identified interactions (hydrogen bonds/salt bridges and van der Waals contacts) are listed in Appendix F.

Table 9. Identified inter-dimer and inter-domain hydrogen bonds found in *Ll*TrxR, *Ec*TrxR and *Sa*TrxR in FO and FR conformations by the program LigPlot⁺.

*Ll*TrxR, FO conformation	*Ec*TrxR, FO conformation	*Sa*TrxR, FO conformation
Cys137-Arg26 (3.1 Å)	Thr47-Gly129 (3.1 Å)	Gln285-Cys137 (3.2 Å)
Cys137-Arg26 (3.2 Å)	Glu48-Arg130 (3.0 Å)	Arg188-Asp309 (2.5Å)
Val136-Arg26 (2.9 Å)	Cys138-Arg26 (3.1 Å)	Arg188-Asp309 (2.8 Å)
Arg143-Glu28 (2.6 Å)	Cys138-Arg26 (2.9 Å)	Val136-Arg26 (3.0 Å)
Ser27-Arg165 (2.7 Å)	Arg144-Asn28 (3.0 Å)	Cys137-Arg26 (3.0 Å)
	Arg144-Asn28 (3.1 Å)	Cys137-Arg26 (3.0 Å)
	Asn166-Asn28 (2.9 Å)	Lys165-Asn28 (3.1 Å)
	Asn166-Asp314 (3.2 Å)	Lys191-Asn308 (3.2 Å)
	Arg189-Asp314 (2.9 Å)	
	Lys193-Asp314 (3.2 Å)	
Total 5 hydrogen bonds	**Total 10 hydrogen bonds**	**Total 8 hydrogen bonds**
*Ll*TrxR, FR conformation	*Ec*TrxR, FR conformation	*Sa*TrxR, FR conformation
Glu50-Arg188 (2.8 Å)	Glu50-Arg189 (2.9 Å)	N.A.
Glu50-Arg188 (2.9 Å)	Glu50-Arg189 (3.0 Å)	N.A.
Gln182-Arg26 (2.8 Å)	Lys188-Asn28 (3.1 Å)	N.A.
Ile184-Arg26 (2.9 Å)	Glu183-Arg26 (2.5 Å)	N.A.
Glu183-Tyr301 (2.6 Å)	Ile185-Arg26 (3.0 Å)	N.A.
Total 5 hydrogen bonds	**Total 5 hydrogen bonds**	N.A.

In *Ll*TrxR 5 hydrogen bonds were identified in both FO and FR conformations. This is in contrast to *Ec*TrxR that has 10 identified hydrogen bonds in FO conformation and only 5 hydrogen bonds in FR conformation. This significant difference in hydrogen bonds between FO- and FR-conformation in *Ec*TrxR changes the enthalpy of the two conformations, which should impact the FO/FR equilibrium in the direction of the FO conformation. In *Sa*TrxR (PDB 4GCM) 8 hydrogen bonds have been identified in the FO conformation. Unfortunately no structure of *Sa*TrxR in FR conformation is available, which could have served in a comparison of stabilizing hydrogen bonds. FO/FR equilibrium of *Sa*TrxR shifted towards the FO conformation could explain why *Sa*TrxR is much less light sensitive than *Ll*TrxR (section 2.4.10), for reasons explained in section 3.2.7. The equal numbers of hydrogen bonds in the two conformations of *Ll*TrxR potentially explains why this enzyme displays a broader variety of crystallized conformations. Interestingly, photo-inactivation of *Ll*TrxR at pH 4.0 seemed to have a protective effect on the activity (Paper 1, figure 3). This could potentially be explained by protonation of aspartate and

glutamate residues involved in salt bridges in the FR-conformation, thus shifting the equilibrium towards the FO-conformation, which according to the FO-FR-conformation-hypothesis proposed in section 3.2.7 offers protection from superoxide generation.

3.2.5 FAD *si*-face open space and the Met-Pro motif

Even though most residues surrounding the FAD isoalloxazine ring are conserved in *Ll*TrxR and *Ec*TrxR, minute differences are revealed when the structures are closely examined. Most noticeable is the presence of an open space at the *si*-face of the FAD in the *Ll*TrxR, which has not been described previously in other TrxR. The FAD *si*-face open space is confined by isoalloxazine ring, the 2′-ribityl hydroxyl group, Met43, Ile49, Thr46 and Leu286, and occupied with a well-defined electron density assigned to a water molecule, which is observed in all structures (figure 52).

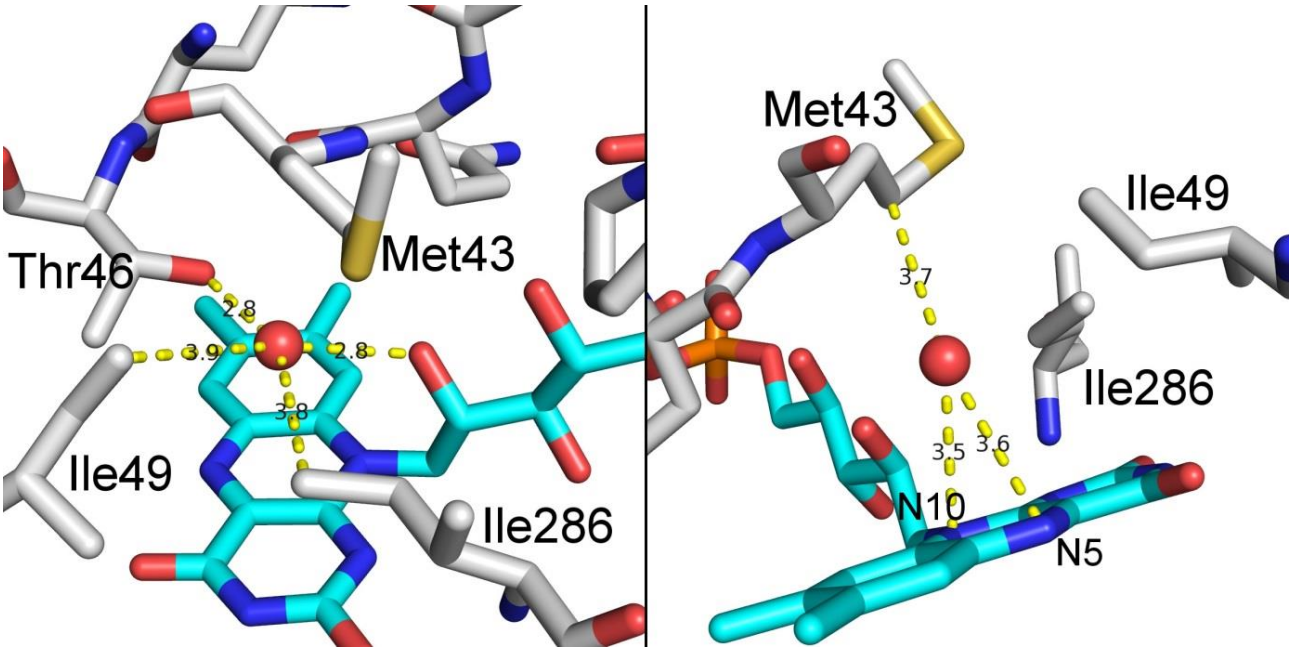

Figure 52. The *Ll*TrxR isoalloxazine *si*-face open space occupied by a water molecule (red sphere). The open space is defined by the isoalloxazine ring, the ribityl and the key residues Met43, Ile49, Thr46 and Leu286. The water is in hydrogen distance to 2′-ribityl hydroxyl group and the alcohol group of Thr46.

The water molecule is perfectly centered over the central ring of the isoalloxazine with hydrogen bond distance to the 2′-ribityl hydroxyl group (2.8 Å) and the alcohol group of Thr46 (2.8 Å), and the distance

from the water to the N5 and N10 atom of the isoalloxazine is 3.5–3.6 Å and 3.7 Å to the γ-carbon of Met43 (figure 52). The dimension of the FAD *si*-face open space is defined by the distance from the β-carbon of Met43 and the isoalloxazine ring (7.2–7.4 Å) and from Leu286 to Thr46 (~6.4Å) and Leu49 to the 2′-ribityl hydroxyl group (~6.3Å).

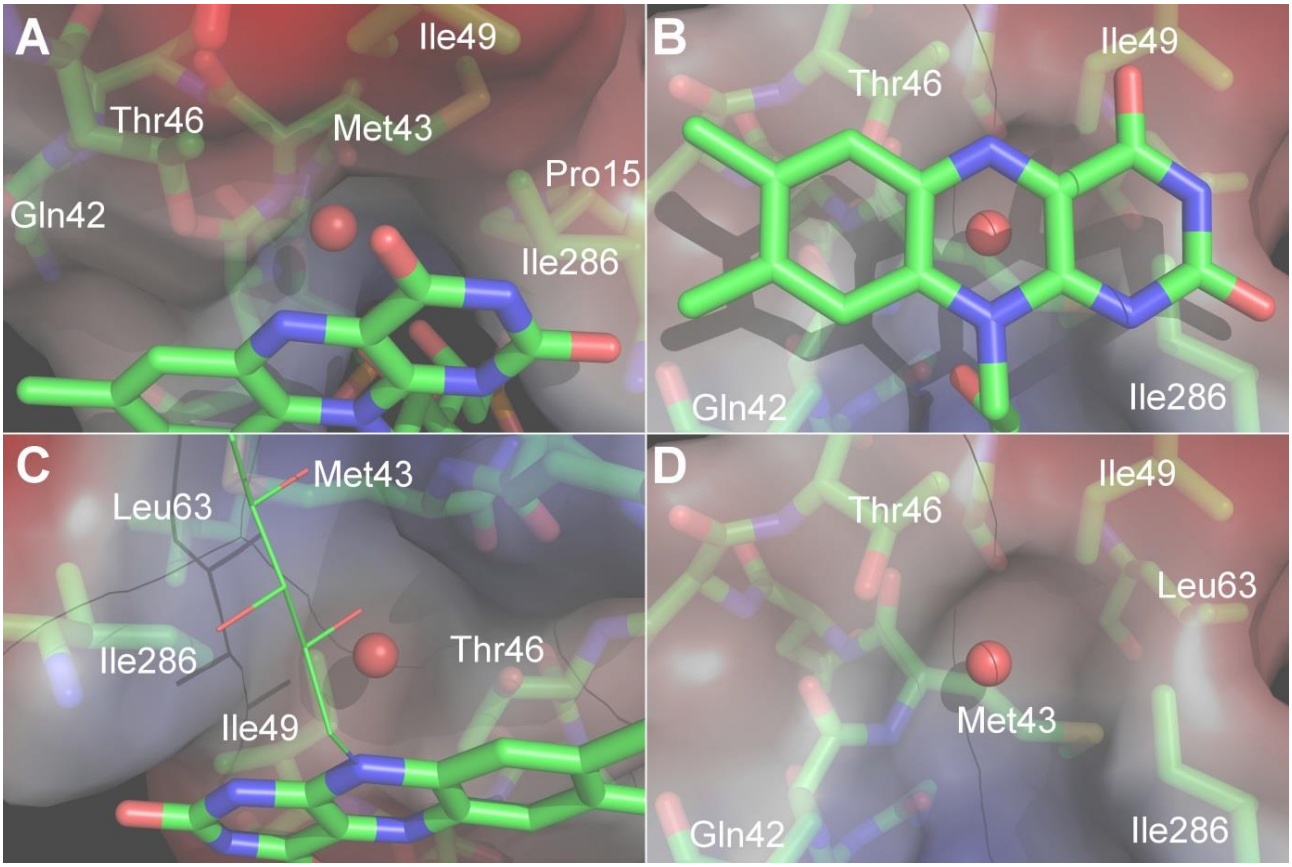

Figure 53. The vacuum electrostatic potential surfaces around the *si*-face open space occupied by a conserved water molecule surrounded by key residues. A and B are facing the N5 and N10 of the isoalloxazine ring, respectively. B and D are viewing the open space from the *re*-face with and without FAD, respectively.

The electrostatic environment at the *si*-face constitutes an overall hydrophobic environment because of the mentioned residues (Met43, Ile49, Thr46 and Leu286) and the π-electron cloud of the conjugated isoalloxazine ring system (figure 53, A-D). It is therefore predicted that the FAD *si*-face open space has the potential to accommodate molecular oxygen (O_2), thus serving as an oxygen pocket. The water *si*-face molecule is then in an exchange/dynamic equilibrium with O_2 molecules. An alternative O_2

accommodation in the vicinity of the isoalloxazine ring would be at the *re*-face, but this seems to be an unlikely option, as the *re*-face in the FO conformation is occupied by the Cys134-Cys137 disulfide, while in the FR conformation it is surrounded by hydrophilic residues (Asp154, Glu158, Ser155 and Gln285).

The described oxygen pocket is not observed in *Ec*TrxR, which has a Leu44$_{EcTrxR}$ centered at the *si*-face of the isoalloxazine with a 3.8–4.0 Å distance from the δ-carbon to the N10 and N5 atoms. Leu44$_{EcTrxR}$ is restricted from bending away from the isoalloxazine towards the Pro15$_{EcTrxR}$ because of the steric hindrance of the bulky Met66$_{EcTrxR}$, which in *Ll*TrxR is substituted by the smaller Ser64$_{LlTrxR}$ (figure 4b, Paper 2). Thus, oxygen is blocked from the *si*-face of *Ec*TrxR (figure 4d, Paper 2), which offers an explanation to the differences between the two enzymes' sensitivity towards visible light and ability to reduce oxygen in presence of NADPH. Residues acting as "gate keepers" have previously been described blocking the access of oxygen to the flavin, thus preventing dehydrogenases from acting as oxidases (Leferink et al., 2009). The feature of *Ll*TrxR to accommodate O_2 at the *si*-face, gives the isoalloxazine ring the ability to act as a photosensitizer either by a type 1 process and/or type 2 processes, as described in section 1.1.3, generating damaging ROS.

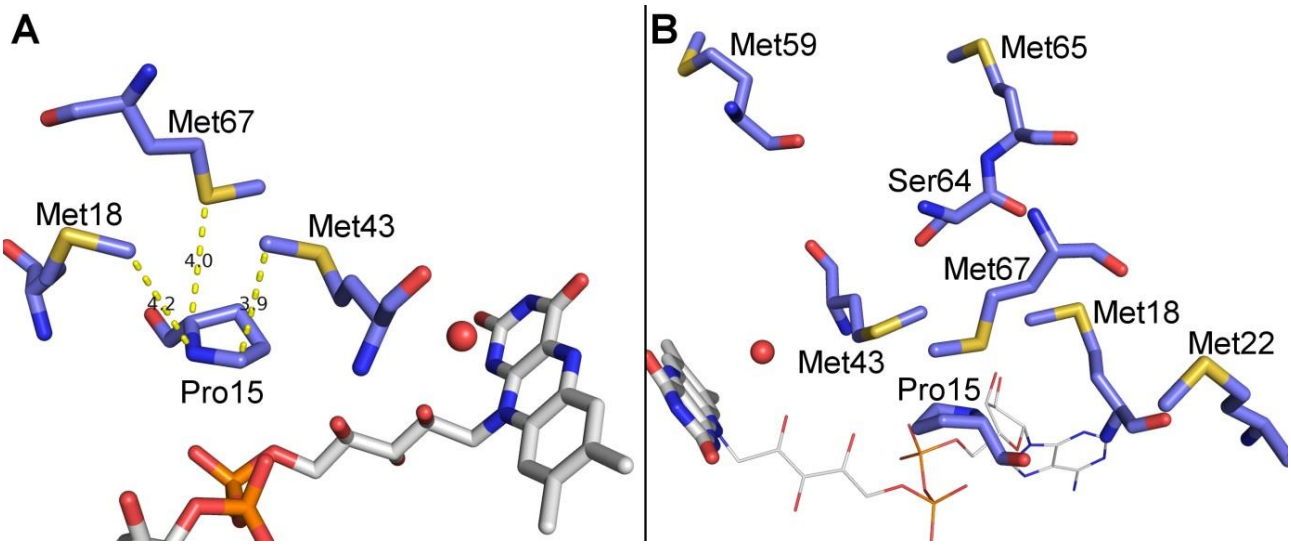

Figure 54. (A) The Met-Pro motif constituted of Met43, Met67, Met65 and Pro15 in conjunction with the oxygen pocket. (B) The Met59 and Met65 are exposed on the surface can potentially connect with the interior methionines. The small size of Ser64 leaves space for Met43 to bend towards the Pro15, a feature which is restricted in *Ec*TrxR (see text).

The oxygen pocket arises as Met43, located in the short α-helix (residues 40-46) in the FAD domain, is bending away from the isoalloxazine towards Pro15 and the sidechains of Met18 and Met67, constituting (what in this work is referred to as) a Met-Pro motif (figure 54, A).

This Met-Pro motif is observed in most LMW TrxR, but mainly with only two methionines (*i.e.* without Met43). In the vicinity of the Met18 and Met 67 is Met22 located which together with Pro70 or Pro53 (of the neighboring monomer) could be an alternative Met-Pro motif. Even at the surface another two methionine residues (Met 59 and Met65) are observed, which might be interconnected with the interior methionines (figure 54, B). The functional explanation for the Met-Pro motif is unclear, but the high density of methionines in this region of the enzyme is worth noting. Examples of proteins using methionines as oxidant scavangers are previously described (Luo and Levine, 2008), where norleucine-substituted (methionine with sulfur substituted with –CH2–) cells showed increased oxidation, *e.g.* at elongation factor Tu, indicating that methionines protect against ROS by being reversibly oxidized to methionine sulfoxide exposed on the surface of the protein, for later reduction by methionine sulfoxide reductase.

3.2.6 Structures of photo-inactivated *Ll*TrxR

The initial investigations had established a gradual blue shift of the 456 nm peak to ~440 nm as a function of light exposure, with a simultaneous loss in enzyme activity. MS data of heat extracted FAD from light exposed (16 h) *Ll*TrxR identified an aldehyde (13.98 Da mass increase) and a mass increase of 29.98 Da (carboxylic acid or aldehyde+alcohol) at the isoalloxazine ring. 2,4-dinitrophenylhydrazine (DNPH) analysis gave positive result for a carbonyl group. Based on spectroscopic data it was concluded that the aldehyde formation was most likely confined to the C7α methyl group of the isoalloxazine ring (Paper 1).

In order to monitor the structural consequences of photo-oxidation, crystallization trials were initiated with *Ll*TrxR exposed to light. The best quality of crystals was obtained in co-crystallizing experiments with $NADP^+$, which therefore became standard conditions. Structures of good quality were obtained from *Ll*TrxR exposed to light for 30, 60, 120, 180 and 240 min, making it possible to monitor the oxidation as a function of light exposure. No overall structural change was observed in the five light-exposed structures, which were all obtained in FR-FR conformation with well-defined electron structures around the $NADP^+$ co-enzyme and FAD molecule. The following section provides an expanded discussion that is not included Paper 2.

3.2.6.1 Oxidation of the isoalloxazine ring

As expected an increased electron density is indeed observed at the C7α methyl group in the *Ll*TrxR structures over the course of visible light exposure. In the first 60 min it is difficult to evaluate whether or not extra electron density occurs at this methyl group, but gradually at 120 min and most clearly at 180 and 240 min the extra electron density is confirmed (figure 55).

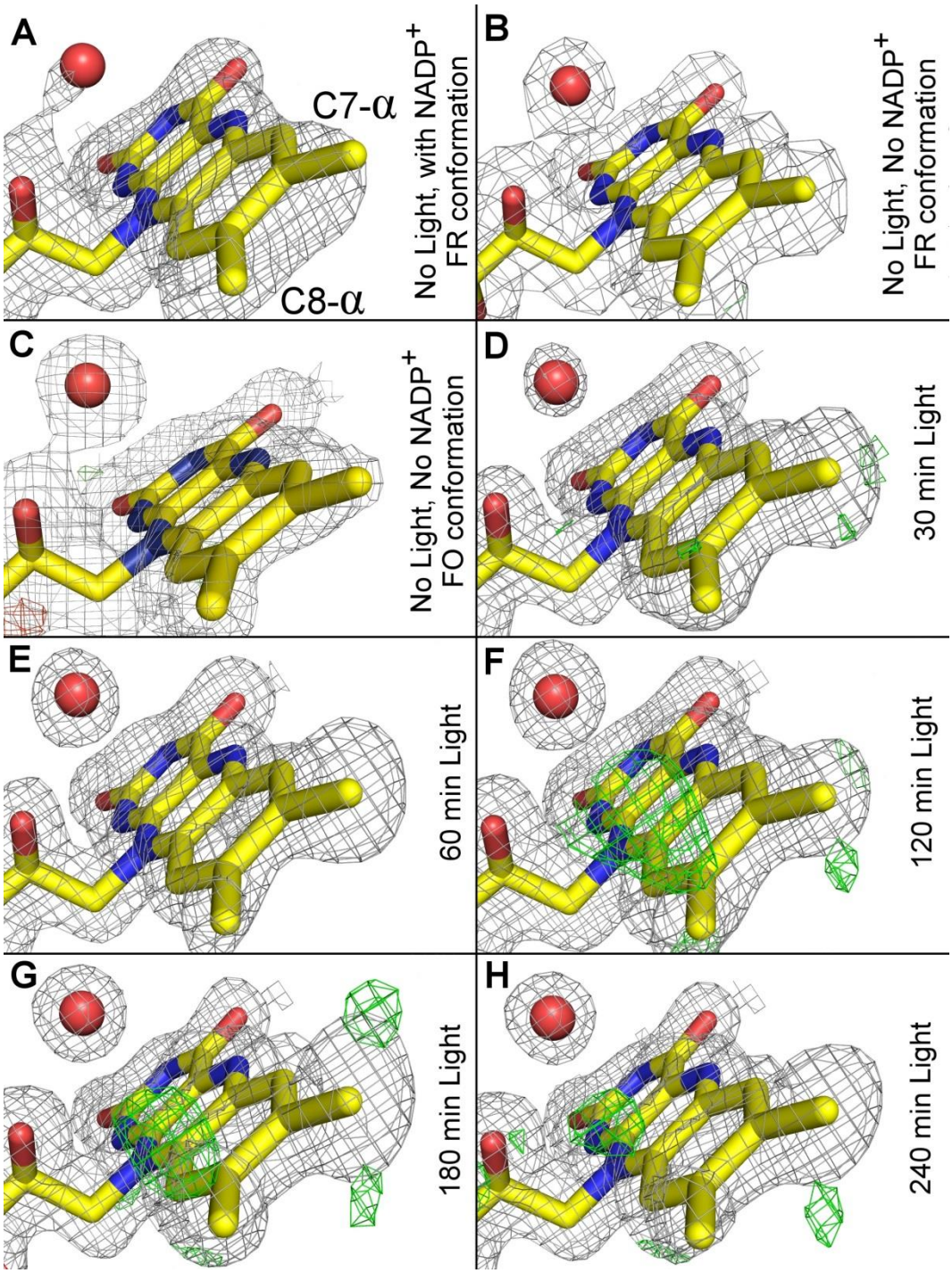

Figure 55. Increased electron density around the C7α methyl group of the isoalloxazine ring in *Ll*TrxR develops over the course of irradiation (0–240 min). The σ_A-weighted $2F_o–F_c$ maps (grey) have been contoured at 1.0 σ. The difference $F_o–F_c$ maps (green/red) have been contoured at ±3.0 σ, respectively. The C7α methyl group develops increased difference densities mainly in the σ_A-weighted $2F_o–F_c$ maps and to a minor extent in the $F_o–F_c$ maps. The conserved *si*-face water is observed in all structures.

According to the data presented in Paper 1 this electron density most likely corresponds to an aldehyde group. Such an aldehyde attached to the isoalloxazine conjugated system should according to established chemistry be part of the conjugation, making the aldehyde group planar with the ring system. However the electrostatic environment may favor hydrogen bonding of the aldehyde to either Ser155 and/or Glu159, turning the aldehyde out of planarity of the conjugation. However, it is difficult to judge from the electron density to what extent the aldehyde is planar.

This oxidation at the C7α is the main focus Paper 2, but furthermore an increase in electron density in the positive difference map is observed on the C8α methyl group almost perpendicular to the *si*-face to the ring system. This increase in electron difference map is accompanied by a simultaneous change in orientation of the electron density of C8α methyl group towards the *si*-face turning the conjugated ring out of plane (figure 56).

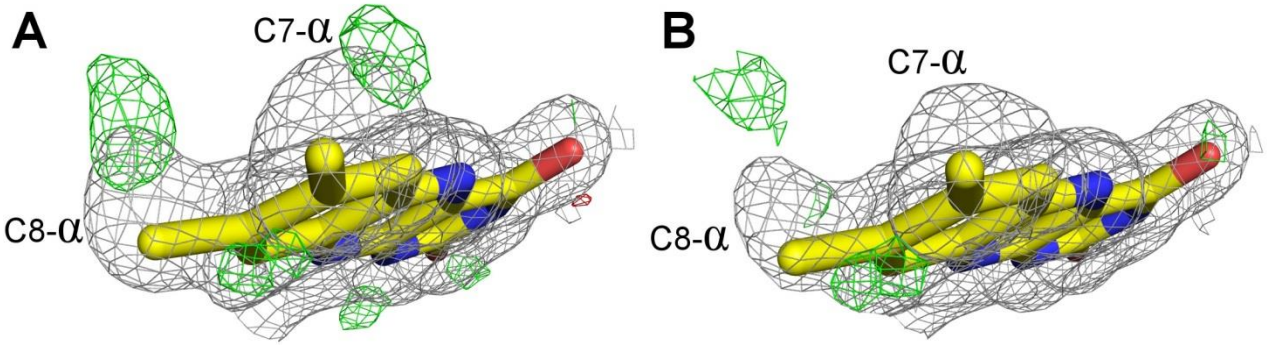

Figure 56. Increased electron density at the C8-α methyl group after 180 min (A) and 240 min (B) light exposure. The increase in electron density at C8-α is less than that of C7-α. The increase could possibly be assigned to the +16.00 Da (an alcohol) increase or the +29.98 Da (alcohol+aldehyde) increase detected in MS data of FAD from irradiated *Ll*TrxR.

These features are only observed for the structures exposed for 180 and 240 min. MS data indicates the formation of a +16 Da peak, representing an alcohol, formed in the first period of the photo-inactivation (figure 30 and data not included). This explains how the isoalloxazine can be oxidized on both methyl groups. The alcohol peak diminishes quickly and the "carboxylic acid" peak becomes the major peak after longer irradiation. As discussed in section 2.2.4 this +29.98 Da peak might actually represent an aldehyde and an alcohol located at C7α and C8α methyl groups, respectively. However, the current available data cannot conclude on this. An attractive approach is to react the heat extracted FAD prior to

MS analysis with oxim or bortrifluoride to verify/falsify the presence of an aldehyde and/or carboxylic acid, respectively. This would clarify if various types of oxidations occur, as well as give further details regarding types of oxidant generation (O_2^-, $^1O_2$, H_2O_2) during irradiation.

3.2.6.2 Oxidation of Tyr237

In addition to the FAD oxidations the nearby Tyr237, located at a distance of 4.4 Å from C7α, is also oxidized upon light exposure. A clear increase in electron density at the meta-position (ortho to the hydroxyl group) of Tyr237 is observed over the course of light exposure (Appendix G and Paper 2, figure 3). The increased electron density at the meta-position most likely represents formation of a hydroxy group that transforms the tyrosine to a 3,4-dihydroxyphenylalanine (DOPA). Mass spectrometric analysis of GluC (endoproteinase) digested photo-inactivated *Ll*TrxR confirmed a mass shift of 16 Da confined to Tyr237 (Paper 2, supplementary). This additional hydroxy group of Tyr237 is turning away from the isoalloxazine, but during the oxidant attack the carbon center most likely faces towards the isoalloxazine, thus the hypothesized site of ROS generation. More interestingly Tyr237 is located in the NADPH domain, which means that Tyr237 oxidation takes place only when *Ll*TrxR is in the FR conformation, *e.g.* in proximity of the FAD. When *Ll*TrxR is in FO conformation another tyrosine (Tyr133) is located in the same position as Tyr237 in the FR conformation, but Tyr133 showed no indications of oxidation in any of the irradiated structures. These observations are in line with the proposed stabilization of *Ll*TrxR in the FR conformation.

3.2.7 Comparison of the isoalloxazine environment in *Ll*TrxR and *Sa*TrxR

The highly similar TrxR from *S. aureus* (*Sa*TrxR) is the only published structure with an identical oxygen pocket, Met-Pro motif as well as a conserved Tyr237 as described for *Ll*TrxR. As discussed in section 2.2.9 *Sa*TrxR and *Bs*TrxR share the characteristic with *Ll*TrxR to reduce O_2 in the presence of NADPH, but their light sensitivity are significantly lower (section 2.2.8). *Sa*TrxR (PDB 4GCM) is the most closely related solved structure (53% sequence identity) in PDB, though no article has been published regarding the structure. Superposition of *Sa*TrxR with the *Ll*TrxR in FO conformation gives a RMSD of 1.095 $Å^2$ for the C_α-carbons.

Interestingly, the light sensitivity of *Sa*TrxR was not as pronounced as for *Ll*TrxR. As the *si*-face environment is identical in the two enzymes (*Sa*TrxR: Val49, Ile286, Thr46; *Ll*TrxR: Ile49, Ile286, Thr46) and the oxygen pocket and Met-Pro motif is conserved (*Sa*TrxR: Met43, Ser64 & Pro15, Met18, Met43, Met67; *Ll*TrxR: Met43, Ser64 & Pro15, Met18, Met43, Met67), other factors might influence the light sensitivity. The O_2 transport to the oxygen pocket might be impacted by the two residues Gln42 and Asn45 that are located at the entrance to the *si*-face open space, but they are very similar in the two structures. Another factor influencing light-sensitivity could be the difference in FO/FR equilibrium. Cysteines are known to act as quencher of photoexcited triplet state flavins, but cystine (oxidized dimer of cysteine) was not observed as a quencher (Cardoso et al., 2004). So TrxR shifted towards FO-conformation may at first glance not be able to act as a quencher of excited FAD. A more likely protective mechanism envisioned is that an electron subtraction from the isoalloxazine (type I reaction) is transferred to the disulfide bond of the active site on the *re*-face, rather than the O_2 on the *si*-face. A similar electron transfer is described for excited tryptophan to a disulfide in a small cyclic peptide (Mozziconacci and Schöneich, 2014). It is not unlikely that a similar protective mechanism indeed would make TrxR in FO conformation less susceptible to light induced oxidation. An open question is also what happens to the one-electron reduction of the disulfide bond generating a disulfide radical anion. UV-excited-tryptophan generated disulfide radical anion is expected to rupture into a thiolate ion and a thiyl radical (Vanhooren et al., 2002), but the energies in the wavelength used in the photo-inactivation of TrxR is much lower (>400 nm). Alternatively, the disulfide radical can transfer its electron to O_2 generating superoxide (Kerwin and Remmele, 2007). With the current data for TrxR it is definitely worth investigating this FO-FR-conformation-hypothesis as an explanation for light sensitive/robust TrxR.

Regarding ROS protecting residues, both enzymes have Tyr237 and Tyr133 conserved, while *Sa*TrxR has a third tyrosine $Tyr115_{SaTrxR}$ in contrast to $His115_{LlTrxR}$. The presence of tyrosines close to the site of ROS generation could provide a temporary protection from oxidation of methyl groups in the isoalloxazine by being oxidized themselves to DOPA.

Even though TrxR mainly transfers reducing equivalents to the redox-active CXXC motif it is possible for *Ll*TrxR to oxidize NADPH in the absence of Trx, forcing O_2 to be the final electron donor, as shown in section 2.2.9. *Sa*TrxR displays approximately the same level of NADPH oxidation as *Ll*TrxR upon O_2 reduction. The structure of *Bs*TrxR is not available but the Met-Pro motif is conserved in the sequence

alignment. *Bs*TrxR shows about half the NADPH oxidation level of *Ll*TrxR and *Sa*TrxR, but still has a threefold higher turnover than *Ec*TrxR. The bacterial flavoenzyme AhpF, which harbors a similar *si*-face open space (PDB 1HYU, 1FL2 and more), also has the ability to reduce molecular oxygen to hydrogen peroxide with a turnover of 1.07 s^{-1} for *S. typhimurium* under the same NAD(P)H concentration. This rate is much lower than hydrogen peroxide NADH oxidases, that typically operate with k_{cat} values above 100 s^{-1} (Niimura et al., 1995), underlining that *Ll*TrxR, *Sa*TrxR and *Bs*TrxR operates via a different mechanism.

3.3 Materials and Methods

3.3.1 Expression and purification of *Ll*TrxR

Recombinant *Ll*TrxR was produced in *E. coli* Rosetta (DE3) by insertion into the vector pET15b (Novagen) with an N-terminal His-tag $_{N}$MGSSHHHHHHSSGLVPRGSH$_{C}$ and transformation as described previously (Björnberg et al., 2014). Harvested cell pellets were lysed in BugBuster protein extraction reagent (Novagen) containing Benzonase nuclease (Merck) in the presence of 0.2 mM FAD (Sigma). After centrifugation the supernatant was filtered (Corning syringe filters, pore size 0.45 µm). The His$_6$-*Ll*TrxR was applied onto HisTrap column (GE Healthcare) equilibrated with loading buffer (20 mM potassium phosphate pH 7.4, 500 mM NaCl, 10 mM imidazole). Target proteins were eluted using a linear gradient of 10–100% elution buffer (20 mM potassium phosphate pH 7.4, 500 mM NaCl, 400 mM imidazole). Fractions (selected based on 280 nm absorbance) were pooled and dialyzed against 100 mM potassium phosphate, 1 mM EDTA, pH 7.4, concentrated to approximately 5 mL (Amicon Ultra 6-8 MWCO) and stored at −80 °C in aliquots as previously described (Björnberg et al., 2014).

3.3.2 Light induced-inactivation of *Ll*TrxR for crystallization purpose

His-trapped purified *Ll*TrxR was thawed on ice and diluted in 100 mM potassium phosphate, 2 mM EDTA, pH 7.5 to a final concentration of 50 µM. The diluted sample was transferred to an Eppendorf tube and kept 20 cm below a 1225 Lumen (21 W) lamp with a color temperature of 6500 K corresponding to a maximum intensity λ_{max} = 460 nm (Manufacture Leuci (Relco group)) in the cold room (4°C) as previous, described (Björnberg et al., 2015).

3.3.3 Purification of *Ll*TrxR for crystallization purpose

*Ll*TrxR samples (irradiated or non-irradiated) without thrombin cleavage were applied to a HiLoad Superdex 75 16/60 column and eluted by 10 mM HEPES, 200 mM NaCl, 2 mM EDTA, pH 7.0 (FR-FR and FO-FO conformation) or 100 mM potasium phosphate, 1 mM EDTA, pH7.4 (FO-FR conformation) at a flow rate of 1 mL min^{-1}. Fractions were selected to only include the main peak in the pooled sample (excluding any shoulders) and the size was checked by SDS-PAGE. Proteins crystallizing in FO-FO and

FR-FR conformations were dialyzed against 10 mM HEPES, 2 mM EDTA, pH 7.0 O.N., while no dialysis was performed of protein crystallizing in FO-FR conformation. Finally the samples were concentrated (Amicon Ultra, 6-8 MWCO) to 8–10 mg/mL and used directly/instantly for setting up crystals. The concentration of *Ll*TrxR was determined by FAD absorbance (ε_{456} = 11,300 M^{-1} cm^{-1}) (Williams et al., 1967).

3.3.4 Activity measurements

The degree of inactivation of the irradiated samples was measured using a DTNB assay (Ellman, 1959). The activity was determined in the presence of 20 nM *Ll*TrxR, 2 µM *Ll*TrxA, 0.20 mM NADPH (Sigma), and 0.20 mM DTNB (Sigma) in a 1 mL cuvette format, measuring the TNB formation at 412 nm. Standard buffer used was 100 mM potassium phosphate, 2 mM EDTA, 0.1 mg/mL BSA, pH 7.5. The initial rates were calculated from the linear slopes made as a minimum in triplicate. The relative inactivation was calculated from the activity of sample taken prior to irradiation. *Ll*TrxA was expressed and purified as described in section 2.4.1.

3.3.5 Crystallization conditions

3.3.5.1 Crystal structures obtained in FR-FR conformation

*Ll*TrxR (2 µL, 8–10 mg/mL) was mixed with 2 µL reservoir buffer and co-crystallized with 1 µL 25 mM $NADP^+$ (Sigma-Aldrich) and equilibrated as hanging-drops over a 500 µL reservoir containing 35% PEG 1500 (Fluka), 400 mM Li_2SO_4, 20 mM HEPES of pH varying in the range 6.0–8.5. Bright yellow octahedron crystals (100 µm) appeared after about 5 d at 19°C and grew to about 200 µm in length by 14 d. Crystals of light-exposed (30, 60, 120, 180 and 240 min) and light-protected *Ll*TrxR were harvested and flash-cooled directly from the drop without additional cryoprotectants, as the presence of PEG1500 prevented ice formation.

3.3.5.2 Crystal structure obtained in FO-FO conformation

*Ll*TrxR (2 µL, 8–10 mg/mL) was mixed with 2 µL reservoir buffer, added 2 µL 60 mM DTT and equilibrated as vapor diffusion hanging-drops over a 500 µL reservoir containing 20% PEG 4000 (Fluka), 400 mM Li_2SO_4. Only non-irradiated *Ll*TrxR crystallized under these reducing conditions. Crystals appeared after ~14 d at 292 K. Crystals were transferred to a cryoprotectant solution consisting of reservoir buffer with 10% ethylene glycol before storing in liquid nitrogen.

3.3.5.3 Crystal structure obtained in FO-FR conformation

*Ll*TrxR (2 µL, 8–10 mg/mL) was mixed with 2 µL reservoir buffer and equilibrated as vapor diffusion hanging-drop over a 500 µL reservoir containing 15% PEG 4000 (Fluka), 400 mM Li_2SO_4. Crystals appeared after ~10 d at 302 K. Crystals were transferred to a cryoprotectant solution consisting of 20% PEG1500 (Fluka), 400 mM Li_2SO_4, 10% ethylene glycol before placing directly into the liquid nitrogen stream at the beamline.

3.3.5.4 Crystal structures obtained from inactivated *Ll*TrxR obtained in FR-FR conformation

Light-inactivated *Ll*TrxR was co-crystallized with $NADP^+$ in the same way as non-inactivated *Ll*TrxR as described in section 3.3.5.1. Increased irradiation time of *Ll*TrxR lowered the quality of the crystals and it was not possible to obtain crystals of suitable quality from protein that was light exposed for more than 240 min. Moreover, it was of greatest importance to harvest the crystals when they reached max 200 µm, as they thereafter started to lose their contour and grew into a four-arm star shape, typically within 14–21 d. However, after several trial-and-error, crystals were obtained of light-exposed *Ll*TrxR (30, 60, 120, 180 and 240 min) which gave suitable diffraction patterns. For *Ll*TrxR crystallized without $NADP^+$ it was more difficult to obtain diffraction at high resolution after long inactivation time. However, the best crystals obtained without $NADP^+$ diffracted to 1.85 Å (30 min irradiation) and 2.2 Å (120 min irradiation), respectively. Crystal structures of inactivated *Ll*TrxR were only possible to obtain in FR-FR conformation. Addition of DTT to the drop with inactivated *Ll*TrxR did not give single crystals.

3.3.6 Data collection, refinement and analysis

X-ray diffraction data were collected at 100 K at I911-3, MAXII, Sweden or at ID30A-1, ESRF, France, with wavelengths range of 0.97–1.00 Å. Diffraction data were indexed, integrated, scaled and merged with XDS and XSCALE (Kabsch, 2010) or MOSFLM (Battye et al., 2011). Molecular replacement was performed with the program MOLREP (Vagin and Teplyakov, 1997) from the CCP4 suite (Winn et al., 2011) using the structure of *Sa*TrxR (PDB 4GCM) as the initial search model for the FO conformation, while *Ec*TrxR (PDB 1F6M) was used as template for the FR conformation. Restrained refinement was carried out using Refmac5 (Vagin et al., 2004) and manual inspection was done in Coot (Emsley et al., 2010). Local non-crystallographic symmetry restraints were imposed when appropriate. *Ll*TrxR obtained in FR-FR conformation crystallized in space group $P4_12_12_1$ with 1 monomer per asymmetric unit, FO-FO conformations crystallized in $P2_1$ with 4 monomers per asymmetric unit, while FO-FR conformation crystallized in P1 with 4 monomers per asymmetric unit. All RMSD values for structural alignments of the Cα-atoms were calculated using the program Superpose in CCP4 (Krissinel and Henrick, 2004). Figures displaying structural data were made with PyMOL (http://www.pymol.org/). The vacuum electrostatic potential surfaces were generated in PyMOL and should only be used for qualitative inspection. Parameters for LigPlot$^+$ were 2.70–3.35 Å for hydrogen bonds/salt bridges and 2.90–3.90 Å for "Non-bounded contact parameters".

Chapter 4. Concluding Remarks and Perspectives

In this chapter the results from chapter 2 and 3 are integrated to bring about a unifying model of the *Ll*TrxR light sensitivity.

The novel isoalloxazine *si*-face open space motif described in chapter 3 is proposed to enable isoalloxazine to act as a photosensitizer in the active site of the enzyme, due to its ability to accommodate O_2. The triplet state excited isoalloxazine is hypothesized to react with O_2 generating a superoxide radical ($O_2^{\bullet-}$) and/or generate singlet oxygen ($^1O_2$) corresponding to type I and type II reactions, respectively. It is known that singlet oxygen formation often competes with electron transfer reactions giving rise to a mix of ROS products (Derosa and Crutchley, 2002), which opens up for a scenario with a combination of the two reactions, potentially explaining how the various oxidized FAD species are generated during irradiation. One way to probe the involvement of singlet oxygen is by performing the photo-inactivation reaction in deuterated water. Singlet oxygen has a longer lifetime in deuterated water and as a consequence the oxidation level will increase if this ROS is involved. However, this approach may not be fully applicable in this context, as the ROS is hypothesized to be generated and reacting in a confined area within the protein, and hence the oxidant will not be in contact with the solvent. Another way to measure the presence of singlet oxygen is by the characteristic band emission at 1268 nm upon decay of singlet oxygen to its ground state (Khan and Kasha, 1979). This luminescence has a very weak quantum yield, since most collisions of singlet oxygen with solvent molecules generates heat (Miyamoto et al., 2014) and the expected low quantities generated in light-exposed TrxR might not be measurable. The fact that Met43 is not oxidized in the irradiated structures indicates that singlet oxygen is not generated in significant amounts, as the reaction rate constant towards this type of residue is high (2×10^7 dm^3 mol^{-1} s^{-1}), opposite of the superoxide radical that react with methionine with rate constant lower than 0.33 dm^3 mol^{-1} s^{-1} (Davies, 2016), though it has to be noted that these values are obtained for the free methionine. Peculiarly, the standard SOD activity assay utilizes the ability of photoexcited riboflavin to produce superoxide in the presence of methionine, using a 15 W fluorescent lamp (Beauchamp and Fridovich, 1971). In addition, superoxide is also known to be involved in DOPA formation upon reaction with Tyr phenoxyl radicals, as described in reaction mechanism proposed in Paper 2, which further indicates that superoxide is a generated in the photo-oxidation reaction. The difference in redox potential of reduced flavin and the active site disulfide is only 7 mV in *Ec*TrxR (O'Donnell and Williams, 1983; Lennon and

Williams, 1996), which can be compared to an increased redox potential of at least 50 mV for the 7,8-substituted oxidized flavin analogues (Edmondson and Ghisla, 1999). A consequence of these types of modifications of the FAD is therefore that the transfer of electrons from the isoalloxazine to the active-side disulfide is prevented, thus inactivating the enzyme. The fact that the photo-inactivated *Ll*TrxR preserves the ability to reduce O_2 in the presence of NADPH, underlines that the inactivation cannot be explained by inability to switch between the FO and FR conformations. Besides the presence of a *si*-face open space acting as an oxygen pocket, other factors play key roles in the light sensitivity of LMW TrxR, as evaluated from the lower inactivation rates of *Sa*TrxR and *Bs*TrxR. As the FAD interactions with the surrounding protein are almost identical for *Ll*TrxR, *Ec*TrxR and *Sa*TRxR, the explanation for the outstanding features of *Ll*TrxR could instead be found in a shift in the FO-FR equilibrium. Comparing stabilizing hydrogen bonds of *Ll*TrxR, *Ec*TrxR and *Sa*TrxR, the two latter have more hydrogen bonds in FO conformation that *Ll*TrxR, which potentially indicates that *Ll*TrxR is less stabilized in FO conformation, and hence the FO-FR equilibrium is shifted towards the FR conformation. This may explain why *Sa*TrxR and *Bs*TrxR, despite having a *si*-face oxygen pocket and conserved Tyr237 and Tyr133, are less sensitive to light. The active site disulfide in the vicinity of the excited isoalloxazine in the FO conformation might to some degree prevent superoxide formation, by the transfer of an electron to the disulfide bond. An electron transfer from excited tryptophan to a disulfide in a small cyclic peptide is previously described (Mozziconacci and Schöneich, 2014) and it is not unlikely that a similar protective mechanism indeed would make TrxR in FO conformation less susceptible to light induced oxidation. Protonation of the glutamate residues at low pH would weaken the salt bridge formation with the arginines between the FAD and NADPH domains (table 9), which might impact the FO/FR equilibrium, potentially changing the light sensitivity/robustness. This is seemingly supported by the protective effect observed at pH 4.0 (figure 3, Paper 1). From the above considerations the light sensitivity can be hypothesized to depend on two factors; the presence of the FAD *si*-face oxygen pocket as well as a conformational shift towards the FR conformation. The oxygen pocket is a consequence of Met43 (*L. lactis* numbering) bending away from the isoalloxazine ring system towards Pro15 (section 3.2.5), where space is available nearby the relatively small Ser64. In *Ec*TrxR the FAD *si*-face is occupied by $Leu44_{EcTrxR}$ and is restricted from bending away from the FAD because of the steric hindrance of the bulky Met66, ensuring an isoalloxazine *si*-face "closed" space (figure 4b, Paper 2). Combining the highlighted structural information with a multiple sequence alignment, it is possible to predict other TrxR

that potentially harbor the FAD *si*-face oxygen pocket. Appendix C shows an alignment of TrxR from selected organisms. Worth noticing is that the combination of Met43 and Ser64 (*L. lactis* numbering) is conserved together with the Met-Pro motif (Met18, Met67 and Pro15) in all organisms predicted to have an oxygen pocket. This is in contrast to most other aligned LMW TrxR that combine an aliphatic *si*-face residue with methionine at the Ser64 position (Appendix C). Another striking detail is that all TrxR with predicted oxygen pockets distinctly have Tyr133 and Tyr237 fully conserved, as well as a single deletion between amino acid 55–56 compared to aligned sequences. Phylogenetic analysis suggests that the predicted oxygen pocket is found in the genera of *Streptococcus*, *Bacillus*, *Staphylococcus*, *Listeria*, *Lactobacillus*, *Enterococcus*, *Lactococcus* and *Erysipelothrix*, distinctively grouped as indicated from the phylogenetic tree (figure 57, Appendix C). The residues forming the oxygen pocket is conserved in all aligned TrxR from organisms belonging to the phylum of *Firmicutes*, except the atypical *E. acidaminophilum* belonging to the genus of *Eubacterium*. Other selected TrxR from Gram-positive (*B. longum* and *P. acnes*) and Gram-negative bacteria as well as eukaryotes do not possess residues associated with the oxygen pocket (Appendix C). The oxygen pocket is predicted in homologous enzymes from pathogen bacteria such as *S. aureus, B. anthracis*, *Listeria monocytogenes*, *Streptococcus pyogenes*, *Enterococcus faecalis* and *Erysipelothrix rhusiopathiae*, which might afford applications in clinical photo-therapy.

Preliminary experiments showed that a long light exposure time is required to kill *L. lactis* cells kept at 4°C, as evaluated from viability count, coinciding with loss of TrxR activity. The low temperature during the irradiation has the downside that the general enzyme activity is lowered, which means that scavengers like peroxiredoxins (Prx) are not providing proper protection against ROS. Blue light therapy has the advantage over photodynamic therapy (PDT) that it does not depend on the addition of an exogenous photosensitizer. Instead it takes advantage of the natural occurring molecules within the cell that can act as photosensitizer, when excited at the proper wavelength. Furthermore, potential harmful effects of light in the UV region are avoided. Light of wavelengths in the violet/blue range of 405–470 nm has shown to inactivate important wound pathogenic bacteria, including *Pseudomonas aeruginosa*, *Propionibacterium acnes*, *Helicobacter pylori* and *S. aureus* (Dai et al., 2012). Phototherapy is known to be beneficial for some skin diseases like acne vulgaris with *P. acnes* as the causing agent, and commercial lamps in the blue light range are available on the market. A combination of blue (415 nm)

and red (660 nm) light therapy have been shown be a better treatment compared to blue light only (Papageorgiou et al., 2000). Studies of light (>400 nm) treated *S. aureus* verify that the availability of oxygen is the rate-limiting factor for the viability (Maclean et al., 2008). The molecular basis for the blue light inactivation of bacteria is not known, but believed to be involving generation of singlet oxygen by excited porphyrins. This hypothesis was indirectly supported by accumulation of porphyrins correlates with death rates (Hamblin et al., 2005). However, this model is not applicable for *L. lactis* and related bacteria that lack the genes encoding enzymes in the porphyrin biosynthesis pathway. Thus other compounds must be responsible for inactivating the cells by ROS formation during light exposure in *L. lactis*.

Light is in many organisms used as a signal to assess the status of the environment. Photoreceptors like the blue-light-utilizing FAD (BLUF) domain, the light-oxygen-voltage (LOV) domain and the cryptochrome (Cry) are induced by flavin photoexcitation. This process involves changes of the protein structure and flavin reactivity, such as covalent bond formation (LOV), rearrangements of hydrogen bonds (BLUF), and redox reactions (Cry) (Losi and Gärtner, 2012). LOV photoreceptors involves a flavin-cysteine adduct whereas BLUF are activated by changes in the hydrogen bond network to the flavin. The photoreceptor domains are *e.g.* linked to kinases, thus inducing a cascade upon light induction (Purcell et al., 2007). A recent study in yeast showed how light and hydrogen peroxide is involved in signaling (Bodvard et al., 2017). The yeast peroxisomal oxidase generates hydrogen peroxide upon light exposure, which is sensed by a peroxiredoxin that transfers the signal to cytosolic Trx, which counteract phosphorylation transcription factor Msn2, causing Msn2 to oscillations in and out of the nucleus (Bodvard et al., 2017). This mechanism provides another layer of information on how cells are known to rhythmically regulate their genes (Lin et al., 2015). Even though yeast is one of the few organisms that lacks dedicated photoreceptors, this example underlines that the interplay of light and cellular response has many facets. Even though no experimental evidence has been presented to support the involvement of TrxR in light signaling, it cannot be rules out that *L. lactis* uses *Ll*TrxR as a sensor of light and/or O_2 which would prevent electron flow to *Ll*NrdH and ribonucleotide reductase with consequences for DNA replication and cell division.

The evolutionary background and physiological relevance of light-sensitive TrxR is not clear. As an inhabitant of plant and animal surfaces, *L. lactis* inevitably is exposed to light. Even though the results

presented in this thesis demonstrate photo-inactivation of TrxR, the O_2 scavenging systems of *L. lactis* in dividing cells at ambient temperatures may be so efficient that *Ll*TrxR inactivation is avoided. In this context it is also interesting to discuss the side reaction of *Ll*TrxR as an O_2 reductant generating H_2O_2. Because of the low rate of this reaction compared to for example NADH oxidase *Ll*TrxR most likely does not contribute significantly as an oxygen scavenger under physiological conditions. The oxygen pocket could possibly be an evolutionary remain of the closely related protein AhpF (Poole, Reynolds, et al., 2000; Hirt et al., 2002), but this seems unlikely, as the *si*-face methionine with the adjacent Met-Pro motif conserved among *Firmicutes* is not found in AhpF.

Future work in shedding light on the photo-sensitivity of *Ll*TrxR and homologs includes verification of the oxygen pocket hypothesis by performing site-directed mutagenesis on *Ll*TrxR and *Ec*TrxR by designing *Ll*TrxR light robust (Met43Leu and Ser64Met) and *Ec*TrxR sensitive (Leu44Met and Met66Ser) mutants. In addition an *Ll*TrxR Tyr237Phe mutant may be useful to further investigate the photo-inactivation mechanism. Yet another, but somewhat more difficult task would be mutating amino acids responsible in stabilizing either FO- or FR-conformation, hence providing new information of the impact on light sensitivity. For this type of analysis it is however important to establish robust and reliable procedures to determine the conformational equilibrium of the investigated TrxR. A pH profile of the equilibrium constant could turn out to be of great value to map potential correlation between light sensitivity and the FR conformation. It is also crucial to establish a new more well-defined irradiation design, controlling the effect (W/cm^2) and wavelength. This could potentially increase the inactivation of *Sa*TrxR and *Bs*TrxR at the proper wavelength and give a more precise picture of the degree of light sensitivity. The current *in vivo* irradiation result was only the starting point that provided the proof-of-concept and having a more well-defined system would give a clearer idea about to what extent *L. lactis* and other microorganisms respond to light.

References

Abrahamse, H. & Hamblin, M. R. (2016) New photosensitizers for photodynamic therapy. *Biochemical Journal*. **473** (4), 347–364.

Alderton, W. K. et al. (2001) Nitric oxide synthases: structure, function and inhibition. *The Biochemical journal*. **357** (Pt 3), 593–615.

Arenas, F. A. et al. (2010) The *Escherichia coli* btuE gene, encodes a glutathione peroxidase that is induced under oxidative stress conditions. *Biochemical and biophysical research communications*. **398** (4), 690–694.

Argyrou, A. & Blanchard, J. S. (2004) Flavoprotein disulfide reductases: advances in chemistry and function. *Progress in Nucleic Acid Research and Molecular Biology*. **78,** 89–142.

Arioli, S. et al. (2013) Increasing the heme-dependent respiratory efficiency of *Lactococcus lactis* by inhibition of lactate dehydrogenase. *Applied and environmental microbiology*. **79** (1), 376–380.

Arnér, E. S. J. & Holmgren, A. (2000) Physiological functions of thioredoxin and thioredoxin reductase. *European Journal of Biochemistry* **267** (20), 6102–6109.

Baker, J. L. et al. (2014) Streptococcus mutans NADH Oxidase Lies at the Intersection of Overlapping Regulons Controlled by Oxygen and NAD^+ Levels. *Journal of Bacteriology*. **196** (12), 2166–2177.

Baker, L. M. S. et al. (2001) Essential Thioredoxin-Dependent Peroxiredoxin System from Helicobacter pylori: Genetic and Kinetic Characterization. *Journal of Bacteriology*. **183** (6), 1961–1973.

Balmer, Y. et al. (2003) Proteomics gives insight into the regulatory function of chloroplast thioredoxins. *Proceedings of the National Academy of Sciences of the United States of America*. **100** (1), 370–375.

Balmer, Y. et al. (2004) Thioredoxin links redox to the regulation of fundamental processes of plant mitochondria. *Proceedings of the National Academy of Sciences*. **101** (8), 2642–2647.

Barkholt, V. & Jensen, A. L. (1989) Amino acid analysis: determination of cysteine plus half-cystine in proteins after hydrochloric acid hydrolysis with a disulfide compound as additive. *Analytical biochemistry*. **177** (2), 318–322.

Battye, T. G. G. et al. (2011) iMOSFLM: A new graphical interface for diffraction-image processing with MOSFLM. *Acta Crystallographica Section D: Biological Crystallography*. **67** (4), 271–281.

Beauchamp, C. & Fridovich, I. (1971) Superoxide dismutase: Improved assays and an assay applicable to acrylamide gels. *Analytical Biochemistry*. **44** (1), 276–287.

Bielski, B. H. et al. (1983) A study of the reactivity of HO_2/O_2^- with unsaturated fatty acids. *The Journal of biological chemistry*. **258** (8), 4759–4761.

Biterova, E. I. et al. (2005) Crystal structures of oxidized and reduced mitochondrial thioredoxin reductase provide molecular details of the reaction mechanism. *Proceedings of the National Academy of Sciences of the United States of America*. **102,** 15018–15023.

Björnberg, O. et al. (2012) Dissecting molecular interactions involved in recognition of target disulfides by the barley thioredoxin system. *Biochemistry*. **51** (49), 9930–9939.

Björnberg, O. et al. (2014) *Lactococcus lactis* TrxD represents a subgroup of thioredoxins prevalent in Gram-positive bacteria containing WCXDC active site motifs. *Archives of biochemistry and biophysics*. **564,** 164–172.

Björnberg, O. et al. (2015) *Lactococcus lactis* Thioredoxin Reductase Is Sensitive to Light Inactivation. *Biochemistry*. **54** (8), 1628–1637.

Blankenhorn, G. (1975) Flavin-Nicotinamide Biscoenzymes: Models for the Interaction between NADH (NADPH) and Flavin in Flavoenzymes. Reaction Rates and Physicochemical Properties of Intermediate Species. *European Journal of Biochemistry*. **50** (2), 351–356.

Blankenhorn, G. (1976) Nicotinamide-Dependent One-Electron and Two-Electron (Flavin) Oxidoreduction : Thermodynamics, Kinetics, and Mechanism. *European Journal of Biochemistry*. **67** (1), 67–80.

Bodvard, K. et al. (2017) Light-sensing via hydrogen peroxide and a peroxiredoxin. *Nature Communications*. **8,** 14791.

Bolotin, A. et al. (2001) The Complete Genome Sequence of the Lactic Acid Bacterium. *Genome Research*. **11,** 731–753.

Brigelius-Flohé, R. & Maiorino, M. (2013) Glutathione peroxidases. *Biochimica et Biophysica Acta (BBA) - General Subjects*. **1830** (5), 3289–3303.

Buettner, G. R. (1993) The Pecking Order of Free Radicals and Antioxidants: Lipid Peroxidation, α-Tocopherol, and Ascorbate. *Archives of Biochemistry and Biophysics*. **300** (2), 535–543.

Calhoun, L. N. & Kwon, Y. M. (2011) Structure, function and regulation of the DNA-binding protein Dps and its role in acid and oxidative stress resistance in *Escherichia coli*: a review. *Journal of applied microbiology*. **110** (2), 375–386.

Cardoso, D. R. et al. (2004) Reactivity of Bovine Whey Proteins, Peptides, and Amino Acids toward Triplet Riboflavin as Studied by Laser Flash Photolysis. *Journal of Agricultural and Food Chemistry*. **52** (21), 6602–6606.

Carlioz, a & Touati, D. (1986) Isolation of superoxide dismutase mutants in *Escherichia coli*: is superoxide dismutase necessary for aerobic life? *The EMBO journal*. **5** (3), 623–630.

Chartron, J. et al. (2007) 3‘-Phosphoadenosine-5‘-phosphosulfate Reductase in Complex with Thioredoxin: A Structural Snapshot in the Catalytic Cycle *Biochemistry*. **46** (13), 3942–3951.

Cohen, G. et al. (1994) The thioredoxin system of Penicillium chrysogenum and its possible role in penicillin biosynthesis. *Journal of Bacteriology*. **176** (4), 973–984.

Collet, J.-F. et al. (2003) Thioredoxin 2, an Oxidative Stress-induced Protein, Contains a High Affinity Zinc Binding Site. *Journal of Biological Chemistry*. **278** (46), 45325–45332.

Collet, J.-F. & Messens, J. (2010) Structure, Function, and Mechanism of Thioredoxin Proteins. *Antioxidants & Redox Signaling*. **13** (8), 1205–1216.

Condon, S. (1983) Aerobic Metabolism of Lactic Acid Bacteria. Irish Journal of Food Science and Technology **7** (1), 15–25.

Condon, S. (1987) Responses of lactic acid bacteria to oxygen. *FEMS Microbiology Letters*. **46** (3), 269–280.

Lo Conte, M. & Carroll, K. S. (2013) The redox biochemistry of protein sulfenylation and sulfinylation. *Journal of Biological Chemistry*. **288** (37), 26480–26488.

Cross, A. R. & Segal, A. W. (2004) The NADPH oxidase of professional phagocytes—prototype of the NOX electron transport chain systems. *Biochimica et Biophysica Acta (BBA) - Bioenergetics*. **1657** (1), 1–22.

D'Autréaux, B. & Toledano, M. B. (2007) ROS as signalling molecules: mechanisms that generate specificity in ROS homeostasis. *Nature Reviews Molecular Cell Biology*. **8** (10), 813–824.

Dai, T. et al. (2012) Blue light for infectious diseases: Propionibacterium acnes, Helicobacter pylori, and beyond? *Drug Resistance Updates*. **15** (4), 223–236.

Davies, M. J. (2016) Protein oxidation and peroxidation. *Biochemical Journal*. **473** (7), 805–825.

Davies, M. J. (2003) Singlet oxygen-mediated damage to proteins and its consequences. *Biochemical and Biophysical Research Communications*. **305** (3), 761–770.

Derosa, M. C. & Crutchley, R. J. (2002) Photosensitized singlet oxygen and its applications. *Coordination Chemistry Reviews*. **233-234,** 351-371.

Dizdaroglu, M. et al. (1991) Chemical nature of in vivo DNA base damage in hydrogen peroxide-treated mammalian cells. *Archives of Biochemistry and Biophysics*. **285** (2), 388–390.

Drazic, A. & Winter, J. (2014) The physiological role of reversible methionine oxidation. *Biochimica et Biophysica Acta - Proteins and Proteomics*. **1844** (8), 1367–1382.

Dubbs, J. M. & Mongkolsuk, S. (2007) Peroxiredoxins in bacterial antioxidant defense. *Sub-cellular biochemistry*. **44,** 143–193.

Duwat, P. et al. (2001) Respiration Capacity of the Fermenting Bacterium *Lactococcus lactis* and Its Positive Effects on Growth and Survival. *Journal of Bacteriology*. **183** (15), 4509–4516.

Edmondson, D. E. & Ghisla, S. (1999) Electronic effects of 7 and 8 ring substituents as predictors of flavin oxidation-reduction potentials. *Flavin and Flavoproteins*. **76,** 71–76.

Edmondson, D. E. & Newton-Vinson, P. (2001) The Covalent FAD of Monoamine Oxidase: Structural and Functional Role and Mechanism of the Flavinylation Reaction. *Antioxidants & Redox Signaling*. **3** (5), 789–806.

Edmondson, D. E. & Singer, T. P. (1973) Oxidation-Reduction Properties of the 8α-Substituted Flavins. *Journal of Biological Chemistry* . **248** (23), 8144–8149.

Edwards, A. M. (2006) Flavins: Photochemistry and Photobiology. Silva E. & Edwards, A. M. (eds.). Cambridge: Royal Society of Chemistry.

Efimov, I. & McIntire, W. S. (2004) A study of the spectral and redox properties and covalent flavinylation of the flavoprotein component of p-cresol methylhydroxylase reconstituted with FAD analogues. *Biochemistry*. **43** (32), 10532–10546.

Efler, P. et al. (2015) Two Lactococcus lactis thioredoxin paralogues play different roles in responses to arsenate and oxidative stress. *Microbiology*. **161** (3), 528–538.

Eichner, A. et al. (2015) Fast and effective inactivation of *Bacillus atrophaeus* endospores using light-activated derivatives of vitamin B2. *Photochemical & photobiological sciences.* **14** (2), 387–396.

Ellman, G. L. (1959) Tissue sulfhydryl groups. *Archives of Biochemistry and Biophysics*. **82** (1), 70–77.

Emsley, P. et al. (2010) Features and development of Coot. *Acta Crystallographica Section D Biological Crystallography*. **66** (4), 486–501.

Erlendsson, L. S. et al. (2003) *Bacillus subtilis* ResA is a thiol-disulfide oxidoreductase involved in cytochrome c synthesis. *Journal of Biological Chemistry*. **278** (20), 17852–17858.

Erlendsson, L. S. et al. (2004) *Bacillus subtilis* StoA is a thiol-disulfide oxidoreductase important for spore cortex synthesis. *Journal of Bacteriology*. **186** (18), 6230–6238.

Fang, X. et al. (1998) Reaction of the superoxide radical with the N-centered radical derived from N-acetyltryptophan methyl ester. *Journal of the Chemical Society, Perkin Transactions*. **2,** 259–263.

Farmer, E. E. & Mueller, M. J. (2013) ROS-Mediated Lipid Peroxidation and RES-Activated Signaling. *Annual Review of Plant Biology*. **64** (1), 429–450.

Felipe, F. L. De et al. (1998) Cofactor engineering: a novel approach to metabolic engineering in *Lactococcus lactis* by controlled expression of NADH oxidase. *Journal of bacteriology*. **180** (15), 3804–3808.

Fernandes, A. P. & Holmgren, A. (2004) Glutaredoxins: Glutathione-Dependent Redox Enzymes with Functions Far Beyond a Simple Thioredoxin Backup System. *Antioxidants & Redox Signaling*. **6** (1), 63–74.

Finkel, T. & Holbrook, N. J. (2000) Oxidants, oxidative stress and the biology of ageing. *Nature*. **408** (6809), 239–247.

Flint, D. H. et al. (1993) The inactivation of Fe-S cluster containing hydro-lyases by superoxide. *Journal of Biological Chemistry*. **268** (30), 22369–22376.

Fritz-Wolf, K. et al. (2011) Crystal structure of the human thioredoxin reductase-thioredoxin complex. *Nature Communications*. **2**, 383.

Fritz-Wolf, K. et al. (2007) The Structure of Human Thioredoxin Reductase 1 Provides Insights into C-terminal Rearrangements During Catalysis. *Journal of Molecular Biology*. **370** (1), 116–127.

Garrigues, C. et al. (1997) Control of the shift from homolactic acid to mixed-acid fermentation in *Lactococcus lactis*: predominant role of the NADH/NAD+ ratio. *Journal of bacteriology*. **179** (17), 5282–5287.

Gerschman, R. et al. (1954) Oxygen Poisoning and X-irradiation: A Mechanism in Common. *Science*. **119** (3097), 623–626.

Gilbert, B. H. F. & Mclean, M. (1963) Molecular and cellular aspects of thiol-disulfide exchange. *Advances in Enzymology and Related Areas of Molecular Biology*. **63**, 69-172.

Gonzalez-Flecha, B. & Demple, B. (1995) Metabolic sources of hydrogen peroxide in aerobically growing *Escherichia coli*. Journal of Biological Chemistry **270** (23), 3681–13687.

Gromer, S. et al. (2003) Active sites of thioredoxin reductases: why selenoproteins? *Proceedings of the National Academy of Sciences of the United States of America*. **100** (22), 12618–12623.

Gustafsson, T. N. et al. (2007) High-resolution structures of oxidized and reduced thioredoxin reductase from Helicobacter pylori. *Acta Crystallographica Section D Biological Crystallography*. **63** (7), 833–843.

Halliwell, B. (1982) Superoxide-dependent formation of hydroxyl radicals in the presence of iron salts is a feasible source of hydroxy radicals in vivo. *The Biochemical journal*. **205** (2), 461–463.

Hamblin, M. R. et al. (2005) Helicobacter pylori accumulates photoactive porphyrins and is killed by visible light. *Antimicrobial agents and chemotherapy*. **49** (7), 2822–2827.

Harman, D. (1956) Aging: a theory based on free radical and radiation chemistry. *Journal of gerontology*. **11** (3), 298–300.

Heelis, P. F. (1982) The photophysical and photochemical properties of flavins (isoalloxazines). *Chemical Society Reviews*. **11**, 15-39.

Heuts, D. P. H. M. et al. (2009) What's in a covalent bond?: On the role and formation of covalently bound flavin cofactors. *FEBS Journal*. **276**, 3405–3427.

Heux, S. et al. (2006) Cofactor engineering in *Saccharomyces cerevisiae*: Expression of a H_2O-forming NADH oxidase and impact on redox metabolism. *Metabolic Engineering*. **8** (4), 303–314.

Higuchi, M. et al. (1999) Functions of two types of NADH oxidases in energy metabolism and oxidative stress of Streptococcus mutans. *Journal of Bacteriology*. **181** (19), 5940–5947.

Hillion, M. & Antelmann, H. (2015) Thiol-based redox switches in prokaryotes. *Biological chemistry*. **396**, 415-44

Hirt, R. P. et al. (2002) The diversity and evolution of thioredoxin reductase: new perspectives. *Trends in Parasitology*. **18** (7), 302–308.

Holmgren, A. (1976) Hydrogen donor system for *Escherichia coli* ribonucleoside-diphosphate reductase dependent upon glutathione. *Proceedings of the National Academy of Sciences of the United States of America*. **73** (7), 2275–2279.

Holmgren, A. (1989) Thioredoxin and glutaredoxin systems. *The Journal of biological chemistry*. **264** (24), 13963–13966.

Holmgren, A. et al. (1975) Three-dimensional structure of *Escherichia coli* thioredoxin-S2 to 2.8 A resolution. *Proceedings of the National Academy of Sciences*. **72** (6), 2305–2309.

Holmgren, A. & Sengupta, R. (2010) The use of thiols by ribonucleotide reductase. *Free Radical Biology and Medicine*. **49** (11), 1617–1628.

Hougland, J. L. et al. (2013) Molecular Basis of Oxidative Stress: Chemistry, Mechanisms, and Disease Pathogenesis. 1st edition. Villamena, F. A. (ed.). Wiley.

Huson, D. H. & Scornavacca, C. (2012) Dendroscope 3: an interactive tool for rooted phylogenetic trees and networks. *Systematic biology*. **61** (6), 1061–1067.

Hägglund, P. et al. (2008) Identification of thioredoxin disulfide targets using a quantitative proteomics approach based on isotope-coded affinity tags. *Journal of proteome research*. **7** (12), 5270–5276.

Hägglund, P. et al. (2010) Identification of thioredoxin target disulfides in proteins released from barley aleurone layers. *Journal of Proteomics*. **73** (6), 1133–1136.

Imlay, J. a (2003) Pathways of oxidative damage. *Annual review of microbiology*. **57**, 395–418.

Imlay, J. A. (2008) Cellular defenses against superoxide and hydrogen peroxide. *Annual review of biochemistry*. **77**, 755–776.

Imlay, J. A. (2014) Transcription Factors That Defend Bacteria Against Reactive Oxygen Species. *Annual review of microbiology*. **69** (1), 93-108.

Imlay, J. A. (1995) A metabolic enzyme that rapidly produces superoxide, fumarate reductase of *Escherichia coli*. Journal of Biological Chemistry **270** (34), 19767–19777.

Ischiropoulos, H. (2009) Protein tyrosine nitration-An update. *Archives of Biochemistry and Biophysics*. **484** (2), 117–121.

Jaeger, T. (2007) Peroxiredoxin systems in mycobacteria. *Sub-cellular biochemistry*. **44**, 207–217.

Jancarik, J. & Kim, S. H. (1991) Sparse matrix sampling: a screening method for crystallization of proteins. *Journal of Applied Crystallography*. **24** (4), 409–411.

Jang, S. & Imlay, J. A. (2007) Micromolar intracellular hydrogen peroxide disrupts metabolism by damaging iron-sulfur enzymes. *Journal of Biological Chemistry*. **282** (2), 929–937.

Jensen, J. M. et al. (2012) Inactivation of barley limit dextrinase inhibitor by thioredoxin-catalysed disulfide reduction. *FEBS Letters*. **586** (16), 2479–2482.

Jensen, P. R. & Hammer, K. (1993) Minimal Requirements for Exponential-Growth of *Lactococcus lactis*. *Applied and Environmental Microbiology*. **59** (12), 4363–4366.

Jiang, R. et al. (2005) Comparison of Alkyl Hydroperoxide Reductase (AhpR) and Water-Forming NADH Oxidase from *Lactococcus lactis* ATCC 19435. *Advanced Synthesis & Catalysis*. **347** (7–8), 1139–1146.

Jin, J. et al. (2008) Covalent flavinylation of vanillyl-alcohol oxidase is an autocatalytic process. *FEBS Journal*. **275** (20), 5191–5200.

Kabsch, W. (2010) XDS. *Acta Crystallographica Section D Biological Crystallography*. **66** (2), 125–132.

Katti, S. K. et al. (1990) Crystal structure of thioredoxin from *Escherichia coli* at 1.68 Å resolution. *Journal of Molecular Biology*. **212** (1), 167–184.

Kemal, C. et al. (1977) Reaction of $^{3}O_{2}$ with dihydroflavins. 1. N-^{3,5}-dimethyl-1,5-dihydrolumiflavin and 1,5-dihydroisoalloxazines. *Journal of the American Chemical Society*. **99** (22), 7272–7286.

Kenney, W. C. et al. (1974) The Covalently Bound Flavin of Chromatium Cytochrome c552. *Eur. J. Biochem.* **48**, 449-453.

Kerwin, B. A. & Remmele, R. L. (2007) Protect from Light: Photodegradation and Protein Biologics. *Journal of Pharmaceutical Sciences*. **96** (6), 1468–1479.

Khan, A. U. & Kasha, M. (1979) Direct spectroscopic observation of singlet oxygen emission at 1268 nm excited by sensitizing dyes of biological interest in liquid solution. *Proceedings of the National Academy of Sciences of the United States of America*. **76** (12), 6047–6049.

Kikugawa, K. et al. (1994) Damage of amino acids and proteins induced by nitrogen dioxide, a free radical toxin, in air. *Free Radical Biology and Medicine*. **16** (3), 373–382.

Kim, G. et al. (2014) Methionine oxidation and reduction in proteins. *Biochimica et Biophysica Acta - General Subjects*. **1840** (2), 901–905.

Kirkensgaard, K. G. et al. (2009) Structure of Hordeum vulgare NADPH-dependent thioredoxin reductase 2. Unwinding the reaction mechanism. *Acta Crystallographica Section D Biological Crystallography*. **65** (9), 932–941.

Kirkensgaard, K. G. et al. (2014) A novel twist on molecular interactions between thioredoxin and nicotinamide adenine dinucleotide phosphate-dependent thioredoxin reductase. *Proteins*. **82** (4), 607–619.

Koetter, J. W. A. & Schulz, G. E. (2005) Crystal structure of 6-hydroxy-D-nicotine oxidase from Arthrobacter nicotinovorans. *Journal of Molecular Biology*. **352** (2), 418–428.

Krieger-Liszkay, A. (2005) Singlet oxygen production in photosynthesis. *Journal of Experimental Botany*. **56** (411), 337–346.

Krissinel, E. & Henrick, K. (2004) Secondary-structure matching (SSM), a new tool for fast protein structure alignment in three dimensions. *Acta Crystallographica Section D Biological Crystallography*. **60** (12), 2256–2268.

König, H. & Fröhlich, J. (2009) Biology of Microorganisms on Grapes, in Must and in Wine. Helmut König et al. (eds.). Berlin, Heidelberg: Springer Berlin Heidelberg.

Laskowski, R. A. & Swindells, M. B. (2011) LigPlot^{+}: Multiple ligand-protein interaction diagrams for drug discovery. *Journal of chemical information and modeling*. **51** (10), 2778–2786.

Laurent, C. T. et al. (1964) Enzymatic Synthesis of Deoxyribonucleotides. *The Journal of Biological Chemistry*. **239** (10), 3436–3444.

Lechardeur, D. et al. (2011) Using heme as an energy boost for lactic acid bacteria. *Current Opinion in Biotechnology*. **22** (2), 143–149.

Lee, S. et al. (2013) Thioredoxin and Thioredoxin Target Proteins: From Molecular Mechanisms to Functional Significance. *Antioxidants & Redox Signaling*. **18** (10), 1165–1207.

Leferink, N. G. H. et al. (2009) Identification of a gatekeeper residue that prevents dehydrogenases from acting as oxidases. *Journal of Biological Chemistry*. **284** (7), 4392–4397.

Lennon, B. W. et al. (2000) Twists in catalysis: alternating conformations of *Escherichia coli* thioredoxin reductase. *Science (New York, N.Y.)*. **289** (5482), 1190–1194.

Lennon, B. W. & Williams, C. H. (1996) Enzyme-monitored turnover of *Escherichia coli* thioredoxin reductase: insights for catalysis. *Biochemistry*. **35** (15), 4704–4712.

Lennon, B. W. & Williams, C. H. (1997) Reductive half-reaction of thioredoxin reductase from *Escherichia coli*. *Biochemistry*. **36** (31), 9464–9477.

Li, Y. et al. (2007) Conformational fluctuations coupled to the thiol-disulfide transfer between thioredoxin and arsenate reductase in *Bacillus subtilis*. *The Journal of biological chemistry*. **282** (15), 11078–11083.

Li, Y. et al. (2003) Glutathione Protects *Lactococcus lactis* against Oxidative Stress Glutathione Protects *Lactococcus lactis* against Oxidative Stress. *Applied and Environmental Microbiology* **69** (10), 5739-5745 .

Lin, Y. et al. (2015) Combinatorial gene regulation by modulation of relative pulse timing. *Nature*. **527** (7576), 54–58.

Loi, V. Van et al. (2015) Redox regulation by reversible protein S-thiolation in bacteria. *Frontiers in microbiology*. **6**, 187.

Losi, A. & Gärtner, W. (2012) The evolution of flavin-binding photoreceptors: an ancient chromophore serving trendy blue-light sensors. *Annual review of plant biology*. **63**, 49–72.

Lu, J. & Holmgren, A. (2014) The thioredoxin antioxidant system. *Free radical biology & medicine*. **66**, 75–87.

Luo, S. & Levine, R. L. (2008) Methionine in proteins defends against oxidative stress. *The FASEB Journal*. **23** (2), 464–472.

Ma, X. X. et al. (2011) Structural plasticity of the thioredoxin recognition site of yeast methionine s-sulfoxide reductase Mxr1. *Journal of Biological Chemistry*. **286** (15), 13430–13437.

Maclean, M. et al. (2008) The role of oxygen in the visible-light inactivation of Staphylococcus aureus. *Journal of photochemistry and photobiology. B, Biology*. **92** (3), 180–184.

Maeda, K. et al. (2006) Structural basis for target protein recognition by the protein disulfide reductase thioredoxin. *Structure (London, England : 1993)*. **14** (11), 1701–1710.

Maisch, T. et al. (2014) Fast and effective photodynamic inactivation of multiresistant bacteria by cationic riboflavin derivatives. *PLOS ONE*. **9** (12), e111792 .

Makarova, K. S. & Koonin, E. V. (2007) Evolutionary genomics of lactic acid bacteria. *Journal of Bacteriology*. **189** (4), 1199–1208.

Martin, J. L. (1995) Thioredoxin -a fold for all reasons. *Structure*. **3** (3), 245–250.

Mattevi, A. (2006) To be or not to be an oxidase: Challenging the oxygen reactivity of flavoenzymes. *Trends in biochemical sciences*. **31** (5), 276–283.

McCord, J. M. & Fridovich, I. (1969) Superoxide dismutase. An enzymic function for erythrocuprein (hemocuprein). *The Journal of biological chemistry*. **244** (22), 6049–6055.

McDonald, C. A. et al. (2011) Oxygen Reactivity in Flavoenzymes: Context Matters. *Journal of the American Chemical Society*. **133** (42), 16809–16811.

McWilliam, H. et al. (2013) Analysis Tool Web Services from the EMBL-EBI. *Nucleic acids research*. **41**, W597-600.

Messner, K. R. & Imlay, J. A. (2002) Mechanism of superoxide and hydrogen peroxide formation by fumarate reductase, succinate dehydrogenase, and aspartate oxidase. *Journal of Biological Chemistry*. **277** (45), 42563–42571.

Meyer, Y. et al. (2009) Thioredoxins and glutaredoxins: unifying elements in redox biology. *Annual review of genetics*. **43**, 335–367.

Miller, A.-F. (2012) Superoxide dismutases: Ancient enzymes and new insights. *FEBS Letters*. **586** (5), 585–595.

Miyamoto, S. et al. (2014) Singlet molecular oxygen generated by biological hydroperoxides. *Journal of Photochemistry and Photobiology B: Biology*. **139**, 24–33.

Miyoshi, A. et al. (2003) Oxidative stress in *Lactococcus lactis*. *Genetics and molecular research : GMR*. **2** (4), 348–359.

Montrichard, F. et al. (2009) Thioredoxin targets in plants: The first 30 years. *Journal of Proteomics*. **72** (3), 452–474.

Moore, E. C. et al. (1964) Enzymatic Synthesis of Deoxyribonucleotides.V. Purification and Properties of Thioredoxin Reductase From *Escherichia coli* B. *The Journal of biological chemistry*. **239** (10), 3445–3452.

Mozziconacci, O. & Schöneich, C. (2014) Effect of Conformation on the Photodegradation of Trp- And Cystine-Containing Cyclic Peptides: Octreotide and Somatostatin. *Molecular Pharmaceutics*. **11** (10), 3537–3546.

Muller, E. G. D. (1996) A Glutathione Reductase Mutant of Yeast Accumulates High Levels of Oxidized Glutathione and Requires Thioredoxin for Growth. *Molecular biology of the cell*. **7** (11), 1805–1813.

Mulrooney, S. B. & Williams, C. H. (1997) Evidence for two conformational states of thioredoxin reductase from *Escherichia coli*: use of intrinsic and extrinsic quenchers of flavin fluorescence as probes to observe domain rotation. *Protein science : a publication of the Protein Society*. **6** (10), 2188–2195.

Murphy, M. P. (2009) How mitochondria produce reactive oxygen species. *Biochemical Journal*. **417** (1), 1–13.

Möller, M. N. et al. (2012) Superoxide Reaction with Tyrosyl Radicals Generates para-Hydroperoxy and para-Hydroxy Derivatives of Tyrosine. *Journal of the American Chemical Society*. **134** (40), 16773–16780.

Nagy, P. et al. (2009) Superoxide-mediated formation of tyrosine hydroperoxides and methionine sulfoxide in peptides through radical addition and intramolecular oxygen transfer. *Journal of Biological Chemistry*. **284** (22), 14723–14733.

Nakano, S. et al. (2003) Spx-dependent global transcriptional control is induced by thiol-specific oxidative stress in *Bacillus subtilis*. *Proceedings of the National Academy of Sciences of the United States of America*. **100** (23), 13603–13608.

Navrot, N. et al. (2015) A redox-dependent dimerization switch regulates activity and tolerance for reactive oxygen species of barley seed glutathione peroxidase. *Plant Physiology and Biochemistry*. **90**, 58–63.

Niimura, Y. et al. (1995) *Amphibacillus xylanus* NADH Oxidase and Salmonella typhimurium Alkyl-hydroperoxide Reductase Flavoprotein Components Show Extremely High Scavenging Activity for Both Alkyl Hydroperoxide and Hydrogen Peroxide in the Presence of *S. typhimurium* Alkyl-hydroper. *Journal of Biological Chemistry*. **270** (43), 25645–25650.

Nonell, S. & Flors, C. (2016) Singlet Oxygen : Applications in Biosciences and Nanosciences, Volume 1. Santi Nonell & Cristina. Flors (eds.). Royal Society of Chemistry.

Nordberg, J. & Arnér, E. S. J. (2001) Reactive oxygen species, antioxidants, and the mammalian thioredoxin system. *Free Radical Biology and Medicine*. **31** (11), 1287–1312.

Nuriel, T. et al. (2011) Protein nitrotryptophan: Formation, significance and identification. *Journal of Proteomics*. **74** (11), 2300–2312.

O'Brien, P. J. (1991) Molecular mechanisms of quinone cytotoxicity. *Chemico-Biological Interactions*. **80** (1), 1–41.

O'Donnell, M. E. & Williams, C. H. (1983) Proton stoichiometry in the reduction of the FAD and disulfide of *Escherichia coli* thioredoxin reductase. Evidence for a base at the active site. *The Journal of biological chemistry*. **258** (22), 13795–13805.

Palde, P. B. & Carroll, K. S. (2015) A universal entropy-driven mechanism for thioredoxin–target recognition. *Proceedings of the National Academy of Sciences*. **112** (26), 7960–7965.

Panday, A. et al. (2015) NADPH oxidases: an overview from structure to innate immunity-associated pathologies. *Cellular and Molecular Immunology*. **12** (1), 5–23.

Papadimitriou, K. et al. (2016) Stress Physiology of Lactic Acid Bacteria. *Microbiology and Molecular Biology Reviews*. **80** (3), 837–890.

Papageorgiou, P. et al. (2000) Phototherapy with blue (415 nm) and red (660 nm) light in the treatment of acne vulgaris. *The British journal of dermatology*. **142** (5), 973–978.

Park, S. & Imlay, J. a (2003) High Levels of Intracellular Cysteine Promote Oxidative DNA Damage by Driving the Fenton Reaction. *Journal of bacteriology*. **185** (6), 1942–1950.

Pedersen, M. B. et al. (2012) Aerobic Respiration Metabolism in Lactic Acid Bacteria and Uses in Biotechnology. *Annual Review of Food Science and Technology*. **3** (1), 37–58.

Poole, L. B., Reynolds, C. M., et al. (2000) AhpF and other NADH: peroxiredoxin oxidoreductases, homologues of low Mr thioredoxin reductase. *European Journal of Biochemistry*. **267** (20), 6126–6133.

Poole, L. B. et al. (2004) Protein sulfenic acids in redox signaling. *Annual review of pharmacology and toxicology*. **44** (1), 325–347.

Poole, L. B., Higuchi, M., et al. (2000) *Streptococcus mutans* H_2O_2-forming NADH oxidase is an alkyl hydroperoxide reductase protein. *Free Radical Biology and Medicine*. **28** (1), 108–120.

Pradenas, G. A. et al. (2012) Reduction of the monounsaturated fatty acid content of *Escherichia coli* results in increased resistance to oxidative damage. *Microbiology*. **158** (5), 1279–1283.

Prinz, W. a et al. (1997) The Role of the Thioredoxin and Glutaredoxin Pathways in Reducing Protein Disulfide Bonds in the *Escherichia coli*Cytoplasm. *Journal of Biological Chemistry*. **272** (25), 15661–15667.

Purcell, E. B. et al. (2007) A photosensory two-component system regulates bacterial cell attachment. *Proceedings of the National Academy of Sciences of the United States of America*. **104** (46), 18241–18246.

Quinto, E. J. et al. (2014) Probiotic Lactic Acid Bacteria: A Review. *Food and Nutrition Sciences*. **5** (18), 1765–1775.

Rai, P. et al. (2001) Localization of Fe(2+) at an RTGR sequence within a DNA duplex explains preferential cleavage by Fe(2+) and H_2O_2. *Journal of molecular biology*. **312** (5), 1089–1101.

Ritz, D. et al. (2000) Thioredoxin 2 is involved in the oxidative stress response in *Escherichia coli*. *The Journal of biological chemistry*. **275** (4), 2505–2512.

Rouhier, N. et al. (2001) Isolation and characterization of a new peroxiredoxin from poplar sieve tubes that uses either glutaredoxin or thioredoxin as a proton donor. *Plant physiology*. **127** (3), 1299–1309.

Russel, M. & Model, P. (1988) Sequence of thioredoxin reductase from *Escherichia coli*. Relationship to other flavoprotein disulfide oxidoreductases. *Journal of Biological Chemistry*. **263** (18), 9015–9019.

Sabharwal, S. S. & Schumacker, P. T. (2014) Mitochondrial ROS in cancer: initiators, amplifiers or an Achilles' heel? *Nature Reviews Cancer*. **14** (11), 709–721.

Sawyer, D. T. & Valentine, J. S. (1981) How super is superoxide? *Accounts of Chemical Research*. **14** (12), 393–400.

Scharf, C. et al. (1998) Thioredoxin is an essential protein induced by multiple stresses in *Bacillus subtilis*. *Journal of bacteriology*. **180** (7), 1869–1877.

Seaver, L. C. & Imlay, J. a (2001) Hydrogen Peroxide Fluxes and Compartmentalization inside Growing *Escherichia coli* Hydrogen Peroxide Fluxes and Compartmentalization inside Growing *Escherichia coli*. *Journal of bacteriology*. **183** (24), 7182–7189.

Sikorska, E. et al. (1998) Efficiency of singlet oxygen generation by alloxazines and isoalloxazines. *Journal of the Chemical Society, Faraday Transactions*. **94** (16), 2347–2353.

Spadaro, D. et al. (2010) The redox switch: Dynamic regulation of protein function by cysteine modifications. *Physiologia Plantarum*. **138** (4), 360–371.

Stone, J. R. & Yang, S. (2006) Hydrogen peroxide: a signaling messenger. *Antioxidants & redox signaling*. **8** (3–4), 243–270.

Sysak, P. K. et al. (1977) Chemistry of singlet oxygen - XXV. Photooxygenation of methionine. *Photochemistry and Photobiology*. **26** (1), 19–27.

Tartaglia, L. A. et al. (1990) Alkyl hydroperoxide reductase from Salmonella typhimurium. Sequence and homology to thioredoxin reductase and other flavoprotein disulfide oxidoreductases. *Journal of Biological Chemistry*. **265** (18), 10535–10540.

Toledano, M. B. et al. (1994) Redox-dependent shift of OxyR-DNA contacts along an extended DNA-binding site: A mechanism for differential promoter selection. *Cell*. **78** (5), 897–909.

Triantaphylidès, C. et al. (2008) Singlet oxygen is the major reactive oxygen species involved in photooxidative damage to plants. *Plant physiology*. **148** (2), 960–968.

Trickey, P. et al. (1999) Monomeric sarcosine oxidase: Structure of a covalently flavinylated amine oxidizing enzyme. *Structure*. **7** (3), 331–345.

Uziel, O. et al. (2004) Transcriptional regulation of the Staphylococcus aureus thioredoxin and thioredoxin reductase genes in response to oxygen and disulfide stress. *Journal of bacteriology*. **186** (2), 326–334.

Vagin, A. & Teplyakov, A. (1997) *MOLREP* : an Automated Program for Molecular Replacement. *Journal of Applied Crystallography*. **30** (6), 1022–1025.

Vagin, A. A. et al. (2004) REFMAC 5 dictionary: organization of prior chemical knowledge and guidelines for its use. *Acta Crystallographica Section D Biological Crystallography*. **60** (12), 2184–2195.

Vanhooren, A. et al. (2002) Photoexcitation of tryptophan groups induces reduction of two disulfide bonds in goat alpha-lactalbumin. *Biochemistry*. **41** (36), 11035–11043.

Vido, K. et al. (2005) Roles of Thioredoxin Reductase during the Aerobic Life of *Lactococcus lactis*. *Journal of Bacteriology*. **187** (2), 601–610.

Waksman, G. et al. (1994) Crystal Structure of *Escherichia coli* Thioredoxin Reductase Refined at 2 Å Resolution. *Journal of Molecular Biology*. **236** (3), 800–816.

Watanabe, S. et al. (2008) Crystal structure of the [2Fe-2S] oxidative-stress sensor SoxR bound to DNA. *Proceedings of the National Academy of Sciences of the United States of America*. **105** (11), 4121–4126.

Wegmann, U. et al. (2007) Complete genome sequence of the prototype lactic acid bacterium *Lactococcus lactis* subsp. cremoris MG1363. *Journal of bacteriology*. **189** (8), 3256–3270.

Wilkinson, F. et al. (1995) Rate Constants for the Decay and Reactions of the Lowest Electronically Excited Singlet State of Molecular Oxygen in Solution. An Expanded and Revised Compilation. *Journal of Physical and Chemical Reference Data*. **24** (2), 663–677.

Williams, C. H. et al. (1967) Lipoamide dehydrogenase, glutathione reductase, thioredoxin reductase, and thioredoxin. *The Journal of biological chemistry*. **242** (22), 5226–5231.

Williams, C. H. et al. (2000) Thioredoxin reductase two modes of catalysis have evolved. *European journal of biochemistry / FEBS*. **267** (20), 6110–6117.

Winn, M. D. et al. (2011) Overview of the *CCP* 4 suite and current developments. *Acta Crystallographica Section D Biological Crystallography*. **67** (4), 235–242.

Winterbourn, C. C. (1979) Comparison of superoxide with other reducing agents in the biological production of hydroxyl radicals. *The Biochemical journal*. **182** (2), 625–628.

Winterbourn, C. C. et al. (2004) Requirements for superoxide-dependent tyrosine hydroperoxide formation in peptides. *The Biochemical journal*. **381** (1), 241–248.

Winterbourn, C. C. (2008) Reconciling the chemistry and biology of reactive oxygen species. *Nature chemical biology*. **4** (5), 278–286.

Wood, Z. a et al. (2003) Peroxiredoxin evolution and the regulation of hydrogen peroxide signaling. *Science (New York, N.Y.)*. **300** (5619), 650–653.

Woodmansee, A. N. & Imlay, J. A. (2002) Reduced flavins promote oxidative DNA damage in non-respiring *Escherichia coli* by delivering electrons to intracellular free iron. *Journal of Biological Chemistry*. **277** (37), 34055–34066.

Wooh, J. W. et al. (2003) Comparison of three commercial sparse-matrix crystallization screens. *Acta crystallographica. Section D, Biological crystallography*. **59** (Pt 4), 769–772.

Wright, A. et al. (2002) Singlet Oxygen-mediated Protein Oxidation: Evidence for the Formation of Reactive Side Chain Peroxides on Tyrosine Residues. *Photochemistry and Photobiology*. **76** (1), 35–46.

Zeller, T. & Klug, G. (2006) Thioredoxins in bacteria: functions in oxidative stress response and regulation of thioredoxin genes. *Die Naturwissenschaften*. **93** (6), 259–266.

Zheng, M. et al. (1998) Activation of the OxyR transcription factor by reversible disulfide bond formation. *Science*. **279** (5357), 1718–1721.

Zuber, P. (2009) Management of oxidative stress in *Bacillus*. *Annual review of microbiology*. **63**, 575–597.

Åslund, F. et al. (1999) Regulation of the OxyR transcription factor by hydrogen peroxide and the cellular thiol-disulfide status. *Proceedings of the National Academy of Sciences of the United States of America*. **96** (11), 6161–6165.

Appendix A. Paper 1

Björnberg, O., Viennet, T., **Skjoldager, N.**, Ćurović, A., Nielsen, K. F., Svensson, B. and Hägglund, P. *Lactococcus lactis* Thioredoxin Reductase Is Sensitive to Light Inactivation. *Biochemistry* **54**, 1628–1637 (2015).

BIOCHEMISTRY
including biophysical chemistry & molecular biology

Article

pubs.acs.org/biochemistry

Lactococcus lactis Thioredoxin Reductase Is Sensitive to Light Inactivation

Olof Björnberg,[†] Thibault Viennet,[†] Nicklas Skjoldager,[†] Aida Ćurović,[†] Kristian Fog Nielsen,[‡] Birte Svensson,[†] and Per Hägglund*[,†]

[†]Enzyme and Protein Chemistry, Department of Systems Biology, Technical University of Denmark, Building 224, Søltofts Plads, DK-2800 Kongens Lyngby, Denmark

[‡]Metabolic Signaling and Regulation group, Department of Systems Biology, Technical University of Denmark, Building 221, Søltofts Plads, DK-2800 Kongens Lyngby, Denmark

Supporting Information

ABSTRACT: Thioredoxin, involved in numerous redox pathways, is maintained in the dithiol state by the nicotinamide adenine dinucleotide phosphate-dependent flavoprotein thioredoxin reductase (TrxR). Here, TrxR from *Lactococcus lactis* is compared with the well-characterized TrxR from *Escherichia coli*. The two enzymes belong to the same class of low-molecular weight thioredoxin reductases and display similar k_{cat} values (~25 s^{-1}) with their cognate thioredoxin. Remarkably, however, the *L. lactis* enzyme is inactivated by visible light and furthermore reduces molecular oxygen 10 times faster than *E. coli* TrxR. The rate of light inactivation under standardized conditions (λ_{max} = 460 nm and 4 °C) was reduced at lowered oxygen concentrations and in the presence of iodide. Inactivation was accompanied by a distinct spectral shift of the flavin adenine dinucleotide (FAD) that remained firmly bound. High-resolution mass spectrometric analysis of heat-extracted FAD from light-damaged TrxR revealed a mass increment of 13.979 Da, relative to that of unmodified FAD, corresponding to the addition of one oxygen atom and the loss of two hydrogen atoms. Tandem mass spectrometry confined the increase in mass of the isoalloxazine ring, and the extracted modified cofactor reacted with dinitrophenyl hydrazine, indicating the presence of an aldehyde. We hypothesize that a methyl group of FAD is oxidized to a formyl group. The significance of this not previously reported oxidation and the exceptionally high rate of oxygen reduction are discussed in relation to other flavin modifications and the possible occurrence of enzymes with similar properties.

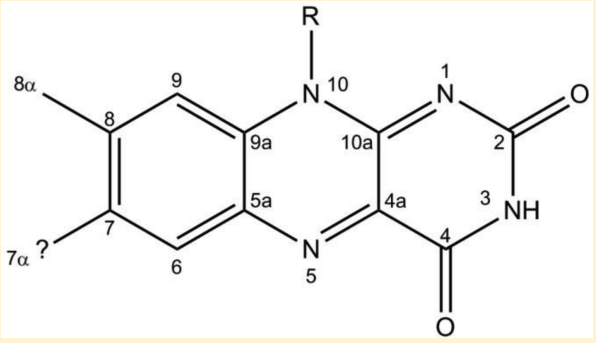

Thioredoxin (Trx) is a ubiquitous 12 kDa dithiol protein regulating the cellular redox environment and providing reducing equivalents to enzymes like ribonucleotide reductase, peroxiredoxin, and methionine sulfoxide reductase, which employ redox-active cysteine residues in catalysis. After oxidation to the disulfide, Trx is recycled to the dithiol form by nicotinamide adenine dinucleotide phosphate (NADPH)-dependent thioredoxin reductase (TrxR, also termed NTR). TrxR and Trx together constitute the Trx system.[1]

All known TrxRs are homodimers and carry one molecule of FAD per monomer but are divided into two types with distinctly different structures and molecular mechanisms. The high-molecular weight (HMW) TrxRs from, e.g., mammals, dipteran insects, and protozoan parasites and the low-molecular weight (LMW) TrxRs from bacteria, fungi, and plants have subunits of ~55 and ~35 kDa, respectively. Both types of TrxR, like other flavoenzymes, can produce hydrogen peroxide upon reaction with molecular oxygen (O_2), a hazardous side reaction probably generally suppressed during evolution, except in cases of dedicated enzymes like macrophage NADPH oxidase that has a role in combating infections.[2]

HMW TrxR is similar in sequence to glutathione reductase (GR) and displays a similar mechanism of transfer of reducing equivalents that involves interfaces between monomers and domains.[3] The hydride from NADPH is delivered to the *re* face of FAD and leaves the opposite *si* face to reduce the pair of redox-active cysteines within a conserved motif (CVNVGC), assisted by a histidine residue from the other subunit. A distinguishing feature between HMW TrxR and GR is the C-terminal extension of a flexible segment (of ~15 residues) having an additional redox center that shuttles reducing equivalents from the internal redox-active cysteines near the FAD to Trx.[4] In HMW TrxRs from mammals, this additional redox center is a selenosulfide pair, but organisms such as *Drosophila melanogaster* instead have a second redox-active disulfide that intriguingly works with a similar efficiency.[5] Several structures of HMW TrxRs are available as well as complexes with Trx.[6,7]

Received: November 3, 2014
Revised: February 6, 2015
Published: February 12, 2015

DOI: 10.1021/bi5013639
Biochemistry 2015, 54, 1628−1637

LMW TrxRs by contrast undergo a large conformational change allowing the transfer of electrons to Trx.[8] The two FAD domains are central for LMW TrxR dimer formation and keep their relative positions, while the NADPH domains rotate, with respect to the FAD domains, by 66° to switch between the flavin-oxidizing (FO) and flavin-reducing (FR) conformations in the catalytic cycle. In the FO conformation, the FAD and the redox-active disulfide are buried and positioned for internal electron transfer (from the *re* face of FAD), which excludes both thioredoxin and NADPH from productive interaction. In the more open FR conformation, the *re* face of FAD is exposed for the delivery of hydride from NADPH and the active site cysteines are exposed for interaction with Trx. Reducing equivalents thus enter and leave FAD at the same face. A nearby aspartic acid residue ($CA^T/_VCD$) assists the thiol–disulfide exchange with Trx.[9,10] The differences in mechanisms between the HMW and LMW types of enzymes make bacterial TrxR a promising target for new antimicrobial drugs.[11−13]

There is substantial structural information about LMW TrxRs from several eubacterial species, including a crystal structure of TrxR from *Helicobacter pylori* in reduced form at an excellent resolution of 1.45 Å.[14] In addition, TrxR structures were determined from archea, yeast, plants, and a unicellular eukaryote. The FR conformation, however, has so far only been observed for *Escherichia coli* TrxR (EcTrxR), in a structure of the complex with Trx, stabilized by an intermolecular disulfide bond formed using single-active site cysteine mutants.[8,15,16] Stopped-flow analysis of EcTrxR with NADPH conducted under anaerobic conditions at 1 °C demonstrated that the reductive half-reaction is very fast.[17] Although the oxidative half-reaction is slower, it is the rearrangement between the FO and FR conformations that appears to limit turnover.[8]

Lactococcus lactis is a model organism for lactic acid bacteria and industrially important as a starter culture in the dairy industry. Like many Gram-positive bacteria within the genera *Bacillus*, *Staphylococcus*, and *Streptococcus*, *L. lactis* lacks a glutathione biosynthesis system. *L. lactis* furthermore has no bacillithiol found in *Bacillus* species, *Staphylococcus aureus*, or *Deinococcus radiodurans*.[18] Remarkably, the knockout mutant of *trxB* (encodes TrxR) in *L. lactis* is viable with no special requirements for the growth medium,[19] while the corresponding gene appears to be more or less essential in *Bacillus subtilis* and *S. aureus*.[20,21] LlTrxR is an efficient reductant for three different redoxin substrates: LlTrxA, similar to the well-characterized Trx1 from *E. coli* (EcTrx1), with a WCGPC active site motif; LlTrxD having a WCGDC motif; and LlNrdH.[22] The latter is a glutaredoxin-like protein providing electrons to ribonucleotide reductase class Ib.[23,24] LlTrxA appears to act as a general disulfide reductase, whereas LlTrxD seems to have more specialized functions, possibly including arsenate detoxification.[25] In this study, comparison of the *L. lactis* and *E. coli* Trx systems showed that the activity of LlTrxR is unstable *in vitro*. Ambient light in the laboratory is sufficient to destroy the activity, which motivated the closer investigation of the nature of light inactivation. Native LlTrxR, protected from light, and a light-inactivated form both show a high rate of turnover with molecular oxygen (O_2) as the electron acceptor.

EXPERIMENTAL PROCEDURES

Protein Purification. The genetic constructs, growth conditions, and purification of recombinant His-tagged TrxRs and Trxs from *E. coli* and barley have been described previously.[26−28] LlTrxA and LlTrxR were prepared similarly also using the pET15a expression vector.[22] Cultures producing EcTrxR and LlTrxR were incubated either overnight at 20 °C or for 6 h at 30 °C following addition of IPTG (0.1 mM). The cell pellet from a 1 L culture was resuspended in 20 mL of Bugbuster protein extraction reagent (Novagen) containing Benzonase nuclease (Merck) and supplemented with FAD (0.2 mM). Without the FAD supplement, the occupancy of FAD in the preparations of EcTrxR and LlTrxR was 10−40% as judged from the comparison of the protein concentration and absorbance (456 nm). The extract was shaken slowly (30 min at room temperature). After centrifugation at 4 °C, the supernatant was filtered (pore size of 0.45 μm) and applied to a 5 mL HisTrap column (GE Healthcare) equilibrated with loading buffer [20 mM potassium phosphate (pH 7.4), 500 mM NaCl, and 10 mM imidazole]. The column was washed with 2 column volumes of loading buffer with 50 mM imidazole. Finally, the TrxRs were eluted by a linear gradient of 50 to 200 mM imidazole in loading buffer. Yellow fractions were pooled, dialyzed [6−8 molecular weight cutoff (MWCO), Spectra/Por 1] against 0.1 M potassium phosphate (pH 7.4) and 1 mM EDTA, and concentrated to at least 5 mg/mL in a volume of ≤5 mL (Ultra-15 10 kDa MWCO, Amicon). Protein samples were stored at −80 °C in aliquots. The yields of protein were higher for the TrxRs (>50 mg/L culture) than for the Trxs.

Spectrophotometric Analysis of Enzyme and Cofactor. Absorption spectra of oxidized TrxRs (300−600 nm) were routinely recorded (Ultrospec 2100 *pro*, Amersham Biosciences). The ε_{456} of FAD in EcTrxR determined to be 11300 M^{-1} cm^{-1} and equal to that of free FAD at 450 nm[29] was used for quantification of FAD in LlTrxR both before (456 nm) and after light inactivation (445 nm) as well as for isolated light-damaged cofactor (445 nm). FAD occupancy was assessed by comparison to the protein concentration determined by the aid of amino acid analysis after hydrolysis for 24 h in 6 M HCl.[30] Fluorescence emission spectra of 5.0 μM LlTrxR or EcTrxR were recorded (PerkinElmer luminescence spectrometer LS55). Excitation and emission wavelengths (10 nm slit widths) were 450 and 470−700 nm, respectively.

Measurement of TrxR Activity. LlTrxR, EcTrxR, and HvNTR2 were assayed in a 1 mL format at 2.0 μM LlTrxA, EcTrx1, and barley HvTrx1, respectively, close to the experimentally determined K_M values of 3.5, 2.2, and 1.2 μM, respectively.[22,31] The assay mixture contained 0.2 mM NADPH with 0.2 mM DTNB as the final electron acceptor in 0.1 M potassium phosphate (pH 7.5), 2 mM EDTA, and 0.1 mg/mL BSA, and reactions were started by the addition of TrxR to a final concentration of 20 nM. The formation of TNB anion was measured at 412 nm (ε_{412} = 13600 M^{-1} cm^{-1}).

Activity of LlTrxR and EcTrxR was also measured as described above but in the absence of Trx and DTNB, forcing the enzymes to use O_2 as an electron acceptor, termed the NADPH/O_2 assay. The oxidation of NADPH was recorded at 340 nm (ε_{340} = 6220 M^{-1} cm^{-1}), and the concentration of TrxR was varied between 50 and 200 nM to obtain a turnover number. The two TrxRs were also compared with respect to the use of 40 μM dichlorophenolindophenol (DCPIP) as an unspecific electron acceptor monitoring the disappearance of absorbance at 600 nm (ε_{600} = 20000 M^{-1} cm^{-1}) at a TrxR concentration of 100 nM.

Conditions for Light Inactivation. The standard buffer during light incubations contained 0.1 M potassium phosphate (pH 7.5), 2 mM EDTA, 0.1 mg/mL BSA, and 2.0 μM TrxR in

DOI: 10.1021/bi5013639
Biochemistry 2015, 54, 1628−1637

an Eppendorf tube kept 20 cm below a 1225 Lumen (21 W) lamp in the cold room (4 °C). According to the manufacturer Leuci (Relco group), the color temperature is 6500 K corresponding to a λ_{max} of 460 nm. Samples (10 μL) were withdrawn at intervals during the inactivation and assayed after dilution to 1 mL in standard buffer (to obtain a final TrxR concentration of 20 nM). The LlTrxR concentration was varied (2.0−40 μM) in separate experiments with intermediate dilutions to achieve a concentration of 20 nM in the assay. Overnight exposure for preparative-scale formation of light-damaged enzyme was performed at 50−200 μM LlTrxR. To study the influence of pH on the light inactivation process, samples contained the standard components (2.0 μM LlTrxR, 2 mM EDTA, and 0.1 mg/mL BSA), but the major buffering component of the standard buffer [0.1 M potassium phosphate (pH 7.5)] was replaced with potassium acetate, adjusted by acetic acid at pH 4.0 and 5.0, a mix of monobasic and dibasic potassium phosphate at pH 6.0, 7.0, and 8.0, and bicine adjusted with NaOH at pH 9.0.

The influence of dissolved molecular oxygen (O_2) on light inactivation was probed using an O_2 scavenging system in the standard buffer consisting of 10 mM glucose, glucose oxidase from *Aspergillus niger* (0.1 mg/mL), and bovine catalase (0.2 mg/mL). Glucose was omitted from the control sample. The influence of iodide ions was tested by including potassium iodide (0.1 M KI) in the standard buffer. As a reference, potassium chloride (0.1 M KCl) was included in the standard buffer to account for the increased ionic strength.

Reconstitution of Light-Treated LlTrxR. To LlTrxR (20 μM in 1 mL) exposed to light treatment for 3 h under standard conditions as described above (and a light-protected control) was added a large excess of FAD (8 mM in 1.5 mL). Subsequently, guanidinium chloride (GdmCl) was gradually added to a final concentration of 2 or 3 M followed by incubation for 21 h with gentle shaking at 4 °C. The samples were then diluted in 0.1 M potassium phosphate (pH 7.5), 2 mM EDTA, and 0.1 mg/mL BSA in several steps to reach GdmCl concentrations of 1, 0.5, and 0.1 M followed by incubations for 18, 1.5, and 3 h, respectively, at 4 °C. The samples were then concentrated to 1 mL by ultrafiltration (Ultra-15 10 kDa MWCO, Amicon), loaded on a PD-10 column, and further concentrated (Ultra-0.5 10 kDa MWCO, Amicon) to a final volume of 0.5 mL. The TrxR activity of the samples before and after reconstitution was analyzed as described above and compared to controls incubated without GdmCl.

Heat Extraction of the Light-Damaged Cofactor. A LlTrxR sample (190 μM) was exposed for 16 h under standard conditions for light inactivation (see above) and inspected for the resulting spectrum to show the typical appearance of light damage. The buffer was exchanged by loading the sample (0.8 mL) on a PD10 column equilibrated in 62 mM ammonium acetate (pH 6.6). Protein from the recovered fractions was incubated at 75 °C over 20 min, resulting in a large precipitate. After centrifugation, the supernatant was loaded on an ultrafiltration device (Ultra-0.5, Ultracel-10 Membrane, Amicon) and the permeate was retained.

Mass Spectrometric Analysis of FADs. Undamaged and light-damaged FAD was analyzed by high-resolution mass spectrometry (HRMS) on a maXis G3 quadrupole time-of-flight (qTOF) mass spectrometer (Bruker Daltonics), equipped with an electrospray ionization (ESI) source and connected to an Ultimate 3000 ultra-high-performance liquid chromatography (UPHLC) system with a UV/vis diode array detector (Dionex) and a Kinetex 2.6 μm pentafluorophenyl (PFP), 100 mm × 2.1 mm column (Phenomenex, Torrance, CA) maintained at 40 °C. A linear 20 min, 0 to 100% gradient from 20 mM aqueous formic acid to 20 mM formic acid in acetonitrile at a rate of 0.4 mL/min was used, followed by isocratic elution for 3 min. HRMS was performed in both negative (ESI^-) and positive (ESI^+) ion mode with a data acquisition range of 10 scans per second at m/z 100−1000. Sodium formate was automatically infused before each run and provided a mass accuracy of <1.5 ppm. MS/MS was performed at 20 and 40 eV for both ESI^+ and ESI^-.

Ion-pair UHPLC−MS/MS analysis was conducted using an Agilent 1290 binary UHPLC system coupled with an Agilent 6460 triple quadrupole instrument equipped with an ESI source and operated in negative mode. Nitrogen was used as the collision gas at 30 eV. Separation was performed on an Agilent Poroshell phenyl column using a 10 mM tributylamine, 10 mM acetic acid (pH 5.5), and 90% methanol gradient system as described in detail by Magdenoska et al.[32]

Reactions with Dinitrophenylhydrazine (DNPH). Light-inactivated, heat-extracted 40 μM FAD was incubated at room temperature with 80 μM DNPH (total volume of 200 μL) in 10 mM phosphoric acid to give pH values of 3.0−3.5. Extracted FAD from untreated LlTrxR and EcTrxR was used as a reference. Cinnamaldehyde (40 μM) was used as a positive control. Blanks containing the compounds described above but no DNPH were incubated in parallel. After 3 days in the dark at room temperature, precipates in samples were visually inspected.

Analysis of Ligand Binding in Three-Dimensional Structures of TrxR. The interactions between FAD and polypeptides in TrxRs were examined by the tool PDBsum (http://www.ebi.ac.uk/thornton-srv/databases/pdbsum), Ligand Explorer (http://www.rcsb.org/pdb/home/home.do), and Pymol.

RESULTS

LlTrxR Is Light-Sensitive. The thoroughly studied *E. coli* Trx system (EcTrxR/EcTrx1) was used as a point of reference in the characterization of *L. lactis* TrxR. The *E. coli* system was subjected to steady state kinetics, and the saturation curve with EcTrx1 as the substrate for EcTrxR generated a k_{cat} of 25 s^{-1} and a K_M of 2.5 μM, in agreement with the parameters reported in the literature.[17,33] The *L. lactis* system (LlTrxR/LlTrxA), however, showed an approximately 10-fold lower k_{cat}. It was noticed that the activity of fresh preparations was higher but decayed considerably upon storage for a few hours on ice. After various principal issues such as the integrity of the DNA clone and the solubility and stability of the enzyme had been interrogated, it became evident that LlTrxR is light-sensitive. The problem of inactivation was solved by avoiding daylight exposure and storing LlTrxR in brown tubes. Light-protected LlTrxR with LlTrxA as a substrate thus yielded a k_{cat} of ∼26 s^{-1}, essentially identical to that of the corresponding *E. coli* system.

The susceptibilities of LlTrxR, EcTrxR, and barley TrxR (HvNTR2) to light inactivation were compared. A compact fluorescent lamp (λ_{max} = 460 nm, i.e., blue light) situated in the cold room was used as the standard condition for light inactivation, and after incubation for 4 h, EcTrxR and HvNTR2 retained >70% activity using their cognate Trx acceptors (EcTrx1 and HvTrxh1) while LlTrxR retained <4% activity (Figure 1). In the dark, all three enzymes retained >90%

DOI: 10.1021/bi5013639
Biochemistry 2015, 54, 1628−1637

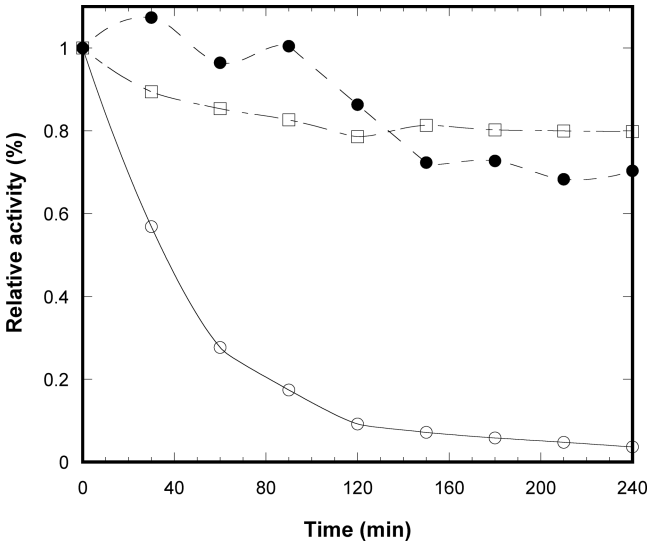

Figure 1. Inactivation of TrxR from *L. lactis*, *E. coli*, and *Hordeum vulgare* (HvNTR2) at pH 7.5. Samples at 2.0 μM LlTrxR (○), EcTrxR (●), and HvNTR2 (□) were exposed to light under standard conditions (20 cm below a 21 W lamp with a maximal intensity at 460 nm). Samples were withdrawn over 4 h and directly assayed together with their cognate Trx. The activities at different time points relative to the initial activity before light exposure are shown.

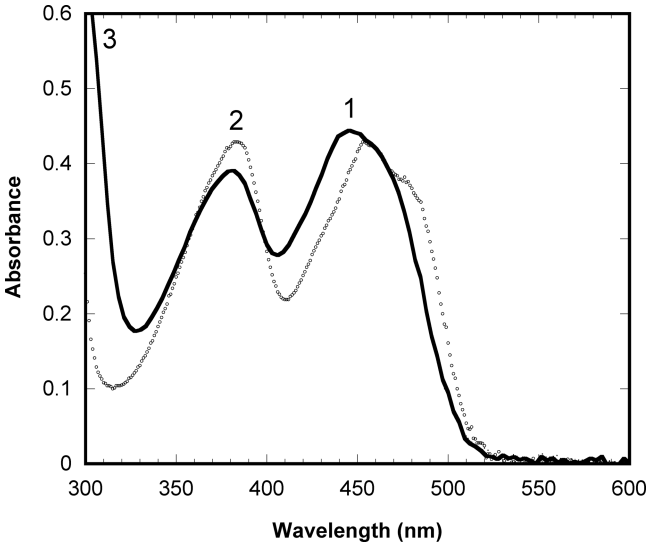

Figure 2. Spectral shift of LlTrxR upon light treatment. The spectrum between 300 and 600 nm of LlTrxR (40 μM) is shown before (small empty cicles) and after 3 h (solid line) of exposure under the 21 W lamp. Three major changes (1−3) are indicated: a blue shift of the main peak (1), a suppression of the second peak (2), and an increase in absorbance below 330 nm (3). Spectra of 10 μM LlTrxR to display the region at 250−300 nm are shown in Figure S3 of the Supporting Information. Additional spectra of time points from this experiment are shown in Figure S4 of the Supporting Information.

activity. Inactivation curves of LlTrxR repeated on four separate occasions indicated a half-life of ∼35 min (Figure S1 of the Supporting Information), and a very low level of residual activity (0.2%) was determined after 16 h. Inactivation of 2−40 μM LlTrxR (Figure S2 of the Supporting Information) showed that only the highest concentrations (20 and 40 μM) provided significant protection.

Light-Damaged LlTrxR Shows a Distinctly Changed Flavin Spectrum. Spectrophotometric analysis revealed that light inactivation is accompanied by major spectral changes in LlTrxR (Figure 2). The spectra of a 40 μM sample of LlTrxR displayed large changes in three regions after illumination for 3 h. The main peak (1), giving rise to the yellow color, was blue-shifted from ∼455 to ∼445 nm but retained a slight shoulder toward higher wavelengths (465−475 nm in undamaged LlTrxR). The magnitude of the second peak (2), around 380 nm, decreased. Finally, a large increase at 300−330 nm (3) not extending to the maximal absorbance at 260−270 nm (Figure S3 of the Supporting Information) where the adenosine moiety contributes. Additional spectra from the experiment showed a reinforcement of the described spectral features and a negligible degree of light scattering (Figure S4 of the Supporting Information). The presence of isosbestic points, e.g., at 400 nm, suggests that light damage involves direct conversion to a photoproduct without observable intermediates. The maintained maximal absorbance at 445 nm indicates a very low level of photodestruction of the isoalloxazine ring system (Figure S4 of the Supporting Information). Consistent with the spectral characteristics of oxidized flavin, diffuse daylight from a window was very harmful, while standard "warm-white" bulbs (typical λ_{max} values of >1000 nm) shifted the spectrum only slowly. EcTrxR and free FAD used as reference substances for these initial spectral observations were insensitive to light (data not shown).

The fluorescence emission of the flavin bound to LlTrxR was 3-fold higher than that of EcTrxR before inactivation (Figure S5 of the Supporting Information). This difference in quantum yield between the two enzymes suggests that the isoalloxazine ring is less rigidly fixed in LlTrxR.[34] After light exposure of LlTrxR, the emission intensity decreased to a level slightly lower than that of EcTrxR, and the maximal emission showed a small shift from 515 to 510 nm. These properties of EcTrxR were not affected by light treatment (Figure S5 of the Supporting Information).

Analysis of LlTrxR by reducing sodium dodecyl sulfate−polyacrylamide gel electrophoresis revealed a band of apparent cross-linked dimer that increased in intensity after light inactivation. More than 95% of light-inactivated LlTrxR, however, appeared in the monomeric form (data not shown). Inactivated LlTrxR was subjected to trypsin digestion, but subsequent analysis by matrix-assisted laser desorption ionization time-of-flight MS did not reveal any differences in the peptide profile compared to that of a sample not exposed to light.

Addition of a large excess of exogenous FAD to light-damaged LlTrxR in the presence of 2−3 M GdmCl (see Experimental Procedures for details) resulted in increased activity from approximately 7 to 40% relative to the level prior to inactivation. No increase in activity was observed after reconstitution of light-protected samples.

Taken together, these observations indicate that light inactivation is accompanied by structural changes in the tightly bound flavin cofactor, but modification on the protein level cannot be excluded.

The Rate of Light Inactivation Is Affected by pH, Oxygen Concentration, and the Presence of Iodide Ions. LlTrxR was subjected to light inactivation in buffers with a range of different pH values. At pH 4.0 and 9.0, activity declined already prior to light exposure [time zero (Figure 3)], suggesting that the enzyme is destabilized. The lowest pH

DOI: 10.1021/bi5013639
Biochemistry 2015, 54, 1628−1637

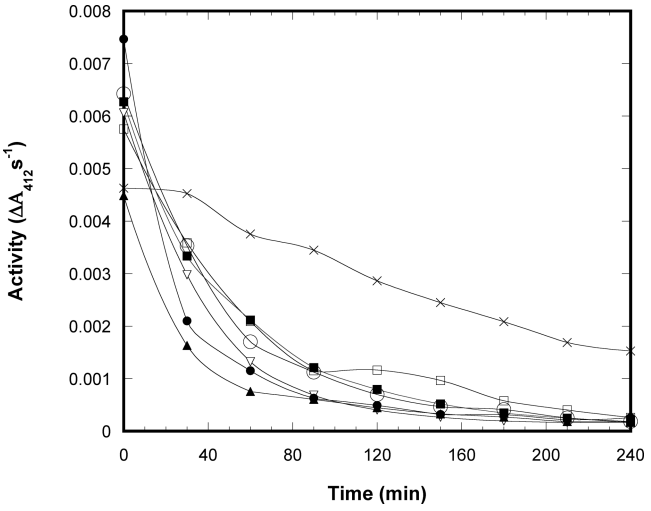

Figure 3. Dependence of pH on light inactivation. LlTrxR was diluted to 2.0 μM in buffers in the pH range from 4.0 to 9.0, and samples were removed over a 4 h light inactivation period for activity measurements with LlTrxA as the substrate and DTNB as the final electron acceptor. Symbols used for the pH buffers: (×) 4.0, (□) 5.0, (■) 6.0, (▽) 7.0, (◯) 7.5 (standard buffer), (●) 8.0, and (▲) 9.0. Absolute activity values, in ΔA_{412} s^{-1}, are shown.

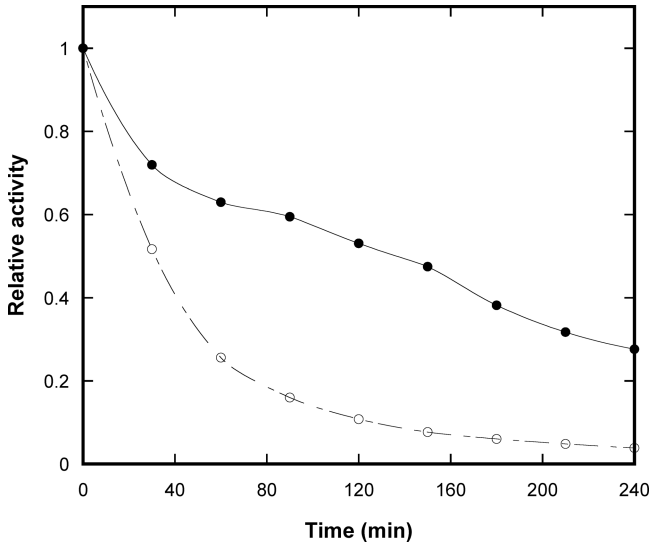

Figure 4. Influence of O_2 on light inactivation. LlTrxR was diluted to 2.0 μM in standard buffer supplemented with glucose oxidase and catalase (0.05 and 0.2 mg/mL, respectively). Glucose (10 mM) was added to activate the enzymatic system for removal of O_2 and H_2O_2 (●) and a control without glucose (○). Samples were removed over a 4 h light inactivation period for activity measurements with LlTrxA as the substrate and DTNB as the final electron acceptor. The activities relative to the initial activity before light exposure are shown.

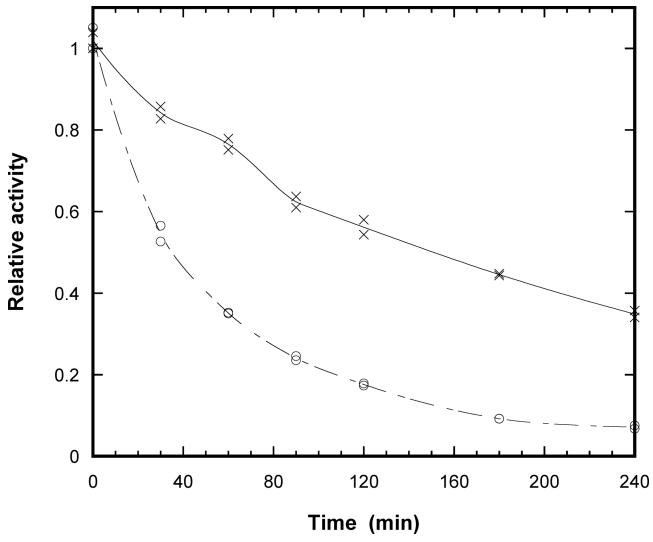

Figure 5. Influence of iodide ions on light inactivation. LlTrxR was diluted to 2.0 μM in standard buffer supplemented with 0.1 M KI (×) or in the control with 0.1 M KCl (○). Samples were removed over a 4 h light inactivation period for activity measurements with LlTrxA as the substrate and DTNB as the final electron acceptor. The activities relative to the initial activity before light exposure are shown.

(4.0), however, conferred a strong protective effect against light inactivation possibly because of non-native conformations of LlTrxR in the vicinity of the flavin. At pH 9.0, inactivation is clearly faster than at the standard pH of 7.5. A mechanism of breakdown initiated by hydroxylation similar to what is observed for riboflavin analogues at alkaline pH may take place if a hydroxide ion can be stabilized in the vicinity of the flavin.[35] However, the moderate increase in the rate of inactivation above pH 7.5 does not suggest that hydrolysis is involved in the light inactivation process.

The O_2 concentration in the inactivation buffer was lowered by addition of glucose, glucose oxidase, and catalase. The scavenging system was validated by a >10-fold decreased activity of LlTrxR in the NADPH/O_2 assay, likely explained by a correspondingly decreased amount of dissolved O_2. The scavenging system strongly slowed the inactivation (Figure 4), suggesting the involvement of O_2. Next, addition of potassium iodide, a quencher of photoexcited triplet state flavins, was investigated. Indeed, iodide has a protective effect at least as strong as that caused by a lowered O_2 content (Figure 5). To account for the additional ionic strength, potassium chloride was included in the reference sample.

The influence of LlTrxA and LlNrdH (1 μM), superoxide dismutase (0.02 and 0.1 mg/mL), FAD and riboflavin (20 μM), DTT (2 mM), and tryptophan (1 mM) as additives was tested separately using a 2 h illumination. Only riboflavin and FAD offered minor protection, albeit less than the O_2-scavenging system. No effect on inactivation was obtained by removing 2 mM EDTA (often employed at a higher concentration in anaerobic photoreduction)[36] from LlTrxR by gel filtration. These various findings suggested the involvement of molecular oxygen (O_2) and photoexcited FAD in the process of inactivation.

LlTrxR Reduces Molecular Oxygen (O_2) Faster Than EcTrxR. EcTrxR is the most well-characterized LMW TrxR, and its sequence is 37% identical to that of LlTrxR. These two TrxRs displayed similar k_{cat} values when they were assayed with their cognate Trx, and DTNB as the final electron acceptor. EcTrxR displayed a turnover of 1.7 s^{-1} for reduction of the classical redox dye DCPIP, twice that of LlTrxR (data not shown). These results suggest that the two reduced TrxRs have somewhat different surface properties.

When assayed without an added electron acceptor, TrxR reduces O_2 to H_2O_2 and LlTrxR showed a turnover of 0.33 s^{-1} in the NADPH/O_2 assay, 10-fold faster than that of EcTrxR (Figure. 5). Assuming the commonly accepted O_2 concentration of 200 μM in aqueous solutions, EcTrxR reduces O_2 at a rate of 160 M^{-1} s^{-1}, i.e., slightly more slowly than free reduced

DOI: 10.1021/bi5013639
Biochemistry 2015, 54, 1628−1637

flavin (250 M^{-1} s^{-1}),[37] while the corresponding 10-fold higher rate for LlTrxR is 1600 M^{-1} s^{-1}. In comparison, flavin-dependent oxidases dedicated to the use of O_2 typically reduce with much higher rate constants in the range of 10^5−10^6 M^{-1} s^{-1}.[38,39] Light-inactivated LlTrxR with <2% residual activity in the DTNB assay retained the high reduction rate of O_2 as seen for the noninactivated enzyme. In fact, a slightly higher turnover of 0.4 s^{-1} was recorded, demonstrating that NADPH is able to reduce the light-inactivated enzyme. However, in the NADPH/O_2 assay, the reductive half-reaction is conceivably at least 2 orders of magnitude faster than the oxidative.[17] A correspondingly large decrease in the reductive half-reaction can thus pass undetected in the assay.

Mass Spectrometric Analysis of the Light-Damaged FAD Suggests Aldehyde Formation. Flavins from both light-inactivated and untreated material were extracted by heat, with a recovery of >50%, suggesting that a majority of the cofactors are not covalently bound to the enzyme. Analysis of the extract from light-inactivated LlTrxR by UHPLC−ESI^+-HRMS revealed a major ion at m/z 800.1433 with an elution profile similar to that of the nonmodified flavin (m/z 786.1642) on a PFP column (Figure S6 of the Supporting Information). The mass difference (m/z 13.979) unambiguously corresponds to the addition of one oxygen atom and the loss of two hydrogen atoms, consistent with conversion of a methyl group to an aldehyde. Furthermore, a minor ion at m/z 816.1385 indicated further oxidation of the aldehyde to a carboxylate group or, alternatively, but less likely, hydroxylation of a second methyl group (Figure S6 of the Supporting Information). The native and presumed aldehyde-modified forms of FAD were readily baseline separated by ion-pair chromatography, and the shorter retention time of the modified FAD is consistent with a higher polarity of the oxidized species. ESI^+ MS/MS spectra of the presumed FAD aldehyde and the nonmodified flavin were highly similar and only displayed fragment ions originating from only the ribityl and phosphoadenosyl groups (data not shown). ESI^- MS/MS of the nonmodified flavin on the other hand showed a low-intensity ion at m/z 241.0729 originating from the isoalloxazine ring system that was shifted up by m/z 13.979 in the aldehyde form, suggesting that the site of modification is localized within this part of the FAD molecule (Figure S7 of the Supporting Information).

To consolidate the results of the mass spectrometric analysis, we probed the inactivated LlTrxR with DNPH that reacts with ketone and aldehyde groups to form insoluble derivatives. Brick-red precipitates appeared with FAD extracted from light-inactivated LlTrxR and cinnamaldehyde (the positive control), while precipitate was not observed with FAD extracted from EcTrxR or untreated LlTrxR. Although the precipitate was similar to the positive control, stoichiometric oxidation to an aldehyde cannot be concluded.

The two methyl groups defined as positions 7α and 8α on the isoalloxazine ring system are the possible sites of aldehyde formation. Oxidation of position 8α was previously observed in a flavoenzyme.[40] In the R268K mutant of lactate oxidase from *Aerococcus viridans*, FMN was almost completely transformed into 8-formyl-FMN upon aging. However, the positional identification relied on the spectral properties being similar to those of the synthesized analogue 8-formyl tetraacetylriboflavin.[41] Spectra of oxidized forms formylated at position 8α are different from the spectrum of the light-damaged FAD in LlTrxR (see Discussion). Edmondson[41] showed that 8-formylriboflavin forms a blue 8-formylflavin hydroquinione cation upon reduction by $TiCl_3$ in 6 M HCl, and the reaction does not require removal of O_2. Incubating the extracted light-damaged cofactor from LlTrxR under these conditions (a 5-fold excess of $TiCl_3$) did not increase absorbance above 550 nm, indicating that 8-formyl-FAD is not a major constituent of the light-damaged FAD in LlTrxR.

■ DISCUSSION

Here we report on the surprising inactivation of LlTrxR by blue light under aerobic conditions, a phenomenon not reported for any other TrxR. In fact, light inactivation under these conditions is unusual or at least slow for other flavoenzymes. On the basis of the mass spectrometric analysis and a positive reaction with DNPH, our results suggest generation of an aldehyde derived from a methyl group. Mass spectrometric fragmentation pinpointed the modification to be localized in the isoalloxazine ring, which has two methyl groups. Iodide seems to exert a protective effect by scavenging photoexcited FAD. It appears likely that triplet state flavin formed upon photoexcitation reacts with O_2, generating a reactive oxygen species ($^1O_2$ or O_2^-), which in turn attacks and oxidizes the methyl group to a formyl group. A modification of the methyl group at position 7α has, to the best of our knowledge, never been reported in a flavoenzyme, but it has been observed at the level of riboflavin. Yagi and co-workers thus isolated both 7α- and 8α-hydroxyriboflavin from urine and showed that liver microsomes catalyze this NADPH-dependent hydroxylation.[42,43]

Modifications of position 8α are implicated in covalent attachment of flavins to some enzymes, e.g., succinate dehydrogenase and monoamine oxidase.[44] The influence of these linkages on activity and redox potential has been studied using synthetic flavin analogues.[45] 8-Formyl-FAD, 8-formyl-tetraacetylriboflavin, and 8-formyl-FMN extracted from the aged R286K mutant of L-lactate oxidase show nearly identical spectral properties (in the range of 300−800 nm).[40,41,46] Like that of light-damaged LlTrxR, the spectrum of oxidized flavin with an 8-formyl substitution displays an elevated absorbance at 300 nm (Figure 2). Otherwise, the spectrum is very different; the main peak is red-shifted (460 nm) in contrast to the blue-shift in light-damaged LlTrxR, and the second peak around 380 nm is elevated. These differences suggest that the aldehyde instead is formed at position 7α, which is a testable hypothesis, and crystallization trials with the light-inactivated enzyme have been initiated. The strong negative effect on activity may be caused by changes in redox potential and/or positioning of redox-active flavin atoms (e.g., N5) hindering electron transfer to the dithiol motif. Experimental and theoretical work on 7,8-substituted flavin analogues predicts increases in redox potentials of at least 50 mV.[47] The light-damaged enzyme is, however, still redox-active with O_2.

Is there any biological significance of the deviating properties of LlTrxR? A naïve idea is simply that *L. lactis*, which thrives at low levels of O_2, uses light inactivation as a sensor of light and O_2 with immediate effects on DNA replication via ribonucleotide reductase. There are several established examples of photoexcited flavoproteins that function as photoreceptors of blue light,[48] for example, YtvA from *B. subtilis*.[49] It could also be suggested that inactivation of TrxR results in an oxidized thiol redox environment that activates redox-sensitive transcription factors such as Spx.[50] In general, blue light at wavelengths of ≤470 nm has an antibacterial effect. Optimal cell killing of *S. aureus* was found to occur at 405 nm, and the mechanism has

DOI: 10.1021/bi5013639
Biochemistry 2015, 54, 1628−1637

been proposed to involve photoexcitation of porphyrins, reaction with O_2, and subsequent formation of reactive oxygen species.[51,52]

LlTrxR showed a rate of O_2 reduction 10-fold higher than that of EcTrxR (Figure 6). Similar results were obtained with

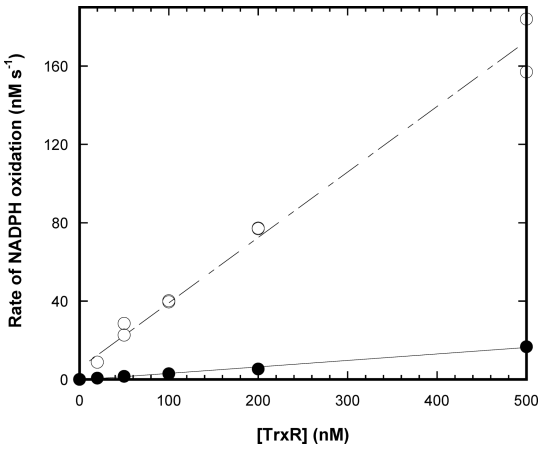

Figure 6. Oxidation of NADPH via TrxR using O_2 as an electron acceptor. LlTrxR (○) and EcTrxR (●) were incubated in the presence of NADPH (0.2 mM). A background rate of 0.00000762 ΔA_{340} s^{-1}, conceivably NADPH destruction, was subtracted from all rates, and the activity recorded (ΔA_{340} s^{-1}) was converted to nanomolar NADPH oxidized per second.

the flavoenzyme dihydroorotate dehydrogenase from *E. coli* and *L. lactis*, i.e., a 7-fold higher reduction rate for the *L. lactis* enzyme.[53] During fermentative growth, *L. lactis* utilizes NADH oxidases to reduce O_2 to restore the NAD^+ pool. These flavoenzymes display different mechanisms and release either H_2O or H_2O_2 as main product of catalysis.[54] Similar to many other lactic acid bacteria, *L. lactis* lacks catalase and relies on peroxiredoxins and NADH peroxidases to degrade H_2O_2. Strains of *Streptococcus pneumoniae* were shown to both tolerate and excrete H_2O_2, which has been suggested to be a strategy for outcompeting other microorganisms, possibly utilized widely among lactic acid bacteria.[55,56] *L. lactis* contains a low number of enzymes with iron−sulfur clusters, generally sensitive to H_2O_2 and O_2^-

Might other LMW TrxRs have the features shown here for LlTrxR, i.e., sensitivity to light and a high rate of O_2 reduction? Both processes are oxidative; however, only the O_2 reduction in the NADPH/O_2 assay is without doubt dependent on the fully reduced form, obtained by hydride transfer, while the comparatively slower light inactivation may involve a one-electron-reduced species of FAD. Furthermore, the site of oxidative attack is probably different; we identified carbon 7α as a probable site for light inactivation, and the C4a carbon is likely to be employed for O_2 reduction. Both oxidases and hydroxylases, dedicated to the use of O_2, employ C4a-hydroperoxide intermediates in catalysis.[2] Dehydrogenase flavoenzymes in contrast seem to have evolved toward low reactivity with O_2, and reduction can be considered as an inappropriate side reaction. A113 on the *re* side of the C4a locus was identified as a gatekeeper for O_2 reduction in L-galactono-γ-lactone dehydrogenase, and the corresponding A113G mutation, creating more free space above the locus, converted the enzyme to a catalytically competent oxidase.[57] A change in the opposite direction, toward less reduction of O_2, was achieved in lactate monooxygenase by a mutation that diminished the amount of free space above the C4a locus.[58] TrxR structures in the FO conformation are defined by having the active site disulfide within 3.0−4.0 Å of C4a and N5, thus preventing access of O_2. Exposure of the reactive locus, however, probably takes place during the switch between conformations and in the FR conformation without bound NADPH or $NADP^+$. The structure of HvNTR2 shows a conformation between the FR and FO conformations, with the active site disulfide closer to carbon 7α.[59] Like EcTrxR, HvNTR2 shows a low rate of O_2 reduction, observed as a background rate in measurements of insulin reduction by the barley Trxs.[60] Apart from the accessibility of O_2, stabilization of the activated oxygen species in the reaction intermediate greatly affects the rate, e.g., by a lysine residue, identified to be primarily responsible for stabilization of the transient negative charge on FAD C(4a)-hydroperoxide in sarcosine oxidase.[2,61]

At present, LMW TrxR structures in the FO conformation from 14 species are available in the Protein Data Bank (PDB). There are several interactions with FAD, most of which concern the ribityl group, the two phosphate groups, and the adenosine moiety. With respect to polar interactions with the chemically active isoalloxazine ring, only two direct hydrogen bonds recur in all 14 structures. They involve O2 as the acceptor and N3 as the donor, respectively. The corresponding residues involved are the main chain NH group of a nonpolar residue ($A295_{EcTrxR}$) and a completely conserved Asn residue ($N51_{EcTrxR}$). These two hydrogen bonds, also seen in the FR conformation of EcTrxR, appear to be central to LMW TrxRs, certainly serving both to keep the ring system in position and to control its reactivity. Other residues surrounding the isoalloxazine ring show less conservation, as outlined below.

The enzyme from *S. aureus* (SaTrxR) is the closest homologue of LlTrxR with a determined structure (PDB entry 4GCM). The sequence identity is 53% (with no need for introducing gaps) in a pairwise alignment (Figure S8 of the Supporting Information). Five residues in SaTrxR (Q42, N45, T46, Y133, and D138) have atoms within 6.0 Å of the 7α-methyl carbon of FAD, and only one of them is completely conserved, D138, the active site acid/base corresponding to $D139_{EcTrxR}$. $Q42_{SaTrxR}$ ($Q42_{EcTrxR}$) is strongly conserved, although its substitution with alanine in *Mycobacterium tuberculosis* TrxR maintains a conserved hydrogen bond to a phosphate through its main chain NH group.[62] $N45_{SaTrxR}$ and $Y133_{SaTrxR}$ occupy less conserved positions, while $T46_{SaTrxR}$ is conserved with substitutions only with serine. These residues in SaTrxR are conserved in the TrxRs from *L. lactis*, *Streptococcus mutans*, and *Bacillus anthracis* (BaTrxR), which group together in the alignment (Figure S8 of the Supporting Information). BaTrxR has been thoroughly investigated, including spectral characterization, but no unexpected properties were reported.[63]

In comparison to EcTrxR, the 7α-methyl carbon is buried less tightly in the SaTrxR structure; e.g., the distance to the phenolic oxygen atom of $Y118_{EcTrxR}$ is 3.8 Å, while the closest atom (NZ) of the corresponding residue in SaTrxR, K117, is 7.6 Å from the 7α-methyl carbon. Moreover, $Ala134_{EcTrxR}$ (CB) is positioned within 4.0 Å, while the corresponding residue $Y133_{SaTrxR}$ shows a closest distance of 5.4 Å (ring carbon CD). This substitution is notable in a segment that is highly conserved in the context of the active site cysteines and acid/base aspartate residue (SYCAVCDG). Furthermore, these residues are displaced during the transition to the FR conformation. Subtle differences related to the conformational

DOI: 10.1021/bi5013639
Biochemistry 2015, 54, 1628−1637

change can make LlTrxR differently reactive with O_2, and the structure of SaTrxR is not a sufficiently good model for making predictions about the mechanisms. However, we find it likely that TrxRs from more closely related genera, e.g., *Streptococcus* (with ~70% sequence identity), display properties like those of LlTrxR.

■ ASSOCIATED CONTENT

Supporting Information

Eight figures as indicated in the text. This material is available free of charge via the Internet at http://pubs.acs.org.

■ AUTHOR INFORMATION

Corresponding Author

*Telephone: +45 4525 5503. Fax: +45 4588 6307. E-mail: ph@bio.dtu.dk.

Funding

The work was supported by the Danish Council for Technology and Production Sciences (FTP, Grant 274-08-0413) and the Carlsberg Foundation (Grant 2010_01-0098).

Notes

The authors declare no competing financial interest.

■ ACKNOWLEDGMENTS

We thank Dale Edmondson, Kaj Frank Jensen, and Peter Macheroux for sharing their experiences with flavins and flavoenzymes, Oskar Axelsson (Spago Nanomedical) for advice concerning the DNPH reaction, and Anita Iversen and Olivera Magdenoska for help with accurate HRMS and ion-pair UHPLC–MS/MS, respectively. Anne Blicher is thanked for performing amino acid analysis, and finally, we acknowledge Bo Svensson (Saromics Biostructure) for the inspection of the SaTrxR structure.

■ ABBREVIATIONS

DCPIP, dichlorophenolindophenol; DNPH, 2,4-dinitrophenylhydrazine; DTNB, 5,5′-dithiobis(2-nitrobenzoic acid); EcTrx1, *E. coli* Trx1; EcTrxR, *E. coli* TrxR; ESI, electrospray ionization; FO, flavin-oxidizing; FR, flavin-reducing; GR, glutathione reductase; HMW, high-molecular weight; HRMS, high-resolution mass spectrometry; HvNTR2, thioredoxin reductase from barley; LlNrdH, *L. lactis* NrdH; LlTrxA, *L. lactis* TrxA; LlTrxD, *L. lactis* TrxD; LlTrxR, *L. lactis* TrxR; LMW, low-molecular weight; MS, mass spectrometry; MS/MS, tandem MS; qTOF, quadrupole time-of-flight; TNB, 2-nitro-5-thiobenzoate; Trx, thioredoxin; TrxR, NADPH-dependent thioredoxin reductase; UHPLC, ultra-high-performance liquid chromatography.

■ REFERENCES

(1) Arnér, E. S. J., and Holmgren, A. (2000) Physiological functions of thioredoxin and thioredoxin reductase. *Eur. J. Biochem. 267*, 6102–6109.

(2) Fagan, R. L., and Palfey, B. A. (2010) Flavin-Dependent Enzymes. In *Comprehensive Natural Products II Chemistry and Biology* (Mander, L., and Lui, H.-W., Eds.) pp 37–113, Elsevier, Oxford, U.K.

(3) Arscott, L. D., Gromer, S., Schirmer, R. H., Becker, K., and Williams, C. H., Jr. (1997) The mechanism of thioredoxin reductase from human placenta is similar to the mechanisms of lipoamide dehydrogenase and glutathione reductase and is distinct from the mechanism of thioredoxin reductase from *Escherichia coli*. *Proc. Natl. Acad. Sci. U.S.A. 94*, 3621–3626.

(4) Cheng, Q., Sandalova, T., Lindqvist, Y., and Arner, E. S. (2009) Crystal structure and catalysis of the selenoprotein thioredoxin reductase 1. *J. Biol. Chem. 284*, 3998–4008.

(5) Gromer, S., Johansson, L., Bauer, H., Arscott, L. D., Rauch, S., Ballou, D. P., Williams, C. H., Jr., Schirmer, R. H., and Arner, E. S. (2003) Active sites of thioredoxin reductases: Why selenoproteins? *Proc. Natl. Acad. Sci. U.S.A. 100*, 12618–12623.

(6) Fritz-Wolf, K., Kehr, S., Stumpf, M., Rahlfs, S., and Becker, K. (2011) Crystal structure of the human thioredoxin reductase-thioredoxin complex. *Nat. Commun. 2*, 1–8.

(7) Fritz-Wolf, K., Urig, S., and Becker, K. (2007) The structure of human thioredoxin reductase 1 provides insights into C-terminal rearrangements during catalysis. *J. Mol. Biol. 370*, 116–127.

(8) Lennon, B. W., Williams, C. H., and Ludwig, M. L. (2000) Twists in catalysis: Alternating conformations of *Escherichia coli* thioredoxin reductase. *Science 289*, 1190–1194.

(9) Mulrooney, S. B., and Williams, C. H. (1994) Potential active-site base of thioredoxin reductase from *Escherichia coli*: Examination of histidine245 and aspartate139 by site-directed mutagenesis. *Biochemistry 33*, 3148–3154.

(10) Oliveira, M. A., Discola, K. F., Alves, S. V., Medrano, F. J., Guimaraes, B. G., and Netto, L. E. (2010) Insights into the specificity of thioredoxin reductase-thioredoxin interactions. A structural and functional investigation of the yeast thioredoxin system. *Biochemistry 49*, 3317–3326.

(11) Koch, O., Jager, T., Heller, K., Khandavalli, P. C., Pretzel, J., Becker, K., Flohe, L., and Selzer, P. M. (2013) Identification of *M. tuberculosis* thioredoxin reductase inhibitors based on high-throughput docking using constraints. *J. Med. Chem. 56*, 4849–4859.

(12) Lu, J., and Holmgren, A. (2014) The thioredoxin antioxidant system. *Free Radical Biol. Med. 66*, 75–87.

(13) Lu, J., Vlamis-Gardikas, A., Kandasamy, K., Zhao, R., Gustafsson, T. N., Engstrand, L., Hoffner, S., Engman, L., and Holmgren, A. (2013) Inhibition of bacterial thioredoxin reductase: An antibiotic mechanism targeting bacteria lacking glutathione. *FASEB J. 27*, 1394–1403.

(14) Gustafsson, T. N., Sandalova, T., Lu, J., Holmgren, A., and Schneider, G. (2007) High-resolution structures of oxidized and reduced thioredoxin reductase from *Helicobacter pylori*. *Acta Crystallogr. D63*, 833–843.

(15) Veine, D. M., Mulrooney, S. B., Wang, P. F., and Williams, C. H. (1998) Formation and properties of mixed disulfides between thioredoxin reductase from *Escherichia coli* and thioredoxin: Evidence that cysteine-138 functions to initiate dithiol-disulfide interchange and to accept the reducing equivalent from reduced flavin. *Protein Sci. 7*, 1441–1450.

(16) Wang, P. F., Veine, D. M., Ahn, S. H., and Williams, C. H. (1996) A stable mixed disulfide between thioredoxin reductase and its substrate, thioredoxin: Preparation and characterization. *Biochemistry 35*, 4812–4819.

(17) Lennon, B. W., and Williams, C. H. (1997) Reductive half-reaction of thioredoxin reductase from *Escherichia coli*. *Biochemistry 36*, 9464–9477.

(18) Newton, G. L., Rawat, M., La Clair, J. J., Jothivasan, V. K., Budiarto, T., Hamilton, C. J., Claiborne, A., Helmann, J. D., and Fahey, R. C. (2009) Bacillithiol is an antioxidant thiol produced in Bacilli. *Nat. Chem. Biol. 5*, 625–627.

(19) Vido, K., Diemer, H., Van Dorsselaer, A., Leize, E., Juillard, V., Gruss, A., and Gaudu, P. (2005) Roles of thioredoxin reductase during the aerobic life of *Lactococcus lactis*. *J. Bacteriol. 187*, 601–610.

(20) Kobayashi, K., Ehrlich, S. D., Albertini, A., Amati, G., Andersen, K. K., Arnaud, M., Asai, K., Ashikaga, S., Aymerich, S., Bessieres, P., Boland, F., Brignell, S. C., Bron, S., Bunai, K., Chapuis, J., Christiansen, L. C., Danchin, A., Debarbouille, M., Dervyn, E., Deuerling, E., Devine, K., Devine, S. K., Dreesen, O., Errington, J., Fillinger, S., Foster, S. J., Fujita, Y., Galizzi, A., Gardan, R., Eschevins, C., Fukushima, T., Haga, K., Harwood, C. R., Hecker, M., Hosoya, D., Hullo, M. F., Kakeshita, H., Karamata, D., Kasahara, Y., Kawamura, F., Koga, K., Koski, P., Kuwana, R., Imamura, D., Ishimaru, M., Ishikawa, S., Ishio, I., Le Coq,

DOI: 10.1021/bi5013639
Biochemistry 2015, 54, 1628–1637

D., Masson, A., Mauel, C., Meima, R., Mellado, R. P., Moir, A., Moriya, S., Nagakawa, E., Nanamiya, H., Nakai, S., Nygaard, P., Ogura, M., Ohanan, T., O'Reilly, M., O'Rourke, M., Pragai, Z., Pooley, H. M., Rapoport, G., Rawlins, J. P., Rivas, L. A., Rivolta, C., Sadaie, A., Sadaie, Y., Sarvas, M., Sato, T., Saxild, H. H., Scanlan, E., Schumann, W., Seegers, J. F., Sekiguchi, J., Sekowska, A., Seror, S. J., Simon, M., Stragier, P., Studer, R., Takamatsu, H., Tanaka, T., Takeuchi, M., Thomaides, H. B., Vagner, V., van Dijl, J. M., Watabe, K., Wipat, A., Yamamoto, H., Yamamoto, M., Yamamoto, Y., Yamane, K., Yata, K., Yoshida, K., Yoshikawa, H., Zuber, U., and Ogasawara, N. (2003) Essential *Bacillus subtilis* genes. *Proc. Natl. Acad. Sci. U.S.A. 100*, 4678−4683.

(21) Uziel, O., Borovok, I., Schreiber, R., Cohen, G., and Aharonowitz, Y. (2004) Transcriptional regulation of the *Staphylococcus aureus* thioredoxin and thioredoxin reductase genes in response to oxygen and disulfide stress. *J. Bacteriol. 186*, 326−334.

(22) Björnberg, O., Efler, P., Ebong, E. D., Svensson, B., and Hägglund, P. (2014) *Lactococcus lactis* TrxD represents a subgroup of thioredoxins prevalent in Gram-positive bacteria containing WCXDC active site motifs. *Arch. Biochem. Biophys. 564*, 164−172.

(23) Jordan, A., Åslund, F., Pontis, E., Reichard, P., and Holmgren, A. (1997) Characterization of *Escherichia coli* NrdH. A glutaredoxin-like protein with a thioredoxin-like activity profile. *J. Biol. Chem. 272*, 18044−18050.

(24) Jordan, A., Pontis, E., Åslund, F., Hellman, U., Gibert, I., and Reichard, P. (1996) The ribonucleotide reductase system of *Lactococcus lactis*. Characterization of an NrdEF enzyme and a new electron transport protein. *J. Biol. Chem. 271*, 8779−8785.

(25) Efler, P., Kilstrup, M., Johnsen, S., Svensson, B., and Hägglund, P. M. (2015) Two *Lactococcus lactis* thioredoxin paralogues play different roles in responses to arsenate and oxidative stress. *Microbiology*, DOI: 10.1099/mic.0.000029.

(26) Björnberg, O., Maeda, K., Svensson, B., and Hägglund, P. (2012) Dissecting molecular interactions involved in recognition of target disulfides by the barley thioredoxin system. *Biochemistry 51*, 9930−9939.

(27) Maeda, K., Hägglund, P., Finnie, C., Svensson, B., and Henriksen, A. (2006) Structural basis for target protein recognition by the protein disulfide reductase thioredoxin. *Structure 14*, 1701−1710.

(28) Shahpiri, A., Svensson, B., and Finnie, C. (2008) The NADPH-dependent thioredoxin reductase/thioredoxin system in germinating barley seeds: Gene expression, protein profiles, and interactions between isoforms of thioredoxin h and thioredoxin reductase. *Plant Physiol. 146*, 789−799.

(29) Williams, C. H., Zanetti, G., Arscott, L. D., and McAllister, J. K. (1967) Lipoamide dehydrogenase, glutathione reductase, thioredoxin reductase, and thioredoxin. *J. Biol. Chem. 242*, 5226−5231.

(30) Barkholt, V., and Jensen, A. L. (1989) Amino acid analysis: Determination of cysteine plus half-cystine in proteins after hydrochloric acid hydrolysis with a disulfide compound as additive. *Anal. Biochem. 177*, 318−322.

(31) Kirkensgaard, K. G., Hägglund, P., Shahpiri, A., Finnie, C., Henriksen, A., and Svensson, B. (2014) A novel twist on molecular interactions between thioredoxin and nicotinamide adenine dinucleotide phosphate-dependent thioredoxin reductase. *Proteins 82*, 607−619.

(32) Magdenoska, O., Martinussen, J., Thykaer, J., and Nielsen, K. F. (2013) Dispersive solid phase extraction combined with ion-pair ultra high-performance liquid chromatography tandem mass spectrometry for quantification of nucleotides in *Lactococcus lactis*. *Anal. Biochem. 440*, 166−177.

(33) Dyson, H. J., Jeng, M. F., Tennant, L. L., Slaby, I., Lindell, M., Cui, D. S., Kuprin, S., and Holmgren, A. (1997) Effects of buried charged groups on cysteine thiol ionization and reactivity in *Escherichia coli* thioredoxin: Structural and functional characterization of mutants of Asp 26 and Lys 57. *Biochemistry 36*, 2622−2636.

(34) Heelis, P. F. (1982) The photophysical and photochemical properties of flavins (isoalloxazines). *Chem. Soc. Rev. 11*, 15−39.

(35) Harayama, T., Tezuka, Y., Taga, T., and Yoneda, F. (1984) Hydrolysis products of flavins (isoalloxazines). *Tetrahedron Lett. 25*, 4015−4018.

(36) Zanetti, G., Williams, C. H., Jr., and Massey, V. (1968) Influence of photoirradiation on the oxidation-reduction state of thioredoxin reductase. *J. Biol. Chem. 243*, 4013−4019.

(37) Kemal, C., Chan, T. W., and Bruice, R. C. (1977) Reaction of $^3O_2$ with dihydroflavins. 1. $N^{3,5}$-Dimethyl-1,5-dihydrolumiflavin and 1,5-dihydroisoalloxazines. *J. Am. Chem. Soc. 99*, 7272−7286.

(38) Gadda, G. (2012) Oxygen activation in flavoprotein oxidases: The importance of being positive. *Biochemistry 51*, 2662−2669.

(39) McDonald, C. A., Fagan, R. L., Collard, F., Monnier, V. M., and Palfey, B. A. (2011) Oxygen reactivity in flavoenzymes: Context matters. *J. Am. Chem. Soc. 133*, 16809−16811.

(40) Yorita, K., Matsuoka, T., Misaki, H., and Massey, V. (2000) Interaction of two arginine residues in lactate oxidase with the enzyme flavin: Conversion of FMN to 8-formyl-FMN. *Proc. Natl. Acad. Sci. U.S.A. 97*, 13039−13044.

(41) Edmondson, D. E. (1974) Intramolecular hemiacetal formation in 8-formylriboflavine. *Biochemistry 13*, 2817−2821.

(42) Ohkawa, H., Ohishi, N., and Yagi, K. (1983) New metabolites of riboflavin appear in human urine. *J. Biol. Chem. 258*, 5623−5628.

(43) Ohkawa, H., Ohishi, N., and Yagi, K. (1983) Hydroxylation of the 7- and 8-methyl groups of riboflavin by the microsomal electron transfer system of rat liver. *J. Biol. Chem. 258*, 5629−5633.

(44) Mewies, M., McIntire, W. S., and Scrutton, N. S. (1998) Covalent attachment of flavin adenine dinucleotide (FAD) and flavin mononucleotide (FMN) to enzymes: The current state of affairs. *Protein Sci. 7*, 7−20.

(45) Edmondson, D. E., and Newton-Vinson, P. (2001) The covalent FAD of monoamine oxidase: Structural and functional role and mechanism of the flavinylation reaction. *Antioxid. Redox Signaling 3*, 789−806.

(46) Meah, Y., and Massey, V. (2002) Studies on 8-CHO-flavins, 8-CN-flavins and 8-CHO-flavoproteins. In *Flavins and flavoproteins* (Chapman, S. K., Perham, R., and Scrutton, N., Eds.) pp 281−286, Rudolf Weber, Berlin.

(47) Edmondson, D. E., and Ghisla, S. (1999) Electronic effects of 7 and 8 ring substituents as predictors of flavin oxidation-reduction potentials. In *Flavins and flavoproteins* (Ghisla, S., Kroneck, P., Macheroux, P., and Sund, H., Eds.) pp 71−76, Rudolf Weber, Berlin.

(48) Losi, A., and Gartner, W. (2012) The evolution of flavin-binding photoreceptors: An ancient chromophore serving trendy blue-light sensors. *Annu. Rev. Plant Biol. 63*, 49−72.

(49) Losi, A., Polverini, E., Quest, B., and Gartner, W. (2002) First evidence for phototropin-related blue-light receptors in prokaryotes. *Biophys. J. 82*, 2627−2634.

(50) Nakano, S., Kuster-Schock, E., Grossman, A. D., and Zuber, P. (2003) Spx-dependent global transcriptional control is induced by thiol-specific oxidative stress in *Bacillus subtilis*. *Proc. Natl. Acad. Sci. U.S.A. 100*, 13603−13608.

(51) Dai, T., Gupta, A., Murray, C. K., Vrahas, M. S., Tegos, G. P., and Hamblin, M. R. (2012) Blue light for infectious diseases: *Propionibacterium acnes*, *Helicobacter pylori*, and beyond? *Drug Resist. Updates 15*, 223−236.

(52) Maclean, M., Macgregor, S. J., Anderson, J. G., and Woolsey, G. A. (2008) The role of oxygen in the visible-light inactivation of *Staphylococcus aureus*. *J. Photochem. Photobiol., B 92*, 180−184.

(53) Björnberg, O., Gruner, A. C., Roepstorff, P., and Jensen, K. F. (1999) The activity of *Escherichia coli* dihydroorotate dehydrogenase is dependent on a conserved loop identified by sequence homology, mutagenesis, and limited proteolysis. *Biochemistry 38*, 2899−2908.

(54) Higuchi, M., Yamamoto, Y., Poole, L. B., Shimada, M., Sato, Y., Takahashi, N., and Kamio, Y. (1999) Functions of two types of NADH oxidases in energy metabolism and oxidative stress of *Streptococcus mutans*. *J. Bacteriol. 181*, 5940−5947.

(55) Mishra, S., and Imlay, J. (2012) Why do bacteria use so many enzymes to scavenge hydrogen peroxide? *Arch. Biochem. Biophys. 525*, 145−160.

DOI: 10.1021/bi5013639
Biochemistry 2015, 54, 1628−1637

(56) Pericone, C. D., Overweg, K., Hermans, P. W., and Weiser, J. N. (2000) Inhibitory and bactericidal effects of hydrogen peroxide production by *Streptococcus pneumoniae* on other inhabitants of the upper respiratory tract. *Infect. Immun. 68*, 3990−3997.
(57) Leferink, N. G., Fraaije, M. W., Joosten, H. J., Schaap, P. J., Mattevi, A., and van Berkel, W. J. (2009) Identification of a gatekeeper residue that prevents dehydrogenases from acting as oxidases. *J. Biol. Chem. 284*, 4392−4397.
(58) Sun, W., Williams, C. H., Jr., and Massey, V. (1996) Site-directed mutagenesis of glycine 99 to alanine in L-lactate monooxygenase from *Mycobacterium smegmatis*. *J. Biol. Chem. 271*, 17226−17233.
(59) Kirkensgaard, K. G., Hägglund, P., Finnie, C., Svensson, B., and Henriksen, A. (2009) Structure of *Hordeum vulgare* NADPH-dependent thioredoxin reductase 2. Unwinding the reaction mechanism. *Acta Crystallogr. D65*, 932−941.
(60) Maeda, K., Hägglund, P., Björnberg, O., Winther, J. R., and Svensson, B. (2010) Kinetic and thermodynamic properties of two barley thioredoxin h isozymes, HvTrxh1 and HvTrxh2. *FEBS Lett. 584*, 3376−3380.
(61) Zhao, G., Bruckner, R. C., and Jorns, M. S. (2008) Identification of the oxygen activation site in monomeric sarcosine oxidase: Role of Lys265 in catalysis. *Biochemistry 47*, 9124−9135.
(62) Akif, M., Suhre, K., Verma, C., and Mande, S. C. (2005) Conformational flexibility of *Mycobacterium tuberculosis* thioredoxin reductase: Crystal structure and normal-mode analysis. *Acta Crystallogr. D61*, 1603−1611.
(63) Gustafsson, T. N., Sahlin, M., Lu, J., Sjöberg, B. M., and Holmgren, A. (2012) *Bacillus anthracis* thioredoxin systems, characterization and role as electron donors for ribonucleotide reductase. *J. Biol. Chem. 287*, 39686−39697.

DOI: 10.1021/bi5013639
Biochemistry 2015, 54, 1628−1637

SUPPLEMENTARY FIGURES

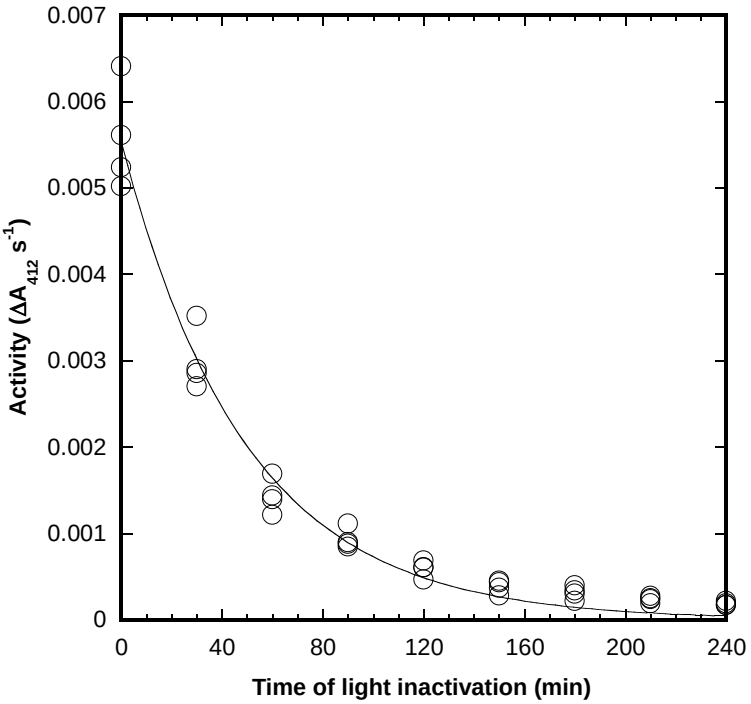

Figure S1. Reproducibility of light-inactivation. LlTrxR (2 µM) was illuminated and samples were removed during a four hour period for activity measurements (at 20 nM LlTrxR). The absolute activities after light-inactivation at standard conditions performed at four different occasions are shown. Assuming no residual activity, data is fitted to a single exponential decay function, giving a half-life of ca 35 min.

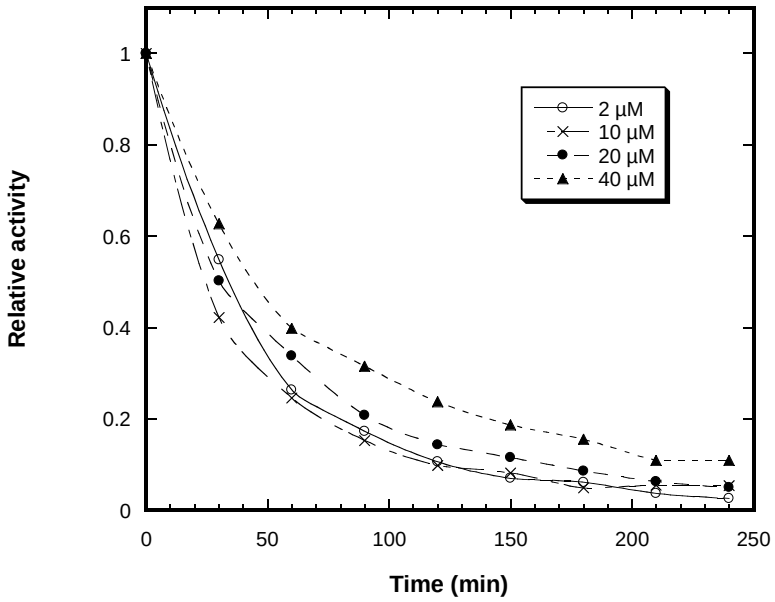

Figure S2. Influence of concentration on light-inactivation. The symbols used for 2, 10, 20 and 40 µM are shown in the plot. LlTrxR was illuminated and samples were removed during a four hour period for activity measurements (at 20 nM LlTrxR). The absolute rates measured at time point zero were 0.0064, 0.0062, 0.0069, and 0.0061, respectively. The average of 0.0065 Δ 412 s^{-1} corresponds to a turnover of 12 s^{-1} in the presence of 2.0 µM LlTrxA.

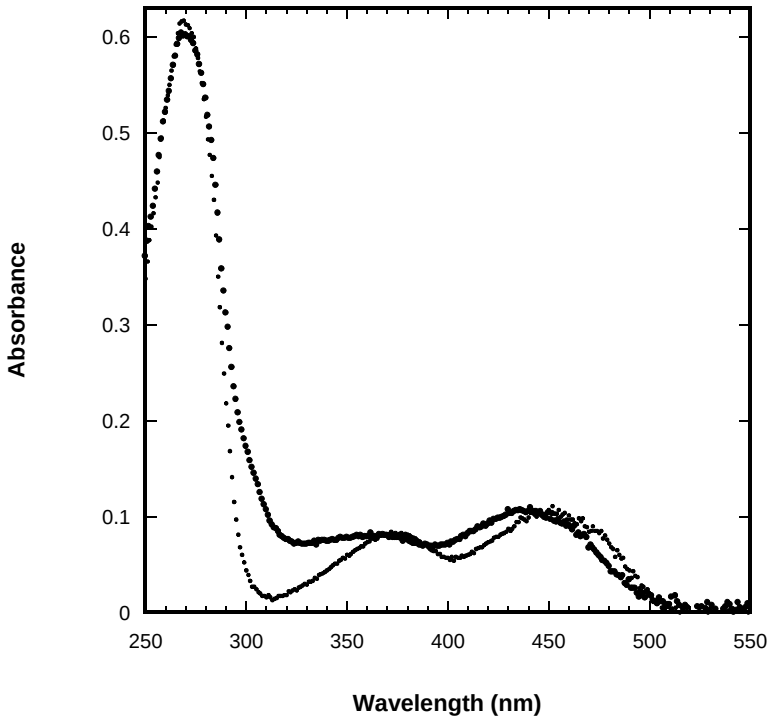

Figure S3. Spectral shift upon light-treatment. An extended spectral region of 250−550 nm of LlTrxR (10 µM) is included in the plot to allow comparison at the absorbance maximum around 270 nm. A sample stored on ice at ambient light (large circles) is compared to a sample protected from light (small circles).

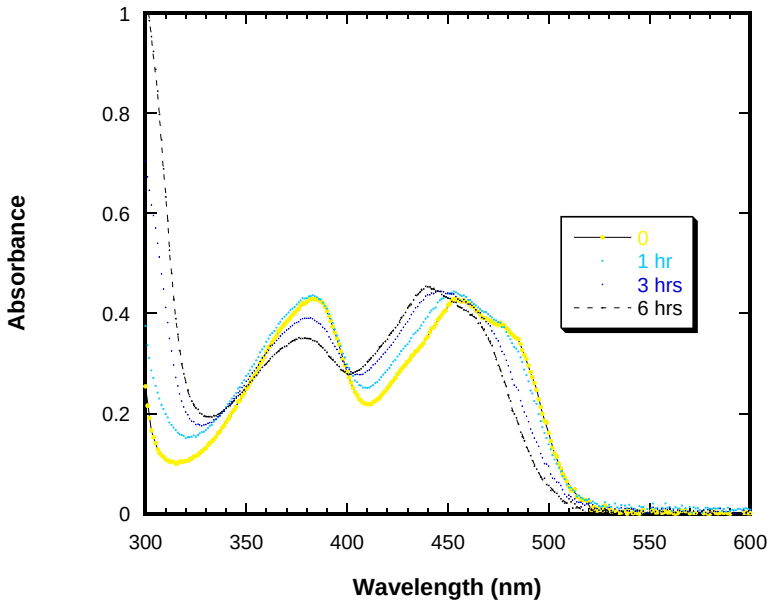

Figure S4. Spectral shift after 0 (yellow), 1 (blue) , 3 (purple) and 6 hrs (black) of illumination. A solution of 40 µM LlTrxR was exposed and after determined time points, samples were centrifuged and spectra recorded. The first spectrum, before illumination (t=0), is marked with a continuous thin line. The spectrum after 6 hours is marked with a dashed line. An isosbestic point at 400 nm is noteworthy.

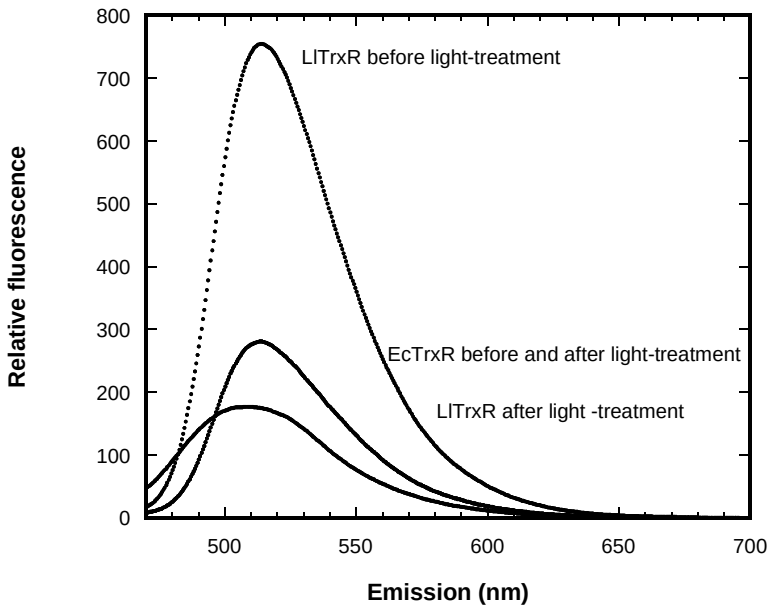

Figure S5. Fluorescence emission spectra of LlTrxR and EcTrxR before and after light exposure. Enzymes were diluted to 40 µM and the light-treated samples were exposed for 20 hrs. To record fluorescence emission, the samples were further diluted to 5 µM. LlTrxR is strongly fluorescent before exposure. After light-exposure, the fluorescence is diminished by a factor of four. In addition, there is a small blue-shift of the emission peak. In contrast, spectra of EcTrxR show no difference resulting in two overlaying spectra.

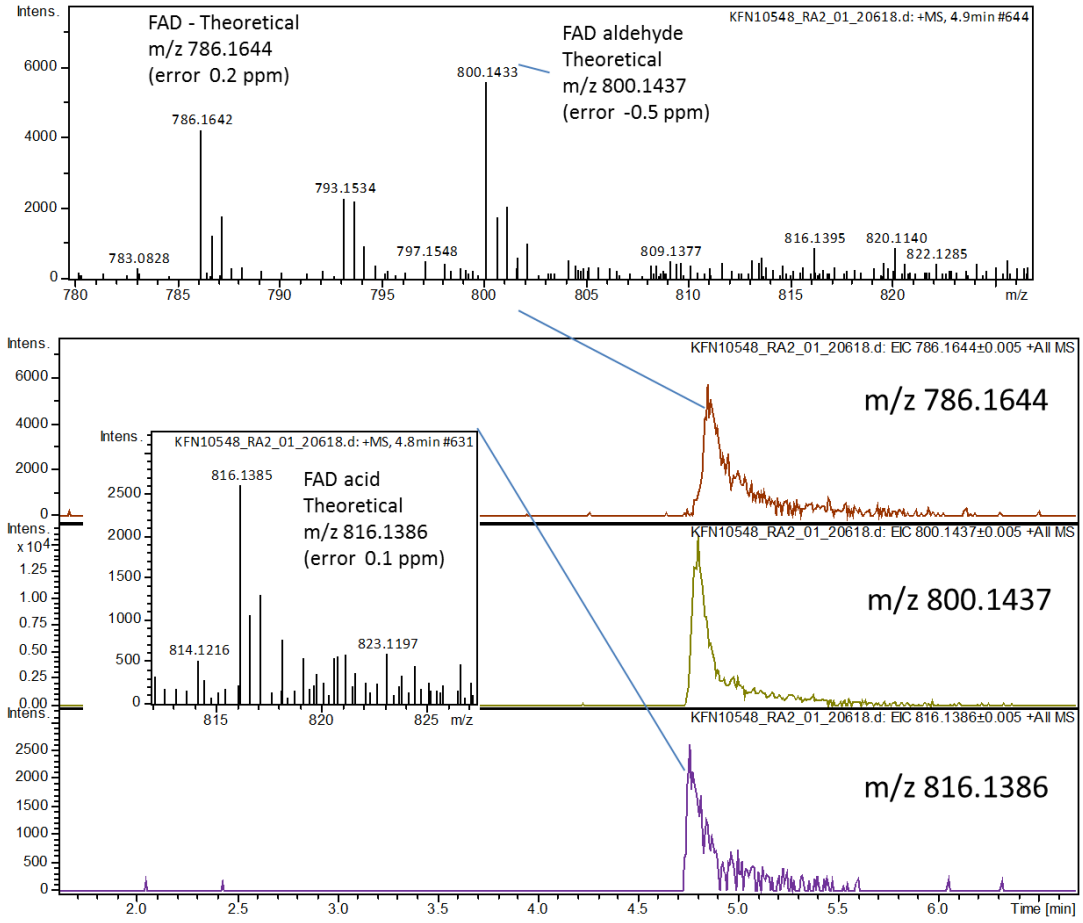

Figure S6. UHPLC ESI$^+$ qTOF analysis of flavins extracted from light inactivated LlTrxR. Extracted ion chromatograms showing partial separation of FAD (m/z 786.1644), the presumed FAD aldehyde (m/z 800.1437) and FAD acid (m/z 816.1386) along with mass spectra showing the pseudomolecular ions with mass deviations relative to the theoretical masses.

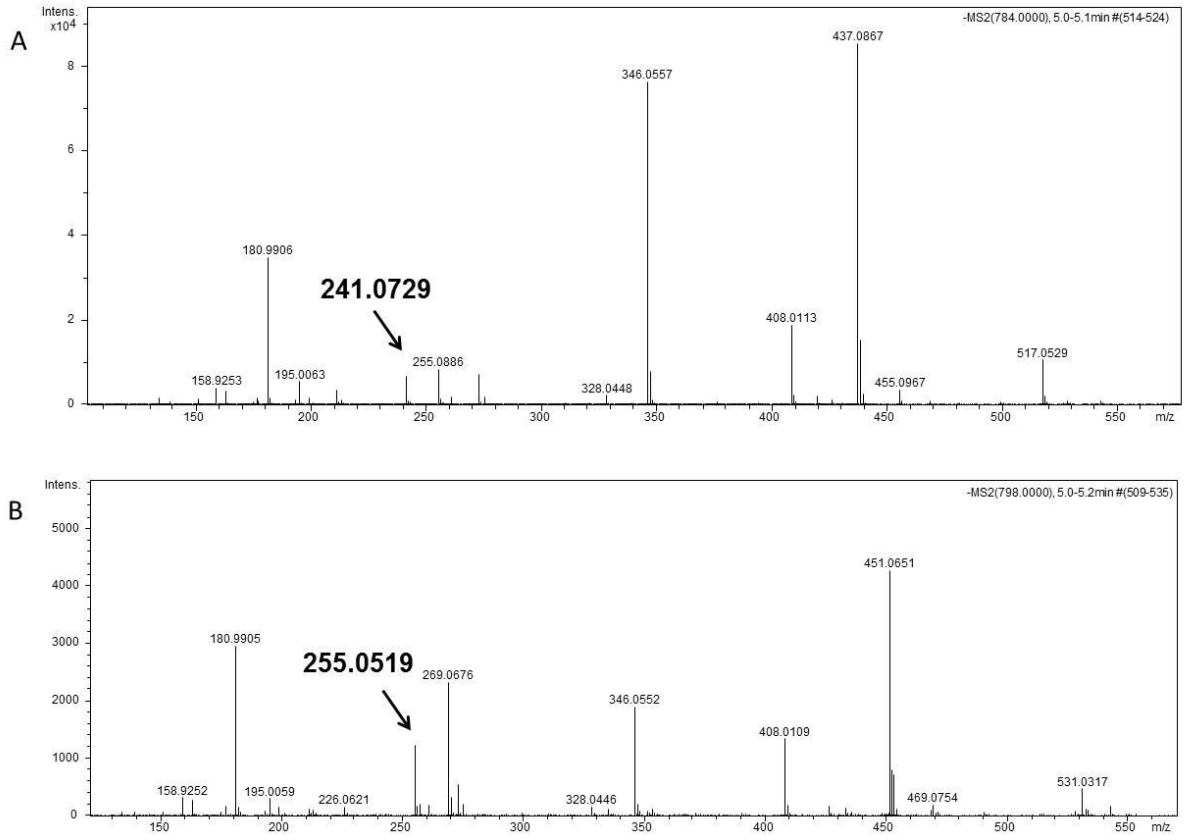

Figure S7. ESI^- qTOF tandem mass spectra of FAD (A; parent m/z 784) and presumed FAD aldehyde (B; parent m/z 798). The ion at m/z 241.0729 (marked with arrow in A) originates from the isoalloxazine ring system ($C_{12}H_9N_4O_2$ (theoretical m/z 241.0725) generated by fragmentation between the isoalloxazine N10 and C1 of the ribityl group) and is shifted by m/z 13.979 to 255.0519 (marked with arrow in B) corresponding to aldehyde formation. Please note change in accurate mass from 255.0886 (A) to 255.0519 (B).

```
H_pylori            --------------MIDCAIIGGGPAGLSAGLYATRGGVKNAVLFEKG-----MPGGQIT
D_radiodurans       -------MTAPTAHDYDVVIIGGGPAGLTAAIYTGRAQLS-TLILEKG-----MPGGQIA
S_aureus            ----------MTEIDFDIAIIGAGPAGMTAAVYASRANLK-TVMIERG-----IPGGQMA
B_anthacis          ---------MSEEKIYDVIIIGAGPAGMTAAVYTSRANLS-TLMLERG-----IPGGQMA
L_lactis            ----------MTEKKYDVVIIGSGPAGMTAAMYTARSEMK-TLLLERG-----VPGGQMN
S_mutans            --------------MYDTIIIGSGPAGMTAALYAARSNLK-VALIEQG-----APGGQMN
E_coli              ---------MGTTKHSKLLILGSGPAGYTAAVYAARANLQ-PVLITGM-----EKGGQLT
M_tuberculosis      MTAPPVHDRAHHPV-RDVIVIGSGPAGYTAALYAARAQLA-PLVFEGT-----SFGGALM
H_vulgare           -----MEGSAAAPLRTRVCIIGSGPAAHTAAIYAARAELK-PVLFEGWMANDIAAGGQLT
                                     ::*.***. :*.:*: *. :    ::          ** :

H_pylori            GSSEIENYPGVKEVVSGLDFMQPWQEQCFRFGLKHEMTAVQRVSKKDS----HFVILAED
D_radiodurans       WSEEVENFPGFPEPIAGMELAQRMHQQAEKFGAKVEMDEVQGVQHDATSHPYPF-TVRGY
S_aureus            NTEEVENFPGFE-MITGPDLSTKMFEHAKKFGAVYQYGDIKSVEDKGEYK-----VINFG
B_anthacis          NTEDVENYPGYE-SILGPDLSNKMFEHAKKFGAEYAYGDVKEVIDGKEYK-----TIIAG
L_lactis            NTAEIENYPGYE-TIMGPELSMKMAEPLEGLGVENAYGFVTGIEDHGDYK-----KIITE
S_mutans            NTSDIENYPGYD-LISGPELSMKMHEPLEKFGVENLYGIVTAVEDHGNFK-----KVLTD
E_coli              TTTEVENWPGDPNDLTGPLLMERMHEHATKFETEIIFDHINKVDLQNR----PF-RLNGD
M_tuberculosis      TTTDVENYPGFRNGITGPELMDEMREQALRFGADLRMEDVESVSLHGP----LKSVVTAD
H_vulgare           TTTDVENFPGFPTGIMGIDLMDNCRAQSVRFGTNILSETVTEVDFSAR----PF-RVTSD
                     : ::**:**    : *  :          :        :  :             :

H_pylori            GKTFEAKSVIIATGGSPKRTGIKGESEYWGKGVSTCATCDGF-FYKNKEVAVLGGGDTA
D_radiodurans       NGEYRAKAVILATGADPRKLGIPGEDNFWGKGVSTCATCDGF--FYKGKKVVVIGGGDAA
S_aureus            NKELTAKAVIIATGAEYKKIGVPGEQELGGRGVSYCAVCDGA--FFKNKRLFVIGGGDSA
B_anthacis          KKEYKARAIIVASGAEYKKIGVPGETELGGRGVSYCAVCDGA--FFKGKELVVIGGGDSA
L_lactis            DDEFITKSIIIATGANHRKLEIPGEEEYGARGVSYCAVCDGA--FFRNQEILVIGGGDSA
S_mutans            DNSYETKTVIIATGAKHRPLAVAGEETYNSRGVSYCAVCDGA--FFRGQDLLVVGGGDSA
E_coli              NGEYTCDALIIATGASARYLGLPSEEAFKGRGVSACATCDGF--FYRNQKVAVIGGGNTA
M_tuberculosis      GQTHRARAVILAMGAAARYLQVPGEQELLGRGVSSCATCDGF--FFRDQDIAVIGGGDSA
H_vulgare           STTVLADTVVVATGAVARRLYFSGSDTYWNRGISACAVCDGAAPIFRNKPIAVIGGGDSA
                           ::::* *.  :   . ..     :*:* **.***   ::: : : *:***::*

H_pylori            VEEAIYLANICKKVYLIHRRDGFRCAPITLEHAKNN---DKIEFLTPYVVEEIKGD--AS
D_radiodurans       VEEGMFLTKFADEVTVIHRRDTLRANKVAQARAFAN---PKMKFIWDTAVEEIQGA--DS
S_aureus            VEEGTFLTKFADKVTIVHRRDELRAQRILQDRAFKN---DKIDFIWSHTLKSINEK--DG
B_anthacis          VEEGVFLTRFASKVTIVHRRDTLRAQKILQDRAFQN---EKVDFIWNHTIKEINEA--NG
L_lactis            VEEALYLTRFGQSVTIMHRRDKLRAQEIIQQRAFKE---EKINFIWDSVPMEIKGD--DK
S_mutans            VEEALFLTRFANKVTIVHRRDELRAQKVLQERAFAN---DKVDFIWDSVVKEIKGN--DL
E_coli              VEEALYLSNIASEVHLIHRRDGFRAEKILIKRLMDKVENGNIILHTNRTLEEVTGD--QM
M_tuberculosis      MEEATFLTRFARSVTLVHRRDEFRASKIMLDRARNN---DKIRFLTNHTVVAVD---GDT
H_vulgare           MEEGNFLTKYGSQVYIIHRRNTFRASKIMQARALSN---PKIQVVWDSEVVEAYGGAGGG
                    :**. :*:.   .* ::***: :*.  :   :   :    :: .

H_pylori            GVSSLSIKNTA-TNEKRELVVPGFFIFVGYDVNNAVLKQEDNSMLCKCDEYGSIVVD---
D_radiodurans       -VSGVKLRNLK-TGEVSELATDGVFIFIGHVPNTAFVKDTV-----SLRDDGYVDVR---
S_aureus            KVGSVTLTSTK-DGSEETHEADGVFIYIGMKPLTAPFKDLG-----ITNDVGYIVTK---
B_anthacis          KVGSVTLVDVN-SGEEKEVKTDGVFVYIGMLPLSKPFVELG-----ITNENGYLETN---
L_lactis            KIQSVVYKNVK-TGEVTEKAFGGIFIYVGLDPVAEFVSDLG-----ITDEAGWIITD---
S_mutans            KVTNVDIENVK-TGQVNNYAFGGVFIYVGLDPVSSMVKELD-----ITDEAGWIPTD---
E_coli              GVTGVRLRDTQNSDNIESLDVAGLFVAIGHSPNTAIFEGQL-----ELE-NGYIKVQSGI
M_tuberculosis      TVTGLRVRDTN-TGAETTLPVTGVFVAIGHEPRSGLVREAI-----DVDPDGYVLVQ---
H_vulgare           PLAGVKVKNLV-TGEVSDLQVSGLFFAIGHEPATKFLNGQL-----ELHADGYVATK---
                     :  :   .             *.*. :*       .              * : .

H_pylori            --FSMKTNVQGLFAAGDIRIFAPKQVVCAASDGATAALSVISYLEHH-------------
D_radiodurans       --DEIYTNIPMLFAAGDVSDYIYRQLATSVGAGTRAAMMTERQLAALEVEGEEVTAAD--
S_aureus            --DDMTTSVPGIFAAGDVRDKGLRQIVTATGDGSIAAQSAAEYIEHLNDQA---------
B_anthacis          --ERMETKVPGIFAAGDVREKMLRQIVTATGDGSIAAQSAQHYVEELLEELKTVSEK---
L_lactis            --DHMRTNIPGIFAVGDVRQKDFRQITTAVGDGAQAAQEAYKFVVELG------------
S_mutans            --DHMKTKVAGVFAIGDVRQKDLRQITTAVGDGAVAAQEAYQYIVNNY------------
E_coli              HGNATQTSIPGVFAAGDVMDHIYRQAITSAGTGCMAALDAERYLDGLADAK---------
M_tuberculosis      -GRTTSTSLPGVFAAGDLVDRTYRQAVTAAGSGCAAAIDAERWLAEHAATGEADSTDALI
H_vulgare           -PGSTHTSVEGVFAAGDVQDKKYRQAITAAGSGCMAALDAEHYLQEVGAQVGKSD-----
                          *.:  :** **:     :*   :.. *  **  .   :

H_pylori            ----
D_radiodurans       ----
S_aureus            ----
B_anthacis          ----
L_lactis            ----
S_mutans            ----
E_coli              ----
M_tuberculosis      GAQR
H_vulgare           ----
```

Figure S8. Sequence comparison of nine selected LMW TrxRs. Sequences of six structure-determined TrxRs, from *M. tuberculosis* (PDB code 2A87), barley (HvNTR2, 2WHD), *E. coli* (several entries *e.g.* 1TDF), *S. aureus* (4GCM), *D. radiodurans* (2Q7V), and *H. pylori* (e.g. 2Q0L) were included. Three TrxRs with unknown structure are also included in the alignment. Residues mentioned in the discussion are labelled. Yellow: residues (Q42, N45, T46 and Y133) within 6.0 Å from the 7α-methyl carbon of FAD in *S. aureus* TrxR (4GCM). Red: five critical residues, the active site cysteine residues, the active site acid/base aspartate residue (also within 6.0 Å from the 7α-methyl carbon of FAD in 4GCM), and the two residues forming hydrogen bonds to FAD O2 and N3.

Appendix B. Paper 2

Skjoldager, N., Blanner Bang, M., Rykær, M., Björnberg, O., Davies, M. J., Svensson, B., Harris, P. and Hägglund, P. The structure of *Lactococcus lactis* thioredoxin reductase reveals molecular features of photo-oxidative damage. *Sci. Rep.* **7**, 46282 (2017).

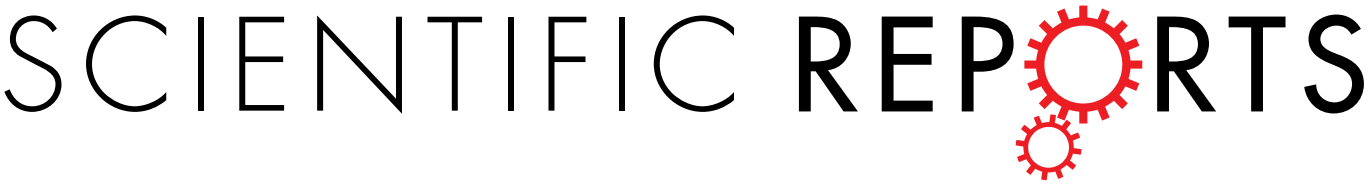

OPEN

The structure of *Lactococcus lactis* thioredoxin reductase reveals molecular features of photo-oxidative damage

Received: 20 January 2017
Accepted: 13 March 2017
Published: 11 April 2017

Nicklas Skjoldager[1], Maria Blanner Bang[2], Martin Rykær[1], Olof Björnberg[1], Michael J. Davies[3], Birte Svensson[1], Pernille Harris[2] & Per Hägglund[1]

The NADPH-dependent homodimeric flavoenzyme thioredoxin reductase (TrxR) provides reducing equivalents to thioredoxin, a key regulator of various cellular redox processes. Crystal structures of photo-inactivated thioredoxin reductase (TrxR) from the Gram-positive bacterium *Lactococcus lactis* have been determined. These structures reveal novel molecular features that provide further insight into the mechanisms behind the sensitivity of this enzyme toward visible light. We propose that a pocket on the *si*-face of the isoalloxazine ring accommodates oxygen that reacts with photo-excited FAD generating superoxide and a flavin radical that oxidize the isoalloxazine ring C7α methyl group and a nearby tyrosine residue. This tyrosine and key residues surrounding the oxygen pocket are conserved in enzymes from related bacteria, including pathogens such as *Staphylococcus aureus*. Photo-sensitivity may thus be a widespread feature among bacterial TrxR with the described characteristics, which affords applications in clinical photo-therapy of drug-resistant bacteria.

The protein disulfide reductase thioredoxin (Trx) maintains thiol groups in a reduced form through thiol-disulfide exchange reactions involving a redox-active WCXXC motif. Trx also provides reducing equivalents to enzymes like ribonucleotide reductase, peroxiredoxins and methionine sulfoxide reductase[1]. The recycling of Trx is catalysed by the homodimeric flavoprotein thioredoxin reductase (TrxR) that utilizes electrons from NADPH which are shuttled through a tightly bound FAD co-enzyme and a redox active dithiol motif. The TrxR monomers in bacteria, fungi and plants are about 35 kDa and composed of an NADPH- and an FAD-binding domain. By contrast, the monomers of TrxR from mammals, dipteran insects and protozoan parasites are larger (ca 50–55 kDa) and harbor an interface domain and a C-terminal flexible extension with an additional redox-active motif. In mammalian enzymes this motif contains a selenocysteine residue, while in e.g. *Drosophila melanogaster* this is replaced by a cysteine apparently without altering the catalytic efficiency[2]. Based on pioneering work on the three-dimensional structure and biophysical characteristics of *Escherichia coli* TrxR (EcTrxR) it was proposed that this bacterial enzyme undergoes a major molecular re-arrangement from the so-called Flavin Oxidizing (FO) conformation to the Flavin Reducing (FR) conformation in order to complete a catalytic cycle[3–5]. The FR conformation structure of EcTrxR in complex with Trx indeed confirmed a 66° rotation of the NADPH domain relative to the FAD domain, which relocates NADPH for hydride transfer to FAD and positions the TrxR CXXC motif in proximity of Trx[6]. Mammalian TrxR does not undergo such a conformational change during catalysis and the reducing equivalents delivered on the *re*-face of FAD are instead directly transferred to a redox-active CVNVGC motif positioned on the *si*-face[7,8]. Subsequently, the electrons are transferred to the C-terminal redox center, in turn reducing the CXXC motif in Trx. These mechanistic differences make TrxR an attractive target for antimicrobial drugs and a range of inhibitors have been explored for this purpose[9,10].

The physiological importance of Trx and TrxR are highly dependent on the lifestyle of the organisms as well as access to alternative redox control systems and antioxidant enzymes. For example in *E. coli* and other glutathione-producing bacteria, Trx is complemented by glutaredoxin as an electron donor to ribonucleotide

[1]Department of Biotechnology and Biomedicine, Technical University of Denmark, DK-2800 Kgs. Lyngby, Denmark. [2]Department of Chemistry, Technical University of Denmark. [3]Department of Biomedical Sciences, University of Copenhagen. Correspondence and requests for materials should be addressed to P.H. (email: hagglundperm@gmail.com) or P.H. (email: ph@kemi.dtu.dk)

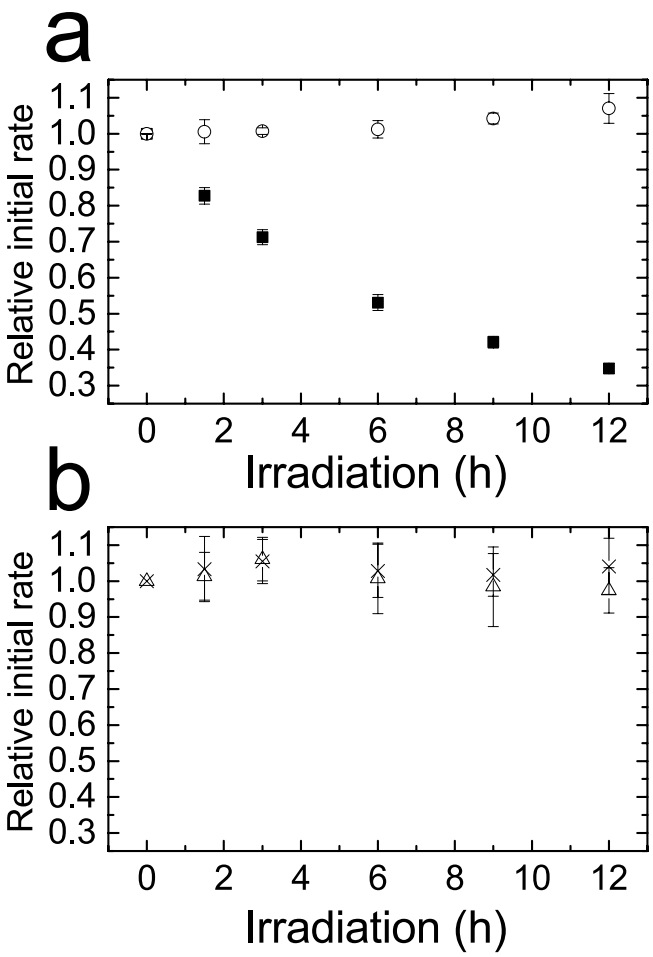

Figure 1. Inactivation of native TrxR in cell extracts. Activity of TrxR quantified by DTNB reduction, was assayed in light exposed cell extracts from *L. lactis* (**a,** ■) and *E. coli* (**b,** △) by adding 0.2 mM DTNB, 0.2 mM NADPH and 5 μM of the respective Trx. "No Light" controls (○ (**a**) and × (**b**)) were samples wrapped in foil; these exhibited no loss of activity. A similar relative change in activity was obtained in assays without addition of Trx (data not shown). All experiments were performed with three biological replicates.

reductase, whereas glutathione-negative bacteria such as *Bacillus subtilis* and *Staphylococcus aureus* lack this pathway[11,12]. The function of Trx as an electron donor to peroxiredoxins is particularly important in catalase-negative bacteria that rely on thiol-dependent peroxidases to remove damaging peroxides. Many lactic acid bacteria (LAB) lack both glutathione and catalase, suggesting that Trx plays a particularly central role in protection against oxidative stress in these bacteria. *Lactococcus lactis*, an industrially important LAB model bacterium, contains a TrxR that recycles two Trx (TrxA and TrxD) as well as NrdH, a glutaredoxin-like protein providing electrons to ribonucleotide reductase class Ib[13]. Additionally, it was recently discovered that reducing equivalents for ribonucleotide reduction can be provided in a TrxR-independent manner through flavoredoxin[14]. This may explain why knock-out mutants lacking either TrxR or Trx are viable even under oxidative stress conditions[15]. While investigating the biochemical properties of *L. lactis* TrxR (LlTrxR) we discovered that the enzyme is susceptible to photo-inactivation by visible light in an oxygen-dependent manner[16]. This inactivation coincided with a shift in the absorbance spectrum of the tightly bound FAD co-enzyme and oxidation of an isoalloxazine methyl group. To characterize the consequences of this photo-oxidation process in greater detail the three-dimensional structure of inactivated LlTrxR is here solved by X-ray crystallography. We propose possible mechanisms that account for the observed oxidative damage of the enzyme.

Results

TrxR from *L. lactis* is sensitive to photo-inactivation. We have previously shown that recombinant TrxR from *L. lactis* is inactivated by visible light *in vitro*, while the corresponding enzyme from *E. coli* is more resistant to photo-inactivation under these conditions[16]. In order to evaluate the sensitivity of native TrxR in an environment resembling the conditions *in vivo*, cell extracts of mid-late exponential phase cultures of *L. lactis* and *E. coli* K-12 were subjected to irradiation over a period of 12 h and TrxR activity was measured at different time points by use of a coupled assay with Trx, applying DTNB as the final electron acceptor. A marked decrease in TrxR activity was observed in the *L. lactis* cell extracts over the course of irradiation, while the activity in the *E. coli* cell extract was essentially unchanged (Fig. 1). After 12 h a ~65% drop in activity was observed in *L. lactis*

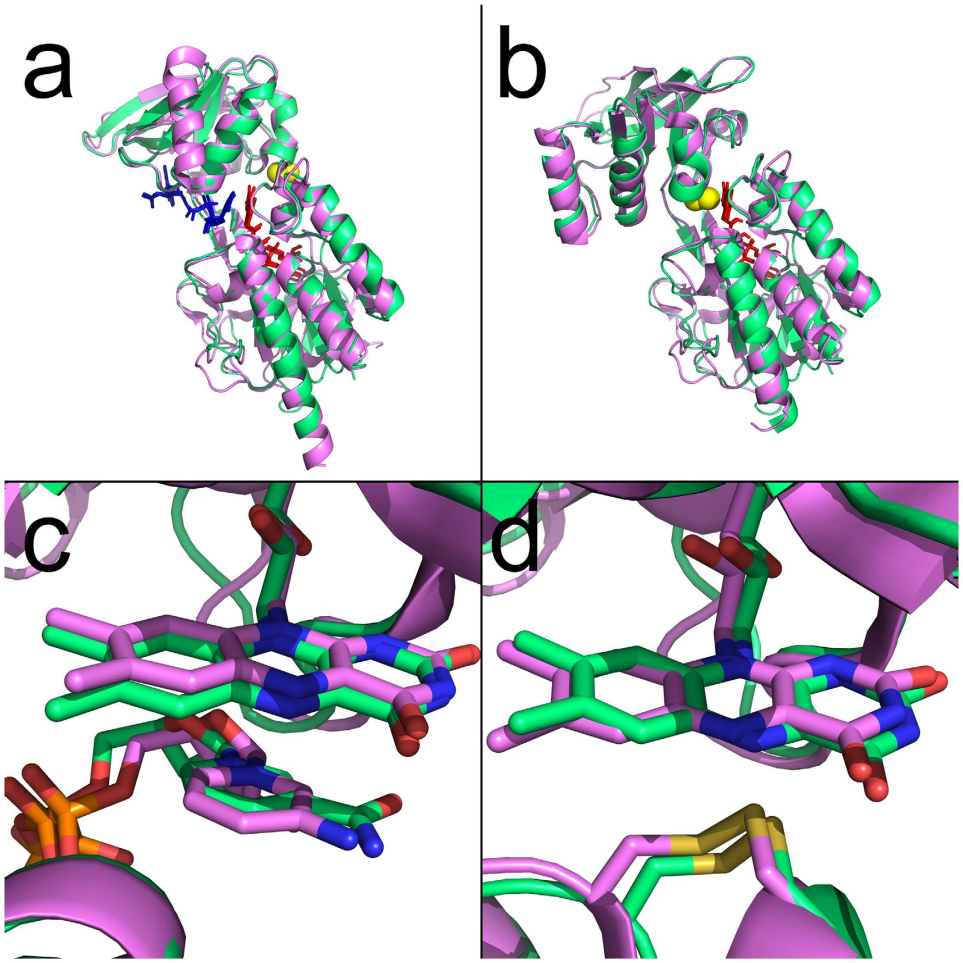

Figure 2. Overall structure of LlTrxR. Superposition of LlTrxR (green) and EcTrxR (violet) in FR (**a**) and FO (**b**) conformations with RMSD values of 0.426 and 1.137 Å, respectively. The FAD and NADPH domains are connected by two anti-parallel β-strands (amino acid residues 113–115 and 240–242). In both the FR and FO conformations the FAD (red sticks), as well as $NADP^+$ and the $NADP^+$ analog $AADP^+$ (blue sticks in the FR conformation) align well as indicated. The active site disulfide bond is marked as yellow spheres. Close-up of the active site of LlTrxR (green) and EcTrxR (violet) in the FR (**c**) and FO (**d**) conformations, indicating that FAD and $NADP^+$/$AADP^+$ are oriented identically in the two enzymes. PDB IDs for the EcTrxR structures are 1F6M and 1TDE for FR and FO conformation, respectively.

cell extract. This apparent slower rate of inactivation of native LlTrxR compared to the recombinant enzyme may be due to light-quenching by endogenous chromophores in the cell extracts.

Overall structure of LlTrxR. The overall structure of LlTrxR is similar to other low molecular weight (LMW) TrxRs[3,17] with a dimeric organization in which each monomer is composed of NADPH and FAD binding domains (Fig. 2). The secondary structure of each subunit consists of 11 α-helices and 19 β-sheets. The FAD-domain consists of residues 1–112 and 243–308 and the NADPH-domain consists of residues 116–239. The LlTrxR structures were obtained mainly in the FR conformation (Fig. 2a,c), which was unexpected since all available structures of LMW TrxR from other organisms are in the FO conformation, except for the engineered complex between EcTrxR and EcTrx[6]. LlTrxR crystallized in the FO conformation (Fig. 2b,d) only under reducing conditions in the presence of DTT (Table 1). The propensity of LlTrxR to crystallize in the FR conformation may indicate that the enzyme is stabilized in this conformation. Superposition of LlTrxR C_α-atoms with the structure of EcTrxR[3,6], gives RMSD of 0.426 Å and 1.137 Å for the enzymes in FR (Fig. 2a,c) and FO conformation (Fig. 2b,d), respectively. The relative orientation of the structures thus matches perfectly with the *E. coli* enzyme and consolidates the catalytic model proposed by Waksman *et al.* (1994) where the NADPH domain rotates 66° relative to the FAD domain in order to switch between the FO and FR conformations in the catalytic cycle.

Oxidation of the FAD co-enzyme and Tyr237 in photo-inactivated LlTrxR. No apparent change in the overall structure of LlTrxR in the FR conformation was observed upon exposure to visible light. Close examination of the isoalloxazine ring however reveals increased electron densities around the C7α methyl group over the course of irradiation (Fig. 3a–f), even though the FAD co-enzyme in general has well-defined electron densities with B-factors typically in the range from 20–24 $Å^2$. This observation is in accordance with our previous

	LlTrxR[a] No Light (PDB 5MH4)	LlTrxR[a] 30 min Light (PDB 5MIP)	LlTrxR[a] 60 min Light (PDB 5MIQ)	LlTrxR[a] 120 min Light (PDB 5MIR)	LlTrxR[a] 180 min Light (PDB 5MIS)	LlTrxR[a] 240 min Light (PDB 5MIT)	LlTrxR[b] No Light (PDB: 5MJK)
Data collection							
Space group	$P4_12_12$	$P4_12_12$	$P4_12_12$	$P4_12_12$	$P4_12_12$	$P4_12_12$	$P2_1$
Cell dimensions							
a, *b*, *c* (Å)	120.54, 120.54, 60.47	121.43, 121.43 60.7	121.46, 121.46, 60.71	121.17, 121.17, 60.62	120.92, 120.92, 60.45	120.69, 120.69, 60.33	73.61, 132.26, 73.5
α, β, γ (°)	90, 90, 90	90, 90, 90	90, 90, 90	90, 90, 90	90, 90, 90	90, 90, 90	90, 112.62, 90
Resolution (Å)	85.24–2.14 (2.22–2.14)	42.94–2.0 (2.05–2.00)[c]	42.95–1.92 (1.97–1.92)	42.86–2.00 (2.05–2.00)	60.45–1.81 (1.84–1.81)	60.34 (1.84–1.80)	47.36–2.00 (2.05–2.00)[c]
R_{merge}	0.127 (1.74)	0.116 (1.224)	0.096 (1.461)	0.073 (0.509)[c]	0.088 (1.063)	0.134 (1.783)	0.088(0.826)[c]
I/σ (I)	12.3 (1.3)	13.24 (1.74)[c]	15.69 (1.18)[c]	20.13 (3.66)[c]	17.5 (1.9)[c]	14.6 (1.5)[c]	12.2(1.8)[c]
CC(½)	99.7(47.7)	99.8(61.9)	99.9(49.5)	99.9(88.9)	99.9(52.1)	99.9(31.7)	99.7(63.3)
Completeness (%)	99.9 (100)	96.2 (98.1)[c]	99.6 (99.8)[c]	99.8 (100.0)[c]	99.9 (99.9)[c]	99.8 (98.9)[c]	99.0 (98.4)[c]
Redundancy	8.4 (8.5)	6.6 (6.5)[c]	7.4 (6.3)[c]	7.5 (7.8)[c]	10.2 (8.1)[c]	13.5 (10.7)[c]	3.8 (3.8)[c]
Refinement							
Resolution (Å)	49.37–2.14	42.94–2.00	42.95–1.92	42.86–2.00	54.13–1.81	54.03–1.80	47.36–2.00
No. reflections	210,842 (20,402)	198,639 (14,547)[c]	260,449 (16,150)[c]	231,711 (17,615)[c]	423,277 (19,394)[c]	560,996 (25,330)[c]	332,553 (24,494)[c]
R_{work}/R_{free}	0.1767/0.2373	0.1947/0.2276	0.1947/0.2276	0.1826/0.2166	0.1895/0.2320	0.1937/0.2335	0.2299/0.2760
No. atoms							
Protein	2,347	2,347	2,347	2,347	2,347	2,347	9,356
Ligand/ion	118	125	125	125	125	125	232
Water	166	224	239	247	256	250	409
B-factors							
Protein	44.3	34.7	35.3	31.5	29.9	31.4	35.1
Ligand/ion	39.1	33.5	33.6	28.0	27.4	29.3	25.1
Water	50.2	44.7	44.8	40.1	39.5	40.9	33.2
R.m.s. deviations							
Bond lengths (Å)	0.018	0.019	0.019	0.018	0.022	0.019	0.015
Bond angles (°)	2.0	2.2	2.0	2.1	2.3	2.1	1.7

Table 1. Data collection and refinement statistics (molecular replacement). [a]The structure was obtained in FR conformation. [b]The structure was obtained in FO conformation. [c]Values in parentheses are for highest-resolution shell. *Number of xtals for each structure should be noted in footnote.

mass spectrometry data demonstrating formation of an aldehyde group in FAD extracted from light-inactivated LlTrxR, which was concluded to be confined to the C7α methyl group based on the spectrophotometric features[16]. Moreover, an increase in electron density at the meta-position (ortho to the hydroxyl group) of Tyr237, located 4.4 Å from C7α is observed as a function of light-exposure (Fig. 3a–f). This density most likely represents the formation of 3,4-dihydroxyphenylalanine (DOPA). Mass spectrometric analysis of proteolytic digests of photo-inactivated LlTxR indeed confirms a mass shift of 16 Da confined to Tyr237 (Supplementary Figure 1). Tyr237 is only close to the isoalloxazine ring when LlTrxR is in the FR conformation (Fig. 3a), suggesting that photo-oxidation reactions are primarily taking place while the enzyme is in this conformation. In the FO conformation, Tyr237 is distant from the flavin-binding site and another tyrosine (Tyr133) is in proximity to the isoalloxazine ring (4.9 Å from C7α), but no indications of oxidation of Tyr133 were observed in the irradiated structures of LlTrxR. Remarkably, Tyr237 appears to be conserved among most TrxR from Gram-positive bacteria in the phylum *Firmicutes*, but is replaced mainly by Ala or Phe in other organisms (Supplementary Figure 2).

An oxygen pocket on the *si*-face of the isoalloxazine ring. The observed oxygen- and triplet isoalloxazine-dependent photo-inactivation of LlTrxR[16] suggests that molecular oxygen is positioned in the vicinity of the FAD and interacts with the photo-excited co-enzyme. A closer look at the isoalloxazine ring indeed reveals a pocket that potentially may accommodate molecular oxygen due to its hydrophobic character. Met43 positioned on the *si*-face bends away from the isoalloxazine towards Pro15 and the sidechains of Met18 and Met67 (Fig. 4a) and as a consequence a pocket on the *si*-face is formed. In the space between the β-carbon of Met43 and the isoalloxazine ring (7.2–7.4 Å distance to N10 and N5) a well-defined electron density appears, assigned to a water molecule perfectly centered above the central ring of the isoalloxazine. This water molecule is present in all structures listed in Table 1. The water is in hydrogen bond distance from the 2′-ribityl hydroxyl group (2.8 Å) and the alcohol group of Thr46 (2.8 Å), and the distance from the water to the N5 and N10 atom of the isoalloxazine is 3.5–3.6 Å (Fig. 4a). A closer look at the electrostatic environment on the *si*-face reveals several hydrophobic residues, most noteworthy are Ile286, Ile49, Leu63 and the β- and γ-carbons of Met43 that together with the π-electron cloud of the conjugated isoalloxazine ring system constitute an overall hydrophobic environment facilitating accommodation of O_2 (Fig. 4c). In the presence of O_2 at this location, it can be speculated that the Thr46 sidechain can flip so the methyl group points towards the O_2, while the 2′-ribityl hydroxyl group can

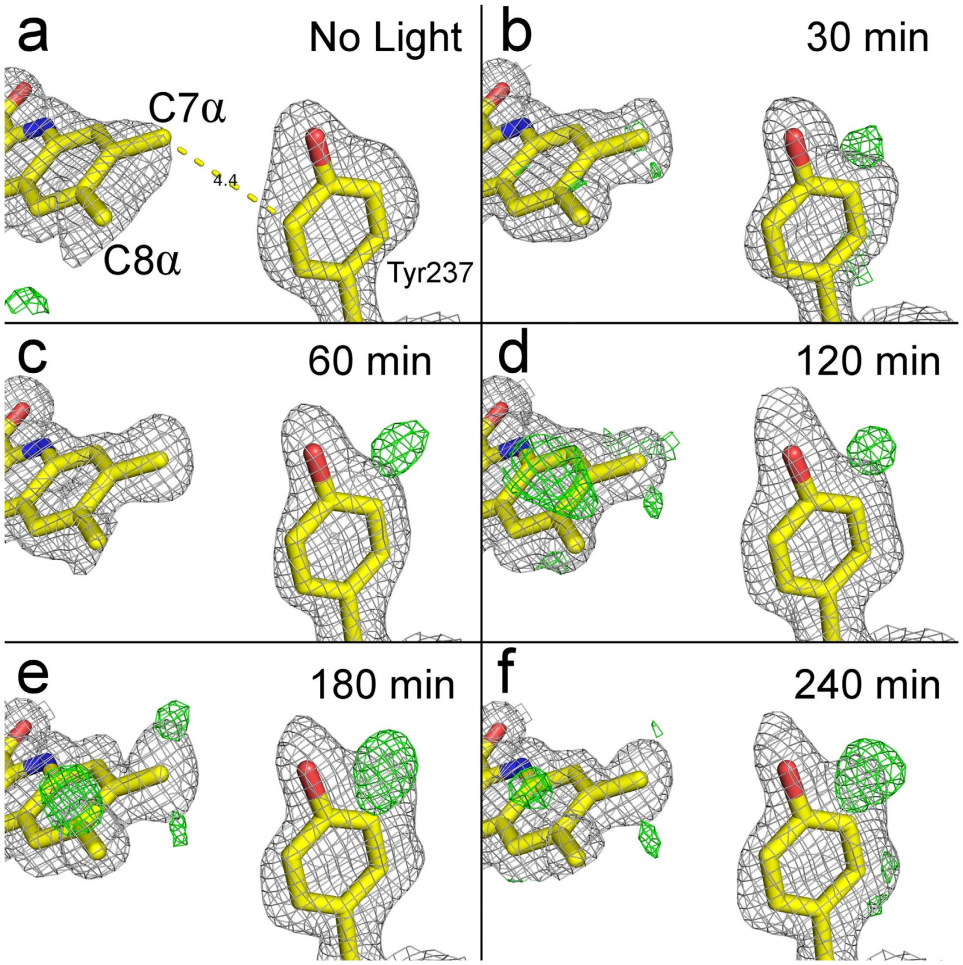

Figure 3. Oxidation of the isoalloxazine ring and Tyr237 in photo-inactivated LlTrxR. Increased electron density around the C7α methyl group of the isoalloxazine ring, and the meta-position of Tyr237 in LlTrxR develops over the course of irradiation (0–240 min). The σ_A-weighted $2F_o–F_c$ maps (grey) have been contoured at 1.0 σ. The difference $F_o–F_c$ maps (green/red) have been contoured at ± 3.0 σ, respectively. The C7α methyl group and the meta-position of Tyr237 develop increased difference densities mainly in the σ_A-weighted $2F_o–F_c$ maps and $F_o–F_c$ maps, respectively.

form a hydrogen bond with the 4′-ribityl hydroxyl group. These changes will further increase the hydrophobicity of the *si*-face, thus increasing the O_2 affinity. The *re*-face of the isoalloxazine ring in the FO conformation is occupied by the Cys134-Cys137 disulfide while in the FR conformation it is surrounded by hydrophilic residues (Asp154, Glu158, Ser155 and Gln285). These features further underlines that the *si*-face open space is the most likely site of O_2 accommodation and thus oxidant generation. The oxygen pocket described here is conserved in *Staphylococcus aureus* TrxR (SaTrxR), the most closely related structure-determined enzyme (53% sequence identity).

Even though several residues on the *si*-face of the isoxoalloxazine ring are conserved among TrxR (Fig. 4e) some subtle yet crucial differences in the local environment are observed. $Met43_{LlTrxR}$ appears to be conserved among bacteria in the phylum *Firmicutes* (Supplementary Figure 2), but in EcTrxR this residue is substituted with $Leu44_{EcTrxR}$ that is centered at the *si*-face of the isoalloxazine with a 3.8–4.0 Å distance from the δ-carbon to the N10 and N5 atoms (Fig. 4b). In addition, $Ser64_{LlTrxR}$ is replaced by the more bulky $Met66_{EcTrxR}$ that hinders $Leu44_{EcTrxR}$ from bending towards Pro15. $Leu44_{EcTrxR}$ thus blocks the pocket on the *si*-face of the isoalloxazine and restricts access of O_2 (Fig. 4d). Noticeably, all available bacterial TrxR structures except those from *L. lactis* and *S. aureus* display Leu/Ile in similar positions as Leu44 in EcTrxR (Fig. 4e).

Discussion

Based on the structural information provided here we propose mechanisms that may account for the observed photo-inactivation of LlTrxR with the involvement of photo-excited FAD and O_2 (Fig. 5). The initial step involves light absorption by the isoalloxazine ring and subsequent electron transfer from the ring to O_2 with concomitant generation of superoxide radicals ($O_2^{-}\cdot$) and an isoalloxazine radical-cation. Subsequent rapid, spontaneous dismutation of $O_2^{-}\cdot$ would give H_2O_2[18], as observed in other flavin photo-oxidation reactions[19]. The isoalloxazine radical-cation may then undergo one of two processes: electron transfer with the nearby Tyr237 to regenerate the isoalloxazine and generate a Tyr237 radical-cation (which would be expected to rapidly deprotonate to give a

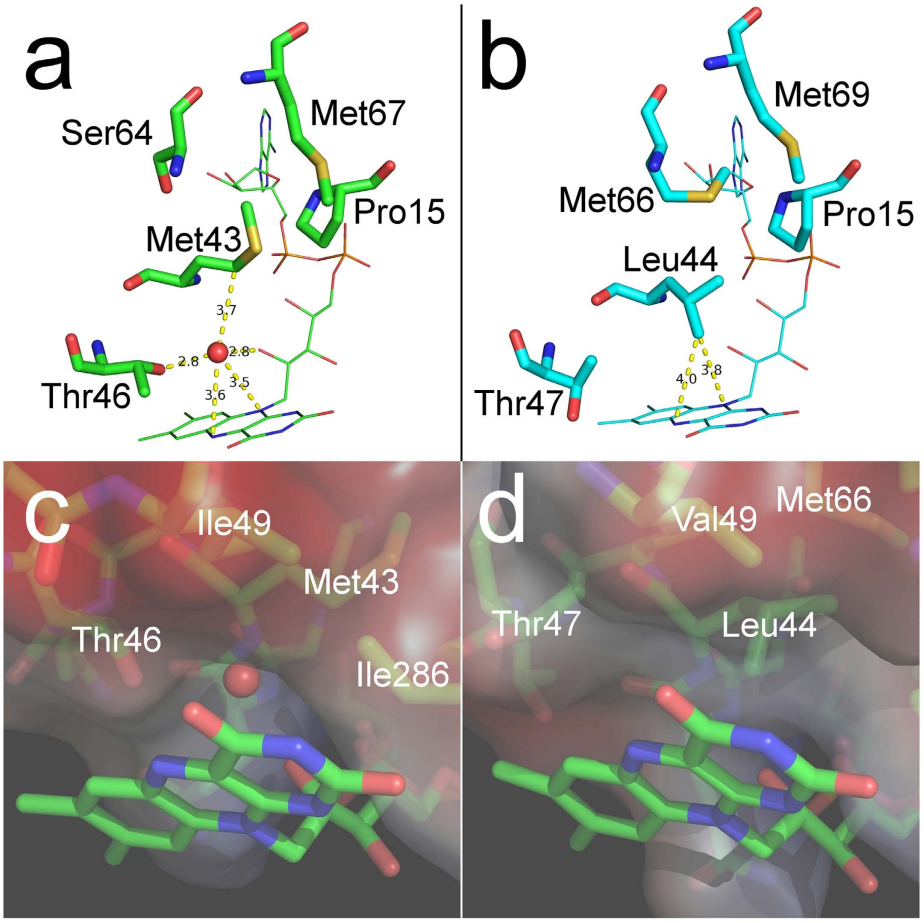

e

***L. lactis* ***	**Pro15**	**Met43**	**Thr46**	**Ser64**	**Met67**
***E. coli* ***	Pro15	Leu44	Thr47	Met66	Met69
***H. pylori* ***	Pro	Ile	Ser	Met	Trp
***S. aureus* ***	Pro	Met	Thr	Ser	Met
S. pyogenes	Pro	Met	Thr	Ala	Met
***D. radiodurans* ***	Pro	Ile	Ser	Ala	Met
B. anthacis	Pro	Met	Thr	Ser	Met
S. mutans	Pro	Met	Thr	Ser	Met
***M. tuberculosis* ***	Pro	Leu	Thr	Met	Met
***H. vulgare* ***	Pro	Leu	Thr	Met	Cys
***S. cerevisiae* ***	Pro	Leu	Thr	Met	Met

Figure 4. An oxygen pocket on the *si*-face of the FAD isoalloxazine ring. (**a**) LlTrxR has a pocket on the *si*-face of the isoalloxazine ring occupied by a water molecule (red sphere), which is in hydrogen bonding distance from the hydroxyl group of the Thr46 sidechain and the 2′-ribityl hydroxyl group of the FAD. Met43 bends towards Pro15 exposing a pocket which is occupied with a water molecule in all obtained structures of LlTrxR. (**b**) In EcTrxR (PDB 1F6M) $Met43_{LlTrxR}$ is substituted with $Leu44_{EcTrxR}$ that is centered at the *si*-face of the isoalloxazine ring and restricts access due to steric hindrance. In addition, $Ser64_{LlTrxR}$ is replaced by the more bulky $Met66_{EcTrxR}$ that hinders $Leu44_{EcTrxR}$ from bending towards Pro15. Distances are given in Å and marked with dashed lines. (**c**) Electrostatic environment at the *si*-face of isoalloxazine in LlTrxR as viewed from the *re*-face showing the pocket where O_2 can be accommodated. The pocket is confined by the π-electron cloud of the isoalloxazine, key hydrophobic residues Ile49, Ile286, Met43 and the methyl group of Thr46. (**d**) Corresponding electrostatic environment at the *si*-face of isoalloxazine in EcTrxR, where the *si*-face pocket is blocked by Leu44. (**e**) Alignment of selected residues that are positioned near the isoalloxazine *si*-face (sequences of structure determined TrxR are marked with an asterisk).

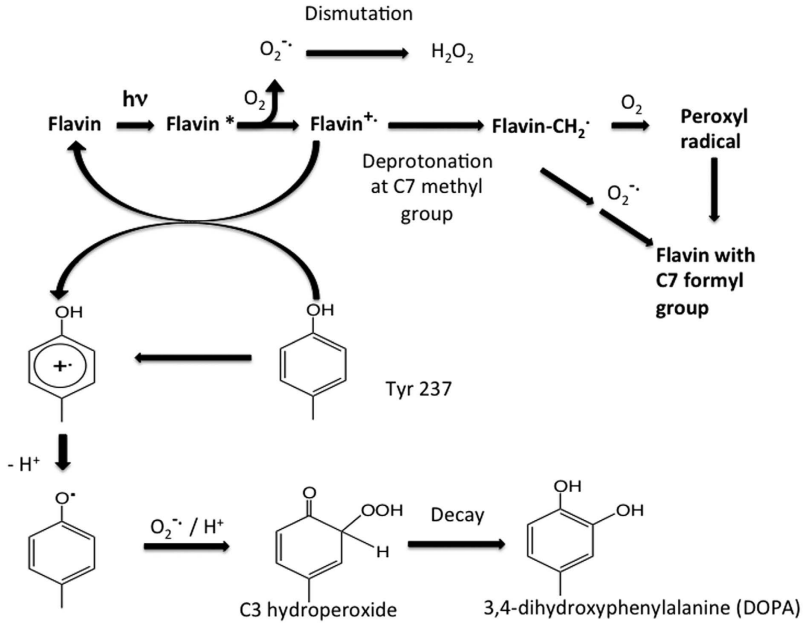

Figure 5. Proposed mechanisms for oxidation of Tyr237 and the FAD methyl group. Upon photo-induced excitation of FAD an electron is transferred to O_2 generating superoxide. The one-electron deficient flavin cation radical can oxidize Tyr237 forming a radical-cation, which rapidly deprotonates to give Tyr phenoxyl radical. The Tyr phenoxyl radical is a target for superoxide and undergoes rapid reaction to give hydroperoxides at either C3 or C5. The resulting Tyr-OOH decays to give 3,4-dihydroxyphenylalanine (DOPA). The flavin radical-cation can upon deprotonation at C7α generate a primary C7α radical (R-$CH_2^{\cdot}$). In the presence of O_2 this would lead to formation of a peroxyl radical, while in the presence of $O_2^{-\cdot}$ a hydroperoxide would be formed. Subsequent decay of the peroxyl radical via the Russell mechanism, or decomposition of the hydroperoxide, would yield an aldehyde.

Tyr phenoxyl radical due to the very low pK_a of these species), or deprotonation at one of the ring methyl groups. Such reactions are supported by literature data on the intramolecular photo-oxidation of target substrates by flavins subject to blue light, by electron transfer pathways[19].

Tyr phenoxyl radicals undergo rapid reaction with $O_2^{-\cdot}$/HOO. to give hydroperoxides, with these being formed at either C3/C5 or C1 due to the high spin density at these sites[20,21]. Such peroxides are unstable and undergo ready decay to the corresponding catechols, potentially accounting for the formation of 3,4-dihydroxyphenyalanine (DOPA) from Tyr237. An alternative route for decay of the isoalloxazine radical-cation involves deprotonation at a methyl group (a well-established decay pathway of radical-cations[22,23]) to give a primary alkyl radical (–$CH_2^{\cdot}$). In the presence of O_2 this would lead to formation of a peroxyl radical, while in the presence of $O_2^{-\cdot}$ a hydroperoxide would be formed. Subsequent decay of the peroxyl radical via the Russell mechanism[24], or decomposition of the hydroperoxide[25], would yield an aldehyde.

An alternative route to oxidation of the C7α methyl group may be direct hydrogen atom abstraction from the methyl group by the Tyr237 phenoxyl radical (i.e. Tyr237-$O^{\cdot}$ + flavin-CH_3 → Tyr237-OH + flavin-$CH_2^{\cdot}$ → formyl group) but such a pathway would be energetically less favorable due to the relative bond strengths of the C-H and O-H bonds. An alternative process involving formation of singlet oxygen ($^1O_2$) by the excited state isoalloxazine could also be envisaged, with this then undergoing decay to H_2O_2 or formation of an endoperoxide from the Tyr237 residue[26]. Subsequent decay of the unstable endoperoxide, potentially involving radical formation[26], could account for the formation of DOPA from Tyr237 and oxidation of the C7α methyl group on the isoalloxazine ring to the formyl group.

The structure of LlTrxR also reveals an oxygen pocket at the *si*-face of the isoalloxazine ring, which is absent in EcTrxR. EcTrxR has previously been shown be highly photo-reactive and forms high yields of FAD semiquinones upon irradiation under anaerobic reaction conditions[27]. In light of the data obtained in the present study, it may therefore be suggested that the difference in photo-sensitivity between LlTrxR and EcTrxR is related to the accessibility of O_2 in the active site, rather than the light-absorbing properties of the isoalloxazine ring *per se*. Besides its proposed role in photo-sensitivity the oxygen pocket might also have implications for the ability of these enzymes to reduce O_2. We have reported that LlTrxR displays a ~10-fold increased rate of O_2 reduction in the presence of NADPH as compared to EcTrxR[16]. LlTrxR thus shows a similar tendency to reduce O_2 as the TrxR homologue AhpF, a dedicated reductase of the peroxide scavenger AhpC in eubacteria[28,29]. Interestingly, X-ray crystal structures of AhpF from *S. typhimurium* and *E. coli* (PDB 1HYU and 1FL2, respectively), also display a pocket on the *si*-face of the isoalloxazine and a tyrosine (Tyr344) located in the same position relative to the C7α as $Tyr237_{LlTrxR}$. It can thus be hypothesized that AhpF also may be sensitive to photo-oxidation. However, it is important to emphasize that a direct comparison between reduction and photo-activation of O_2 cannot be made since the molecular mechanisms and kinetic properties of these processes are different.

The novel molecular features of LlTrxR reported here provide insight into the photo-inactivation mechanism involving a protein-bound FAD acting as a photosensitizer that is highly relevant in a wider context. The conservation of Tyr237 and Met43 among TrxR from related Gram-positive bacteria suggests that photo-sensitivity may be widespread among these types of organisms. This opens up interesting perspectives in terms of clinical light treatment, e.g. blue light therapy of pathogenic and multi-drug resistant bacteria such as *S. aureus, Streptococcus pyogenes* and *Bacillus anthracis*, which all have TrxR predicted to harbour the described oxygen pocket.

Methods

Photo-inactivation of native TrxR in cell extracts. *Lactococcus lactis* subsp. *cremoris* (strain MG1363) was grown in SA medium[30] containing 1% (w/v) glucose and 2 mg/L lipoic acid (GSAL medium). *E. coli* K-12 (strain MG1655) was grown in LB-medium. One liter synchronized cell culture (in biological triplicate) at exponential phase (OD_{600} 0.6–0.7) was placed on ice for 30 min and then centrifuged (4 °C). The cell pellet was resuspended in 0.9% NaCl and distributed in ten 2 mL screw-cap microcentrifuge tubes, centrifuged, and the pellets were stored at −20 °C until use. Proteins were extracted by adding 600 μL 100 mM potassium phosphate pH 7.5, 1 mM EDTA and 400 μL glass beads ≤106 μm (Sigma) to each tube and performing bead beating on a FastPrep FP120 homogenizer (Qbiogene), setting 6 for 30 s, followed by 1 min rest on ice. Bead beating was repeated 6 times followed by centrifugation for 15 min at 13,000 g. Benzonase (2 μL) was added to pooled supernatants (~4.5 mL) and incubated for 1 h at 21 °C. The protein concentration was determined (Bio-Rad Protein Assay, Life Science Research) using BSA as a standard and the samples were aliquoted and stored at −20 °C. Cell extracts were thawed, diluted 1:1 with 100 mM potassium phosphate pH 7.5, 1 mM EDTA and transferred to original 1.5 mL Eppendorf tubes with 6 × 3mm magnets, and placed on a stirrer in a cold room at 4 °C. The samples were irradiated with a 1225 Lumen (21 W) lamp at 15 cm distance as previously described[16]. Control samples wrapped in foil are referred to as "No Light". After 0, 1.5, 3, 6, 9 and 12 h cell extracts were removed and stored at −20 °C for subsequent activity measurements. TrxR activity was assayed as 5,5′-dithiobis(2-nitrobenzoic acid) (DTNB) reduction monitored at 412 nm in 150 μL format with 100 mM potassium phosphate, pH 7.5, 2 mM EDTA, 0.20 mM DTNB and 0.20 mM NADPH. For *L. lactis* 30 μL of undiluted cell extract was used in the assay while the *E. coli* cell extracts were diluted 3 times in 100 mM potassium phosphate, pH 7.5, 1 mM EDTA before being added to the assay mixture. The activity of the cell extracts was measured directly or after addition of their respective recombinant thioredoxins (5 μM final concentration), LlTrxA and EcTrx1[13]. The addition of recombinant thioredoxin in the assay boosted the signal ~4 and ~2.3 times for *L. lactis* and *E. coli*, respectively. The initial activities were determined in at least technical triplicates for each biological replicate.

Photo-inactivation of recombinant TrxR. Production and purification of recombinant His-tagged *L. lactis* and *E. coli* TrxR and Trx and subsequent light inactivation of TrxR were performed essentially as described previously[16]. For crystallization trials 50 μM LlTrxR was irradiated for 30, 60, 120, 180, and 240 min (with remaining relative initial activities of ~73, 27, 26, 15 and 10%, respectively) and subsequently loaded on a HiLoad Superdex 75 gel filtration column (prep grade, 16/60; GE Healthcare) using 10 mM HEPES, 200 mM NaCl, 2 mM Na-EDTA, pH 7.0 as eluent. Fractions that appeared homogeneous according to the chromatogram and SDS-PAGE were pooled, dialyzed (6−8 kDa MWCO, Spectra/Por 1) against 10 mM HEPES, 2 mM Na-EDTA, pH7.0, and concentrated (Amicon Ultra centrifugal filter unit, 10 kDa MWCO) to 8–10 mg/mL as assessed from absorbance ($\varepsilon_{456} = 11{,}300\ M^{-1}cm^{-1}$)[31].

Crystallization and data collection of LlTrxR. Crystals obtained in FR conformation: LlTrxR (2 μL, 8–10 mg/mL) was mixed with 2 μL reservoir buffer and co-crystallized with 1 μL 25 mM $NADP^+$ (Sigma-Aldrich) and equilibrated as hanging-drops over a 500 μL reservoir containing 35% PEG 1500 (Fluka), 400 mM Li_2SO_4, 20 mM HEPES of pH varying in the range 6.0–8.5. Bright yellow octahedron crystals (100 μm) appeared after about 5 days at 19 °C and grew to about 200 μm in length by 14 days. Crystals of light-exposed (30, 60, 120, 180 and 240 min) and light-protected LlTrxR were harvested and flash-cooled directly from the drop without additional cryoprotectants.

Crystals obtained in FO conformation: LlTrxR (2 μL, 8–10 mg/mL) was mixed with 2 μL reservoir buffer, and 2 μL 60 mM DTT and equilibrated as hanging-drops over a 500 μL reservoir containing 20% PEG 4000 (Fluka), 400 mM Li_2SO_4. Only non-irradiated LlTrxR crystallized under these reducing conditions. Crystals appeared after ~14 days at 19 °C. Crystals were transferred to a cryoprotectant solution consisting of reservoir buffer with 10% ethylene glycol before storing in liquid nitrogen.

Data collection, structure determination and refinement. X-ray diffraction data were collected at 100 K at I911–3, MAXII, Sweden and at ID30A-1, ESRF, France, with wavelengths ranging from 0.97–1.00 Å. Diffraction data were indexed, integrated, scaled and merged with XDS and XSCALE[32] or MOSFLM[33]. Molecular replacement was performed with the program MOLREP[34] from the CCP4 suite[35] using the structure of SaTrxR (PDB 4GCM) as the initial search model for the FO conformation, while EcTrxR (PDB 1F6M) was used as template for the FR conformation. Restrained refinement was carried out using Refmac5[36] and manual inspection was done in Coot[37]. Local non-crystallographic symmetry restraints were imposed when appropriate. LlTrxR obtained in FR conformation crystallized in space group $P4_12_12_1$ with 1 monomer per asymmetric unit, while FO conformations crystallized in $P2_1$ with 4 monomers per asymmetric unit. After refinement, the Ramachandran plots of the structures had 94.4–97.3%% residues in favored regions, 2.5–5.0% residues in allowed regions and 0–0.66% residues outliers. Details on the data collection statistics are provided in Table 1. All RMSD values for structural alignments of the Cα-atoms were calculated using the program Superpose in CCP4[38]. Figures displaying structural data were made with PyMOL (http://www.pymol.org/).

Mass spectrometry. LlTrxR (20 μg; irradiated or light-protected) in 8 M urea, 50 mM NH_4CO_3 (45 μL) was added to 2.4 μL 100 mM DTT and incubated (40 min, 21 °C), followed by addition of 2.5 μL 200 mM iodoacetamide and incubation in the dark (40 min, 21 °C). After 1:10 dilution with 50 mM NH_4CO_3, endoproteinase GluC (Roche) was added to the samples in a 1:40 enzyme:protein ratio (w/w) and incubated overnight at 29 °C. Trifluoroacetic acid was added to the digested samples to a final concentration of 0.5% and subjected to StageTip purification with empore C18 disks (3 M) as previously described[39]. Samples (1 μg) were analysed on a Q-Exactive Orbitrap (Thermo Fisher Scientific) coupled to an EASY-nLC 1000 liquid chromatograph (Thermo Fischer Scientific). Peptides were loaded onto a custom-made nanoLC column (15 cm, C18, 100 Å, 1.9 μm particle size, 75 μm ID) packed into a Picofrit emitter (New Objectives) and eluted using a 70 min gradient at a flow rate of 250 nL min^{-1}. Resolution of 70,000, automatic gain control (AGC) value of $3{\cdot}10^6$, maximum injection time (IT) of 20 ms and scan range of 300 to 1500 *m/z* were used for MS scans. MS/MS spectra were acquired in data-dependent mode (Top 10 method) with resolution of 17,500, AGC value of $1{\cdot}10^6$, and maximum fragmentation accumulation time of 60 ms.

References

1. Arnér, E. S. J. & Holmgren, A. Physiological functions of thioredoxin and thioredoxin reductase. *Eur. J. Biochem* **267,** 6102–6109 (2000).
2. Gromer, S. *et al.* Active sites of thioredoxin reductases: Why selenoproteins? *Proc. Natl. Acad. Sci. USA* **100,** 12618–12623 (2003).
3. Waksman, G., Krishna, T. S. R., Williams, C. H. & Kuriyan, J. Crystal structure of *Escherichia coli* thioredoxin reductase refined at 2 Å resolution. *J. Mol. Biol.* **236,** 800–816 (1994).
4. Mulrooney, S. B. & Williams, C. H. Evidence for two conformational states of thioredoxin reductase from *Escherichia coli*: use of intrinsic and extrinsic quenchers of flavin fluorescence as probes to observe domain rotation. *Protein Sci.* **6,** 2188–2195 (1997).
5. Veine, D. M., Mulrooney, S. B., Wang, P. F. & Williams, C. H. Formation and properties of mixed disulfides between thioredoxin reductase from *Escherichia coli* and thioredoxin: evidence that cysteine-138 functions to initiate dithiol-disulfide interchange and to accept the reducing equivalent from reduced flavin. *Protein Sci.* **7,** 1441–1450 (1998).
6. Lennon, B. W., Williams Jr., C. H. & Ludwig, M. L. Twists in catalysis: Alternating conformations of *Escherichia coli* thioredoxin reductase. *Science* **289,** 1190–1194 (2000).
7. Fritz-Wolf, K., Urig, S. & Becker, K. The structure of human thioredoxin reductase 1 provides insights into C-terminal rearrangements during catalysis. *J. Mol. Biol.* **370,** 116–127 (2007).
8. Fritz-Wolf, K., Kehr, S., Stumpf, M., Rahlfs, S. & Becker, K. Crystal structure of the human thioredoxin reductase-thioredoxin complex. *Nat. Commun.* **2,** 383 (2011).
9. Saccoccia, F. *et al.* Thioredoxin reductase and its inhibitors. *Curr. Protein Pept. Sci.* **15,** 621–646 (2014).
10. Gustafsson, T. N. *et al.* Ebselen and analogs as inhibitors of *Bacillus anthracis* thioredoxin reductase and bactericidal antibacterials targeting *Bacillus* species, *Staphylococcus aureus* and *Mycobacterium tuberculosis*. *Biochim. Biophys. Acta - Gen. Subj.* **1860,** 1265–1271 (2016).
11. Kobayashi, K. *et al.* Essential *Bacillus subtilis* genes. *Proc. Natl. Acad. Sci. USA* **100,** 4678–4683 (2003).
12. Uziel, O., Borovok, I., Schreiber, R., Cohen, G. & Aharonowitz, Y. Transcriptional regulation of the *Staphylococcus aureus* thioredoxin and thioredoxin reductase genes in response to oxygen and disulfide stress transcriptional regulation of the *Staphylococcus aureus* thioredoxin and thioredoxin reductase genes in response. *J. Bacteriol.* **186,** 326–334 (2004).
13. Björnberg, O., Efler, P., Ebong, E. D., Svensson, B. & Hägglund, P. *Lactococcus lactis* TrxD represents a subgroup of thioredoxins prevalent in Gram-positive bacteria containing WCXDC active site motifs. *Arch. Biochem. Biophys.* **564,** 164–172 (2014).
14. Chen, J., Shen, J., Solem, C. & Jensen, P. R. A new type of YumC-like ferredoxin (flavodoxin) reductase is involved in ribonucleotide reduction. *MBio* **6,** e01132–15 (2015).
15. Efler, P. *et al.* Two Lactococcus lactis thioredoxin paralogues play different roles in responses to arsenate and oxidative stress. *Microbiology* **161**, 528–538 (2015).
16. Björnberg, O. *et al. Lactococcus lactis* thioredoxin reductase is sensitive to light inactivation. *Biochemistry* **54,** 1628–1637 (2015).
17. Kirkensgaard, K. G., Hägglund, P., Finnie, C., Svensson, B. & Henriksen, A. Structure of *Hordeum vulgare* NADPH-dependent thioredoxin reductase 2. Unwinding the reaction mechanism. *Acta Crystallogr. Sect. D Biol. Crystallogr.* **65,** 932–941 (2009).
18. Bielski, B. H. J., Cabelli, D. E., Arudi, R. L. & Ross, A. B. Reactivity of HO_2/O_2^- radicals in aqueous solution. *J. Phys. Chem. Ref. Data* **14,** 1041–1100 (1985).
19. Lechner, R., Kümmel, S. & König, B. Visible light flavin photo-oxidation of methylbenzenes, styrenes and phenylacetic acids. *Photochem. Photobiol. Sci.* **9,** 1367–1377 (2010).
20. Winterbourn, C. C., Parsons-Mair, H. N., Gebicki, S., Gebicki, J. M. & Davies, M. J. Requirements for superoxide-dependent tyrosine hydroperoxide formation in peptides. *Biochem. J.* **381,** 241–248 (2004).
21. Möller, M. N., Hatch, D. M., Kim, H. Y. H. & Porter, N. A. Superoxide reaction with tyrosyl radicals generates *para*-hydroperoxy and *para*-hydroxy derivatives of tyrosine. *J. Am. Chem. Soc.* **134,** 16773–16780 (2012).
22. Davies, M. J. & Gilbert, B. C. Free radical reactions. Fragmentation and rearrangements in aqueous solution. *Adv. Detail. React. Mech.* **1,** 35–81 (1991).
23. Baciocchi, E. Side-chain reactivity of aromatic radical cations. *Acta Chem. Scand.* **44,** 645–652 (1990).
24. Russell, G. A. Deuterium-isotope effects in the autoxidation of aralkyl hydrocarbons. Mechanism of the interaction of peroxy radicals. *J. Am. Chem. Soc.* **79,** 3871–3877 (1957).
25. Davies, M. J. Protein oxidation and peroxidation. *Biochem. J.* **473,** 805–825 (2016).
26. Wright, A., Bubb, W. A., Hawkins, C. L. & Davies, M. J. Singlet oxygen-mediated protein oxidation: evidence for the formation of reactive side chain peroxides on tyrosine residues. *Photochem. Photobiol.* **76,** 35–46 (2002).
27. Zanetti, G., Williams, C. H. & Massey, V. Influence of photoirradiation on the oxidation-reduction state of thioredoxin reductase. *J. Biol. Chem.* **243,** 4013–4019 (1968).
28. Niimura, Y., Poole, L. B. & Massey, V. *Amphibacillus xylanus* NADH oxidase and *Salmonella typhimurium* alkyl-hydroperoxide reductase flavoprotein components show extremely high scavenging activity for both alkyl hydroperoxide and hydrogen peroxide in the presence of *S. typhimurium* alkyl-hydroperoxide reductase 22-kDa protein component. *J. Biol. Chem.* **270,** 25645–25650 (1995).
29. Poole, L. B. Bacterial defenses against oxidants: mechanistic features of cysteine-based peroxidases and their flavoprotein reductases. *Arch. Biochem. Biophys.* **433,** 240–254 (2005).
30. Jensen, P. R. & Hammer, K. Minimal requirements for exponential-growth of *Lactococcus lactis*. *Appl. Environ. Microbiol.* **59,** 4363–4366 (1993).
31. Williams, C. H., Zanetti, G., Arscott, L. D. & McAllister, J. K. Lipoamide dehydrogenase, glutathione reductase, thioredoxin reductase, and thioredoxin. *J. Biol. Chem.* **242,** 5226–5231 (1967).
32. Kabsch, W. XDS. Acta Crystallogr. Sect. D Biol. *Crystallogr.* **66,** 125–132 (2010).

33. Battye, T. G. G., Kontogiannis, L., Johnson, O., Powell, H. R. & Leslie, A. G. W. *iMOSFLM*: A new graphical interface for diffraction-image processing with *MOSFLM*. *Acta Crystallogr. Sect. D Biol. Crystallogr.* **67,** 271–281 (2011).
34. Vagin, A. & Teplyakov, A. *MOLREP*: An automated program for molecular replacement. *J. Appl. Crystallogr*. **30,** 1022–1025 (1997).
35. Winn, M. D. *et al.* Overview of the *CCP*4 suite and current developments. *Acta Crystallogr. Sect. D Biol. Crystallogr*. **67,** 235–242 (2011).
36. Vagin, A. A. *et al. REFMAC 5* dictionary: Organization of prior chemical knowledge and guidelines for its use. *Acta Crystallogr. Sect. D Biol. Crystallogr*. **60,** 2184–2195 (2004).
37. Emsley, P., Lohkamp, B., Scott, W. G. & Cowtan, K. Features and development of Coot. *Acta Crystallogr. Sect. D Biol. Crystallogr*. **66,** 486–501 (2010).
38. Krissinel, E. & Henrick, K. Secondary-structure matching (SSM), a new tool for fast protein structure alignment in three dimensions. *Acta Crystallogr. Sect. D Biol. Crystallogr*. **60,** 2256–2268 (2004).
39. Rappsilber, J., Mann, M. & Ishihama, Y. Protocol for micro-purification, enrichment, pre-fractionation and storage of peptides for proteomics using StageTips. *Nat. Protoc.* **2,** 1896–1906 (2007).

Acknowledgements

The Q-Exactive Orbitrap mass spectrometer was granted by the Danish Council for Independent Research | Natural Sciences (grant nr. 11-106246). Technical University of Denmark is acknowledged for a PhD stipend (NS) and The Danish Research Foundation, Nordic Bioscience A/S and Technical University of Denmark are acknowledged for a joint PhD scholarship (MR). MJD is supported by a grant from the Novo Nordisk Foundation (grant no: NNF13OC0004294). The MAXIV and ESRF synchrotrons is acknowledged for beam-time and support during data-collection. The research presented has received funding from BioStruct-X (EC FP7 grant agreement N°283570) and DANSCATT (the Danish agency and for Science, Technology and Innovation).

Author Contributions

P.Ha., P.Hä., and B.S. conceived and directed the project; N.S., O.B., P.Ha., P.Hä. designed experiments; N.S. produced proteins and performed biochemical experiments. N.S., M.B.B. and P.Ha. performed X-ray crystallographic experiments and analysed the data; M.R. and P.Hä. performed mass spectrometry and analysed the data; N.S., M.R., O.B., M.J.D., B.S., P.Ha., P.Hä. discussed results and wrote the paper.

Additional Information

Accession codes: Coordinates and structure factors have been deposited in the Protein Data Bank under accession codes: 5MH4 (FR conformation, no light); 5MIP (FR conformation, 30 min light); 5MIQ (FR conformation, 60 min light); 5MIR (FR conformation, 120 min light); 5MIS (FR conformation, 180 min light); 5MIT (FR conformation, 240 min light); 5MJK (FO conformation, no light).

Supplementary information accompanies this paper at http://www.nature.com/srep

Competing Interests: The authors declare no competing financial interests.

How to cite this article: Skjoldager, N. *et al.* The Structure of *Lactococcus lactis* thioredoxin reductase reveals molecular features of photo-oxidative damage. *Sci. Rep.* **7**, 46282; doi: 10.1038/srep46282 (2017).

Publisher's note: Springer Nature remains neutral with regard to jurisdictional claims in published maps and institutional affiliations.

Supplementary information

The structure of *Lactococcus lactis* thioredoxin reductase reveals molecular features of photo-oxidative damage

Nicklas Skjoldager[1], Maria Blanner Bang[2], Martin Rykær[1], Olof Björnberg[1], Michael J Davies[3], Birte Svensson[1], Pernille Harris[2*] & Per Hägglund[1*]

[1]Department of Biotechnology and Biomedicine, Technical University of Denmark, DK-2800 Kgs. Lyngby, Denmark

[2]Department of Chemistry, Technical University of Denmark

[3]Department of Biomedical Sciences, University of Copenhagen

[*]Correspondence should be addressed to Per Hägglund (ph@bio.dtu.dk) or Pernille Harris (ph@kemi.dtu.dk).

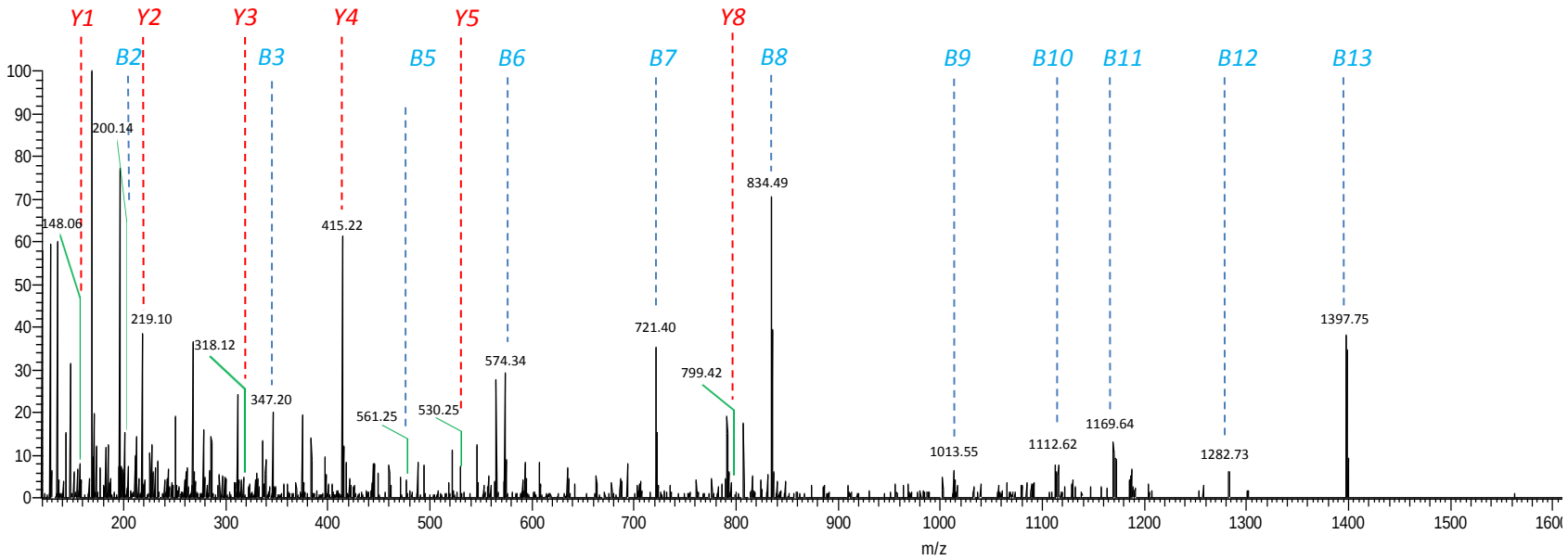

Figure S1a. Annotated MS/MS spectrum of the precursor at m/z 906.98 corresponding to the peptide KAFGGIFIYVGLDPVAE with an oxidized tyrosine (Y*)

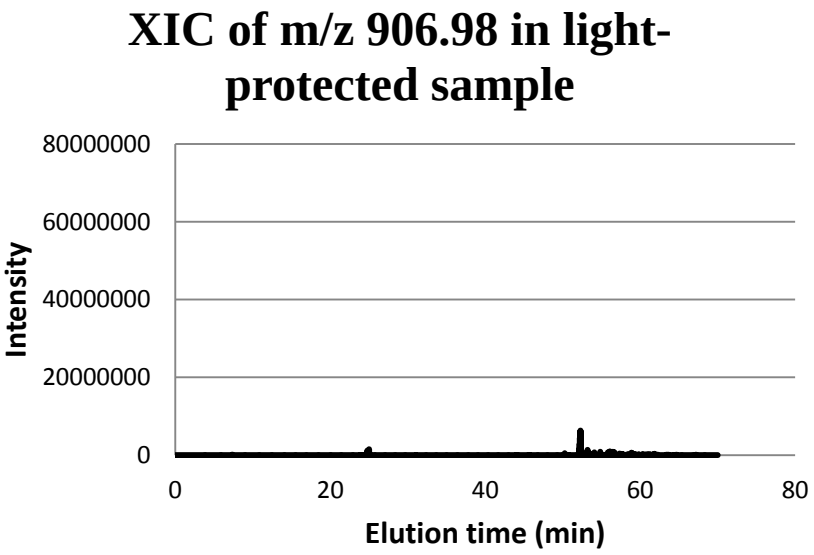

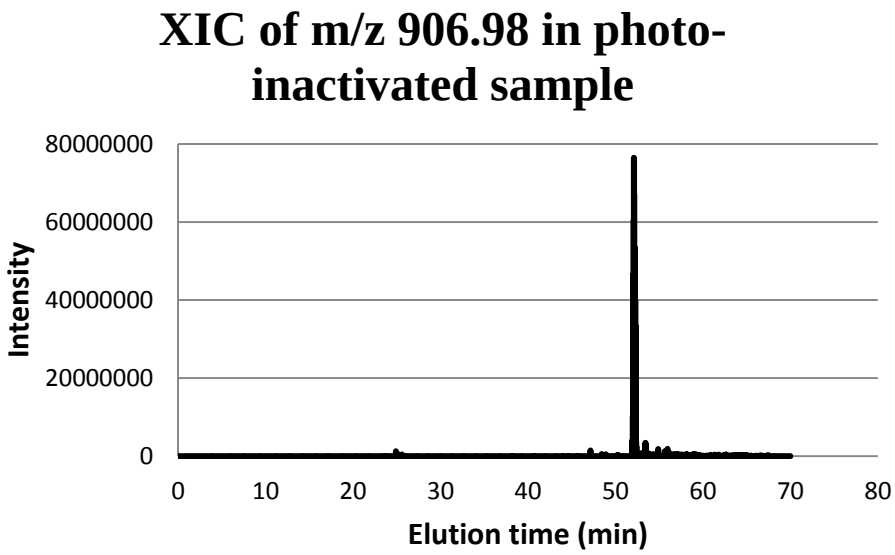

Figure S1b. Extracted ion chromatograms (XIC) of the precursor at m/z 906.98 corresponding to the peptide KAFGGIFIYVGLDPVAE with an oxidized tyrosine

Appendix C. Multiple alignment of selected LMW TrxR and phylogenetic analysis

Yellow: Met-Pro motif (Pro15, Met18, Met67, Met66$_{EcTrxR}$ Met69$_{EcTrxR}$). Green: FAD *si*-face Met43. Cyan: Tyr133, Tyr237 & Ser64/Ala/Gly. TrxR with the predicted *si*-face oxygen pockets are marked in **bold**. *L. lactis* numbering are indicated for key residues.

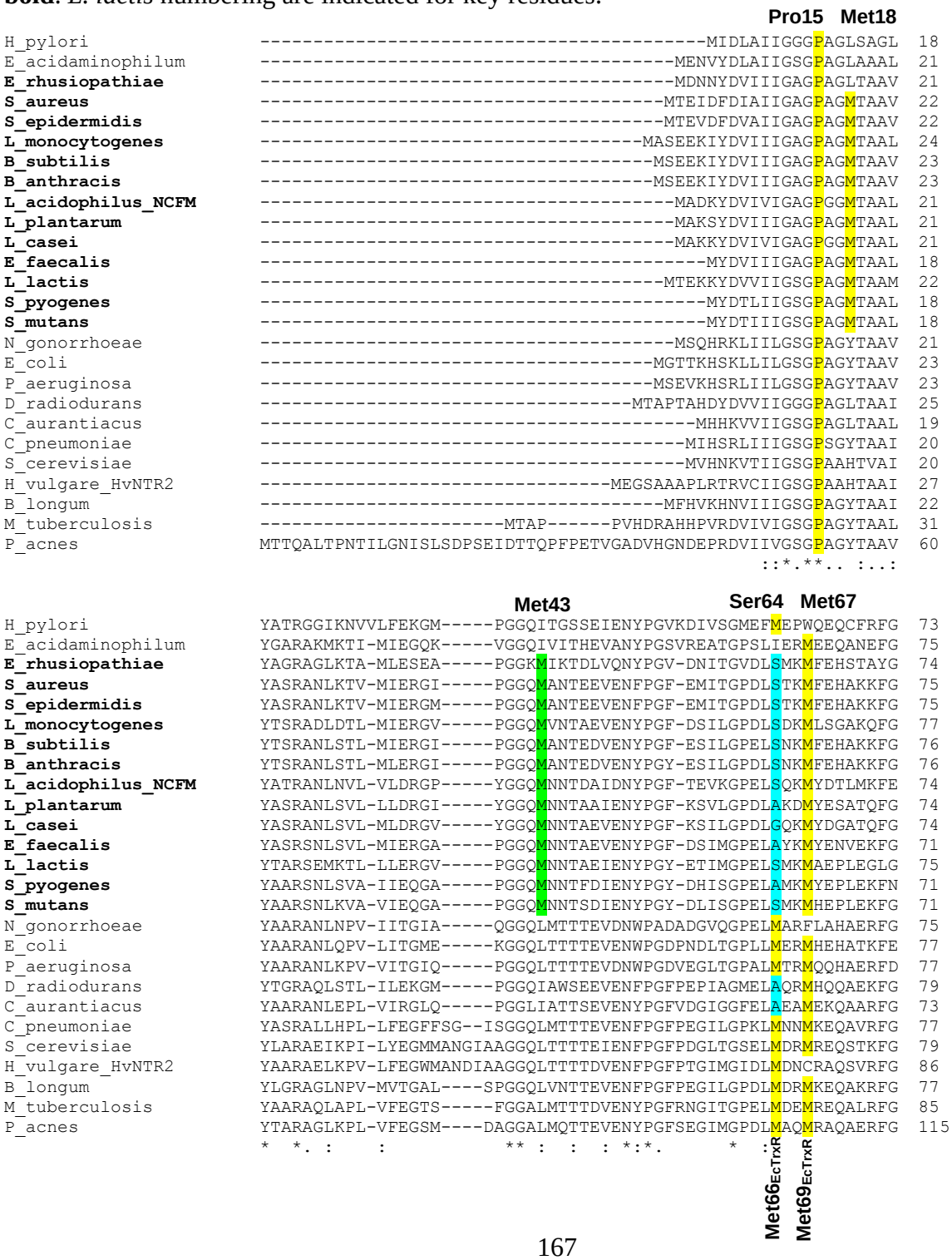

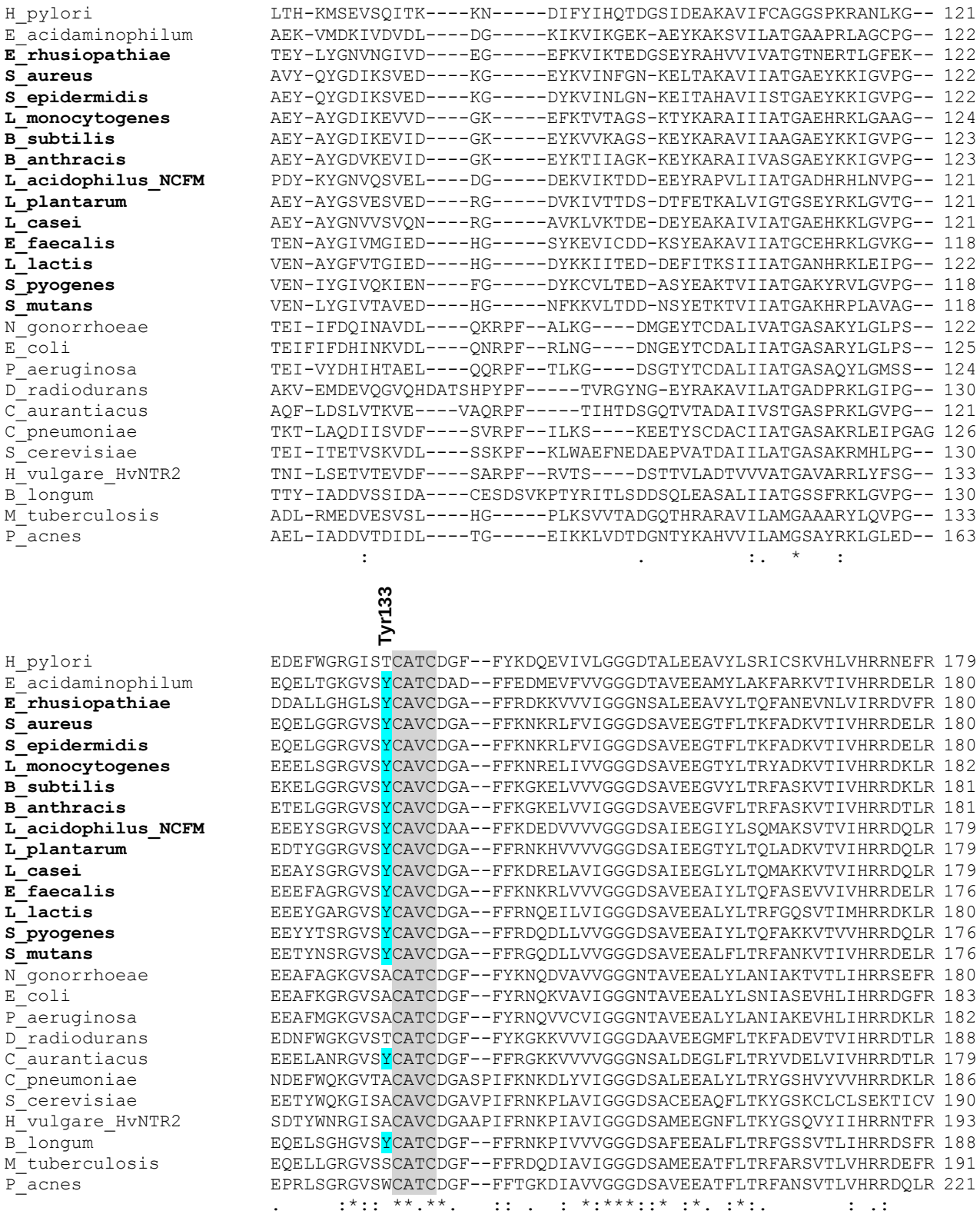
H_pylori LTH-KMSEVSQITK----KN-----DIFYIHQTDGSIDEAKAVIFCAGGSPKRANLKG-- 121
E_acidaminophilum AEK-VMDKIVDVDL----DG-----KIKVIKGEK-AEYKAKSVILATGAAPRLAGCPG-- 122
E_rhusiopathiae TEY-LYGNVNGIVD----EG-----EFKVIKTEDGSEYRAHVVIVATGTNERTLGFEK-- 122
S_aureus AVY-QYGDIKSVED----KG-----EYKVINFGN-KELTAKAVIIATGAEYKKIGVPG-- 122
S_epidermidis AEY-QYGDIKSVED----KG-----DYKVINLGN-KEITAHAVIISTGAEYKKIGVPG-- 122
L_monocytogenes AEY-AYGDIKEVVD----GK-----EFKTVTAGS-KTYKARAIIIATGAEHRKLGAAG-- 124
B_subtilis AEY-AYGDIKEVID----GK-----EYKVVKAGS-KEYKARAVIIAAGAEYKKIGVPG-- 123
B_anthracis AEY-AYGDVKEVID----GK-----EYKTIIAGK-KEYKARAIIVASGAEYKKIGVPG-- 123
L_acidophilus_NCFM PDY-KYGNVQSVEL----DG-----DEKVIKTDD-EEYRAPVLIIATGADHRHLNVPG-- 121
L_plantarum AEY-AYGSVESVED----RG-----DVKIVTTDS-DTFETKALVIGTGSEYRKLGVTG-- 121
L_casei AEY-AYGNVVSVQN----RG-----AVKLVKTDE-DEYEAKAIVIATGAEHKKLGVPG-- 121
E_faecalis TEN-AYGIVMGIED----HG-----SYKEVICDD-KSYEAKAVIIATGCEHRKLGVKG-- 118
L_lactis VEN-AYGFVTGIED----HG-----DYKKIITED-DEFITKSIIIATGANHRKLEIPG-- 122
S_pyogenes VEN-IYGIVQKIEN----FG-----DYKCVLTED-ASYEAKTVIIATGAKYRVLGVPG-- 118
S_mutans VEN-LYGIVTAVED----HG-----NFKKVLTDD-NSYETKTVIIATGAKHRPLAVAG-- 118
N_gonorrhoeae TEI-IFDQINAVDL----QKRPF--ALKG----DMGEYTCDALIVATGASAKYLGLPS-- 122
E_coli TEIFIFDHINKVDL----QNRPF--RLNG----DNGEYTCDALIIATGASARYLGLPS-- 125
P_aeruginosa TEI-VYDHIHTAEL----QQRPF--TLKG----DSGTYTCDALIIATGASAQYLGMSS-- 124
D_radiodurans AKV-EMDEVQGVQHDATSHPYPF-----TVRGYNG-EYRAKAVILATGADPRKLGIPG-- 130
C_aurantiacus AQF-LDSLVTKVE----VAQRPF-----TIHTDSGQTVTADAIIVSTGASPRKLGVPG-- 121
C_pneumoniae TKT-LAQDIISVDF----SVRPF--ILKS----KEETYSCDACIIATGASAKRLEIPGAG 126
S_cerevisiae TEI-ITETVSKVDL----SSKPF--KLWAEFNEDAEPVATDAIILATGASAKRMHLPG-- 130
H_vulgare_HvNTR2 TNI-LSETVTEVDF----SARPF--RVTS----DSTTVLADTVVVATGAVARRLYFSG-- 133
B_longum TTY-IADDVSSIDA----CESDSVKPTYRITLSDDSQLEASALIIATGSSFRKLGVPG-- 130
M_tuberculosis ADL-RMEDVESVSL----HG-----PLKSVVTADGQTHRARAVILAMGAAARYLQVPG-- 133
P_acnes AEL-IADDVTDIDL----TG-----EIKKLVDTDGNTYKAHVVILAMGSAYRKLGLED-- 163
Tyr133
H_pylori EDEFWGRGISTCATCDGF--FYKDQEVIVLGGGDTALEEAVYLSRICSKVHLVHRRNEFR 179
E_acidaminophilum EQELTGKGVSYCATCDAD--FFEDMEVFVVGGGDTAVEEAMYLAKFARKVTIVHRRDELR 180
E_rhusiopathiae DDALLGHGLSYCAVCDGA--FFRDKKVVVIGGGNSALEEAVYLTQFANEVNLVIRRDVFR 180
S_aureus EQELGGRGVSYCAVCDGA--FFKNKRLFVIGGGDSAVEEGTFLTKFADKVTIVHRRDELR 180
S_epidermidis EQELGGRGVSYCAVCDGA--FFKNKRLFVIGGGDSAVEEGTFLTKFADKVTIVHRRDELR 180
L_monocytogenes EEELSGRGVSYCAVCDGA--FFKNRELIVVGGGDSAVEEGTYLTRYADKVTIVHRRDKLR 182
B_subtilis EKELGGRGVSYCAVCDGA--FFKGKELVVVGGGDSAVEEGVYLTRFASKVTIVHRRDKLR 181
B_anthracis ETELGGRGVSYCAVCDGA--FFKGKELVVIGGGDSAVEEGVFLTRFASKVTIVHRRDTLR 181
L_acidophilus_NCFM EEEYSGRGVSYCAVCDAA--FFKDEDVVVVGGGDSAIEEGIYLSQMAKSVTVIHRRDQLR 179
L_plantarum EDTYGGRGVSYCAVCDGA--FFRNKHVVVVGGGDSAIEEGTYLTQLADKVTVIHRRDQLR 179
L_casei EEAYSGRGVSYCAVCDGA--FFKDRELAVIGGGDSAIEEGLYLTQMAKKVTVIHRRDQLR 179
E_faecalis EEEFAGRGVSYCAVCDGA--FFKNKRLVVVGGGDSAVEEAIYLTQFASEVVIVHRRDELR 176
L_lactis EEEYGARGVSYCAVCDGA--FFRNQEILVIGGGDSAVEEALYLTRFGQSVTIMHRRDKLR 180
S_pyogenes EEYYTSRGVSYCAVCDGA--FFRDQDLLVVGGGDSAVEEAIYLTQFAKKVTVVHRRDQLR 176
S_mutans EETYNSRGVSYCAVCDGA--FFRGQDLLVVGGGDSAVEEALFLTRFANKVTIVHRRDELR 176
N_gonorrhoeae EEAFAGKGVSACATCDGF--FYKNQDVAVVGGGNTAVEEALYLANIAKTVTLIHRRSEFR 180
E_coli EEAFKGRGVSACATCDGF--FYRNQKVAVIGGGNTAVEEALYLSNIASEVHLIHRRDGFR 183
P_aeruginosa EEAFMGKGVSACATCDGF--FYRNQVVCVIGGGNTAVEEALYLANIAKEVHLIHRRDKLR 182
D_radiodurans EDNFWGKGVSTCATCDGF--FYKGKKVVVIGGGDAAVEEGMFLTKFADEVTVIHRRDTLR 188
C_aurantiacus EEELANRGVSYCATCDGF--FFRGKKVVVVGGGNSALDEGLFLTRYVDELVIVHRRDTLR 179
C_pneumoniae NDEFWQKGVTACAVCDGASPIFKNKDLYVIGGGDSALEEALYLTRYGSHVYVVHRRDKLR 186
S_cerevisiae EETYWQKGISACAVCDGAVPIFRNKPLAVIGGGDSACEEAQFLTKYGSKCLCLSEKTICV 190
H_vulgare_HvNTR2 SDTYWNRGISACAVCDGAAPIFRNKPIAVIGGGDSAMEEGNFLTKYGSQVYIIHRRNTFR 193
B_longum EQELSGHGVSYCATCDGF--FFRNKPIVVVGGGDSAFEEALFLTRFGSSVTLIHRRDSFR 188
M_tuberculosis EQELLGRGVSSCATCDGF--FFRDQDIAVIGGGDSAMEEATFLTRFARSVTLVHRRDEFR 191
P_acnes EPRLSGRGVSWCATCDGF--FFTGKDIAVVGGGDSAVEEATFLTRFANSVTLVHRRDQLR 221

```
H_pylori                AAPSTIEHVK---KNDKIHIVTPAVVEEIKGDK-----------------------SGV 212
E_acidaminophilum       AAKSIQEKAF---KNPKLDFMWNSAIEEIKGDG-----------------------IVE 213
E_rhusiopathiae         GDDSAQRQVF---NNEKINIIKKHIPVDYIDKD-----------------------GKL 213
S_aureus                AQRILQDRAF---KNDKIDFIWSHTLKSINEKD-----------------------GKV 213
S_epidermidis           AQNILQERAF---KNDKVDFIWSHTLKTINEKD-----------------------GKV 213
L_monocytogenes         AQQILQDRAF---KDEKVDFIWNSTVEEIVGDG-----------------------KKV 215
B_subtilis              AQSILQARAF---DNEKVDFLWNKTVKEIHEEN-----------------------GKV 214
B_anthracis             AQKILQDRAF---QNEKVDFIWNHTIKEINEAN-----------------------GKV 214
L_acidophilus_NCFM      AQPTLQKRAF---ANEKMKFIWNAQTEEILGDG-----------------------NRV 212
L_plantarum             AQQILQDRAF---ANPKMEFVWNSNVTEIIGDD-----------------------KKV 212
L_casei                 AQQIIQKRAF---ANDKMHFVWNAQVQEIQGDD-----------------------MKV 212
E_faecalis              AQKIIQDRAF---ANEKISFVWDTVVEEIVGNE-----------------------MVV 209
L_lactis                AQEIIQQRAF---KEEKINFIWDSVPMEIKGDD-----------------------KKI 213
S_pyogenes              AQKILQDRAF---ANDKVDFIWDSVVKEIKGND-----------------------IKV 209
S_mutans                AQKVLQERAF---ANDKVDFIWNSVVKEIKGND-----------------------LKV 209
N_gonorrhoeae           AEKIMIDKLMKRVEEGKIILKLESNLQEVLGDD-----------------------RGV 216
E_coli                  AEKILIKRLMDKVENGNIILHTNRTLEEVTGDQ-----------------------MGV 219
P_aeruginosa            SEKILQDKLFDKAENGNVRLHWNTTLDEVLGDA-----------------------SGV 218
D_radiodurans           ANKVAQARAF---ANPKMKFIWDTAVEEIQGAD-----------------------SV 220
C_aurantiacus           ADPILQERAF---SNPKVRFIWNSVVVSINGKD-----------------------KV 211
C_pneumoniae            ASKAMEARAQ---NNEKITFLWNSEIVKISG---D-----------------------SIV 218
S_cerevisiae            LLPLCKKRAE---KNEKIEILYNTVALEAKG--DG-----------------------KLL 223
H_vulgare_HvNTR2        ASKIMQARAL---SNPKIQVVWDSEVVEAYGGAGG-----------------------GPL 228
B_longum                ASQIMVDRAK---ANPTITLLTNTVVTSITGTSSPTQNTGAPIAIPGLTIKRPAVAPASV 245
M_tuberculosis          ASKIMLDRAR---NNDKIRFLTNHTVVAVDGDT-----------------------TV 223
P_acnes                 ASQIMADRAA---ADPKITFAWNSEVVAMQGES-----------------------KL 253
                               :      : .: .
```

```
                                                                  Tyr237
H_pylori                TSVLIKHTDSNTN---------EEIPVMGIFIFVGYNVNTATLKQDDGSMLCECDEYGSI 263
E_acidaminophilum       S-AVFKN--LVTGE-TTEYFANEEDGTFGIFVFIGYIPKSDVFKG-----KITLDDAGYI 264
E_rhusiopathiae         TGMKFEH--VETGE-PLV------IDTDGVFPYIGAIPATGFLKD-----LNVLDNEGYL 259
S_aureus                GSVTLTS--TKDGS-EET------HEADGVFIYIGMKPLTAPFKD-----LGITNDVGYI 259
S_epidermidis           GSVTLES--TKDGA-EQT------YDADGVFIYIGMKPLTAPFKN-----LGITNDAGYI 259
L_monocytogenes         TGAKLVS--TVDGS-ESI------MPVDGVFIYVGLVPLTKAFLN-----LGITDDEGYI 261
B_subtilis              GNVTLVD--TVTGE-ESE------FKTDGVFIYIGMLPLSKPFEN-----LGITNEEGYI 260
B_anthracis             GSVTLVD--VNSGE-EKE------VKTDGVFVYIGMLPLSKPFVE-----LGITNENGYL 260
L_acidophilus_NCFM      TGVKYLD--KENGE-TKE------VSAAGVFIYVGVLPQTEPFKK-----LGILNEQGWI 258
L_plantarum             TGVKVNN--NKTGE-DSE------IAVDGVFIYVGINPITKPFSN-----LGITDENGWI 258
L_casei                 TGVKYRDRDKETGE-EHI------LPVAGVFIYVGIMPMTEAFQD-----LGVLDEHGWI 260
E_faecalis              TGVKARN--VKTDE-VSE------IEANGVFIYVGLDPLTEPFKK-----AGITNEAGWI 255
L_lactis                QSVVYKN--VKTGE-VTE------KAFGGIFIYVGLDPVAEFVSD-----LGITDEAGWI 259
S_pyogenes              SNVLIEN--VKTGQ-VTD------HAFGGVFIYVGMNPVTDMVKD-----LEITDQEGWI 255
S_mutans                TNVDIEN--VKTGQ-VNN------YAFGGVFIYVGLDPVSSMVKE-----LDITDEAGWI 255
N_gonorrhoeae           NGALLKN--NDGS--DQQ------IAVSGIFIAIGHKPNTDIFKG-----QLEMDEAGYL 261
E_coli                  TGVRLRD--TQNSDNIES------LDVAGLFVAIGHSPNTAIFEG-----QLELE-NGYI 265
P_aeruginosa            TGVRLKS--TIDGS-TSE------LSLAGVFIAIGHKPNTDLFQG-----QLEMR-DGYL 263
D_radiodurans           SGVKLRN--LKTGE-VSE------LATDGVFIFIGHVPNTAFVKD-----TVSLRDDGYV 266
C_aurantiacus           ESVTLRN--LQTGE-VSE------LPTDGVFPYIGHVPNTDLFRG-----ILELDEGGYI 257
C_pneumoniae            RSVDIKN--VQTQE-ITT------REAAGVFFAIGHKPNTDFLGG-----QLTLDESGYI 264
S_cerevisiae            NALRIKN--TKKNE-ETD------LPVSGLFYAIGHTPATKIVAG-----QVDTDEAGYI 269
H_vulgare_HvNTR2        AGVKVKN--LVTGE-VSD------LQVSGLFFAIGHEPATKFLNG-----QLELHADGYV 274
B_longum                SSIAVRN--VVTGE-EST------LDTNAVFVAIGHTPATDFAAG-----VVDRDDDGYV 291
M_tuberculosis          TGLRVRD--TNTGA-ETT------LPVTGVFVAIGHEPRSGLVRE-----AIDVDPDGYV 269
P_acnes                 ESITLRD--TKTGE-ERQ------LEVAGVFEAIGHDPRSELVRG-----QVDLDDAGYV 299
                                              .:*  :*    :                * :
```

```
H_pylori                KVDLS-----MKTSVEGLFAAGDVRTLAPKQVVCAAGDGATAALQAIAYLEHK------- 311
E_acidaminophilum       ITDDN-----MKTNVEGVFAAGDIRVKSLRQVVTACADGAIAATQAEKYVEANFEE---- 315
E_rhusiopathiae         IVNNQ-----LETAIPGIFGAGDVIQKHLRQIVTATSDGAIAAQNAFHYIQDLKSKA--- 311
S_aureus                VTKDD-----MTTSVPGIFAAGDVRDKGLRQIVTATGDGSIAAQSAAEYIEHLNDQA--- 311
S_epidermidis           VTQDD-----MSTKVRGIFAAGDVRDKGLRQIVTATGDGSIAAQSAADYITELKDN---- 310
L_monocytogenes         VTDEE-----MRTNLPGIFAAGDVRAKSLRQIVTATGDGGLAGQNAQKYVEELKESLEAE 316
B_subtilis              ETNDR-----METKVEGIFAAGDIREKSLRQIVTATGDGSIAAQSVQHYVEELQETLKTL 315
B_anthracis             ETNER-----METKVPGIFAAGDVREKMLRQIVTATGDGSIAAQSAQHYVEELLEELKTV 315
L_acidophilus_NCFM      PTNEH-----METKVSGIFALGDVRDKDLRQIANAVGEGSVAGQAAYNYFQDLKN----- 308
L_plantarum             ETNDH-----METKVPGIFAVGDVRKKDLRQVATAVGEGGTAGQGVYTYITALGDKVNN- 312
L_casei                 PTDEH-----MRTKVPGVFAIGDVRAKDLRQITTAVGEGGTAGQGVFNYIQSLNDTNIEI 315
E_faecalis              ETDQE-----MRTKIPGVYAIGDVREKTLRQITTAVGEGGIAGQQVFNYIEELK------ 304
L_lactis                ITDDH-----MRTNIPGIFAVGDVRQKDFRQITTAVGDGAQAAQEAYKFVVELG------ 308
S_pyogenes              ITDDH-----MRTSIPGIFAIGDVRQKDLRQITTAVGDGAIAGQGVYHYLESFPS----- 305
S_mutans                PTDDH-----MKTKAAGVFAIGDVRQKDLRQITTAVGDGAVAAQEAYQYIVNNY------ 304
N_gonorrhoeae           KTKGGTADNVGATNIEGVWAAGDVKDHTYRQAITSAASGCQAALDAERWLGSQNI----- 316
E_coli                  KVQSGIHGNATQTSIPGVFAAGDVMDHIYRQAITSAGTGCMAALDAERYLDGLADAK--- 322
P_aeruginosa            RIHGGSEGNATQTSIEGVFAAGDVADHVYRQAITSAGAGCMAALDAEKYLDDH------- 316
D_radiodurans           DVRD-E----IYTNIPMLFAAGDVSDYIYRQLATSVGAGTRAAMMTERQLAALEVEGEEV 321
C_aurantiacus           VTDG-R----TRTNIPGIFAAGDVTDHIYRQAVTAAGDGCRAAMEATWYLAEQEHARSKA 312
C_pneumoniae            VTEKGT----SKTSVPGVFAAGDVQDKYYRQAVTSAGSGCIAALDAERFLG--------- 311
S_cerevisiae            KTVPGS----SLTSVPGFFAAGDVQDSKYRQAITSAGSGCMAALDAEKYLTSLE------ 319
H_vulgare_HvNTR2        ATKPGS----THTSVEGVFAAGDVQDKKYRQAITAAGSGCMAALDAEHYLQEVGAQVGKS 330
B_longum                VVQGAS----TVTSAPGIFAAGDCVDRTYRQAISAAGMGCRAALDAQAYLTD-------- 339
M_tuberculosis          LVQGRT----TSTSLPGVFAAGDLVDRTYRQAVTAAGSGCAAAIDAERWLAEHAATGEAD 325
P_acnes                 VCAEPS----TRTNVPGVFACGDLVDSHYQQAVTAAGSGCRAALDAERFLTELGR----- 350
                                     *    .:. **      :*   : . *  *.  .   .

H_pylori                ----------  311
E_acidaminophilum       ----------  315
E_rhusiopathiae         ----------  311
S_aureus                ----------  311
S_epidermidis           ----------  310
L_monocytogenes         AAK-------  319
B_subtilis              K---------  316
B_anthracis             SEK-------  318
L_acidophilus_NCFM      ----------  308
L_plantarum             ----------  312
L_casei                 KA--------  317
E_faecalis              ----------  304
L_lactis                ----------  308
S_pyogenes              ----------  305
S_mutans                ----------  304
N_gonorrhoeae           ----------  316
E_coli                  ----------  322
P_aeruginosa            ----------  316
D_radiodurans           TAAD------  325
C_aurantiacus           TVSVA-----  317
C_pneumoniae            ----------  311
S_cerevisiae            ----------  319
H_vulgare_HvNTR2        D---------  331
B_longum                ----------  339
M_tuberculosis          STDALIGAQR  335
P_acnes                 ----------  350
```

Multiple alignment of selected LMW TrxR generated with Clustal Omega (McWilliam et al., 2013).

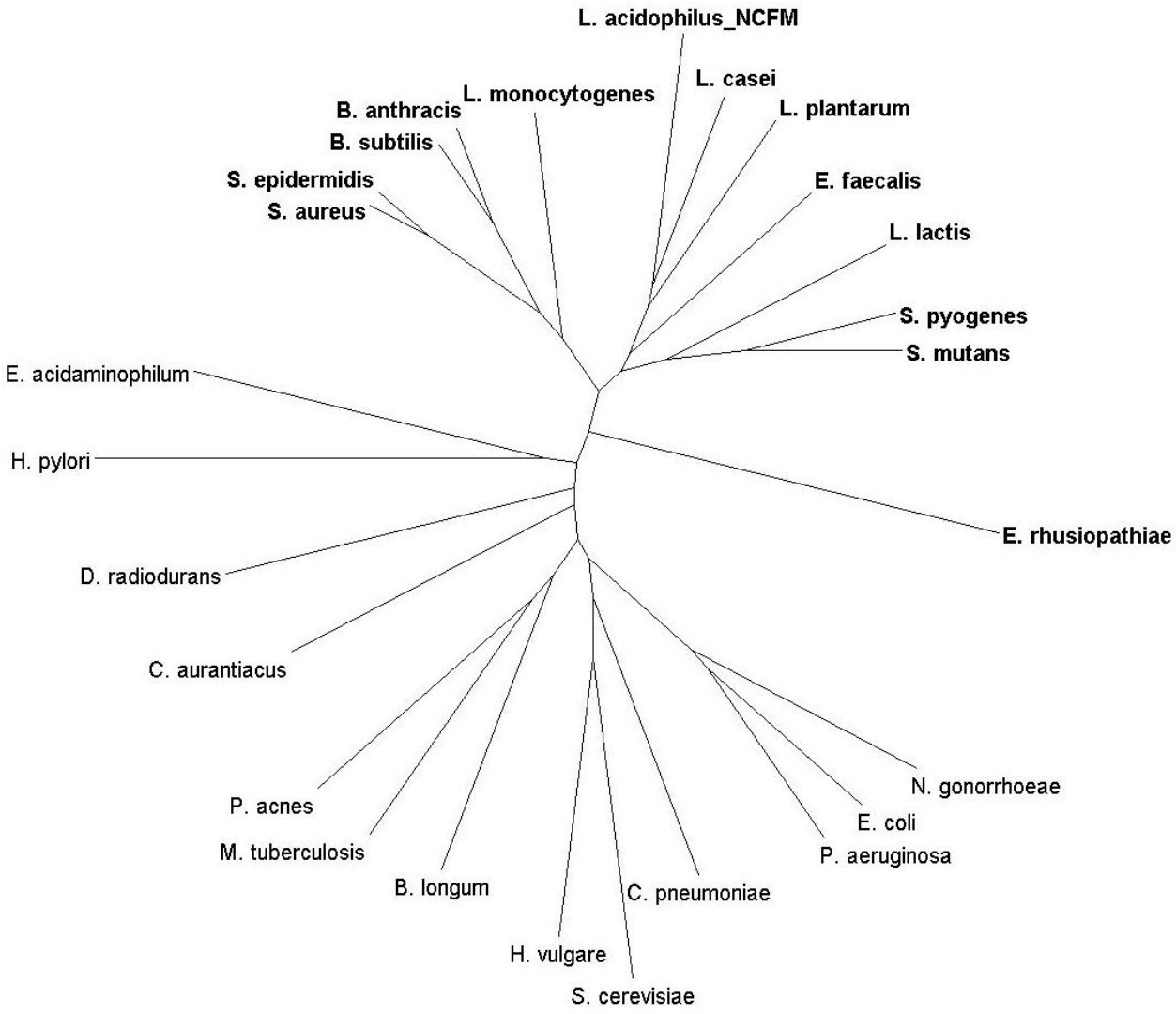

Figure 57. Phylogenetic tree of LMW TrxR of selected organisms. Organisms marked in bold are predicted to harbor the FAD *si*-face oxygen pocket, as evaluated from the sequence alignment above. The phylogenetic tree is calculated with Clustal Omega (McWilliam et al., 2013) and represented by Dendroscope (Huson and Scornavacca, 2012) version 3.5.7 with *D. radiodurans* as outgroup.

Gram-positive bacteria: *Lactococcus lactis* (A2RLJ5), *Propionibacterium acnes* (D1Y8R6), *Staphylococcus aureus* (P66011), *Bacillus subtilis* (P80880), *Lactobacillus acidophilus* NCFM (Q5FL69), *Bifidobacterium longum* subsp. Infantis (B7GPF0), *Lactobacillus casei* (G1U9U6), *Lactobacillus plantarum* (T5JY88), *Bacillus anthracis* (Q81X56), *Streptococcus pyogenes* (J7M1U4), *Erysipelothrix rhusiopathiae* (F5WV12), *Enterococcus faecalis* (Q835N8), *Streptococcus mutans* (J3JQX2), *Staphylococcus epidermidis* (Q8CPY8), *Eubacterium acidaminophilum* (P50971), *Listeria monocytogenes* (O32823). Gram-negative bacteria: *E. coli* (P0A9P4), *Helicobacter pylori* (D0IS18), *Neisseria gonorrhoeae* (Q5F926), *Pseudomonas aeruginosa* (Q9I0M2), *Chlamydia pneumoniae* (Q9Z8M4). Other classes of bacteria: *Chloroflexus aurantiacus* (A9WEL6), *Deinococcus radiodurans* (Q9RSY7), *Mycobacterium tuberculosis* (P9WHH0). Eukaryotes: *Hordeum vulgare* (barley), hvNTR2 (A9LN30), *Saccharomyces cerevisiae* (P29509).

Appendix D. Overview of all crystallization trials

This is an overview of all crystallization trials, represented in the 4x6 well trays (A–D x 1–6) used. The reservoir buffers are combined of the solutions mentioned in the columns and rows, thus giving a grid of crystallization buffer conditions. The ratio mixing of protein solution and reservoir buffer for the vapor diffusion hanging drop experiments are indicated. Structure Screen 1 (MD1-01) and Structure Screen 2 (MD1-02) from Molecular Dimensions (Jancarik & Kim 1991; Wooh et al. 2003) are not mentioned here. All trays made as hanging drop with 500 µL Reservoir volume unless otherwise stated.

Protein buffer solutions used:

Crystallization screens and tray #3–10: 100 mM ammonium acetate, pH 7.4.

Tray#11–21: 100 mM potasium phosphate, 1 mM EDTA, pH7.4

Tray #22–54: 10 mM HEPES, 2 mM Na-EDTA, pH7.0

#3	Light exposed LITrx	**1**	**2**	**3**	**4**	**5**	**6**
		10% PEG 8000	15% PEG 8000	20% PEG 8000	10% PEG 8000	15% PEG 8000	20% PEG 8000
A	0,3 M Li_2SO_4						
B	0,4 M Li_2SO_4						
C	0,5 M Li_2SO_4						
D	0,6 M Li_2SO_4						
	Protein : Reservoir	2:2	2:2	2:2	2:1	2:1	2:1

Tray #4: As tray #3

#5	Additive screen 1 (HR2-420), Hamilton. Sitting drop	**1**	**2**	**3**	**4**	**5**	**6**
		15% PEG 8000	15% PEG 8000	15% PEG 8000	15% PEG 8000	15% PEG 8000	25% PEG 8000
A	0,5 M Li_2SO_4						
B	0,5 M Li_2SO_4						
C	0,5 M Li_2SO_4						
D	0,5 M Li_2SO_4						
	Protein : Reservoir	2:2	2:2	2:2	2:1	2:1	2:1

#6		**1**	**2**	**3**	**4**	**5**	**6**
		10% PEG 8000	15% PEG 8000	20% PEG 8000	10% PEG 8000	15% PEG 8000	20% PEG 8000
A	0,3 M Li_2SO_4						
B	0,4 M Li_2SO_4						
C	0,5 M Li_2SO_4						
D	0,6 M Li_2SO_4						
	Protein : Reservoir	2:2	2:2	2:2	2:1	2:1	2:1

#7	No Light	**1**	**2**	**3**	**4**	**5**	**6**
		15% PEG 8000	15% PEG 8000	15% PEG 8000	15% PEG 8000	15% PEG 8000	25% PEG 8000
A	0,5 M Li_2SO_4						
B	0,5 M Li_2SO_4						
C	0,5 M Li_2SO_4						
D	0,5 M Li_2SO_4						
	Protein : Reservoir	2:2	2:2	2:2	2:1	2:1	2:1

Tray #8: As tray #7, just exposed to light for 2 hours.

#9	No Light	1	2	3	4	5	6
		20% PEG 8000	25% PEG 8000	30% PEG 8000	20% PEG 8000	25% PEG 8000	30% PEG 8000
A	0,2 M Li_2SO_4						
B	0,3 M Li_2SO_4						
C	0,4 M Li_2SO_4						
D	0,5 M Li_2SO_4						
	Protein : Reservoir	2:2	2:2	2:2	2:3	2:3	2:3

#10	68 timers belysning	4	5	6
		20% PEG 8000	25% PEG 8000	30% PEG 8000
A	0,2 M Li_2SO_4			
B	0,3 M Li_2SO_4			
C	0,4 M Li_2SO_4			
D	0,5 M Li_2SO_4			
	Protein : Reservoir	3:3	3:3	3:3

Crystallization #11 (8,9 mg/mL)	15% PEG	20% PEG	25 % PEG	15% PEG	20% PEG	25 % PEG
0,2 M Li_2SO_4						
0,3 M Li_2SO_4						
0,4 M Li_2SO_4						
0,5 M Li_2SO_4						
Protein:Reservoir	2:2	2:2	2:2	2:1	2:1	2:1

Crystallization #12 (8,9 mg/mL)	10 % (V/V) EtOH	10 % (V/V) EtOH				
1,5 M NaCl						
1,5 M NaCl						
1,5 M NaCl						
1,5 M NaCl						
Protein:Reservoir	2:2	2:1				

Constant: 0.4 M Li_2SO_4 .Volume: 500 µL reservoir

Crystallization #13 (8,9 mg/mL, RT)	15% PEG	20% PEG	25 % PEG	15% PEG	20% PEG	25 % PEG
PEG8000						
PEG4000						
PEG1500						
PEG400						
Protein:Reservoir	2:2	2:2	2:2	2:3	2:3	2:3

Tray #14: As tray #33, just incubated at 30°C. Drop B1 gave **structure LlTrxR#1**.

Constant: 0.4 M Li_2SO_4 .Volume: 500 µL reservoir

Crystallization #15 (7.13 mg/mL, RT)	PEG1000	PEG1500	PEG3350			
20% PEG						
25% PEG						
30% PEG						
35% PEG						
Protein:Reservoir	2:2	2:2	2:2			

Tray #16: As tray #15, just incubated at 30°C.

Constant: 0.4 M Li_2SO_4 .Volume: 500 µL reservoir

Crystallization #17 (8.9 mg/mL, RT)	PEG1000	PEG1500	PEG3350	PEG1000	PEG1500	PEG3350
20% PEG						
25% PEG						
30% PEG						
35% PEG						
Protein:Reservoir	2:2	2:2	2:2	2:3	2:3	2:3

Tray #17: As tray #16, just incubated at 30°C.

Constant: 0.4 M Li_2SO_4 .Volume: 500 µL reservoir

Crystallization #19 (8.9/7.74/7.84 mg/mL, RT)	15% PEG	20% PEG	25% PEG	15% PEG	20% PEG	25% PEG
PEG 1500						
PEG 3350						
PEG 1500						
PEG 3350						
Protein:Reservoir	2:2	2:2	2:2	2:2	2:2	2:2

Tray #20: As tray #19, just incubated at 30°C.

Constant: 0.4 M Li_2SO_4 .Volume: 500 µL reservoir

Crystallization #21 (6.3 mg/mL, 30ºC*)	15% PEG	20% PEG	25% PEG	15% PEG	20% PEG	25% PEG
PEG 1500						
PEG 3350						
PEG 1500						
PEG 3350						
Protein:Reservoir	2:2	2:2	2:2	3:2	3:2	3:2

Constant: 200 mM Li_2SO_4. No DTT added

Crystallization #22. No Light (11.0 mg/mL, RT)	20% PEG	25% PEG	30% PEG	20% PEG	25% PEG	30% PEG
PEG 1500						
PEG 4000						
PEG 1500 with 50 mM HEPES, pH7.0						
PEG 4000 with 50 mM HEPES, pH7.0						
Protein:Reservoir	2:2	2:2	2:2	2:2	2:2	2:2

Constant: 400 mM Li_2SO_4. No DTT added

Crystallization #23. No Light (11.0 mg/mL, RT)	20% PEG	25% PEG	30% PEG			30% PEG
PEG 1500						
PEG 4000						
PEG 1500 with 50 mM HEPES, pH7.0						
PEG 4000 with 50 mM HEPES, pH7.0						
Protein:Reservoir	2:2	2:2	2:2			2:2

Constant: 200 mM Li_2SO_4. 1 part protein solution + 1 part reservoir + 1 part DTT (60 mM)

Crystallization #24. No Light (11.0 mg/mL, RT)	20% PEG	25% PEG	30% PEG	20% PEG	25% PEG	30% PEG
PEG 1500						
PEG 4000						
PEG 1500 with 50 mM HEPES, pH7.0						
PEG 4000 with 50 mM HEPES, pH7.0						
Protein:Reservoir	2:2:2	2:2:2	2:2:2	2:2:2	2:2:2	2:2:2

Tray #25: As tray #24, just using 400 mM Li_2SO_4. Drop B1 gave structure **LITrxR#2.**

Constant: 200 mM Li_2SO_4. No DTT added

Crystallization #26. With Light (9.3 mg/mL, RT)	20% PEG	25% PEG	30% PEG	20% PEG	25% PEG	30% PEG
PEG 1500						
PEG 4000						
PEG 1500 with 50 mM HEPES, pH7.0						
PEG 4000 with 50 mM HEPES, pH7.0						
Protein:Reservoir	2:2	2:2	2:2	2:2	2:2	2:2

Tray #27: As tray #26, just using 400 mM Li_2SO_4.

Constant: 200 mM Li_2SO_4. 1 part DTT (60 mM) added to 1 part protein solution + 1 part reservoir.

Crystallization #28. With Light (9.3 mg/mL, RT)	20% PEG	25% PEG	30% PEG	20% PEG	25% PEG	30% PEG
PEG 1500						
PEG 4000						
PEG 1500 with 50 mM HEPES, pH7.0						
PEG 4000 with 50 mM HEPES, pH7.0						
Protein:Reservoir	2:2:2	2:2:2	2:2:2	2:2:2	2:2:2	2:2:2

Tray #29: As tray #28, just using 400 mM Li_2SO_4.

Constant: 200 mM Li_2SO_4.

Crystallization #30. With NADPH+ Light (~10 mg/mL, RT)	1 20% PEG	2 25% PEG	3 30% PEG	4 20% PEG	5 25% PEG	6 30% PEG
PEG 1500				+DTT	+DTT	+DTT
PEG 4000				+DTT	+DTT	+DTT
PEG 1500 with 50 mM HEPES, pH7.0				+DTT	+DTT	+DTT
PEG 4000 with 50 mM HEPES, pH7.0				+DTT	+DTT	+DTT
Protein:Reservoir(:DTT), in µL	1:1	1:1	1:1	1:1:1	1:1:1	1:1:1

Constant: 400 mM Li_2SO_4.

Crystallization #31. With NADPH+ Light (~10 mg/mL, RT)	1 30% PEG	2 30% PEG				
PEG 1500		DTT				
PEG 4000		DTT				
PEG 1500 with 50 mM HEPES, pH7.0		DTT				
PEG 4000 with 50 mM HEPES, pH7.0		DTT				
Protein:Reservoir(:DTT), in µL	1:1	1:1:1				

Constant: 400 mM Li_2SO_4

Crystallization #32. No Light (11.7 mg/mL)						
30% PEG1500						
30% PEG4000 + part 60 mM DTT						No DTT
35% PEG1500						
35% PEG4000 + 1 part 60 mM DTT						No DTT
Protein:Reservoir(:DTT), in µL	2:2(:2)	2:2(:2)	2:2(:2)	2:2(:2)	2:2(:2)	2:2

Constant: 400 mM Li_2SO_4

Crystallization #33. NO Light (11.7 mg/mL)						
30% PEG4000						
35% PEG4000						
40% PEG4000						
40% PEG4000 + 1 part X mM NADPH						
Protein:Reservoir(:NADPH), in µL	2:2(:2)	2:2(:2)	2:2(:2)	2:2(:2)	2:2(:2)	2:2

Constant: 400 mM Li_2SO_4

Crystallization #33A. WITH Light (9.3 mg/mL)						
30% PEG4000						
35% PEG4000				**Protein used: TrxB-NADPH WITH Light**	**Protein used: TrxB-NADPH WITH Light**	**Protein used: TrxB-NADPH WITH Light**
40% PEG4000				**Protein used: TrxB-NADPH WITH Light**	**Protein used: TrxB-NADPH WITH Light**	**Protein used: TrxB-NADPH WITH Light**
40% PEG4000 + 1 part X mM NADPH						
Protein:Reservoir(:NADPH), in µL	**2:2(:2)**	**2:2(:2)**	**2:2(:2)**	**2:2(:2)**	**2:2(:2)**	**2:2**

Constant: 200 mM $(NH_4)_2SO_4$

Crystallization #34. No Light (11.7 mg/mL)						
30% PEG1500						
30% PEG4000 + part 60 mM DTT						
35% PEG1500						
35% PEG4000 + 1 part 60 mM DTT						
Protein:Reservoir(:DTT), in µL	**2:2(:2)**	**2:2(:2)**	**2:2(:2)**	**2:2(:2)**	**2:2(:2)**	**2:2(:2)**

Tray #35: As tray #43, just using 400 mM Li_2SO_4.

Try PDB 4GCM crystallization conditions: 10.00% Glycerol, 1.26M tri-Sodium Citrate, 0.1M HEPES pH 7.5.

Crystallization #36. Reservoir volume: 1 mL	**No Light (11.7 mg/mL)**	**With Light (9.3 mg/mL)**	**With TrxB-NADPH Light (9.36 mg/mL)**	**No Light (11.7 mg/mL)**	**With Light (9.3 mg/mL)**	**TrxB_009 Only his-tag purified.**
				+ NADPH	**+ NADPH**	
				+ NADPH	**+ NADPH**	
				+ NADPH	**+ NADPH**	
				+ NADPH	**+ NADPH**	
Protein:Reservoir(:NADPH), in µL	**2:2**	**2:2**	**2:2**	**2:2(:2)**	**2:2(:2)**	**2:2**

Constant: 400 mM Li_2SO_4

Crystallization #37. TrxB_009, only His-tag purified (11.2 mg/mL) LlTrxR-NADPH WITH Light (9.36 mg/mL)	**400 mM Li_2SO_4**	**400 mM Li_2SO_4**	**200 mM $(NH_4)_2SO_4$**	**200 mM $(NH_4)_2SO_4$**	**400 mM $(NH_4)_2SO_4$**	**400 mM $(NH_4)_2SO_4$**
30% PEG4000						
35% PEG4000						
30% PEG1500						
35% PEG1500						
Protein:Reservoir (in µL)	**2:2**	**2:2**	**2:2**	**2:2**	**2:2**	**2:2**

Constant: 400 mM Li_2SO_4, 35% PEG1500

Crystallization #38. No Light TrxB_010, gel filtrated(8.10 mg/mL)	**pH 5.5 pH 6.0 pH 6.5 pH 7.0**	**pH 7.5 pH 8.0 pH 8.5 % HEPES**	**pH 5.5 pH 6.0 pH 6.5 pH 7.0**	**pH 7.5 pH 8.0 pH 8.5 % HEPES**	**pH 5.5 pH 6.0 pH 6.5 pH 7.0 (NADP+)**	**pH 7.5 pH 8.0 pH 8.5 % HEPES (NADP+)**
Protein:Reservoir:NADPH/NADP+ (in µL)	**2:2**	**2:2**	**2:2**	**2:2**	**2:2:1**	**2:2:1**

Constant: 400 mM Li_2SO_4, 35% PEG1500

Crystallization #39. No Light TrxB_010, gel filtrated(8.10 mg/mL)	**pH 5.5 pH 6.0 pH 6.5 pH 7.0 (NADP+)**	**pH 7.5 pH 8.0 pH 8.5 % HEPES (NADP+)**	**pH 5.5 pH 6.0 pH 6.5 pH 7.0 (NADPH)**	**pH 7.5 pH 8.0 pH 8.5 % HEPES (NADPH)**	**pH 5.5 pH 6.0 pH 6.5 pH 7.0 (NADPH)**	**pH 7.5 pH 8.0 pH 8.5 % HEPES (NADPH)**
Protein:Reservoir:NADPH/NADP+ (in µL)	**2:2:1**	**2:2:1**	**2:2:1**	**2:2:1**	**2:2:1**	**2:2:1**

Constant: 400 mM Li_2SO_4

Crystallization #40. Light TrxB_010, gel filtrated(xx mg/mL)	**Light 30 min**	**Light 60 min**	**Light 30 min**	**Light 60 min**	**Light 30 min**	**Light 60 min**
30% PEG4000, % HEPES						
30 % PEG4000, HEPES, pH=6.0						
35 % PEG1500, % HEPES						
35 % PEG1500, HEPES, pH=6.0						
Protein:Reservoir (in µL)	**2:2**	**2:2**	**2:2**	**2:2**	**2:2**	**2:2**

Constant: 400 mM Li_2SO_4

Crystallization #41. Light TrxB_010, gel filtrated(xx mg/mL)	**Light 30 min**	**Light 60 min**	**Light 30 min**	**Light 60 min**	**Light 30 min**	**Light 60 min**
30% PEG4000, % HEPES						
30 % PEG4000, HEPES, pH=6.0						
35 % PEG1500, % HEPES						
35 % PEG1500, HEPES, pH=6.0						
Protein:Reservoir:NADP+ (in µL)	**2:2:1**	**2:2:1**	**2:2:1**	**2:2:1**	**2:2:1**	**2:2:1**

Constant: 400 mM Li_2SO_4, 35% PEG1500

Crystallization #42. Light TrxB_010, gel filtrated (30 min: 8.2 mg/mL, 120 min: 5.1 mg/mL)	**HEPES, pH=6.5**	**HEPES, pH=6.5**	**HEPES, pH=6.5**	**HEPES, pH=7.5**	**HEPES, pH=7.5**	**HEPES pH=7.5**
Light 30 min						
Light 30 min, NADP+						
Light 120 min						
Light 120 min, NADP+						
Protein(30min):Reservoir:NADP+ (in µL) 2:2:1 Protein(120min):Reservoir:NADP+ (in µL) 3:2:1						

Constant: 400 mM Li_2SO_4, 35% PEG1500

Crystallization #43. Light TrxB_010, gel filtrated (30 min: 8.2 mg/mL, 120 min: 5.1 mg/mL)	**HEPES, pH=8.0**	**HEPES, pH=8.0**	**HEPES, pH=8.0**			
Light 30 min						
Light 30 min, NADP+						
Light 120 min						
Light 120 min, NADP+						
Protein(30min):Reservoir:NADP+ (in µL) 2:2:1 Protein(120min):Reservoir:NADP+ (in µL) 3:2:1						

Constant: 400 mM Li_2SO_4, 35% PEG1500. * Final concentration in reservoir: 2 mM.

Crystallization #44, Light TrxB_010, gel filtrated (30 min: 8.2 mg/mL, 120 min: 5.1 mg/mL)	**Light 30 min + NADP+**	**Light 30 min + NADP+**	**Light 120 min + NADP+**	**Light 120 min + NADP+**	**Light 30 min**	**Light 120 min**
$FeCl_3$*						
$CuSO_4$*						
$MgCl_2$*						
$CaCl_2$*						
Protein(30min):Reservoir:NADP+ (in µL) 2:2:1 Protein(120min):Reservoir:NADP+ (in µL) 2:1:1						

Constant: 400 mM Li_2SO_4, 35% PEG1500

Crystallization #45. 2 hours Light TrxB_010, gel filtrated (2 hours: 7.26 mg/mL)	**HEPES, pH=7.5**	**HEPES, pH=7.5**	**HEPES, pH=7.5**	**HEPES, pH=8.0**	**HEPES, pH=8.0**	**HEPES, pH=8.0**
+$NADP^+$ Protein:Reservoir:NADP+ (in µL) 1:2:1						
+$NADP^+$ Protein:Reservoir:NADP+ (in µL) 2:2:1						
+$NADP^+$ Protein:Reservoir:NADP+ (in µL) 3:2:1						
%$NADP^+$ Protein:Reservoir (in µL) 2:2						

Tray #46: As tray #45, just light exposed for 6 hours.

Constant: 400 mM Li_2SO_4, 35% PEG1500

Crystallization #47. 2 hours Light TrxB_010, gel filtrated (2 hours: 7.26 mg/mL)	**HEPES, pH=7.5**	**HEPES, pH=7.5**	**HEPES, pH=7.5**	**HEPES, pH=8.0**	**HEPES, pH=8.0**	**HEPES, pH=8.0**
+$NADP^+$ Protein:Reservoir:NADP+:DTT (in µL) 1:2:1:1						
+$NADP^+$ Protein:Reservoir:NADP+:DTT (in µL) 2:2:1:1						
+$NADP^+$ Protein:Reservoir:NADP+:DTT (in µL) 3:2:1:1						
%$NADP^+$ Protein:Reservoir:DTT (in µL) 2:2:1						

Tray #48: As tray #47, just light exposed for 6 hours.

Constant: 400 mM Li_2SO_4, 35% PEG1500

Crystallization #49. No Light TrxB_010, gel filtrated (No Light: 7.26 mg/mL)	**HEPES pH=6.0**	**HEPES pH=6.0**	**HEPES pH=6.5**	**HEPES pH=6.5**	**HEPES pH=7.5**	**HEPES pH=7.5**
+$NADP^+$ Protein:Reservoir:NADP+ (in µL) 4:2:1						
+$NADP^+$ Protein:Reservoir:NADP+ (in µL) 4:2:1						
+$NADP^+$ Protein:Reservoir:NADP+ (in µL) 4:2:1						
+$NADP^+$ Protein:Reservoir:NADPH (in µL) 4:2:2						

Tray #50: As tray #49, just without $NADP^+$.

Constant: 400 mM Li_2SO_4, 35% PEG1500

Crystallization #51. 3 hours Light TrxB_010, gel filtrated (3 hours: 10.64 mg/mL)	**HEPES pH=6.0**	**HEPES pH=6.0**	**HEPES pH=6.5**	**HEPES pH=6.5**	**HEPES pH=7.5**	**HEPES pH=7.5**
+$NADP^+$ Protein:Reservoir:NADP+ (in µL) 2:2:1						
+$NADP^+$ Protein:Reservoir:NADP+ (in µL) 2:2:1						
+$NADP^+$ Protein:Reservoir:NADP+ (in µL) 2:2:1						
+$NADP^+$ Protein:Reservoir:NADP+ (in µL) 2:2:1						

Constant: 400 mM Li_2SO_4, 35% PEG1500

Crystallization #52. 3 hours Light TrxB_010, gel filtrated (3 hours: 10.64 mg/mL)	**HEPES pH=6.0**	**HEPES pH=6.0**	**HEPES pH=6.5**	**HEPES pH=6.5**	**HEPES pH=7.5**	**HEPES pH=7.5**
+$NADP^+$ Protein:Reservoir:NADP+ (in µL) 1.5:2:1						
+$NADP^+$ Protein:Reservoir:NADP+ (in µL) 1.5:2:1						
%$NADP^+$ Protein:Reservoir (in µL) 2:2						
%$NADP^+$ Protein:Reservoir (in µL) 1.5:2						

Constant: 400 mM Li_2SO_4, 35% PEG1500

Crystallization #53. 4 hours Light TrxB_010, gel filtrated (4 hours: 11,6 mg/mL)	**HEPES pH=6.0**	**HEPES pH=6.0**	**HEPES pH=6.5**	**HEPES pH=6.5**	**HEPES pH=7.5**	**HEPES pH=7.5**
+$NADP^+$ Protein:Reservoir:NADP+ (in µL) 2:2:1						
+$NADP^+$ Protein:Reservoir:NADP+ (in µL) 2:2:1						
+$NADP^+$ Protein:Reservoir:NADP+ (in µL) 2:2:1						
%$NADP^+$ Protein:Reservoir (in µL) 2:2						

Constant: 400 mM Li_2SO_4, 35% PEG1500

Crystallization #54. 4 hours Light TrxB_010, gel filtrated (4 hours: 11.6 mg/mL)	**HEPES pH=6.0**	**HEPES pH=6.0**	**HEPES pH=6.5**	**HEPES pH=6.5**	**HEPES pH=7.5**	**HEPES pH=7.5**
+$NADP^+$ Protein:Reservoir:NADP+ (in µL) 1.5:2:1						
+$NADP^+$ Protein:Reservoir:NADP+ (in µL) 1.5:2:1						
+$NADP^+$ Protein:Reservoir:NADP+ (in µL) 1.5:2:1						
%$NADP^+$ Protein:Reservoir (in µL) 1.5:2						

Appendix E. Structural analyses

1.

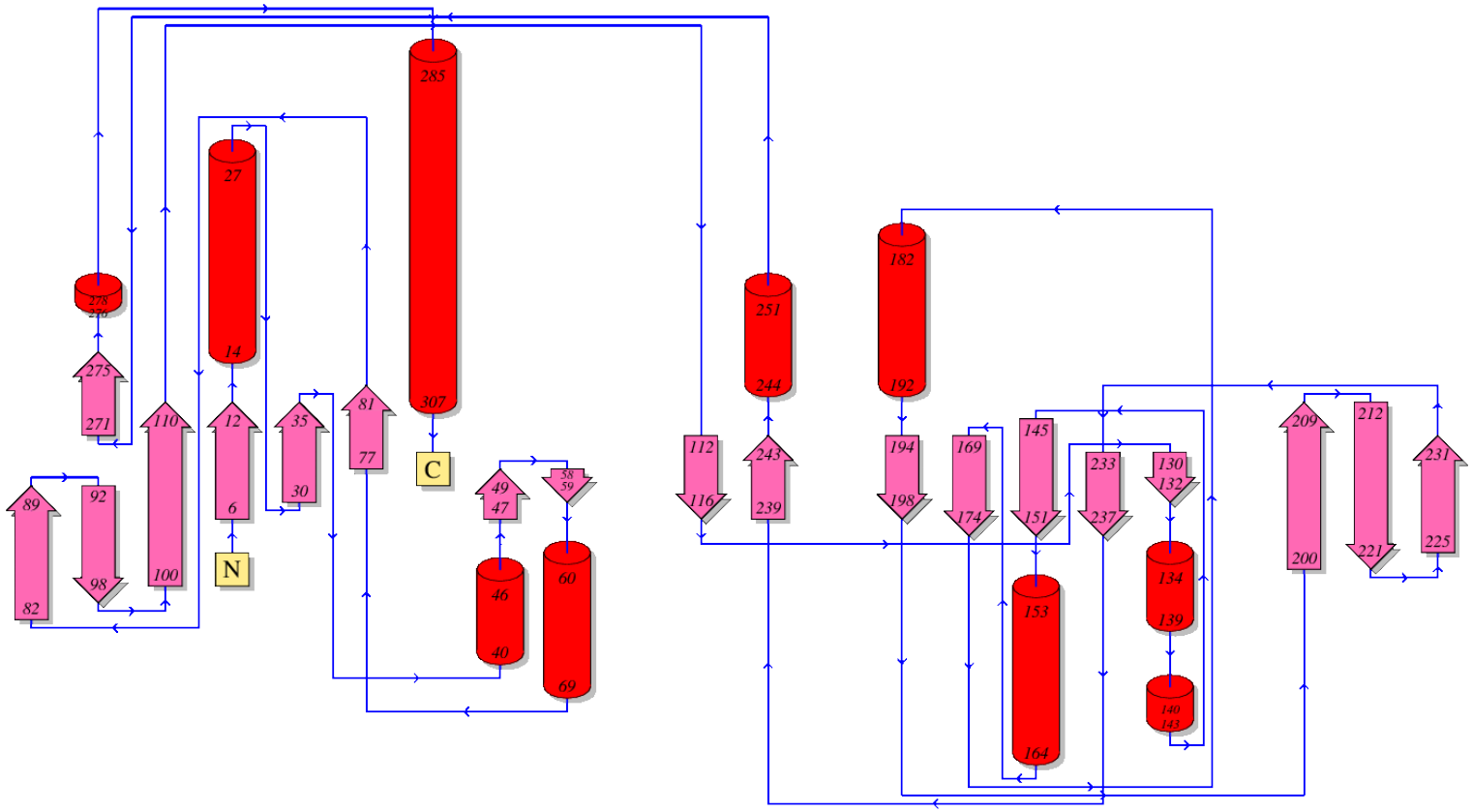

Figure 58. Topology diagram of the secondary structure of LlTrxR with the FAD domain (1-111+244-308) and the NADPH domain (117-238). The domains are connected by two anti-parallel β-sheets (112-116 and 239-243), classically assigned to the FAD domain (Generated by PDBsum).

2.

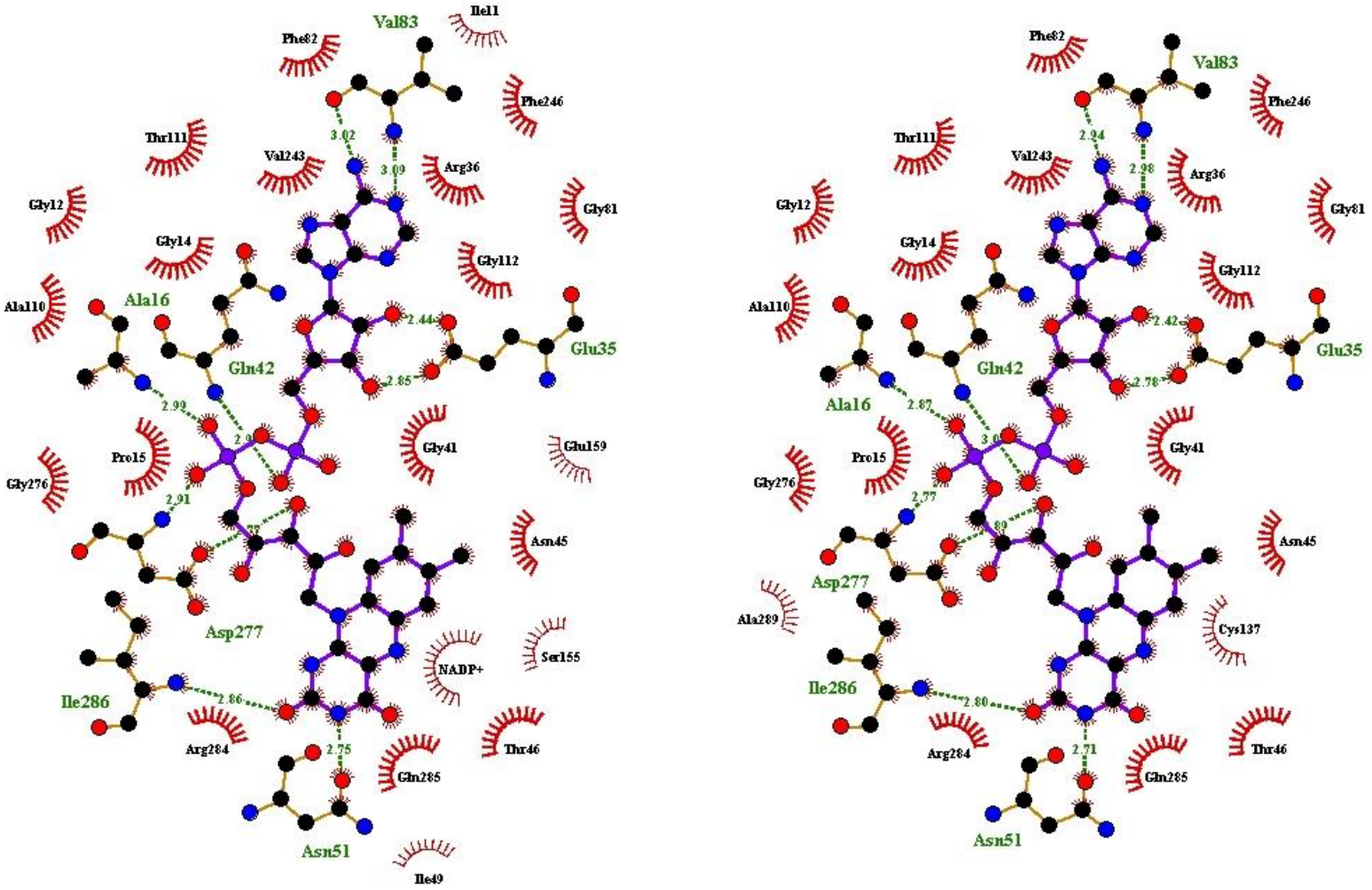

Figure 59. Interactions between FAD and surrounding *Li*TrxR protein in the FR (left) and FO (right) conformation, PDB 5MH4 and 5MJK, respectively. Contacts found with LigPlot^{+}.

3.

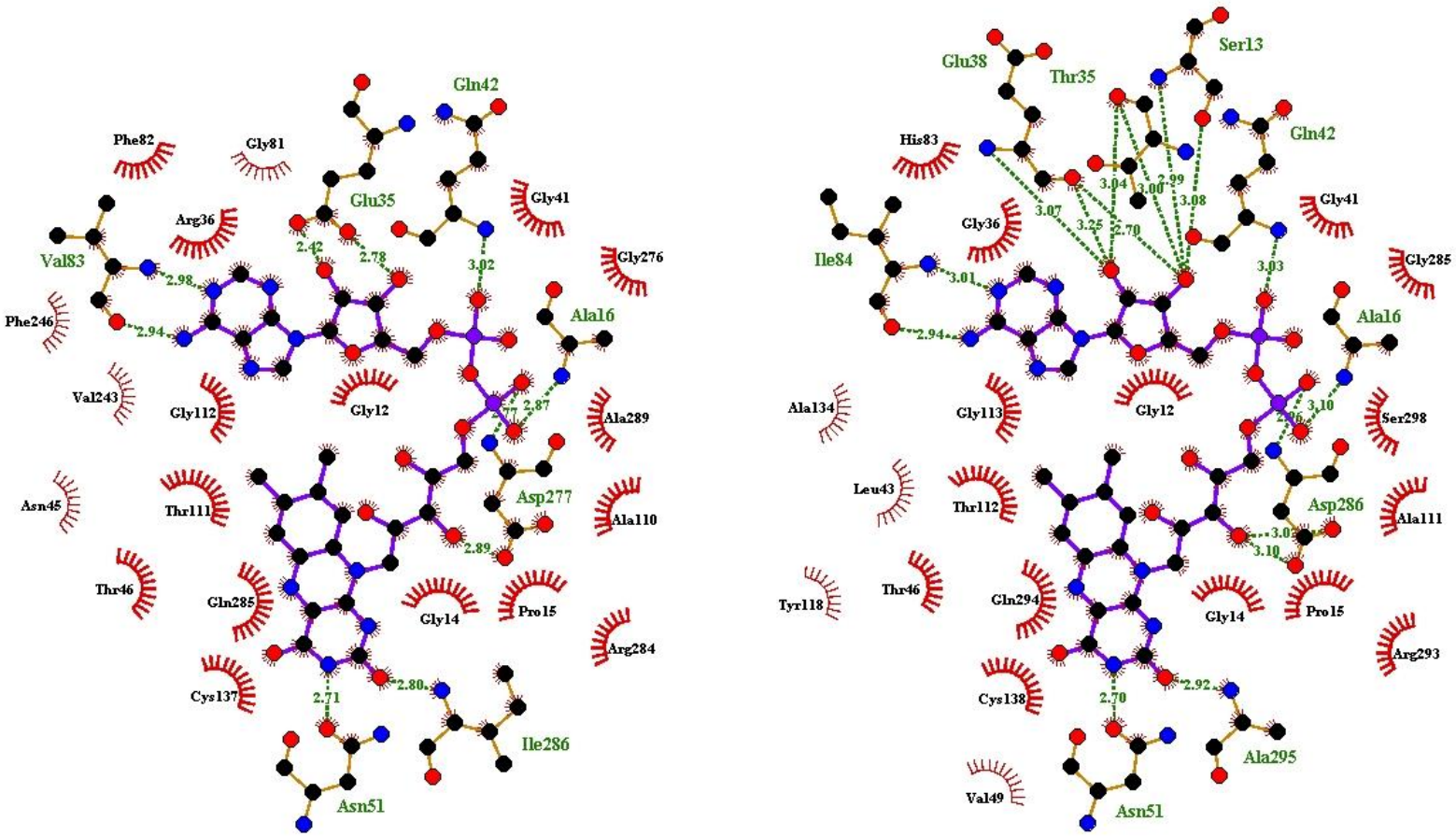

Figure 60. Interactions between FAD and surrounding TrxR in FO conformation comparing *Ll*TrxR (left) and *Ec*TrxR (right), PDB 5MJK and 1TDE, respectively. As seen, only two residues in *Ec*TrxR (Ser13vand Glu38), involved in hydrogen bonding with the ribose of the nucleotide, are different to *Ll*TrxR. The same result was obtained for *Ll*TrxR (PDB 5MH4) and *Ec*TrxR (1F6M) in FR conformation. Contacts found with LigPlot^{+}.

4.

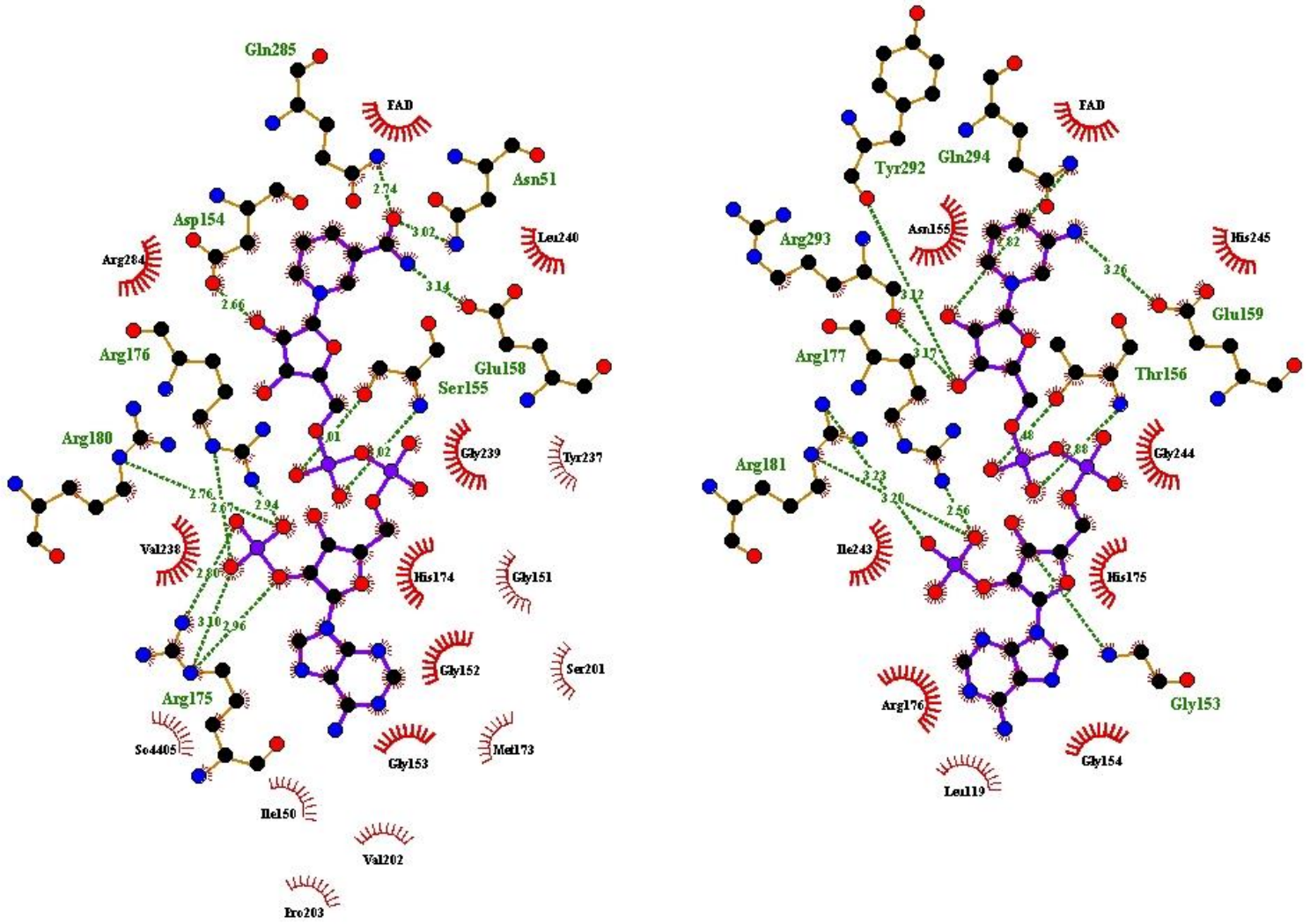

Figure 61. Comparison of interaction between *Ll*TrxR and *Ec*TrxR with NADP$^+$ (left) and AADP$^+$ (right) respectively. PDB 5MH4 and 1F6M for *Ll*TrxR and *Ec*TrxR, respectively. See chapter 3 for detailed description.

Appendix F. Tables of interactions identified with LigPlot^{+}

LigPlot	FAD domain	NADPH domain	Neighboring Monomer	Hinge region	Distance (Å)	Interaction type
***Ll*TrxR, FO**	Glu50	Phe141			3.5	van der Waals
	Gln285	Cys137			3.6	van der Waals
	Gln285	Val136			3.3	van der Waals
	Ala47	Ala128			3.1	van der Waals
		Cys137	Arg26		3.1/3.17	Hydrogen bond
		Val136	Arg26		2.9	Hydrogen bond
		Arg188	Gln306		3.3	van der Waals
		Arg143	Glu28		2.6	Hydrogen bond
		Phe166	Glu28		3.4	van der Waals
		Ser27	Arg165		2.7	Hydrogen bond
		Tyr162	Tyr301		3.7	van der Waals
		Tyr162	Ser27		3.3	van der Waals
		Tyr133		His115	3.9	van der Waals
		Val238		Arg116	3.8	van der Waals
	Val243				Thr111	Hydrogen bond

LigPlot	FAD domain	NADPH domain	Neighboring Monomer	Hinge region	Distance (Å)	Interaction type
***Li*TrxR, FR**	Glu50	Arg188			2.8/2.9	Hydrogen bond
	Ala47	Tyr162			3.5	van der Waals
	Asn45	Cys137			3.7	van der Waals
	Asn45	Cys134			3.9	van der Waals
	Asn45	Val136			3.5	van der Waals
	Asn44	Val136			3.8	van der Waals
		Gln182	Arg26		2.8	Hydrogen bond
		Ile184	Arg26		2.9	Hydrogen bond
		Ile184	Glu28		3.5	van der Waals
		Glu183	Tyr301		2.6	Hydrogen bond
		Glu183	Glu28		3.5	van der Waals
		Glu183	Ser27		3.6	van der Waals
		Tyr133		His115	3.6	van der Waals
		Val238		Arg116	3.7	van der Waals
	Gln42			Ala113	3.2	Hydrogen bond

LigPlot	FAD domain	NADPH domain	Neighboring Monomer	Hinge region	Distance (Å)	Interaction type
***Ec*TrxR, FO**	Thr47	Gly129			3.1	Hydrogen bond
	Glu48	Arg130			3.0	Hydrogen bond
	Glu50	Phe142			3.3	van der Waals
	Asn51	Cys138			3.8	van der Waals
	Gln294	Thr137			3.6	van der Waals
		Cys138	Arg26		3.1/2.9	Hydrogen bond
		Arg144	Asn28		3.0/3.1	Hydrogen bond
		Asn166	Asn28		2.9	Hydrogen bond
		Asn166	Asp314		3.2	Hydrogen bond
		Arg189	Asp314		2.9	Hydrogen bond
		Lys193	Asp314		3.2	Hydrogen bond
		Tyr163	Glu310		3.8	van der Waals
		Tyr163	Ala27		3.7	van der Waals
		Thr137	Leu307		3.8	van der Waals
		Phe141	Phe75		3.8	van der Waals
		Phe141	Ala25		3.5	van der Waals
		Ala134		Ala116	3.8	van der Waals
	Thr114			Asn248	2.9	Hydrogen bond
	Gln42			Ala116	3.1	Hydrogen bond

LigPlot	FAD domain	NADPH domain	Neighboring Monomer	Hinge region	Distance (Å)	Interaction type
***Ec*TrxR, FR**	Glu50	Arg189			2.9/3.0	Hydrogen bond
	Thr47	Thr137			3.8	van der Waals
	Thr45	Thr137			3.0	van der Waals
		Lys188	Asn28		3.1	Hydrogen bond
		Ile185	Arg26		3.0	Hydrogen bond
		Glu183	Arg26		2.5	Hydrogen bond
		Lys184	Ala27		3.6	van der Waals
		Leu186	Arg26		3.8	van der Waals
	Gly261			Pro247	3.8	van der Waals
	Tyr262			Pro247	3.5	van der Waals
	Val287			Gly113	3.8	van der Waals
	Gln42			His245	3.4	van der Waals

LigPlot	FAD domain	NADPH domain	Neighboring Monomer	Hinge region	Distance (Å)	Interaction type
***Sa*TrxR, FO**	Gln285	Cys137			3.2	Hydrogen bond
	Gln285	Val136			3.8	van der Waals
		Arg188	Asp309		2.5/2.8	Hydrogen bond
		Val136	Arg26		3.0	Hydrogen bond
		Cys137	Arg26		3.0/3.0	Hydrogen bond
		Lys165	Asn28		3.1	Hydrogen bond
		Lys191	Asn308		3.2	Hydrogen bond
		Ile184	Asp309		3.9	van der Waals
		Val136	Gln298		3.6	van der Waals
		Ala140	Arg26		3.9	van der Waals
		Phe166	Arg26		3.7	van der Waals
		Phe166	Asn28		3.4	van der Waals
		Lys165	Ala27		3.3	van der Waals
		Tyr133		Lys116	3.8	van der Waals
		Tyr133		Tyr115	3.6	van der Waals
		Cys134		Tyr115	3.6	van der Waals
	Tyr258			Met240	3.4	van der Waals
	Tyr258			Pro242	3.4	van der Waals
	Val256			Pro242	3.6	van der Waals
	Gly257			Pro242	3.4	van der Waals
	Arg36			Leu243	3.8	van der Waals
	Val278			Gly112	3.8	van der Waals
	Gln42			Ala113	3.1	Hydrogen bond

Appendix G. Electron density maps for inspection (wall-eyed stereo)

Maps from all the structures published in PDB have been selected to highlight characteristics of the *Ll*TrxR. The σ_A-weighted $2F_o–F_c$ maps (grey) have been contoured at 1.0 σ. The difference $F_o–F_c$ maps (green/red) have been contoured at ±3.0 σ, respectively.

General backbone and sidechain (PDB 5MJK)

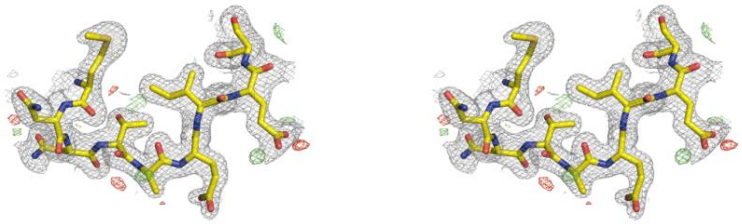

Assigned oxygen pocket with conserved water as viewed from the *re*-face of FAD (PDB 5MIQ). Observed in all structures.

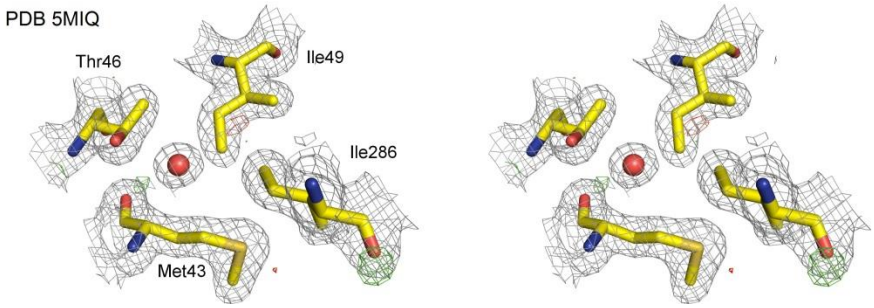

Methionine-Proline motif, located in conjunction with the assigned oxygen pocket (5MIP). Observed in all structures.

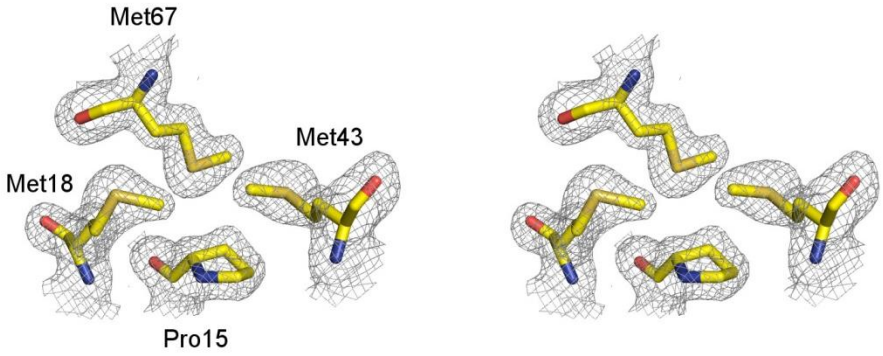

The redox-active disulfide in the proximity of FAD (PDB 5MJK). Observed in structure obtained in FO conformation.

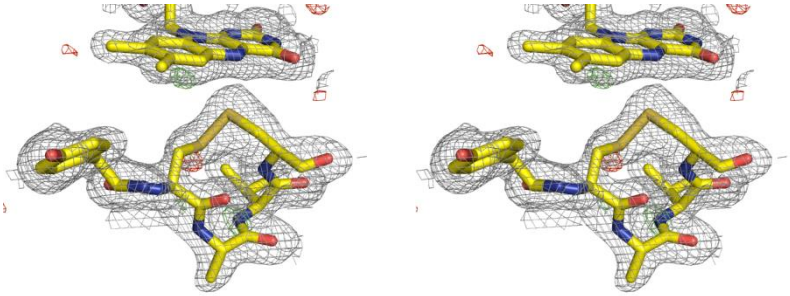

FAD-NADP$^+$ complex with conserved water at *si*-face of FAD (5MH4).

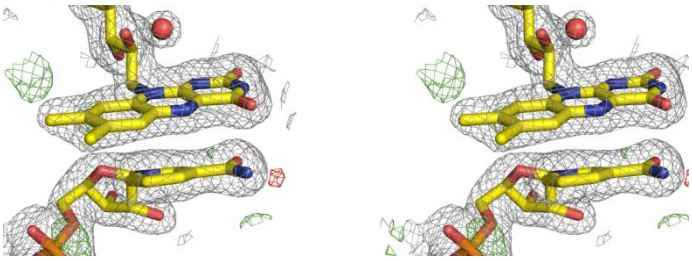

FAD-NADP$^+$ complex with conserved water at *si*-face of FAD (5MIQ).

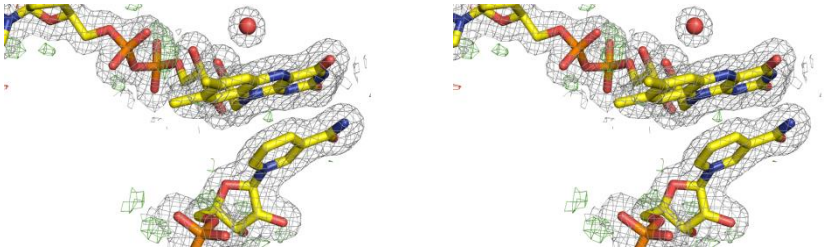

Methyl groups C7-alpha and C8-alpha of FAD without visible light exposure (PDB 5MJK)

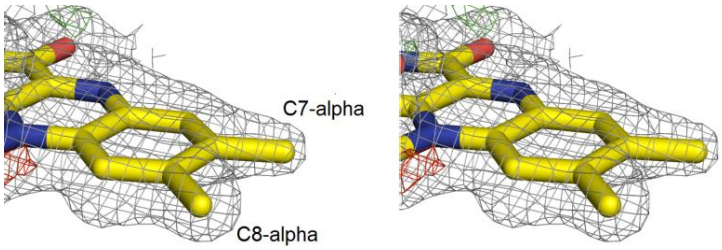

Gradual carbon-7-alpha formyl formation on FAD after 60 minutes visible light exposure (5MIQ)

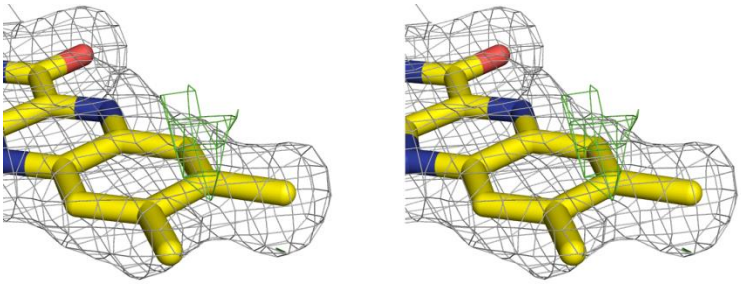

Carbon-7-alpha formyl formation on FAD after 180 minutes visible light exposure (PDB 5MIS), with possible further oxidation on carbon-8-alpha.

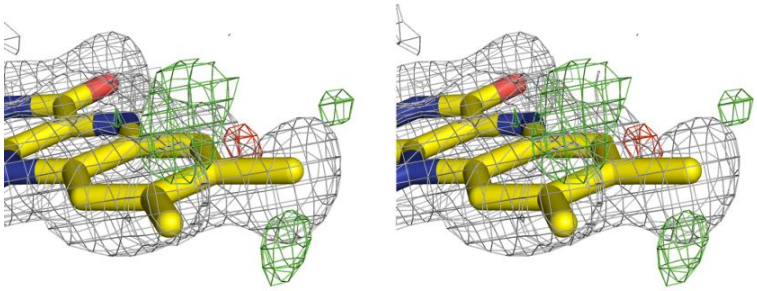

Oxidation of Tyr237 to 3,4-dihydroxyphenylalanine (DOPA) over the course of visible light exposure

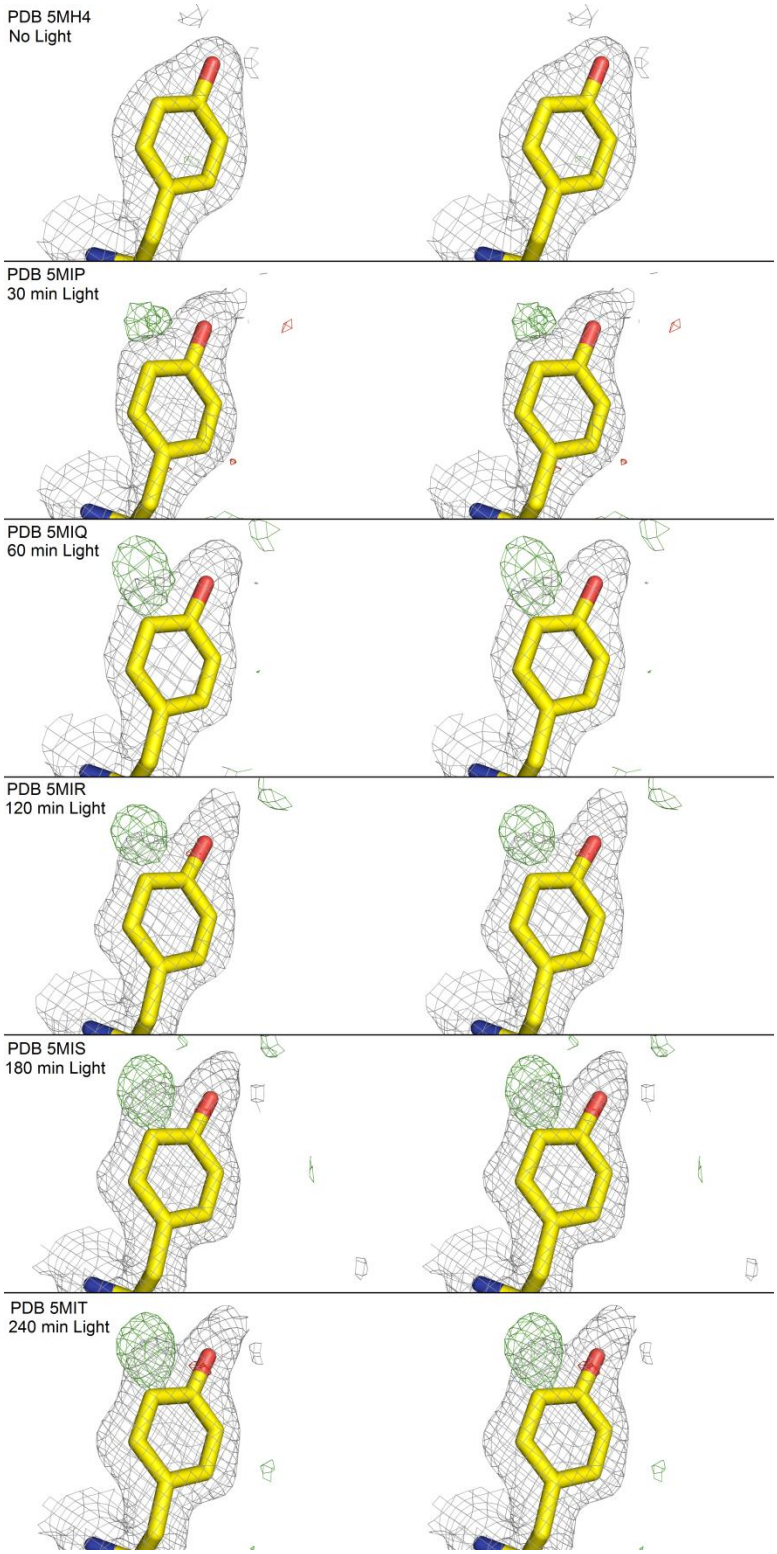

Appendix H. Potential Thioredoxin Protein Targets

Potential *Ll*TrxA and *Ll*TrxD protein targets were cloned, expressed, purified and characterized. All in all seven proteins were expressed and five were tested but it was not possible to firmly establish the rate of disulfide reduction in various DTNB assays. At least as far as for the recombinantly expressed proteins and the *in vitro* conditions tested. The potential *Ll*TrxA and *Ll*TrxD targets were identified by; (A) Petr Efler during his PhD studies as phenotype of *ΔLltrxD*[1] and as up-regulation in the *ΔLltrxA*[2] (Efler et al., 2015), (B) Martin Rykær during his Master's with 2-D electrophoresis followed by MALDI-TOF identification[3] (Identification of *Lactococcus lactis* Thioredoxin Target Proteins, master's thesis, M. Rykær, 2013). (C) Bioinformatics: In same operon as *trxD* and *noxE*[4].

Table 10. Overview of selected potential *Ll*TrxA/*Ll*TrxD protein targets.

	Protein target from *L. lactis*	**Abbreviation**	**UniProt entry**	**Length**	**Cysteines**	**M_w (kDa)**
1	Thiolperoxidase[3]	Tpx	A2RI31	159	2	19.6
2	Alkyl hydroperoxide reductase[3]	AhpC	A2RI68	186	3	22.8
3	Arsenate reductase[1]	ArsC	A2RJP3	133	5	17.2
4	Phenylalanyl-tRNA synthetase beta chain[4]	PheT	A2RIB6	207	3	24.2
5	Llmg_1498[3] (Uncharacterized protein)	Hyp1498	A2RLA9	120	1	15.6
6	Dihydrolipoamid dehydrogenase[3]	DLD	A2RHE1	471	2	51.9
7	Llmg_1475[2] (Uncharacterized protein)	Hyp1475	A2RL87	79	0	11.3

Tpx: *Ll*TrxA does reduce Tpx. But *Ll*TrxD only reduces Tpx at very slow rates. Assays performed with DTNB/H_2O_2/Tert-Butyl hydroperoxide as final electron acceptor. The Michaelis–Menten kinetics constants were determined for *Ll*TrxA/*Ll*TrxD → Tpx.

AhpC: Protein target neither reduced by *Ll*TrxA nor by *Ll*TrxD.

ArsC: *Ll*TrxA does reduce arsenate reductase, but at very low rate. *Ll*TrxD does *not* reduce reductase arsenate.

PheT: Can be reduced by *Ll*TrxA at slow rates. *Ll*TrxD can also reduce *Ll*PheT, but at even lower rates.

Hyp1498: SEC reveals that Hyp1498 is to be fund as a mix of monomers and dimers (figure next page), which was also verified by SDS-PAGE (data not included). The dimer of Hyp1498 can be reduced directly by NADPH (without *Ll*Trx and *Ll*TrxR).

Table 11. Cloning and transformation.

	Primer design	PCR amplification from chromosomal *L. lactis* DNA	Restriction enzymes (BamHI and NdeI)	Cloned into pET15b vector	Transformed into *E. coli* strain DH5α.	Transformed into *E. coli* Rosetta (DE3)
Tpx	**X**	**X**	**X**	**X**	**X**	**X**
AhpC	**X**	**X**	**X**	**X**	**X**	**X**
ArsC	**X**	**X**	**X**	**X**	**X**	**X**
PheT	**X**	**X**	**X**	**X**	**X**	**X**
Hyp1498	**X**	**X**	**X**	**X**	**X**	**X**
DLD	**X**	**X**	**X**	**X**	**X**	**X**
Hyp1475	**X**	**X**	**X**	**X**	**X**	**X**

Table 12. Protein production and purification.

	Temperature optimization for expression	His trap purification	Size exclusion chromatography
Tpx	**X**	**X**	**X**
AhpC	**X**	**X**	**X**
ArsC	**X**	**X**	**X**
PheT	**X**	**X**	**X**
Hyp1498	**X**	**X**	**X**
DLD	-	-	-
Hyp1475	-	-	-

Table 13. Characterization of proteins. Measured with NADPH/DTNB assays.

	*Ll*TrxA target	*Ll*TrxD target	Direct NADPH reduction
Tpx	**YES**	**Slow rate**	**NO**
AhpC	**NO**	**NO**	**NO**
ArsC	**Slow rate**	**NO**	**NO**
PheT	**Slow rate**	**Slow rate**	**NO**
Hyp1498	**NO**	**NO**	**YES (dimer form only)**
DLD	**?**	**?**	**?**
Hyp1475	**?**	**?**	**?**

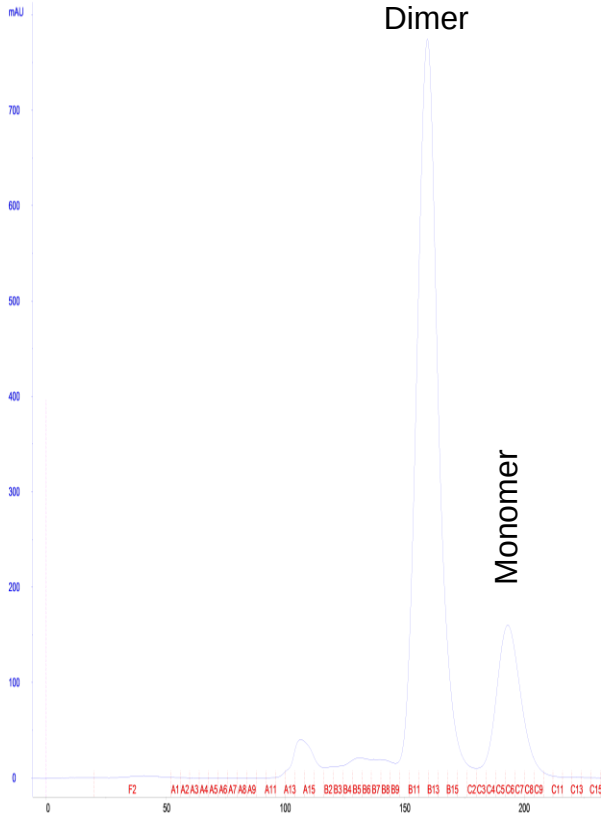

Figure 62. Size exclusion chromatography of His-tag-purified protein Hyp1498, monitored by A_{280}. The chromatogram displays two forms of Hyp1498, a dimer and a monomer form.